Nitrous oxide (N_2O) isotopic composition in the troposphere: instrumentation, observations at Mace Head, Ireland, and regional modeling

by Katherine Ellison Potter

B.S. Chemistry & Environmental Science
College of William and Mary, 2004

SUBMITTED TO THE DEPARTMENT OF EARTH, ATMOSPHERIC, AND PLANETARY SCIENCES
IN PARTIAL FULFULLMENT OF THE REQUIREMENTS FOR THE DEGREE OF

DOCTOR OF PHILOSOPHY IN CLIMATE PHYSICS AND CHEMISTRY
AT THE
MASSACHUSETTS INSTITUTE OF TECHNOLOGY

SEPTEMBER 2011

Signature of Author: _____
Department of Earth, Atmospheric, and Planetary Sciences
19 August 2011

Certified by: _____
Ronald G. Prinn
TEPCO Professor of Atmospheric Chemistry
Thesis Supervisor

Certified by: _____
Shuhei Ono
Assistant Professor
Thesis Co-Supervisor

Accepted by: _____
Maria T. Zuber
E.A. Griswold Professor of Geophysics and Planetary Science
Department Head

Nitrous oxide (N_2O) isotopic composition in the troposphere: instrumentation, observations at Mace Head, Ireland, and regional modeling

by Katherine Ellison Potter

Submitted to the Department of Earth, Atmospheric, and Planetary Sciences
on 19 August 2011 in partial fulfillment of the requirements for the degree of
Doctor of Philosophy in Climate Physics and Chemistry

Abstract

Nitrous oxide (N_2O) is a significant greenhouse gas and main contributor to stratospheric ozone destruction. Surface measurements of N_2O mole fractions have been used to attribute source and sink strengths, but large uncertainties remain. Stable isotopic ratios of N_2O (here considered $^{14}N^{15}N^{16}O$, $^{15}N^{14}N^{16}O$, $^{14}N^{14}N^{18}O$, relative to the abundant $^{14}N^{14}N^{16}O$) linked to source and sink isotopic signatures can provide additional constraints on emissions and counter-balancing stratospheric sink. However, the isotopic composition in the troposphere has been regarded and measured as a fixed value, limited by insufficient measurement precision and few data.

This thesis provides the foundation for high-frequency, high-precision measurements and utilization of N_2O tropospheric isotopic composition. This is achieved through the development of a new measuring capability with sufficient precision to detect the subtle signals of N_2O isotopic composition in tropospheric air and uniquely fully-automated and high-frequency capable. This instrument was applied to produce the first set of tropospheric air observations gathered at a remote research station covering a full annual cycle, paired with air origin information, and providing a valuable assessment of tropospheric composition and its potential utility. The first regional model of tropospheric N_2O isotopic composition was developed for further assessment of expected variability and utility of isotopic composition data.

The optimized fully-automated, liquid-cryogen-free pre-concentration device coupled to continuous flow IRMS resulted in ^{15}N site-specific precisions markedly improved over other systems of 0.11 and 0.14‰ (1σ) for $\delta^{15}N^{\alpha}$ and $\delta^{15}N^{\beta}$, respectively, and among the best bulk composition precisions of 0.05 and 0.10‰ for $\delta^{15}N^{bulk}$ and $\delta^{18}O$, respectively. The high-precision, non-continuous flask observations of N_2O ^{15}N site-specific composition (January 2010 to January 2011; Mace Head Atmospheric Research Station, Ireland) detected statistically significant signals on short-term and annual timescales, and when analyzed with air history information showed consistencies with source-receptor relationships. No seasonal cycle could be detected in the low-frequency observations, but regional model scenarios of the stratospheric seasonal signal resulted in amplitudes at the cusp of current measurement capabilities.

This thesis illustrated detectable variations in tropospheric N_2O isotopic composition which can potentially reduce uncertainty in the N_2O budget with high-frequency, high-precision observations, now feasible by the instrumentation developed here.

Thesis Supervisor: Ronald G. Prinn
Title: TEPCO Professor of Atmospheric Chemistry
Thesis Co-Supervisor: Shuhei Ono
Title: Assistant Professor

Acknowledgments

Ron Prinn and Shuhei Ono have supervised my work with equally valuable and perfectly distinct contributions, and cannot begin to enumerate their assets to me. I have been blessed to have them both at my back. Eric Davidson and Peter Simmonds on my committee provided a marvelous amount of constant inspiration for me as a scientist; through initial nitrogen cycle ignition in Brazil many years ago, to continual ideas and new approaches, to images of ideal scientist models and experience to crave.

The instrumentation work in this thesis began with the dedication and invaluable tutoring of Brian Greally, who jumpstarted Stheno into being. Simon O'Doherty generously made this entire thesis feasible with the welcome at the University of Bristol and munificent lending of Stheno's structure. Gerry Spain at the Mace Head Atmospheric Research Station was beyond air-sample-collector and provided me with valuable measurement knowledge, experience, insights, and confidence. My instrumentation support team including Ben Miller, Jens Mühle, Peter Salameh, Ray Weiss, and Dickon Young never failed to provide on-call instrument support and replies to many many emails regarding instrument failures, breakdowns, and other bits bringing frustration and love of experimental work. Bill Olszewski on-site never failed to serve as an incredible source of knowledge regarding anything lab equipment. Alistair Manning provided the priceless NAME air history estimates for each of my observations, without which this data might be interpreted as simply noise. Matt Rigby deserves thanks for the numerous discussions, insights, and pursuits regarding modeling of N_2O isotopes which educated this experimentalist in the ways of modelers. I am honored to have the enduring collaboration and friendship of Naohiro Yoshida and Sakae Toyoda, and am thankful for the opportunity to work alongside them at the Tokyo Institute of Technology, in the past and in the future, to further isotopomer research.

Additionally, outside of the science realm for keeping me going day-to-day, thanks to Mary Ellen Rhinehart and Erika Johnson for the maintenance and attention, and Mary Elliff for smiles, tokens, and friendship, and always leaving me higher and more hopeful than before.

Contents

Chapter 1: Introduction and thesis overview

1.1 Background

Nitrous oxide (N_2O) is an important trace gas, both a major greenhouse gas and main contributor to stratospheric ozone loss. Preindustrial mole fractions obtained from ice core data dating back to 1785 are around 270 ppb, rising to a present value above 320 ppb, mainly attributed to anthropogenic influences (Kroeze et al 1999, Sowers et al 2002). Over the past couple decades global growth has been monitored as approximately a linear trend in long-term atmospheric measurement programs, including the Advanced Global Atmospheric Gases Experiment (AGAGE) (Figure 1.1). The anthropogenic influence causing this increase is generally attributed to anthropogenically fixed nitrogen and agricultural expansion (e.g. fuel combustion, Haber-Bosch fertilizer production, livestock manure, and cultivation induced fixation), and the rate of increase is consistent with ~2% of manure and fertilizer nitrogen converted to N_2O (Davidson et al 2009). N_2O has a global warming potential 300 times that of carbon dioxide and estimates of its atmospheric lifetime are near 120 years. It currently has the fourth largest contribution to radiative forcing over the past 250 years among the long-lived greenhouse gases behind CF_2Cl_2 (CFC-12), CH_4, and CO_2 (Denman et al 2007). As CFC-12 levels slowly decline and N_2O continues its increasing trend, nitrous oxide will then rank third in its contribution to global warming. In the stratosphere N_2O serves as the source of NO_x in the catalytic destruction of ozone, and following the abatement of chlorofluorocarbons in recent years, N_2O is now considered the most important ozone depleting gas (Ravishankara et al 2009). Despite the importance of N_2O as contributing to climate change and ozone depletion, the understanding of its sources and sinks is still only known in general terms with large uncertainties in magnitudes and distribution in time and space.

Figure 1.1 Observations (in situ) of N_2O non-polluted mole fractions from the Mace Head, Ireland station of the AGAGE monitoring network from 1994. Monthly means (order 10^3 measurements) with standard deviations. http://agage.eas.gatech.edu, Prinn et al (2000)

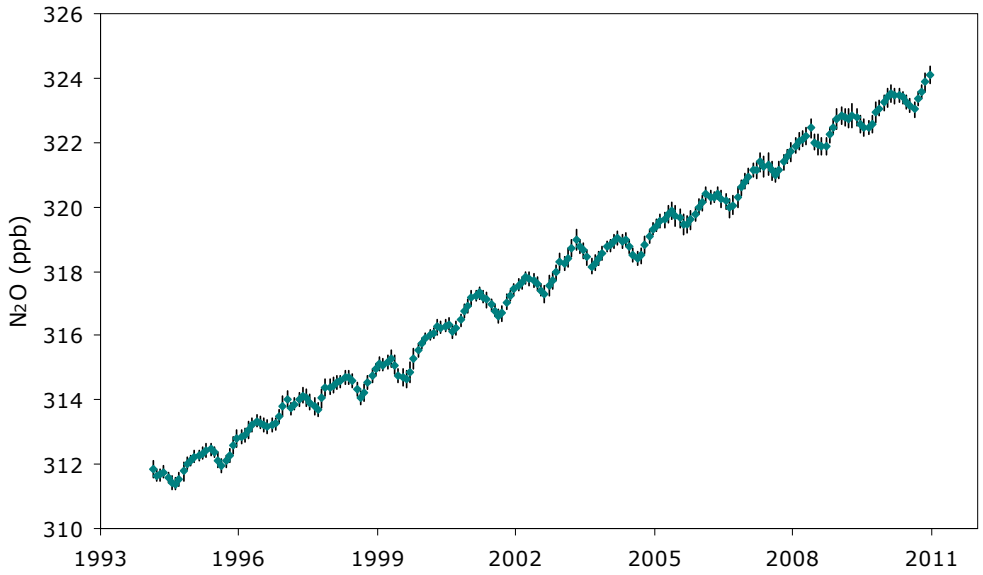

The major sources of N_2O in the atmosphere are microbial processes in the soil and to a lesser extent in the ocean. These processes occur naturally but have been exacerbated by anthropogenic inputs into the nitrogen cycle through expanding agricultural lands, increased fertilizer use, and increased N supply to coastal oceans such that the anthropogenic source now accounts for ~1/3 of the total N_2O source. Smaller anthropogenic sources include fossil fuel combustion, biomass burning, sewage, nylon manufacture, and automobiles. Minor atmospheric sources are from NH_3 oxidation and $N_2 + O(^1D)$. In the troposphere N_2O is chemically inert and the significant sink of nitrous oxide occurs when it ascends to the stratosphere in stratosphere-troposphere exchange (STE) mixing processes where it is photolyzed by ultraviolet radiation (~90% of the total loss) or oxidized by excited atomic oxygen (~10% of loss). Figure 1.2 summarizes N_2O best estimates for source magnitudes from the IPCC AR4 (Denman et al 2007), however the large uncertainty is indicated with the error bars displaying the range of values from compiled estimates. Bottom-up (summing individual source estimates) and top-down (using measurements to constrain sources) approaches to estimating the global N_2O budget show some consistency in the total global source when averaging across the spectrum of estimates, 17.7 and 17.3 TgN/y, respectively. This consistency is misleading, however, because the range in estimates is quite large (bottom-up: 8.5-27.7, top-down: 15.8-18.4 TgN/y) and within the total global estimates the spatial and temporal distributions of source estimations are wildly different.

The considerable uncertainty in the magnitude, distribution, and temporal pattern in the various natural and anthropogenic sources is partly due to the fact that the sources are so variable in space and time. N_2O emissions from soils, the largest source, predominantly are emitted in large pulses dependent upon soil moisture and precipitation, temperature, N availability, organic matter, and other conditions such as root mortality and freeze-thaw sequences (Firestone & Davidson 1989, Dobbie et al 1999, Davidson et al 2000, Keller et al 2005, et al). All of these vary greatly spatially across latitudes and even within the same region, and temporally as emissions fluctuate with seasons, peak after rainfall and fertilization events, and change with the aging of the soil conditions.

Figure 1.2 Global N_2O source estimates as given in the IPCC AR4 (Denman et al 2007). The gray bars indicate the range of source size estimates provided by both bottom-up and top-down analyses. Cool colors correspond to natural sources, warm colors predominately anthropogenic.

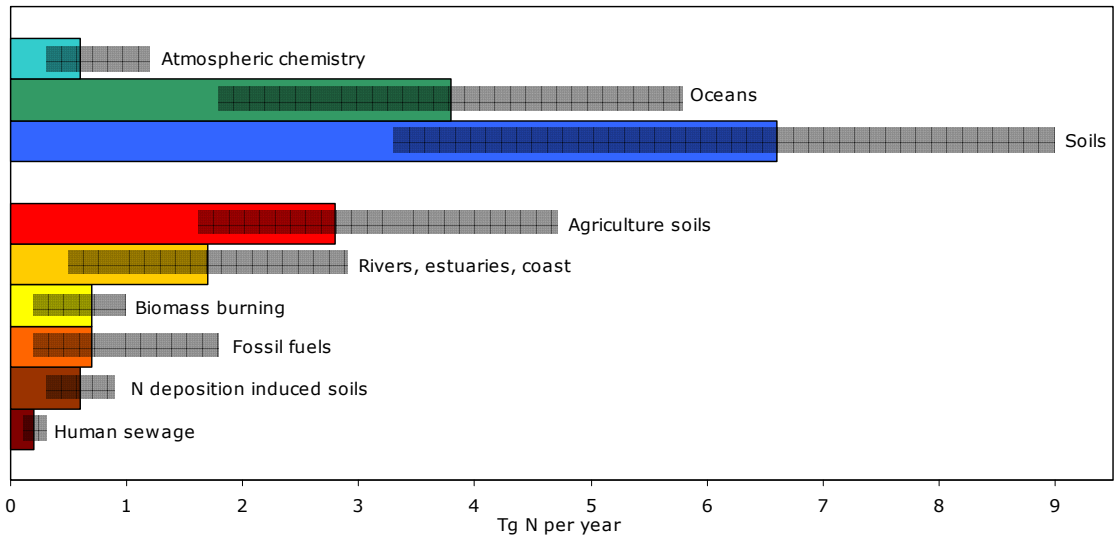

Continuous, long-term surface measurements of N_2O mole fractions have provided an important resource in analysis of the global budget through data analysis (e.g. Jiang et al 2007, Nevison et al 2004, 2005, 2007, 2011) and inversion studies on both global (e.g. Huang et al 2008, Hirsch et al 2006) and regional levels (e.g. Ryall et al 2001, Manning et al 2011, Corazza et al 2011). The utilization of these measurements, however, has largely reached the limit of information that can be extracted about the N_2O budget from mole fraction data and leaves large uncertainty remaining. On this front, the isotopologues of N_2O (here considered the abundant $^{14}N^{14}N^{16}O$ and the main rare isotopologues $^{14}N^{15}N^{16}O$, $^{15}N^{14}N^{16}O$, and $^{14}N^{14}N^{18}O$, diagnosed by $\delta^{15}N^{\alpha}$, $\delta^{15}N^{\beta}$, $\delta^{18}O$, and site preference ($SP = \delta^{15}N^{\alpha} - \delta^{15}N^{\beta}$)) potentially can help elucidate the remaining uncertainties by providing added observables which are linked to distinguishing source and sink isotopic signatures. The various influences on N_2O in the troposphere each have characteristic isotopic compositions due to the different processes involved and associated isotope fractionation effects, and thus the measured isotopic composition can add a powerful constraint on the controls of N_2O.

On the global scale, uncertainties in the exchange between troposphere and stratosphere play a very important role in N_2O emission estimates. For use in inverse modeling studies, this is the most significant source of uncertainty among all types of modeling uncertainties (Huang et al 2008, Hirsch et al 2006). One of the most critical applications of N_2O isotopic measurements will be to better contrain stratosphere-troposphere exchange. The distinguishing isotopic signatures between the stratospheric loss and surface sources are balanced in the tropospheric composition and thus stratospheric influence will be recorded in the tropospheric isotopic composition.

On the regional scale, N_2O isotopic composition has the potential to be critical as well through its ability to separate influencing source types. Manning et al (2011) used the AGAGE continuous N_2O mole fraction data from Mace Head over the years 1990-2007 with a novel inverse modeling technique and generally confirmed emission inventories in the UK and northwest Europe. However, distinction between sources was not possible with mole fractions alone due to the spatial confluence of emitting sectors. Mole fraction data in top-down studies generally are limited to total emissions, but isotopic composition data tied to signatures can potentially be used with the same techniques to delineate between natural and anthropogenic emissions, and between sectors within anthropogenic emissions, on both regional and global levels.

Table 1.1 Isotopic abundances of N_2O isotopologues calculated from IUPAC elemental N and O isotope abundances (Berglund & Wieser 2011).

Isotopologue	Abundance (mole fraction)
$^{14}N^{14}N^{16}O$	0.99032
$^{14}N^{15}N^{16}O$	0.00362
$^{15}N^{14}N^{16}O$	0.00362
$^{14}N^{14}N^{18}O$	0.00204
$^{14}N^{14}N^{17}O$	0.00038
$^{15}N^{15}N^{16}O$	1.32E-5
$^{14}N^{15}N^{18}O$	7.43E-6
$^{15}N^{14}N^{18}O$	7.43E-6
$^{14}N^{15}N^{17}O$	1.38E-6
$^{15}N^{14}N^{17}O$	1.38E-6
$^{15}N^{15}N^{18}O$	2.72E-8
$^{15}N^{15}N^{17}O$	5.03E-9

Uses of N_2O isotopic composition in the troposphere rely upon understanding of the isotopic fractionation and signatures of source and sink processes affecting atmospheric N_2O. Figure 1.3a-c illustrates the $\delta^{15}N^{bulk}$, $\delta^{15}N^{\alpha}$, $\delta^{15}N^{\beta}$, $\delta^{18}O$, and site preference (SP = $\delta^{15}N^{\alpha}$ - $\delta^{15}N^{\beta}$) signatures of the major sources and sinks in relation to the tropospheric composition, compiled from a range of measurement studies as referenced below. They are able to serve as a best guess for the general contributions for isotopic composition influences on N_2O in the troposphere and illustrate general relative depleted/enriched territories for the compositions, but the relatively few data collected in limited spatial regions and the often episodic nature of N_2O emissions means that these contributions cannot yet be perfectly defined.

Biological source and loss processes from the soils and oceans are accompanied by isotopic selectivity associated with the kinetics of bond formation and destruction, as well as the isotopic composition of the precursor molecules (e.g. NH_3 and NO_3^-). These biologically controlled production processes rely upon numerous factors such as oxidation status, temperature, N substrate availability, gas transport, soil type, soil texture, and water content. Apparent in Figure 1.3a-c, the range of compositions for the major soil source is quite variable, but in general the soil source is relatively depleted in across all isotopic values $\delta^{15}N^{\alpha}$, $\delta^{15}N^{\beta}$, and $\delta^{18}O$. Studies of N_2O isotopic composition from soil emissions have found extremely depleted values associated with high release rates (Perez et al 2000, 2006). The majority of total N_2O emitted from soils arises during high flux events rather than as a steady source, particularly after precipitation or irrigation, N fertilizer application, and freeze-thaw events among many other controlling influences. These high flux events arise in response to changing microbial processes between denitirification, nitrification, nitrifier denitrification, denitrifier N_2O consumption, etc., each of which have been found to have variable N_2O isotopic signatures dependent upon the fractionating enzymatic process as well as the original N substrate material in the soil and any oxygen exchange occurring in the substrate (Stein & Yung 2003, Toyoda et al 2005, 2011, Bateman et al 2005, Perez et al 2006, Kool et al 2009, Sutka et al 2006, Ostrom et al 2007, Casciotti et al 2009, Snider et al 2009, Well et al 2009). For the two major processes producing N_2O, nitrification involves formation of the N^{α}-O bond while denitrification involves cleavage, meaning that fractionation will accumulate at these positions. The different fractionations have been demonstrated in studies with pure strains of nitrifying and denitrifying bacteria. Recent observations suggest an isotopic difference between natural and fertilized agricultural soil emissions which have a distinctively more-depleted $\delta^{15}N^{bulk}$ composition (Park et al 2011), supporting the notion previously measured in natural versus fertilized and urine-amended soils (Perez et al 2001, Yamulki et al 2001).

Ocean vertical profiles suggest that while the majority of ocean-produced N_2O is from denitrification occurring in the oxygen minimum zone, different processes occur in the surface ocean which exchanges with the atmosphere (Popp et al 2002). Measurements in the ocean surface layer suggest that the isotopic signature is slightly depleted relative to the troposphere (Yoshinari et al 1997, Dore et al 1998, Naqvi et al 1998, Popp et al 2002, Yamagishi et al 2007). Ocean data of N_2O isotopic composition has mainly focused on the hot spots of N_2O production such as the eastern tropical north Pacific, with a few observations of open ocean waters in the Pacific. Spatial coverage thus does not encompass the globe, including no Atlantic Ocean measurements available yet, and it is possible in these lesser productive regions the ocean will act more like a buffer of N_2O rather than contributing a distinctive signature.

Anthropogenic industrial and combustion sources have very few signature data, with studies on coal (Ogawa & Yoshida 2005b), biomass burning (Ogawa & Yoshida 2005a), and car emissions (Toyoda et al 2008). Coal combustion appears to be dependent upon the exact combustion process and varies on either side of the tropospheric composition for both $\delta^{15}N$ and $\delta^{18}O$ (Ogawa & Yoshida 2005b) despite early measurements of $\delta^{18}O$ enriched coal source (Wahlen & Yoshinari 1985).

Biomass burning yields a slight $\delta^{15}N^{\alpha}$ site preference ($\delta^{15}N^{\alpha} - \delta^{15}N^{\beta} = 2‰$), and an overall bulk $\delta^{15}N$ lighter than the troposphere at 0‰ (Ogawa et al 2003). Yoshida and Toyoda (2000) suggest that there is insignificant fractionation of ^{15}N between the alpha and beta positions because industrial sources are not catalyzed enzymatically. Plotted in Figure 1.3a-c are the sparse estimates from these studies. Generally, the acceptance is that industrial processes have an isotopic signature similar to that of tropospheric N_2O (Rahn & Wahlen 2000).

The sum of the source signatures must balance the downward flux from the stratospheric sink to generate the tropospheric isotope signal. Stratospheric N_2O loss and fractionation effects through photolysis ($N_2O + h\nu \rightarrow N_2 + O(^1D)$) and photooxidation ($N_2O + O(^1D) \rightarrow 2NO$, $N_2 + O_2$) are well-studied and presently well-understood through the use of theory and models (Yung & Miller 1997, Miller & Yung 2000, Johnson et al 2001, Kaiser et al 2002a,b, McLinden et al 2003, Morgan et al 2004) and laboratory and field measurements (Rahn et al 1998, Umemoto 1999, Griffith et al 2000, Röckmann et al 2000, Turatti et al 2000, Yoshida & Toyoda 2000, Zhang et al 2000, Röckmann et al 2001, Toyoda et al 2001, Kaiser et al 2003b, Park et al 2004, Toyoda et al 2004, Kaiser et al 2006). Generally speaking, kinetic isotope effects cause the preferential reaction with isotopically lighter N_2O, thereby leaving ^{15}N- and ^{18}O-enriched N_2O in the stratosphere. This characteristic heavy composition then increases sharply into the upper stratosphere as photolysis increases and N_2O mole fractions taper off. Yung and Miller (1997) argue that because of small differences in their zero point energies, $^{14}N^{15}NO$ and $^{15}N^{14}NO$ should undergo photolysis at significantly different rates, thereby the stratospheric signal carrying ^{15}N site-specific information as well. Plotted in Figure 1.3a-c are rough estimates for the composition of the lower stratosphere which would be mixing with the troposphere taken from two studies (Toyoda et al 2004, Park et al 2004). Stratospheric values at higher altitudes would plot diagonally more enriched for all isotopologues, measured at extremely enriched composition near to or greater than 100‰ in the upper levels of the stratosphere (Toyoda et al 2004).

Figure 1.3 (next page) N_2O isotopic signatures associated with sources and the lower stratosphere compiled from reported measurements are plotted in relation to the tropospheric composition as measured in this thesis. Note these data points are representative and do not account for all possible signature values from a given source type. a) $\delta^{15}N^{bulk}$ v $\delta^{18}O$. b) $\delta^{15}N^{\alpha}$ v $\delta^{15}N^{\beta}$. c) SP v $\delta^{15}N^{bulk}$.
Ocean: Popp et al 2002, Yamagishi et al 2007, Miyafukuro et al 2008, Naqvi et al 1998, Dore et al 1998, Yoshinari et al 1997; Estuary: Bol et al 2004; River: Toyoda et al 2009; Natural soil: Tilsner et al 2003, Well et al 2005, Perez et al 2000, 2006, Goldberg et al 2010, Kim & Craig 1993, Park et al 2011; Agricultural soil: Yamulki et al 2001, Bol et al 2003, Kim & Craig 1993, Opdyke et al 2009, Ostrom et al 2010, Tilsner et al 2003, Perez et al 2000, 2001, Casciotti et al 1997, Park et al 2011, Rock et al 2007; Car: Toyoda et al 2008; Biomass burning: Ogawa & Yoshida 2005a; Coal: Ogawa & Yoshida 2005b; Landfill: Mandernack et al 2000; Lower stratosphere: Toyoda et al 2004, Park et al 2004

a)

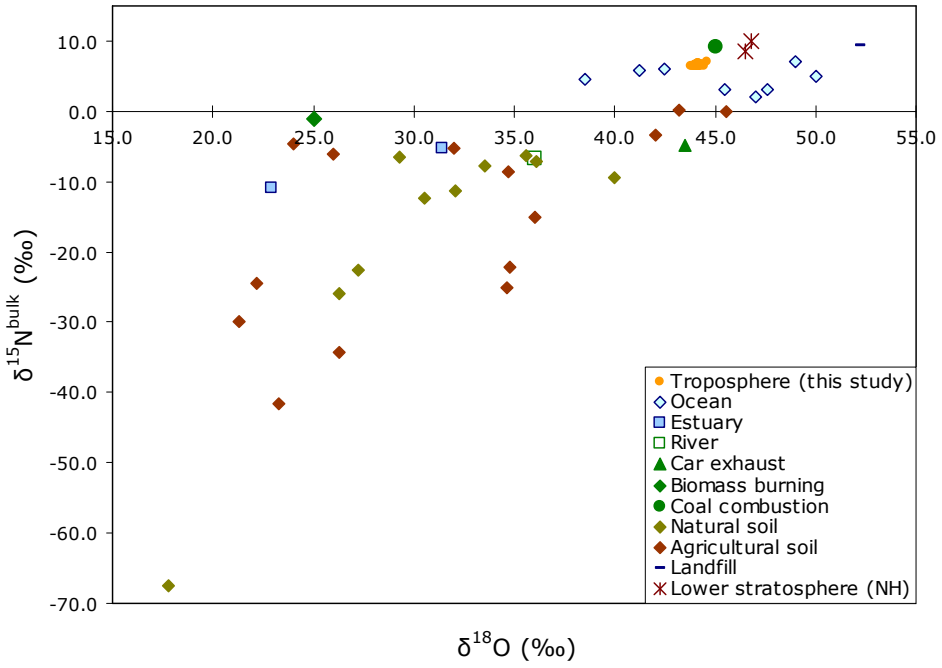
10.0
0.0
-10.0
-20.0
-30.0
-40.0
-50.0
-60.0
-70.0
15.0
20.0
25.0
30.0
35.0
40.0
45.0
50.0
55.0
δ15Nbulk (‰)
δ18O (‰)
Troposphere (this study)
Ocean
Estuary
River
Car exhaust
Biomass burning
Coal combustion
Natural soil
Agricultural soil
Landfill
Lower stratosphere (NH)

b)

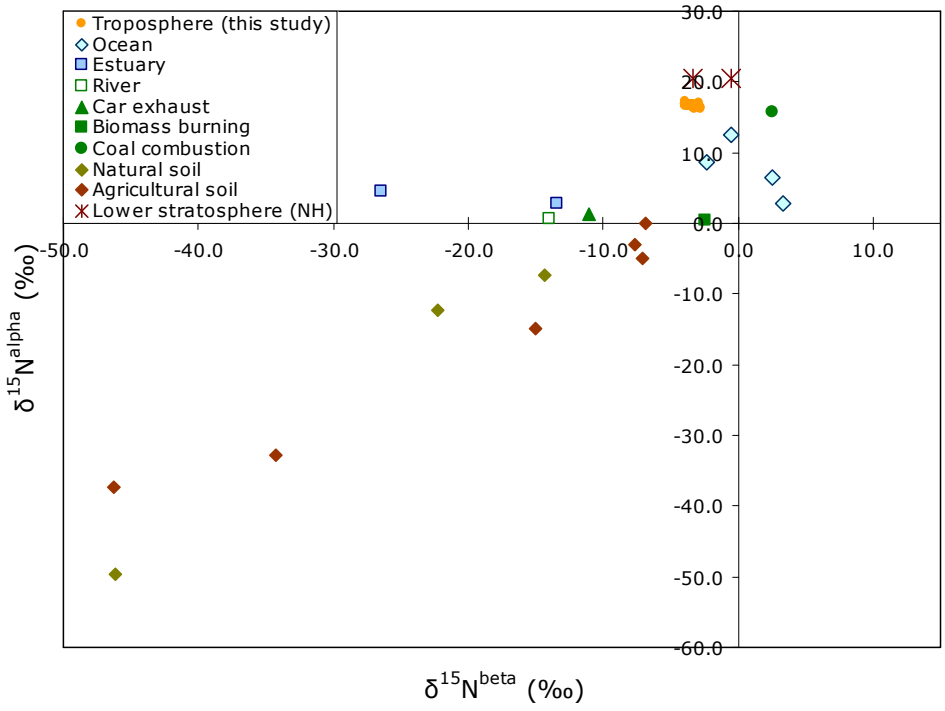
Troposphere (this study)
Ocean
Estuary
River
Car exhaust
Biomass burning
Coal combustion
Natural soil
Agricultural soil
Lower stratosphere (NH)
30.0
20.0
10.0
0.0
-10.0
-20.0
-30.0
-40.0
-50.0
-60.0
-50.0
-40.0
-30.0
-20.0
-10.0
0.0
10.0
δ15Nalpha (‰)
δ15Nbeta (‰)

c)

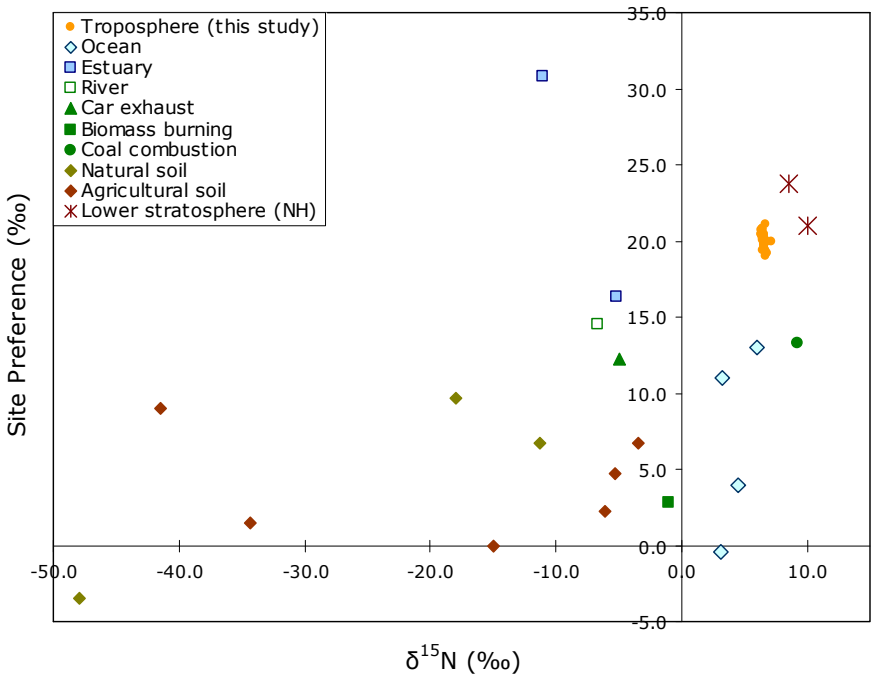

Through the signals generated from changing source and sink influences, the isotopic composition of N_2O in the troposphere has the potential to add new information. However it thus far has been considered an essentially constant value in present-day and only utilized for gross global budget consistency checks (e.g. Yoshida & Matsuo 1983, Kim & Craig 1993, Rahn & Wahlen 2000, Toyoda et al 2002, Rockmann et al 2003, Park et al 2004), limited by insufficient measurement precision to capture the subtle variations and few number of observations. Measurements of tropospheric N_2O isotopic composition are scarce. The most often reported values were collected by Kim and Craig (1993) of $\delta^{15}N^{bulk}$ = 7.0‰ and $\delta^{18}O$ = 44.7‰, and more recently with the improved measurement capabilities to distinguish between the alpha α (central) and beta β (outer) nitrogen positions ($N^{\beta}N^{\alpha}O$) the values by Yoshida & Toyoda (2000), $\delta^{15}N^{bulk}$ = 7.0±0.6‰, $\delta^{18}O$ = 43.7±0.9‰, $\delta^{15}N^{\beta}$ = -2.35‰ and $\delta^{15}N^{\alpha}$ = 16.35‰ ($\delta^{15}N$ referenced to air-N_2, $\delta^{18}O$ referenced to VSMOW). Kaiser et al (2003a) conducted the only focused tropospheric N_2O isotopic composition study with a dataset that spans ~2 years at sites spread throughout Europe and they were unable to discern temporal or spatial patterns related to N_2O processes. However, there was no information about distinguishing background air from regionally polluted air nor attribution of individual collected air samples to specific air mass origins, which is particularly a concern for these European sites surrounded by many regional influences. The study also did not produce a consistent time series of all major isotopologues at a fixed site, which would be important to build a steady characterization of the N_2O regional European influences felt at that location. Early measurements of the bulk nitrogen isotopic composition of N_2O by Yoshida & Matsuo (1983) pointed to the heterogeneity of the N_2O nitrogen isotope in the atmosphere. They made a few measurements of tropospheric air from differing locations and synoptic origins yielding variation greater than experimental uncertainty which were consistent with changing air masses between polar continental and tropical maritime origins.

N_2O has a long atmospheric lifetime of ~120 years which causes its tropospheric mole fraction to have very little variation in response to perturbations, and likewise the isotopic composition will only have subtle, but nevertheless informative, signals. Improved mole fraction measurement techniques and high-frequency in situ observations incorporated into the AGAGE long-term atmospheric monitoring network of globally distributed stations (currently nine plus two affiliated stations) have allowed the detection of a small seasonal cycle (Fraser et al 1997, Prinn et al 2000, Nevison et al 2004). The seasonal mole fraction variation has amplitudes ranging ~0.3 to 0.9 ppb against a background concentration above 320 ppb, only a 0.1 to 0.3% signal. The detection of such a signal has shed significant light on the regionally-varying major sources and stratospheric influence of the N_2O budget (Prinn et al 2000, Nevison et al 2004, Nevison et al 2005, Jiang et al 2007, Nevison et al 2007, Nevison et al 2011). Long term monitoring with high-frequency, high-precision, in situ observations has also allowed for capturing of short-term variability and diagnosis of regional sources (Ryall et al 2001, Manning et al 2011, Corazza et al 2011). The establishment of continuous N_2O isotopic observations, into a long-term global monitoring network would likely similarly create large advances in the understanding of N_2O, particularly with the additional capability to distinguish between N_2O influences.

1.2 Research goals and approach

The increasing presence and important roles of N_2O in the atmosphere propel scientific research to reduce the large uncertainty in the nitrous oxide budget and distinguish between the suggested causes of observed variability in N_2O mole fractions on short, seasonal, and long-term timescales. Such knowledge would aid with assessment of current source emissions, to clarify the cause of N_2O growth as anthropogenic fixed nitrogen input to agriculture and coastal waters, and to assist future projections of this globally impacting gas in the atmosphere. A novel approach is required as methods and data thus far have been insufficient. The stable isotope composition in the troposphere provides information about origin and fate that cannot be determined from mole fraction measurements alone. This thesis work has taken the necessary foundational steps towards realizing continuous in situ, high-frequency, long-term N_2O isotopic composition data. The major aims of this thesis are to:

- Make regular observations of tropospheric air at a remote research station over a full annual cycle and thereby provide a preliminary assessment of N_2O isotope variations in the troposphere on short and seasonal timescales, addressing the questions: Will continuous measurements at remote monitoring stations bring useful information? What are the magnitudes of variation and what level of measurement precision is required to detect such variation? To what N_2O budget uncertainties might isotopic composition in the troposphere be applied- namely, what resolvable, coherent, consistent source-receptor relationships exist in N_2O isotopic composition ?
- Design and construct an instrumentation system with sufficient precision to detect statistically significant signals in tropospheric air samples at a remote research station with high-frequency, fully-automated capabilities, and additionally inform measurement protocol, precision and sampling frequency needed to detect signals, and information regarding isotope referencing practices.
- Design and investigate a regional modeling method for simulation of N_2O isotopic composition centered at a remote research station, enabling a preliminary assessment of the

.

This thesis approaches the aims for the utilization of tropospheric N_2O isotopic composition in a multi-faceted manner.

The assessment of N_2O isotopic composition in the troposphere is conducted through both observations and regional model simulations in the framework of detectable signals in the composition. The isotopic composition of N_2O will have only small variations much like the mole fraction, and the utility of the isotopic data hinges on the measurement precision requirements to detect those variations.

Spanning January 2010 to January 2011, this research produces the first observations of tropospheric N_2O isotopic composition with regular data spanning a full annual cycle at one location. Importantly, these observations are tied to air mass origin information through the use of meteorologically-driven Lagrangian particle dispersion model air history estimates showing the surface influence from the observation backwards in time, as well as the simultaneously collected trace gas measurements and other atmospheric observations. Without such air origin information, potentially useful subtle variation in composition will be interpreted as noise. N_2O isotopic ratios in the troposphere were indeed found to vary within the measurement precision capabilities achieved for this thesis. Variations were consistent with atmospheric mixing processes tied to industrial pollution events, soil source events, and possibly the downflux of stratospheric air reflecting the differing source signatures and impact from downward mixing of stratospheric air, but the low-frequency observations were insufficient to fully interpret these potential source-receptor relationships which will require high-frequency measurements for more accurate interpretation and validation.

The measurement of N_2O isotopic composition is not straightforward, and high-precision instrumentation with fully-automated in situ capabilities was needed to conduct the year-long preliminary assessment time series, and progress towards useful long-term measurements. A pre-concentration device, coined 'Stheno', was designed and constructed for the necessary air sample processing and separation of N_2O from other gases before isotope detection. The ability to assess the isotopic variability in real air samples depends upon the precision and uncertainty in the measurements since it is expected that the modulations will be small in magnitude, and thus Stheno's development incorporated rigorous optimization specifically for N_2O and isotopic measurements. Additionally the measurement of ^{15}N site-specific isotopic composition is challenging and required particular attention for high-precision achievements. For this thesis, Stheno was maintained in the laboratory for initial testing and non-continuous observations interfaced with an isotope ratio mass spectrometer in continuous flow mode (CF-IRMS). Though non-continuous measurements were made, instrumentation design was conducted with the foresight of transitioning to in situ measurements and thus Stheno possesses in situ capabilities: fully-automated, liquid-cryogen-free, durable station-tested temperature controlled housing, and run by shared station instrument software. The precision achieved by Stheno with the CF-IRMS indeed was higher than other reported precisions and additionally included in situ capabilities. Most notably, the site-specific ^{15}N composition is improved by 2-3 fold over the best achieved previously by an online CF-IRMS system (Rockmann et al 2005) and superior to offline IRMS as well (Kaiser et al 2003).

A regional forward model was developed as well to explore the potential information within N_2O isotopic composition. It utilizes the same Lagrangian particle dispersion model air history estimates as paired with the observations along with estimated source signatures to simulate the

influence of regional sources and assess the information contained and potential signal sizes of short-term variation. The model finds coherent relationships between detectable variation and N_2O influences with the precision capabilities achieved in this thesis. The model also includes a simulation of a stratospheric seasonal influence to discern the potential size of this signal in the isotopic composition and the instrumentation precision required. The model furthermore importantly provides a foundation for utilizing these relationships in the future with high-frequency observations, both as a regional forward model to assist in isotopic data interpretation (e.g. Alexander et al 2005), and providing a structure with the air history estimates to utilize the short-term regionally influenced variation for regional N_2O emissions quantification (e.g. Manning et al 2011) and, unique to isotopes, characterization.

The location chosen to focus on for this research is the Mace Head Atmospheric Research Station in Ireland (53.32°N, 9.90°W), a remote research station conducting long-term in situ measurements of trace gases and other atmospheric parameters. On the west coast of Ireland, Mace Head is situated in a particularly useful location for assessing N_2O controls, and thus tropospheric isotopic data from this location will provide vital insight into the N_2O budget and serves well for a preliminary assessment of N_2O isotopic composition in the troposphere. In the higher latitudes of the Northern Hemisphere it receives strong influence from the downwelling of upper stratospheric air into the lower stratosphere and troposphere through stratosphere-troposphere exchange in the Brewer-Dobson circulation. Tropospheric meteorological patterns bring background air from across the Atlantic and Arctic Ocean ~50% of the time and easterly winds from over the UK and Europe ~30-40% of the time. The air originating over soil and anthropogenic sources from Europe will reflect short- and long-term timescale variation in these regional sources, while the oceanic air gives assessment of the background troposphere and is informative of a broader more global picture. Though this thesis does not conduct continuous measurements, the pilot observations with non-continuous measurements and regional modeling ideally would, if found useful, apply where continuous in situ N_2O isotopic measurements would commence. As one of the founding stations of the AGAGE long term atmospheric monitoring network, the Mace Head station is a site with established and well-supported infrastructure to maintain continuous long-term measurements of this important new source of information. N_2O seasonality at Mace Head is characterized by a broad spring (Feb-Apr) maximum and a sharp summer minimum (July-Aug). Studies analyzing mole fraction data collected at Mace Head attribute the August minimum to stratospheric down-welling of low concentration N_2O air during winter/spring and a 3-month delay for propagation of this signal to the surface (Nevison et al 2007, Jiang et al 2007, Nevison et al 2011). Late summer minima in N_2O possibly also reflect seasonal tropospheric transport mechanisms, including seasonal differences in boundary layer height, convection, and interhemispheric transport (Prinn et al 2000, Nevison et al 2007, Jiang et al 2007). Mole fraction data is not informative enough to separately discern the surface source component of the seasonal cycle, but undoubtedly seasonal warming temperatures, changing precipitation, and start of the agricultural season do drive a seasonal soil source impact. These changes in controls on short-, seasonal-, and long- timescales will be reflected in the isotopic composition measured at Mace Head, and the link to distinct signatures will help to tease apart signals in N_2O global and regional budgets and clarify the origins of N_2O variation.

It was from the Mace Head location that this thesis assesses N_2O isotopic composition in the troposphere, through instrumentation development, pilot observations, and regional modeling.

Chapter 1 References

Alexander B, Park RJ, Jacob DJ, Li QB, Yantosca RM, Savarino J, Lee CCW & Thiemens MH (2005). Sulfate formation in sea salt aerosols: Constraints from oxygen isotopes. *J Geophys Res* 110: D10307.

Bateman AS, Kelly SD & Jickells TJ (2005). Nitrogen isotope relationships between crops and fertilizer: implications for using nitrogen isotope analysis as an indicator of agricultural regime. *J Agric Food Chem* 53: 5760-5765.

Berglund M, Wieser ME (2011). Isotopic compositions of the elements 2009 (IUPAC Technical Report). Pure Appl. Chem 83(2): 397-410.

Bol R, Toyoda S, Yamulki S, Hawkins JMB, Cardenas LM & Yoshida N (2003). Dual isotope and isotopomer ratios of N_2O emitted from a temperate grassland soil after fertiliser application. *Rapid Commun Mass Spectrom* 17: 2550-2556.

Bol R, Rockmann T, Blackwell M & Yamulki S (2004). Influence of flooding on $d^{15}N$, $d^{18}O$, $1d^{15}N$ and $2d^{15}N$ signatures of N_2O released from estuarine soils—A laboratory experiment using tidal flooding chambers. *Rapid Commun Mass Spectrom* 18: 1561-1568.

Casciotti K, Rahn T & Wahlen M (1997). Stable isotopes of N and O in nitrous oxide emissions from fertilized soils. *EOS Trans Am Geophys Union* 78: F58 (Fall Meet Suppl).

Casciotti KL (2009). Inverse kinetic isotope fractionation during bacterial nitrite oxidation. *Geochim Cosmochim Acta* 73: 2061-2076.

Corazza M, Bergamaschi P, Vermeulen AT, Aalto T, Haszpra L, Meinhardt F, O'Doherty S, Thompson R, Moncrieff J, Popa E, Steinbacher M, Jordan A, Dlugokencky E, Bruhl C, Krol1 M & Dentener F. Inverse modelling of European N_2O emissions: assimilating observations from different networks. *Atmos Chem Phys* 11: 2381-2398.

Davidson EA, Keller M, Erickson HE, Verchot LV & Veldkamp E (2000). Testing a conceptual model of soil emissions of nitrous and nitric oxides. *BioScience* 50: 667–680.

Davidson EA. (2009) The contribution of manure and fertilizer nitrogen to atmospheric nitrous oxide since 1860. *Nature Geoscience* 2: 659-662.

Dobbie KE, McTaggart IP & Smith KA (1999). Nitrous oxide emissions from intensive agricultural systems: variations between crops and seasons, key driving variables, and mean emission factors. J Geophys Res 104: 26891-26899.

Dore JE, Popp BN, Karl DM & Sansone FJ (1998). A large source of atmospheric nitrous oxide from subtropical North Pacific surface waters. *Nature* 396: 63-66.

Firestone MK & Davidson EA. Microbiological basis of NO and nitrous oxide production and consumption in soil. *In* Exchange of Trace Gases between Terrestrial Ecosystems and the Atmosphere, Andreae MO & Schimel DS, editors, John Wiley & Sons, New York, 1989, pp. 7-21.

Fraser PJ, Steele P, Derek N, Porter L & Sturrock G. Halocarbons, nitrous oxide, methane, carbon monoxide and hydrogen-- The AGAGE program, 1993-1996. *In* Baseline 1996, Gras J *et al.*, editors. Bur Meteorol, CSIRO, Melbourne, Victoria, Australia, 1997, pp. 111-120.

Goldberg SD, Borken W & Gebauer G (2010). N_2O emission in a Norway spruce forest due to soil frost: concentration and isotope profiles shed a new light on an old story. *Biogeochemistry* 97: 21-30.

Griffith DWT, Toon GC, Sen B, Blavier J-F & Toth RA (2000). Vertical profiles of nitrous oxide isotopomer fractionation measured in the stratosphere. *Geophys Res Lett* 27: 2485-2488.

Hirsch AI, Michalak AM, Bruhwiler LM, Peters W, Dlugokencky EJ & Coauthors (2006). Inverse modeling estimates of the global nitrous oxide surface flux from 1998-2001. *Global Biogeochem Cycles* 20: GB1008.

Huang J, Golombek A, Prinn R, Weiss R, Fraser P, Simmonds P, Dlugokencky EJ, Hall B, Elkins J, Steele P, Langenfelds R, Krummel P, Dutton G & Porter L (2008). Estimation of regional emissions of nitrous oxide from 1997 to 2005 using multi-network measurements, a chemical transport model, and a Kalman Filter. *J Geophys Res* 113: D17313.

Denman KL, Brasseur G, Chidthaisong A, Ciais P, Cox PM, Dickinson RE, Hauglustaine D, Heinze C, Holland E, Jacob D, Lohmann U, Ramachandran S, da Silva Dias PL, Wofsy SC & Zhang X (2007). Couplings Between Changes in the Climate System and Biogeochemistry. *In*: Climate Change 2007: The Physical Science Basis. Contribution of Working Group I to the Fourth Assessment Report of the Intergovernmental Panel on Climate Change [Solomon, S., D. Qin, M. Manning, Z. Chen, M. Marquis, K.B. Averyt, M.Tignor and H.L. Miller (eds.)]. Cambridge University Press, Cambridge, United Kingdom and New York, NY, USA.

Jiang X, Ku WL, Shia R-L, Li Q, Elkins JW, Prinn RG & Yung YL (2007). Seasonal cycle of N_2O: Analysis of data. *Global Biogeochem Cycles* 21: GB1006.

Johnson MS, Billing GD, Gruodis A & Janssen MHM (2001). Photolysis of nitrous oxide isotopomers studied by time-dependent hermite propagation. *J Phys Chem A* 105: 8672-8680.

Kaiser J, Brenninkmeijer CAM & Rockmann T (2002a). Intramolecular ^{15}N and ^{18}O fractionation in the reaction of N_2O with $O(^1D)$ and its implications for the stratospheric N_2O isotope signature. *J Geophys Res* 107 (D14): 4214.

Kaiser J, Rockmann T & Brenninkmeijer CAM (2002b). Temperature dependence of isotope fractionation in N_2O photolysis. *Physical Chemistry Chemical Physics* 4 (18): 4220-4230.

Kaiser J, Rockmann T & Brenninkmeijer CAM (2003a). Complete and accurate mass-spectrometric isotope analysis of tropospheric nitrous oxide. *J Geophys Res* 108 (D15): 4476.

Kaiser J, Rockmann T, Brenninkmeijer CAM & Crutzen PJ (2003b). Wavelength dependence of isotope fractionation in N_2O photolysis. *Atmos Chem Phys* 3: 303-313.

Kaiser J, Engel A, Borchers R & Rockmann T (2006). Probing stratospheric transport and chemistry with new balloon and aircraft observations of the meridional and vertical N_2O isotope distribution. *Atmospheric Chemistry and Physics* 6: 3535-3556.

Keller M, Varner R, Dias JD, Silva H, Crill P, Oliveira Jr RC & Asner GP (2005). Soil atmosphere exchange of nitrous oxide, nitric oxide, methane, and carbon dioxide in logged and undisturbed forest in the Tapajos National Forest, Brazil. *Earth Interact* 9: 1-28.

Kim K-R & Craig H (1993). Nitrogen-15 and oxygen-18 characteristics of nitrous oxide: A global perspective. *Science* 262: 1855-1857.

Kool DM, Wrage N, Oenema O, Harris D & van Groenigen JW (2009). The ^{18}O signature of biogenic nitrous oxide is determined by O exchange with water, *Rapid Commun Mass Spectrom* 23: 104-108.

Kroeze C, Mosier AR & Bouwman L (1999). Closing the global N_2O budget: a retrospective analysis 1500-1994. *Global Biogeochemical Cycles* 13: 1-8.

Mandernack KW, Rahn T, Kinney C & Wahlen M (2000). The biogeochemical controls of the $\delta^{15}N$ and $\delta^{18}0$ of N^2O produced in landfill cover soils. *J Geophys Res* 105(D14): 17709-17720.

Manning AJ, O'Doherty S, Jones AR, Simmonds PG & Derwent RG (2011). Estimating UK methane and nitrous oxide emissions from 1990 to 2007 using an inversion modeling approach. *J Geophys Res* 116: D02305.

McLinden CA, Prather MJ & Johnson MS (2003). Global modeling of the isotopic analogues of N_2O: Stratospheric distributions, budgets, and the ^{17}O-^{18}O mass-independent anomaly. *J Geophys Res* 108(D8): 4233.

Miyafukuro T, Toyoda S & Yoshida N (2008). Isotopomer analysis of N_2O dynamics in the eastern North Pacific Ocean, 4th International Symposium on Isotopomers, 4th International Symposium on Isotopomers proceedings, ISI2008 Science Committee, pp. 199-201.

Miller CE & Yung YL (2000). Photo-induced isotopic fractionation. *J Geophys Res* 105: 29039-29051.

Morgan CG, Allen M, Liang MC, Shia RL, Blake GA & Yung YL (2004). Isotopic fractionation of nitrous oxide in the stratosphere: Comparison between model and observations. *J Geophys Res* 109: D04305.

Naqvi SWA, Yoshinari T, Jayakumar DA, Altabet MA, Narvekar PV, Devol AH, Brandes JA & Codispoti LA (1998). Budgetary and biogeochemical implications of N_2O isotope signatures

in the Arabian Sea. *Nature* 394: 462-464.

Nevison CD, Kinnison DE & Weiss RF (2004). Stratospheric influence on the tropospheric seasonal cycles of nitrous oxide and chlorofluorocarbons. *Geophys Res Lett* 31: L20103.

Nevison CD, Keeling RF, Weiss RF, Popp BN, Jin X, Fraser PJ, Porter LW & Hess PG (2005). Southern Ocean ventilation inferred from seasonal cycles of atmospheric N_2O and O_2/N_2 at Cape Grim, Tasmania. *Tellus Ser. B* 57: 218-229.

Nevison CD, Mahowald NM, Weiss RF & Prinn RG (2007). Interannual and seasonal variability in atmospheric N_2O. *Global Biogeochem Cycles* 21: GB3017.

Nevison CD, Dlugokencky E, Dutton G, Elkins JW, Fraser P, Hall B, Krummel PB & Langenfelds RL (2011). Exploring causes of interannual variability in the seasonal cycles of tropospheric nitrous oxide. *Atmos Chem Phys* 11: 3713-3730.

Ogawa M & Yoshida N (2003). Isotopomer analysis of nitrous oxide emitted from burning of agricultural residue. Goldschmidt Conference Abstracts.

Ogawa M & Yoshida N (2005a). Nitrous oxide emission from the burning of agricultural residue. *Atmospheric Environment* 39: 3421-3429.

Ogawa M & Yoshida N (2005b). Intramolecular distribution of stable nitrogen and oxygen isotopes of nitrous oxide emitted during coal combustion. *Chemosphere* 61: 877-887.

Opdyke MR, Ostrom NE & Ostrom PH (2009). Evidence for the predominance of denitrification as a source of N_2O in temperate agricultural soils based on isotopologue measurements. *Global Biogeochem Cycles* 23: GB4018.

Ostrom NE, Pitt A, Sutka R, Ostrom PH, Grandy As, Huizinga KM, Robertson GP (2007). Isotopologue effects during N_2O reduction in soils and in pure cultures of denitrifiers. *J Geophys Res* 112: G02005.

Ostrom NE, Pitt A, Sutka RL, Ostrom PH, Grandy AS, Huizinga KM, Gandhi H, von Fischer JC & Robertson GP (2010). Isotopologue data reveal bacterial denitrification as the primary source of N_2O during a high flux event following cultivation of a native temperate grassland. *Soil Biology and Biochemistry* 42: 499-506.

Park SY, Atlas EL, Boering KA (2004). Measurements of N_2O isotopologues in the stratosphere: Influence of transport on the apparent enrichment factors and the isotopologue fluxes to the troposphere, *J Geophys Res* 109: 462-464.

Park S, Perez T, Boering KA, Trumbore SE, Gil J, Marquina S & Tyler SC (2011). Can N_2O stable isotopes and isotopomers be useful tools to characterize sources and microbial pathways of N_2O production and consumption in tropical soils? *Global Biogeochem Cycles* 25: GB1001.

Perez T, Trumbore SE, Tyler SC, Davidson EA, Keller M & DeCarmargo PB (2000). Isotopic variability of N_2O emissions from tropical forest soils. *Global Biogeochem Cycles* 14: 525-535.

Perez T, Trumbore SE, Tyler SC, Matson PA, Ortiz-Monasterio I, Rahn T & DWT Griffith (2001). Identifying the agricultural imprint on the global N_2O budget using stable isotopes. *J Geophys Res* 106: 9869-9878.

Perez T, Garcia-Montiel D, Trumbore S, Tyler S, De Camargo P, Moreira M & Piccolo M & Cerri C (2006). Nitrous oxide nitrification and denitrification N-15 enrichment factors from Amazon forest soils. *Ecological Applications* 16: 2153-2167.

Popp BN, Westley MB, Toyoda S, Miwa T, Dore JE & coauthors (2002). Nitrogen and oxygen isotopomeric constraints on the origins and sea-to-air flux of N_2O in the oligotrophic subtropical North Pacific gyre. *Global Biogeochem Cycles* 16: doi:2001GB001806.

Prinn, R *et al.* (2000). A history of chemically and radiatively important gases in air deducted from ALE/GAGE/AGAGE. *J Geophys Res* 105: 17751-17792.

Rahn T & Wahlen M (2000). A reassessment of the global isotopic budget of atmospheric nitrous oxide. *Global Biogeochem Cycles* 14: 537-543.

Rahn T, Zang H, Wahlen M & Blake GA (1998). Stable isotope fractionation during ultraviolet photolysis of N_2O. *Geophys Res Lett* 25: 4489-4492.

Ravishankara AR, Daniel JS & Portmann RW (2009). Nitrous oxide (N_2O): the dominant ozone-depleting substance emitted in the 21st Century. *Science* 326: 123-125.

Rock L, Ellert BH, Mayer B & Norman AL (2007). Isotopic composition of tropospheric and soil N_2O from successive depths of agricultural plots with contrasting crops and nitrogen amendments. *J Geophys Res* 112: D18303.

Rockmann T, Brenninkmeijer CAM, Wollenhaupt M, Crowley JN & Crutzen PJ (2000). Measurement of the isotopic fractionation of $^{15}N^{14}N^{16}O$, $^{14}N^{15}N^{16}O$ and $^{14}N^{14}N^{18}O$ in the UV photolysis of nitrous oxide. *Geophys Res Lett* 27: 1399-1402.

Rockmann T, Kaiser J, Brenninkmeijer CAM, Crowley J, Borchers R, Brand W & Crutzen P (2001). Isotopic enrichment of nitrous oxide ($^{15}N^{14}NO$, $^{14}N^{15}NO$, $^{14}N^{14}N^{18}O$) in the stratosphere and in the laboratory. *J Geophys Res* 106: 10403.

Rockmann T, Kaiser J & Brennickmeijer CAM (2003b). The isotopic fingerprint of the pre-industrial and the anthropogenic N_2O source. *Atmospheric Chemistry and Physics* 3: 315-323.

Ryall DB, Derwent RG, Manning AJ, Simmonds PG & O'Doherty S (2001). Estimating source regions of European emissions of trace gases from observations at Mace Head. *Atmos Environ* 35(14): 2507-2523.

Snider DM, Schiff SL & Spoelstra J (2009). $^{15}N/^{14}N$ and $^{18}O/^{16}O$ stable isotope ratios of nitrous oxide produced during denitrification in temperate forest soils. *Geochimica et Cosmochimica Acta* 73: 877-888.

Sowers T, Rodebaugh A, Yoshida N & Toyoda S (2002). Extending records of the isotopic composition of atmospheric N_2O back to 1800 A.D. from air trapped in snow at the South Pole and the Greenland Ice Sheet Project II ice core. *Global Biogeochemical Cycles* 16(4): 0886-6236.

Stein L & Yung Y (2003). Production, isotopic composition, and atmospheric fate of biologically produced nitrous oxide. *Ann Rev Earth Planetary Sci* 31: 329-356.

Sutka RL, Ostrom NE, Ostrom PH, Breznak JA, Gandhi H, Pitt AJ & Li F (2006). Distinguishing nitrous oxide production from nitrification, and denitrification on the basis of isotopomer abundances. *Appl Exp Microbiol* 72: 638-644.

Tilsner J, Wrage N, Lauf J & Gebauer G (2003). Emission of gaseous nitrogen oxides from an extensively managed grassland in NE Bavaria, Germany: II. Stable isotope natural abundance of N_2O. *Biogeochemistry* 63: 249-267.

Toyoda S, Yoshida N, Urabe T, Aoki S, Nakazawa T, Sugawara S & Honda H (2001). Fractionation of N_2O isotopomers in the stratosphere. *J Geophys Res* 106: 7515-7522.

Toyoda S, Yoshida N, Miwa T, Matsui Y, Yamagishi H, Tsunogai U, Nojiri Y & Tsurushima N (2002). Production mechanism and global budget of N_2O inferred from its isotopomers in the western North Pacific. *Geophys Res Lett* 29(3): 1037.

Toyoda S *et al.* (2004). Temporal and latitudinal distributions of stratospheric N_2O isotopomers. *J Geophys Res* 109: D08308.

Toyoda S, Mutobe H, Yamagishi H, Yoshida N & Tanji Y (2005). Fractionation of N_2O isotopomers during production by denitrifier. *Soil Biology and Biochemistry* 37(8): 1535-1545.

Toyoda S, Yamamoto S, Arai S, Nara H, Yoshida N, Kashiwakura K & Akiyama K (2008). Isotopomeric characterization of N_2O produced, consumed, and emitted by automobiles. *Rapid Commun Mass Spectrom* 22: 603-612.

Toyoda S, Iwai H, Koba K & Yoshida N (2009). Isotopomeric analysis of N_2O dissolved in a river in the Tokyo metropolitan area. *Rapid Commun Mass Spectrom* 23: 809-821.

Toyoda S *et al.* (2011). Characterization and production and consumption processes of N_2O emitted from temperate agricultural soils determined via isotopomer ratio analysis. *Global Biogeochem Cycles* 25: GB2008.

Turatti F, Griffith DWT, Wilson SR, Esler MB, Rahn T, *et al.* (2000). Positionally dependent ^{15}N factors in the UV photolysis of N_2O determined by high resolution FTIR spectroscopy. *Geophys Res Lett* 27: 2489-92.

Umemoto H (1999). N-14/N-15 isotope effect in the UV photodissociation of N_2O. *Chem. Phys. Lett.* 314: 267272.

Wahlen M & Yoshinari T (1985). Oxygen isotope ratios in N_2O from different environments, *Nature* 313: 780-782.

Well R, Flessa H, Jaradat F, Toyoda S & Yoshida N (2005). Measurement of isotopomer signatures of N_2O in groundwater. *J Geophys Res* 110: G02006.

Well R & Flessa H (2009). Isotopologue signatures of N_2O produced by denitrification in soils, *J Geophys Res* 114: G02020.

Yamagishi H, Westley MB, Popp BN, Toyoda S, Yoshida N, Watanabe S, Koba K & Yamanaka Y (2007). Role of nitrification and denitrification on the nitrous oxide cycle in the eastern tropical North Pacific and Gulf of California. *J Geophys Res - Biogeosci* 112: G02015.

Yamulki S, Toyoda S, Yoshida N, Veldkamp E, Grant B & Bol R (2001). Diurnal fluxes and the isotopomer ratios of N_2O in a temperate grassland following urine amendment. *Rapid Commun Mass Spectrom* 15: 1263-1269.

Yoshida N & Matsuo S (1983). Nitrogen isotope ratio of atmospheric N_2O as a key to the global cycle of N_2O. *Geochemical Journal* 17: 231-239.

Yoshida N & Toyoda S (2000). Constraining the atmospheric N_2O budget from intramolecular site preference in N_2O isotopomers. *Nature* 405: 330–334.

Yoshinari T, Altabet MA, Naqvi SWA, Codispoti L, Jayakumar A, *et al.* (1997). Nitrogen and oxygen isotopic compositions of N_2O from suboxic waters of the eastern tropical North Pacific and the Arabian Sea-- Measurement by continuous-flow isotope ratio monitoring. *Mar Chem* 56: 253-264.

Yung YL, Miller CE. 1997. Isotopic fraction- ation of stratospheric nitrous oxide. *Science* 278:1778–80.

Zhang H, Wennberg PO, Wu VH & Blake GA (2000). Fractionation of $^{14}N^{15}N^{16}O$ and $^{15}N^{14}N^{16}O$ during photolysis at 213nm. *Geophys Res Lett* 27: 2481-2484.

Chapter 2: Isotopic analysis of N_2O

This chapter will describe the various instrumentation and measurement development and procedures used in this study of N_2O isotopic composition in the troposphere. Monitoring N_2O isotopic composition in the troposphere is not simple. Variation in N_2O isotopic composition in the troposphere is expected to be subtle and for observations to be useful for science requires high-precision instrumentation, and ideally with high-frequency observations capabilities in order for proper interpretation of any detected variation. N_2O isotopic measurement itself is difficult: N_2O rare isotopologues are present at sub- ppb levels this necessitating pre-concentration, and the measurement of site-specific ^{15}N composition is not straightforward and notoriously difficult. Therefore, advancement of N_2O isotopic measurement capabilities was needed to enable useful observations for advancement of atmospheric N_2O research, and was conducted here with the design and construction of a system with sufficient precision to detect and interpret isotopic signals at a remote atmospheric research station with high-frequency, fully-automated capabilities, as no established method previously existed.

Foremost for this instrumental work, Part I is the design, development, and assessment of the 'Stheno' pre-concentration system for use with continuous flow isotope ratio mass spectrometry for measurements of N_2O isotopic composition in tropospheric air, which serves as the heart of the instrumentation for the isotopic measurement of N_2O and of the instrumental work for this thesis. Part II provides details of IRMS analytical methods and configuration for both continuous flow and traditional dual inlet analyses applicable to this work. Calibration of N_2O requires specific attention because no international standard procedure yet exists in terms of $^{15}N^{\alpha}$ and $^{15}N^{\beta}$ site-specific isotopomer calibration. Part III details experimental verification of the commonly accepted calibration. The further work on calibration conducted in close collaboration with Dr. N. Yoshida's laboratory at the Tokyo Institute of Technology is in progress and will not be included in this thesis.

Part I. Optimized fully automated pre-concentration system for the isotopic analyses of tropospheric nitrous oxide by continuous flow isotope ratio mass spectrometry

Introduction

As a long-lived, well-mixed gas, variation in N_2O mole fraction as well as isotopic composition in the troposphere is subtle. With the improvement of measurement precision and high-frequency observations for N_2O mole fraction, since around 1994 a discernable seasonal cycle has emerged, currently with an amplitude ~0.3 to 0.9 ppb atop the ~320 ppb mean, as well as useful short-term variability (Fraser et al 1997, Prinn et al 2000, Nevison et al 2004, Nevison et al 2011). These mole fraction data have been analyzed and modeled, but have seemingly reached the limit of information which can be extracted from whole N_2O observations about the N_2O budget (Hirsch et al 2006, Huang et al 2008). Isotopic composition in the troposphere lends additional information about N_2O tied to the specific signatures and fractionation associated with atmospheric N_2O sources, sinks, and other influences. Despite this promised utility, measurements of tropospheric N_2O isotopic composition are scarce. N_2O isotopic composition in the troposphere has been regarded by many as an essentially constant present-day value due to limitations of measurement precision and low-frequency of observations. As measurement techniques progress and precision improves, and with the advent of in situ high-frequency measurements, the slight variations in the tropospheric isotopic composition are indeed discernable and hold valuable information about the controlling processes of atmospheric N_2O.

For stable isotopic analysis of N_2O here considered are the rare mono-substituted ^{18}O and ^{15}N isotopologue ratios. Nitrous oxide is an asymmetric molecule (N-N-O) such that the two N atoms are distinct, and referred to as beta β and alpha α, $N^{\beta}N^{\alpha}O$. With the only recent advent of new measurement techniques to allow N position specific isotope ratio analysis (isotopomer analysis), the N_2O isotopomer ratios present a unique opportunity to investigate an additional set of parameters beyond the $\delta^{15}N^{bulk}$ value. Even though the molecular masses are identical, the fractionation for the two ^{15}N isotopomers, $^{14}N^{15}NO$ and $^{15}N^{14}NO$, can be distinct as a function of reaction mechanism and precursor source compositions.

Isotope ratios of a sample for the ^{18}O and site-specific ^{15}N rare isotopologues in relation to the abundant $^{14}N^{14}N^{16}O$ are reported relative to atmospheric N_2 and VSMOW (Vienna Standard Mean Ocean Water) standards using delta notation (δ), and are reported in units of per mil (‰). Values are reported as $\delta^{15}N^{\alpha}$, $\delta^{15}N^{\beta}$, $\delta^{18}O$, and the derived average $\delta^{15}N^{bulk}$ and site preference (SP = $\delta^{15}N^{\alpha} - \delta^{15}N^{\beta}$).

$$^{15}R^{\alpha} = [^{14}N^{15}NO] / [^{14}N^{14}NO]$$
$$^{15}R^{\beta} = [^{15}N^{14}NO] / [^{14}N^{14}NO]$$
$$^{18}R = [NN^{18}O] / [NN^{16}O]$$

$$\delta^{15}N^{i} = [((^{15}N/^{14}N)_{sample} - (^{15}N/^{14}N)_{N2}) / (^{15}N/^{14}N)_{N2}]$$
$$= (^{15}R^{i}_{N2O}/^{15}R_{N2}) - 1$$

$$\delta^{18}O = [((^{18}O/^{16}O)_{sample} - (^{18}O/^{16}O)_{VSMOW}) / (^{18}O/^{16}O)_{VSMOW}]$$
$$= (^{18}R_{N2O}/^{18}R_{VSMOW}) - 1$$

Current methods for measurement of N_2O isotopic composition seem often to be inadequate to extract useful variation in the troposphere due to insufficient precision and/or low-frequency capabilities. With N_2O only at ppb levels and the presence of many interfering molecules in ambient air, current technology necessitates that air samples be processed to pre-concentrate and purify the N_2O regardless of isotope detector. Early measurements of the N_2O bulk isotopic composition (Yoshida & Matsuo 1983, Kim & Craig 1990, Cliff & Thiemens 1994, Tanaka et al 1995) has certainly moved toward better precision, and later ^{15}N site-specific analysis (Toyoda & Yoshida 1999, Brenninkmeijer & Rockmann 1999). Kaiser et al (2003) developed an offline pre-concentration system for measurement of N_2O by standard dual inlet IRMS and reported possibly the highest precision for atmospheric samples thus far. However, the offline dual inlet analysis requires μmol quantities of N_2O and thus requiring approximately 400 dm^3 STP of air sample with elaborate sampling techniques, which makes high-frequency observations impractical. Similarly, N_2O isotopic measurements using optical FTIR detection requires μmol quantities of N_2O (Turatti 2001) equivalent to hundred of liters of tropospheric air and is impractical for high-frequency measurements.

Isotope ratio mass spectrometry in continuous flow mode (CF-IRMS) has the benefit of only requiring nanomole quantities of sample thus making relatively high-frequency analysis of the low concentration N_2O in tropospheric air feasible. Manual pre-concentration units for N_2O isotopic analysis by CF-IRMS pioneered the field (Yoshida & Toyoda 2000), however manual operation limits consistent precision and high-frequency in situ measurements. Several off-the-shelf trace gas pre-concentration units exist (e.g. Thermofinnigan Gas Bench/PreCon (Brand 1995), GV instruments Trace Gas) which other groups commonly have used with an IRMS for atmospheric isotopic analysis (e.g. Coplen et al 2004, Schnyder et al 2004, Fisher et al 2006) and specifically for N_2O isotopic studies (e.g. Rockmann et al 2003, Park et al 2004, Rockmann et al 2005, Kaiser et al 2006, Croteau et al 2010). However these devices have a universal design for trace gas applications and thus are not optimized for N_2O isotopic measurements and lack the degree of precision required for comprehensive studies of N_2O isotopic composition in the troposphere.

Additionally, though many of the above mentioned systems are automated in most of the device, all of the pre-concentration systems rely upon liquid cryogen cold traps which greatly hinders the ability for in situ long-term high-frequency measurements.

Optical laser-based detectors based upon infrared absorption properties of the different isotopologues holds promise for both high-precision and high-frequency observations. Presently two groups of note are progressing this technology by quantum cascade laser (Empa, Dubendorf, Switzerland, Mohn et al 2008, 2009; MIT/Aerodyne Research Inc, Cambridge, USA), but both the optical shelf and pre-concentration device components of the instruments are still in development.

This work seeks to create a pre-concentration system specifically tailored to the needs of N_2O separation, with considerable attention to avoiding isotope fractionation during processing and other specific N_2O measurement concerns. The pre-concentration device developed in this thesis, coined 'Stheno', marks the first utilization of fully automated liquid-cryogen-free technology from the 'Medusa' system (Miller et al 2008) of the AGAGE in situ observation network for use with isotopic analysis and coupled with an isotopic ratio mass spectrometer. In this work Stheno is interfaced with a continuous flow IRMS system (Stheno+CF-IRMS), but Stheno is designed to allow future application with other detector options. This system pushes the limits of precision for N_2O isotopic analysis by CF-IRMS technology, while also paving the way for N_2O-tailored pre-concentration methodology for use with other detectors (e.g. laser-based optical methods) and with fully automated liquid-cryogen-free technology to make high-frequency in situ observations feasible for the first time. The optimized design of Stheno+CF-IRMS results in precisions markedly

superior to all other systems for site-specific ^{15}N composition, improved by 2-3 fold over the best achieved previously by an online CF-IRMS systems and superior to offline IRMS as well, and one of the best bulk ^{15}N and ^{18}O precisions. Stheno is thus created to make high-precision measurements capable of detecting isotopic signals in tropospheric air at a remote research station with high-frequency observation capabilities to enable useful measurements for science.

2.1 Stheno+CF-IRMS pre-concentration system

2.1.1 Overview

The Stheno pre-concentration unit used here was custom designed and built for the separation and pre-concentration of N_2O in tropospheric air samples. The current sample measurement system is composed of: the sample inlet manifold, Stheno N_2O pre-concentration/purification system with gas chromatograph (GC), open split interface, and continuous flow isotope ratio mass spectrometer (CF-IRMS). This system places Stheno in the laboratory for initial design, testing, and 1-year of pilot study observations with flask air samples. The Stheno unit is designed, however, with fully automated capabilities and flexible sample inlet design so that with no modifications it can be deployed for in situ measurements.

The optimized system utilizes the liquid-cryogen-free refrigeration unit (Cryotiger, Polycold Division of Brooks Automation, Petaluma, CA) and cryo-trap mounting of the AGAGE Medusa system, a recently developed system for the measurement of atmospheric halocarbon species (Miller et al 2008). Automated control and monitoring of the pre-concentration system devices are with the Medusa system software, GCWerks, and valve numbers in the diagram (V1, V2, V5, V6) refer to the mirrored multi-port valves in the Medusa system for consistency, but this modified system for N_2O eliminating two of the valves. Helium carrier gas flow control is likewise regulated by electronic pressure control devices (EPC) from the gas chromatograph (Agilent 6890). The traps precisely independently controlled temperatures from ~-165 °C to 100 °C, structural design, and mounting to the Cryotiger cold-end use Medusa configuration, but with different packing material (DMCS-treated glass beads instead of HayeSepD). Utilizing the Medusa core technology, the Stheno pre-concentration system is uniquely optimized for N_2O, and specifically for isotopic analysis.

The final design and flow of the system for analysis of air samples by Stheno+CF-IRMS includes the Stheno pre-concentration system, open split and continuous flow interface, and IRMS analysis sequence and referencing for continuous flow air samples. A number of challenges exist in the measurement of tropospheric N_2O isotopes. Specific design measures which uniquely optimize this system for those needs will be highlighted. To assess the instrument and design aiming for the highest precision possible by IRMS detector technology, one-year time series of flask measurements of tropospheric air was conducted. The final section will present the results of the optimized system and precision achieved.

2.1.2 Stheno automated pre-concentration system design and air sample flow

Air sampling analysis on Stheno (flow diagram Figure 2.1, instrumental parameters sequence Figure 2.2) begins with a 150 second 50 ml/min sweep of the sampling line, chemical traps, and Nafion dryer with the air sample while the first cryotrap (T1) is flushed with helium, controlled by a mass flow controller (MFC) (Red-Y Smart Controller GSC, Voegtlin Instruments AG). Approximately 420 ml STP of air sample is introduced to the temperature-stabilized all stainless steel system via one of six possible inlet ports at 30 ml/min controlled by the MFC. The housing of the majority of Stheno valves and tubing is temperature-stabilized (30 °C), as designated by the dotted

outline in Figure 2.1. A diaphragm pump (Barnant AirCadet) downstream of the mass flow controller assists maintaining a pressure differential across the MFC and steady flow regardless of any potential upstream pressure transients. The pump also ensures pressures remain below atmospheric pressure in T1, thus preventing possible condensation of oxygen (vapor pressure ~5 bar at -165 °C). The sample size of 420 ml STP and 30 ml/min flow rate of tropospheric air was optimized with a balance between trapping capacity, lessening time required for sample extraction, and optimizing the amount of pre-concentrated N_2O to maximize measurement precision.

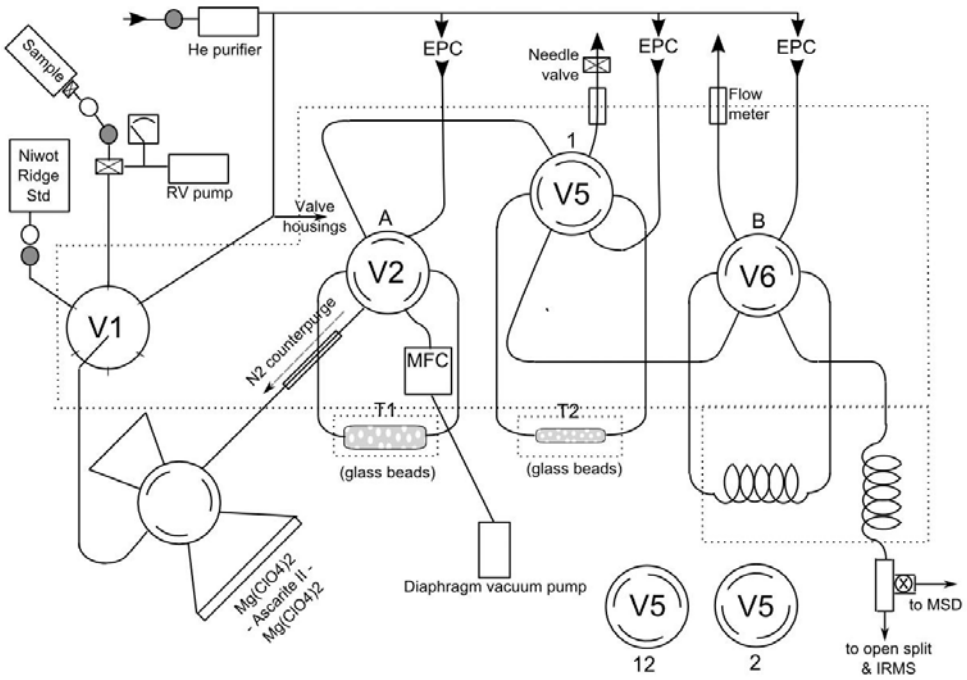

Figure 2.1 Diagram of Stheno flow scheme as described in the text. Dotted boxes encase separate temperature-controlled sections: Stheno housing at 30 °C, T1 from -165 to 100°C, T2 from -165 to 100 °C, and gas chromatograph oven. Positions for multi-position valve 5 with elongated grooves are isolated (1), load (12), backflush inject (2). V1, V2, V5, V6: multi-port valves; MFC: mass flow controller; EPC: electronic pressure controller; T1, T2: cryotraps; MSD: quadrupole mass spectrometer detector; IRMS: isotope ratio mass spectrometer.

Interference by CO_2 poses a particular challenge since at atmospheric concentrations there is ~1000 times more CO_2 than N_2O, for IRMS analysis its molecular ion is as the same m/z 44, 45, 46 masses as N_2O, it has a similar vapor pressure as N_2O so that trapping temperatures and GC elution times are similar, and for optical analysis it also absorbs infrared at similar wavelengths. The air first passes through a series of chemical absorbent traps of $Mg(ClO_4)_2$, Ascarite II, and again $Mg(ClO_4)_2$, for removal of water, CO_2, and water, respectively. Approximately >99.99% of the CO_2 is removed. These chemical traps are made with 9 mmID glass tubes connected using Swagelok nylon ferrules avoiding potentially off-gassing fluorocarbon materials (section 2.2), and configured into the sample flow path with a manual 6-port valve to allow bypassing the traps during chemical replacement without exposing the system to ambient air. The air is further dried through a Nafion membrane (Permapure, Inc.) with N_2 gas counterpurge flow before reaching a cooled stainless steel trap (T1) (1.60 mmID, 76.8 cm) with DMCS-treated glass beads (Alltech, 100/120 mesh, 660 mg/21.50 cm packing) held at -160 °C to trap N_2O and other remaining condensable gases.

A multi-port valve (Valco Instrument Company Inc) with helium purged housing switches the cooled trap inline with helium carrier gas flow and T1 is briefly flushed for 20 s with He to further remove bulk air (N_2,O_2) to vent monitored for trap system errors with a flow meter. During system development this vented fraction was captured and analyzed by quadrupole mass spectrometer (Agilent 5973) to ensure that no N_2O analyte was being lost past T1. Electronic pressure controllers direct all analytical He carrier gas (Ultra High Purity, >99.999%, Airgas). Prior to entering the Stheno system, the ultra high purity helium passes through a 12-micron particle filter (3B Filters, Inc), hydrocarbon trap (Supelco 24449), and high capacity water and oxygen trap (Supelco 23802). Immediately adjacent to the system, He carrier gas is controlled at ~50 psi with a high purity regulator (Tescom, 64-2600 series) equipped with Vespel seat to avoid fluorocarbon contamination and passes through a VICI Helium Purifier with heated getter alloy chemisorbing all non-noble gases.

After flushing T1, another purged housing Valco multi-port valve switches T1 inline with a second small volume cryo-focusing stainless steel trap, T2 (0.51 mmID, 81.9 cm), with DMCS-treated glass beads (Alltech, 100/120 mesh, 20.9 mg/6.45 cm packing) held at -165 °C to sharpen the chromatographic peak. T1 is resistively heated to 80 °C with voltage applied across the trap itself controlled by Omega PID temperature/process controllers, thus releasing the trapped gases into He carrier gas flow which carries the released gases to T2 (position 12 in figure). For desorption from glass beads N_2O does not require temperature this high, but this temperature was found optimal for sharp N_2O release. A downstream flow meter monitors the transfer. A needle valve downstream of T2 during the T1-to-T2 transfer more finely regulates the transfer flow and pressure on T2 and was tested and set in the position for optimal complete and sharp collection of N_2O on the smaller T2 trapping surface area. V5 is a specially designed and custom rotor engraved multi-port valve allows T2 to be completely isolated from flow for static desorption (position 1) as it is resistively heated to 80 °C for 30 seconds before the valve is switched (position 2) and the He carrier gas back-flushes the sample to a gas chromatographic CP-PoraBOND Q fused silica PLOT pre-column (10 m, 0.32 mmID, Agilent). The static desorption prior to dynamic He flow creates a sharper and more symmetrical N_2O peak shape to allow for better IRMS analysis and separation from neighboring compounds.

For further separation the sample is passed to the main column (CP-PoraBOND Q, 25 m, 0.32 mmID) and a multi-port valve switches the pre-column to be backflushed with He to vent after N_2O has passed. This inclusion of a pre-column and backflush is vital for clearing out heavier, late-eluting analytes which can contaminate subsequent samples, particularly fluorocarbons which ionize to CF^+ in the mass spectrometer at the same m/z 31 mass necessary for N_2O isotopomer analysis (section 2.2). The GC pre- and main column type and length were thoroughly assessed for ideal N_2O separation, particularly from the small remaining CO_2 and fluorocarbon compounds (section 2.2). The gas chromatograph is isothermal at 30 °C during separation of the N_2O peak and after N_2O elution is ramped to 200 °C to move through the heavier, slower-moving compounds prior to cooling back to 30 °C in preparation for the next air sample run. During system idle time between analyses, He continuously flows throughout the system and the pre-column is out of line in backflush mode.

Images of Stheno are included in Appendix 2.I.

Figure 2.2 Typical air sampling sequence of instrumental parameters as controlled and recorded by the GCWerks software, following the air sampling method as described in the text. T1, T2: cryotrap temperatures (°C); Base: Cryotiger baseplate temperature (°C); Flow: MFC flowrate (ml/min); Oven: GC oven temperature (°C); EPC3, EPC4, EPC5: electronic pressure controller pressures connected to V2, V5, V6, respectively (mbar×100); Tmod: Stheno housing temperature (°C); T1-P: pressure sensor between T1 and MFC (mbar×100)

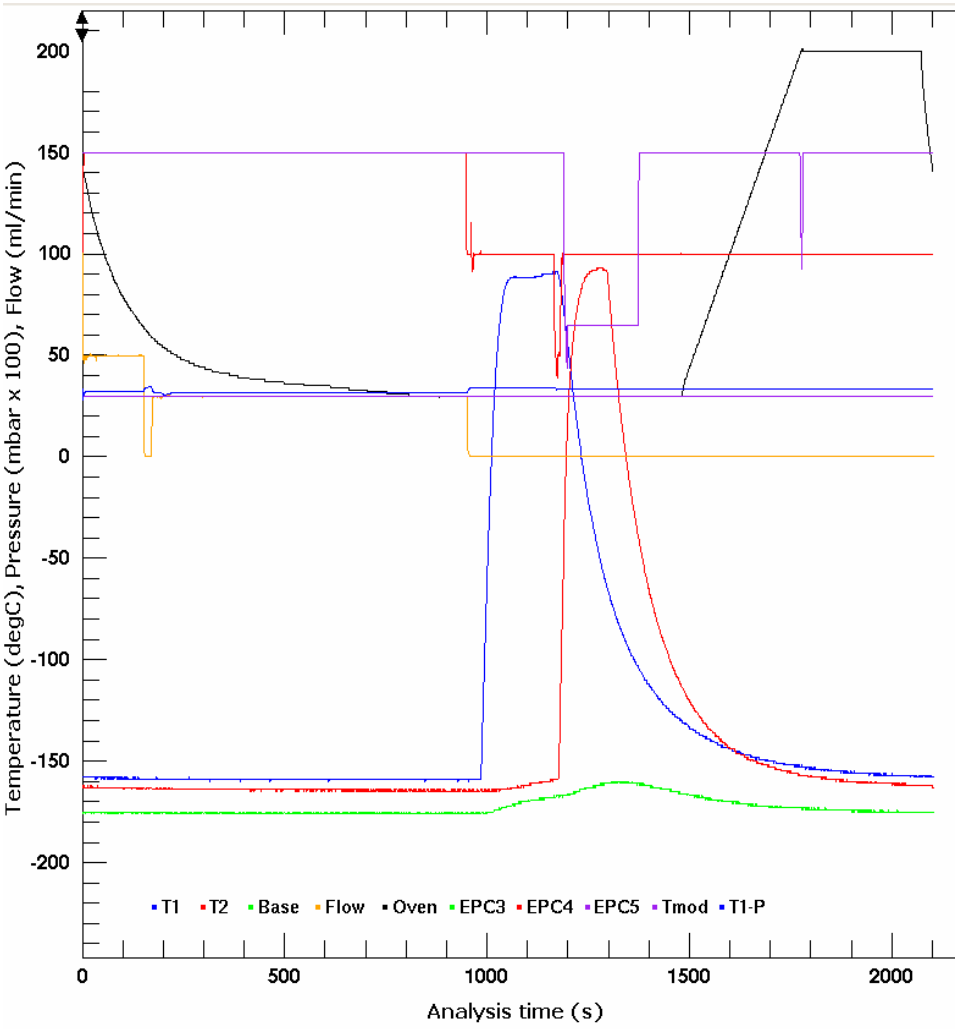

2.1.3 Open split and IRMS continuous flow interface

The eluting N_2O peak is directed from the GC to a modified closed-bottomed open split based on the design of Ferretti et al (2000) and Rockmann et al (2003) (Figure 2.3, images in Appendix 2.I). With the closed-bottom design, the Stheno GC effluent can be entirely diverted from the IRMS or diluted. The ability to divert the sample flow helps with preservation of the IRMS by preventing late-eluting heavier compounds from entering the ion source. In this design the sample capillary originating from the GC column (deactivated glass capillary 0.32 mmID) and a He dilution capillary (0.11 mmID) enter a narrow closed-bottom glass tube (1.5 mmID, 1.9 mmOD, 90 mm long) and are mounted with air-actuated pistons which allow them to be raised and lowered in relation to a fixed transfer capillary leading to the IRMS (0.11 mmID, 150 cm). In this way the GC sample flow can be entirely diverted from the IRMS except during the short and precisely known time of the N_2O peak elution thus preventing additional compounds from entering the ion source,

during which the sample capillary is lowered and the He capillary is raised. In absence of the sample flow the He capillary is lowered and there is always a continuous flow of He to the IRMS, with the option of sample or reference gas dilution. He dilution pressure was optimal at 1 bar above ambient providing constant flow to the IRMS ion source with minimal noise added to the sample flow. Capillary lengths and diameters were specified to obtain a split ratio ~1:8. The stationary transfer capillary exiting the open split feeds into the continuous flow interface of the IRMS (MAT253, Thermofinnigan) via a stainless steel bellows valve (Swagelok 4H) with Valco capillary adaptor fitting. With the CF bellows valve open to the ion source the IRMS vacuum was approximately 2.5E-6 mbar.

Figure 2.3 Closed bottom open-split. Stheno GC and helium dilution deactivated silica capillaries are controlled by separate air-actuated pistons. Sample gas enters from left via a deactivated silica capillary from the Stheno GC and exits to the right to the IRMS via a fixed capillary.

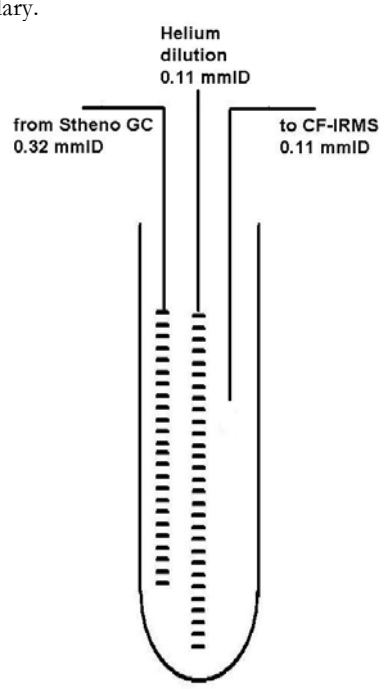

2.1.4 IRMS measurement

Each aliquot of air from Stheno, either from sample or standard air tank, is measured in relation to pure N_2O reference gas (Airgas, VLSI grade >99.9999%) calibrated on the common Tokyo Institute of Technology ^{15}N site-specific scale, which has been accepted in the community as a temporary international reference until an official site-specific N_2O isotope calibration standard exists. Two separate N_2O reference tanks were calibrated on this scale using dual-inlet offline techniques. Only N_2O reference tank II was used during the air sample analyses thus maintaining reference tank I as a stable reference source unaffected by fractionation caused by aliquot removal. Pure N_2O reference tanks are equipped with Ultra High Purity stainless steel single-stage regulators (Tescom, 74-2400 series), specified with Vespel seat and precision electropolish to 5 Ra microinch internal surface, and equipped with stainless steel electropolished high purity pressure gauges (WISE). The quality regulators prevent potential off-gassing of interfering fluorocarbon compounds into the N_2O reference gas, and lessen possibility of isotopic fractionation with the electropolished interior and single-stage design having less internal volume, and no N_2O absorption onto fluorocarbon seats.

To determine the ^{15}N site-specific isotopomers $\delta^{15}N^{\alpha}$ and $\delta^{15}N^{\beta}$ in addition to $\delta^{15}N^{bulk}$ and $\delta^{18}O$ by IRMS, the molecular ion N_2O^+ and fragment ion NO^+ are monitored at m/z 44, 45, 46 and m/z 30, 31, respectively, in the technique simultaneously developed by Brenninkmeijer & Rockmann (1999) and Toyoda & Yoshida (1999). The technique uses the idea that the NO^+ fragment will contain the N predominately from the central N^{α} (N^{α}–O^+), with a small amount of scrambling that occurs in the ion source leading to some N^{β}–O^+ (typically ~8%, see section 2.4). The MAT253 IRMS used here is equipped with ion collector cups that do not allow the simultaneous monitoring of the 5 desired ions, therefore isotopic ratios are determined with sequential aliquots of air sample.

Example measurement series are show in Figure 2.4 for the molecular ion (m/z 44, 45, 46) and fragment ion (m/z 30, 31) runs. (Note that the IRMS resistors on the different ion channels are different thus the ratios and relative peak sizes in these traces are not absolute. Ion channel differences are canceled out with relation to the reference gas.) Reference gas from the dual-inlet bellows is admitted to the IRMS ion source for peak centering immediately preceding analysis. Pure N_2O reference gas for sample value determination is admitted via the IRMS dual-inlet bellows (e.g. Merritt et al 1995, Ferretti et al 2000, Miller at al 2002). Three 20 second wide pulses of reference gas are introduced from the dual-inlet bellows of the IRMS to the source region. After the third reference has returned to baseline the Stheno-GC capillary on the open split is lowered and the He dilution capillary raised during the timed elution of the N_2O peak allowing the sample peak to enter the IRMS via the CF interface. Following N_2O elution the He dilution capillary on the open split is lowered and Stheno-GC capillary raised, followed by a fourth N_2O reference pulse. Average measured ion intensities of the two reference peaks bracketing the sample N_2O peak are used to determine the delta value of the sample peak. The use of two bracketing reference peaks will account for changes in the source that occur over the timescale of a couple minutes and the small distribution of reference gas aliquot compositions. The initial two pulses of reference gas are performed to ensure stable reference gas values for the referencing peaks three and four. These measured reference values of 31/30, 45/44, and 46/44 and the measured ratios of the sample peak are used to determine the isotopic composition of the air sample versus air-N_2 and VSMOW for $\delta^{15}N$ and $\delta^{18}O$ values, respectively.

Details on this calculation and other IRMS conditions and optimization for maximum N_2O measurement precision are detailed in Part II of this chapter.

Figure 2.4 (next page) Example IRMS traces showing the 4 reference gas peaks and the eluting sample peak. for a) the molecular ion N_2O^+ monitoring mode of m/z 44, 45, 46, 47 and b) the fragment ion NO^+ monitoring mode of m/z 30, 31, 32. Upper plots of each are the ion ratios, lower plots are ion current intensities. In figure a, the small peak preceding the large N_2O peak is CO_2. In figure b, the N_2O is the large peak followed by three small unidentified m/z 31 compounds (likely fluorocarbons).

a)

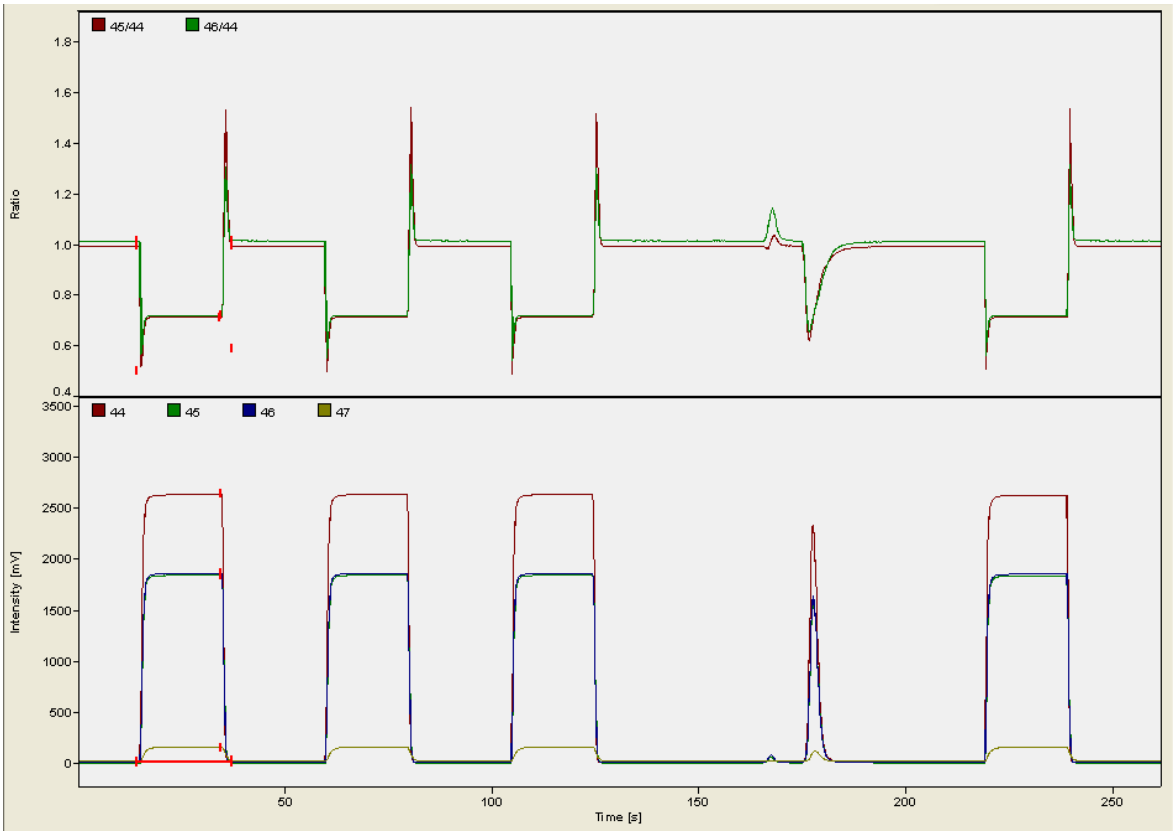
45/44
46/44
Ratio
1.8
1.6
1.4
1.2
1.0
0.8
0.6
0.4
44
45
46
47
Intensity [mV]
3500
3000
2500
2000
1500
1000
500
0
50
100
150
200
250
Time [s]

b)

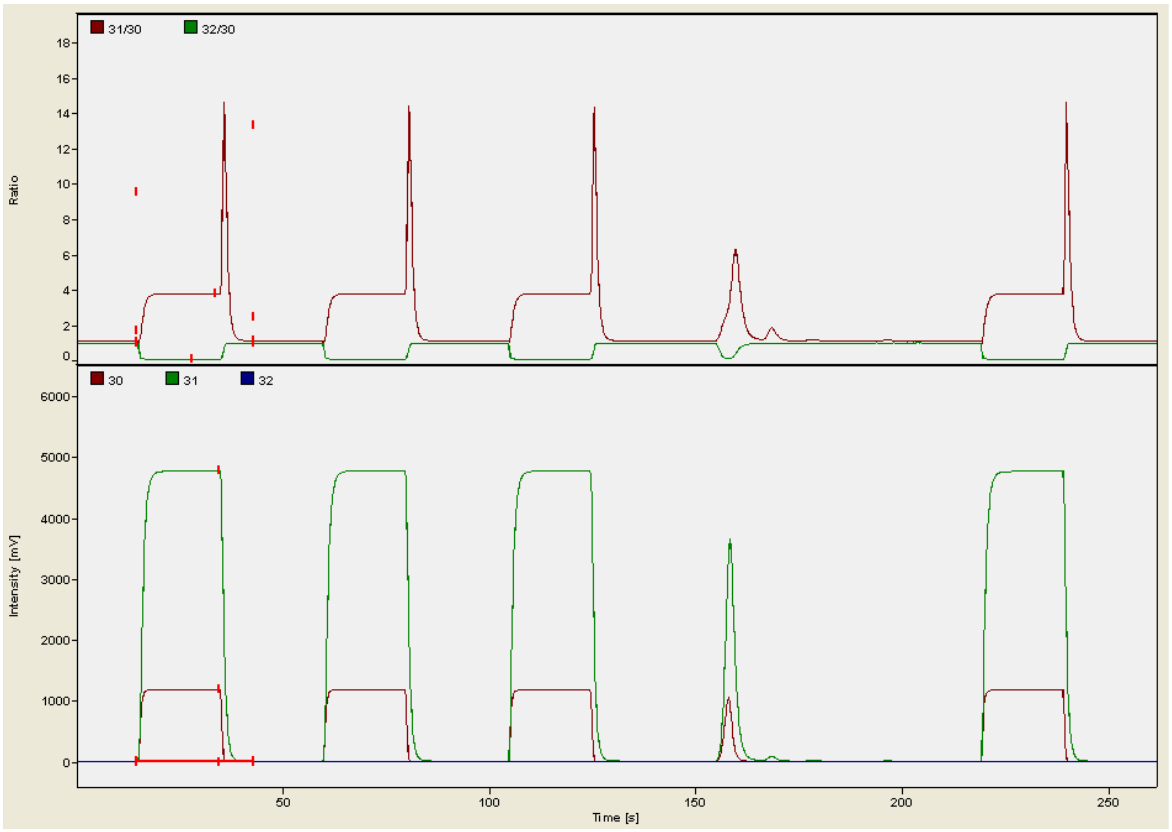
31/30
32/30
Ratio
18
16
14
12
10
8
6
4
2
0
30
31
32
Intensity [mV]
6000
5000
4000
3000
2000
1000
0
50
100
150
200
250
Time [s]

2.1.5 Tropospheric flask samples

For the initial design and pilot testing of this system flask sample canisters were used rather than in situ measurements. Air samples were collected from Mace Head, Ireland Atmospheric Research Station (53.32N, 9.90W), one of the primary AGAGE (http://agage.eas.gatech.edu/) stations making high-precision, continuous measurements of N_2O mole fraction and other trace gases since 1978 (Prinn et al 2000). Details of the air sampling at Mace Head are included in Chapter 4 and Appendix 4.III. Two types of sample flasks are used: 2.9L spherical stainless steel flasks (Biospherics Research Corp) electropolished by Electromatic, Inc. with a single inlet with a bellows valve (Nupro SS-4H), or 3L cylindrical stainless steel flasks (Lab Commerce, Santa Clara, CA, X23L-2N) with two inlets each with bellows valves (Nupro SS-4H). Flasks were filled to about 40 psig. Between air collections, all sampling flasks are cleaned and evacuated to <5 mtorr prior to shipment to Mace Head. Flask "cleaning" entails vacuuming flasks to <5 mTorr (rotary vacuum pump, ULVAC KIKO Inc), followed by 3 cycles of pressurizing to ~40 psi with Research Plus grade N_2 gas (Airgas, >99.9999%, <0.1 ppm CO_2) and evacuating to <5 mTorr, and a final evacuation to <5 mTorr.

The Stheno sample inlet is designed so that with no modifications it can be used with an automatic in situ air sampling intake, such as used with the AGAGE instrumentation. Air samples from the sample flasks enter Stheno through a stainless steel manifold connected to one of six possible inlet ports controlled by a multiposition valve (Valco). Mass flow controllers are highly sensitive to pressure transients. Because the pressure in the sample canisters decreases as the sample is drawn into Stheno, an inline regulator (Tescom 64-3600 series, Vespel seat) is used to maintain stable flask outlet pressure of 1.6 bar (absolute) to the Red-Y flow controller and ensure that pressure on T1 for all samples is equivalent, thus resulting in constant sample size. The Tescom regulator model is specially chosen for this application as low-droop to prevent pressure and flow drift resulting from the large relative change in pressure in the flask as it is depleted, and single-stage to prevent potential fractionation.

The number of repeated analyses of a single flask sample is limited by Mace Head air sample size. A flask air sample is about 6 to 9 L STP (2-3 bar in 2.9 or 3.0 L canisters), however sample canisters are not drawn to lower than ambient to lessen the possibility of fractionation so that analyses can be performed on 3 to 6 L STP per air sample, with individual measurement size of 420 mL STP. To conserve sample, instead of flushing the full volume of the sample manifold connected to Stheno with the sample prior to analyses as could be done when sample size is not limited, a sample inlet manifold was designed which is cleared by vacuum to <10mTorr (rotary vacuum pump, ULVAC KIKO Inc) monitored with a Teledyne Hastings 0-1000mTorr vacuum gauge and gauge tube. The flask and vacuum are interfaced with a 3-way bellow-sealed diaphragm valve with polyimide seat (Swagelok, DP series). Pressure is monitored in the sampling line and flask between the flask and 3-way valve with a -30 inHg vacuum to 40 psig (~4 bar) stainless steel Bourdon tube Ultrahigh purity pressure gauge (Swagelok PGU-50). The vacuum is created only to V1, therefore to clear tubing beyond this, immediately prior to a sample run He carrier gas is pulled from a different port on V1 and flushed through the sampling line including warm T1 (at 30C). This short "flushing" runfile also simultaneously flushes He carrier through all of the tubing, rotates valves to all positions with He flow, and warms T2. This precautionary runfile ensures that there is no residual air or air pockets within Stheno, either from a previous air sample or from any slow system infiltration if it has been static for extended time.

2.1.6 Natural air standard

To monitor day-to-day variations in the entire measurement system (including all of the IRMS components and CF response; Stheno pre-concentration device functioning and components;

possible effects of pressure, temperature, or moisture levels in the instrument surroundings on instrumental functioning, particularly the continuous flow interface; and response to pure N_2O reference gas aliquots) a natural air standard was used, fully mimicking the air sample analysis and flow path. Natural air collected by NOAA at the biosphere preserve Niwot Ridge, Colorado air standard preparation facility (40.03°N, 105.53°W) was dried to a dew point of -80 °C with $Mg(ClO_4)_2$ and stored in a 29.5 L Scott Marrin aluminum cylinder which has been treated with a drying/passivation process and initially pressurized to 2000 psig. Experience from NOAA-ESRL with natural air standards for a variety of gases supports the stability of N_2O in Al cylinders with dry air (Brad Hall, NOAA-ESRL, personal communication, 2009). Nitrous oxide mole fraction in the tank is calibrated by ECD as 322.72 ±0.09 ppb (n = 24) on the NOAA-2006 scale.

Alongside sample analyses were run daily series of the Niwot Ridge (NR) air standard (approximately 3-5 pairs of molecular and fragment ions analyses per day). The NR standard air tank is attached to a Stheno inlet port using stainless steel tubing and ultra high purity single-stage regulator with Vespel seat and electropolished internals (Tescom 74-2400 series) set to 1.6 bar absolute, the same pressure regulated for the sample flasks. The NR analysis serves as a quality control to check the performance of the entire system. Examination of variation in these values over time provides checks on the overall reproducibility and long-term precision, discovers problems in the analytic system, and monitors long-term instrumental drift for all system components.

2.2 Stheno optimization and special measures

The relatively small variations in N_2O isotopic composition in tropospheric air are subtle and difficult to resolve, thus necessitating close attention to data quality control. In addition to the optimization of the analytical system for maximum precision and the details mentioned previously, a number of measures in particular were taken to maximize the system efficiency and address major priorities of tropospheric N_2O isotopic measurements: high-precision and high-frequency capabilities. The addressing of these goals specifically for N_2O is part of what makes this system unique to other off-the-shelf universal pre-concentration systems, in addition to having fully-automated liquid-cryogen-free capabilities.

The final configuration and protocol for the Stheno system were the result of many checks for optimal N_2O pre-concentration with full recovery, eliminated interfering compounds and sample contamination, adequate amount of sample, and in the minimal amount of time, among other concerns. Highlighted here are the major quality control and system optimization measures in the development of this pre-concentration device and the uniqueness in each of these features being tailored for N_2O and isotope analysis, here optimized for CF-IRMS. System performance tests were performed stepwise changing through parameters to achieve successful and optimal N_2O pre-concentration as monitored by quadrupole mass spectrometer (Agilent 5973). The results of these tests are as incorporated into the final Stheno design and method discussed earlier in section 2.1 and presented later in the system assessment in section 2.3. Optimization of the IRMS configuration is presented in Part II of this chapter.

2.2.1 Diagnostic quadrupole mass spectrometer

During Stheno development the system was connected to a quadrupole mass spectrometer (Agilent 5973) which is capable of monitoring of more ions than possible with the individual collector cup system of the sensitive IRMS. This detector served to unambiguously identify known compounds in the retention time region (N_2O, CO_2) and identify compounds of unknown identity.

The identification of N_2O therefore does not solely rely upon comparison of retention times nor does it rely on the assumption that the observed N_2O peak is not aligned with another compound as well. The quadrupole MS was particularly useful because it allowed monitoring for interfering fluorocarbon species with imperceptibly small m/z 31 ion fragments (CF^+), which could still be altering the N_2O 31/30 ratio since mass 31 is the rare isotope and any small change might have a consequential effect on the final δ value. With the aid of AGAGE personnel experience in GC-MS analysis of atmospheric fluorocarbon species, these other ion fragments which commonly result from fluorocarbon compounds which were monitored included m/z 33, 50, 51, 65, 69, and 85. Later in Stheno development the flow after the GC outlet was split via a microneedle T valve (SIS) between the IRMS open split (deactivated fused-silica capillary, 0.32mm ID) and a quadrupole mass spectrometer (Agilient 5973) to allow for simultaneous detection of the N_2O isotopic composition m/z ions by the highly sensitive IRMS while also detecting other ions on the quadrupole MS to assess for underlying interfering compounds. Coupling a traditional MS with an IRMS in parallel to the same pre-concentration + GC system provides concurrent information about chemical nature and isotopic composition under identical pre-concentration, separation, and sample conditions (e.g. Meier-Augenstein et al 1994). The split to the MS was via a 0.075 mmID deactivated fused-silica column with initial flow rate calculations according to the Poiseuille equation to give sample amounts appropriate for each spectrometer detector. Final measured flow resulted in approximately a 1:8 split between the MS and the open split leading to the IRMS. After final Stheno design the flow was diverted entirely to the IRMS to maximize the signal.

Appendix 2.III includes chromatograms at the fluorocarbon diagnostic ion masses from analysis of an AGAGE air standard tank collected at Mace Head (H-106) in the final Stheno configuration, confirming the sufficient separation of N_2O from any interfering compounds.

2.2.2 N_2O-specific separation

For N_2O analysis by IRMS, other gases in general can cause interference in the ion source, and trace gases with mass fragments that overlap with N_2O are especially problematic. This includes CO_2 with the same molecular ion fragments as N_2O (m/z 44, 45, 46), and fluorocarbons which generate the CF^+ m/z 31 fragment the same as the $^{15}N^{16}O^+$ fragment. Water can be damaging to the system and particularly the IRMS. Additionally, N_2 can be oxidized to N_2O in the IRMS ion source. Contamination by CO_2 poses a particular challenge since it has a similar boiling point and elution time as N_2O. In GC analysis of a pure tropospheric sample with carbon dioxide 10^3 times more concentrated than N_2O, the CO_2 peak completely swamps the neighboring N_2O peak. Trace amounts of CO_2 can persist even through many standard GC separations (Tanaka et al 1995).

In optical instruments, the separation of other gases will be simplified slightly to removal of those gases that overlap optically with N_2O in the chosen spectral band (potentially CH_4, CO_2, and H_2O). N_2O will still have to be pre-concentrated by cryo-trapping to remove bulk gases (N_2, O_2) to improve the level of precision by current technology, but no gas chromatography is necessary. Thus, the methodology is selected for effectiveness for an optical detector in addition to IRMS analysis for future application.

i) CO_2 and water removal

CO_2 and H_2O will be trapped alongside N_2O in any cryotrap, therefore the system starts with a chemical trap with Ascarite II which resulted in >99.99% CO_2 removal in combination with magnesium perchlorate ($Mg(ClO_4)_2$) for water removal. Additionally, the chemical traps are connected to the system via a 6-port valve so that the system will not be exposed during absorbent replacement, thus avoiding contamination or condensation by interfering gases. The chemical trap is followed by a Nafion dryer membrane to further reduce water to a dew point of about -18 °C.

ii) Cryo-trapping

Multiple trap packing materials with variable surface areas and material properties were tested for complete N_2O adsorption and desorption, including HayeSepD, DMCS (dimethyldichlorosilane)-treated glass beads, and empty coiled tubing. The ideal N_2O trapping material has minimal absorbent properties to minimize potential fractionation and retain as few other interfering molecules as possible while still capturing all N_2O. Glass beads (100/120 mesh, T1 660 mg, T2 20.9mg) were determined to be the optimal trapping material for N_2O isotopes, with minimal concern for unintended isotope fractionation caused by incomplete trapping ability or preferential adherence and desorption ability. HayeSepD additionally can trap methane (CH_4), which for IRMS analysis would be separated by the later gas chromatography, but could pose interference for infrared optical detectors. The use of glass bead traps for N_2O isolation also provides the opportunity for system expansion to include isotopic analysis of other trace gases not trapped on the glass beads, namely CH_4, with addition of a later HayeSepD trap.

To pre-concentrate further, after collection of the remaining condensable gases on a cold -165 °C T1, the trap is flushed with helium for 20 seconds to remove lingering N_2 and O_2.

Complete gas trapping and transfer on the two traps were tested to determine exact parameters for trapping temperatures, desorption temperatures, sampling flow rate, T1 venting parameters, flow rate for T1 desorption to T2 trapping, T2 heating desorption technique (isolated static then dynamic carrier gas flow, or dynamic flow only), and T2 desorption flow rate. Complete trapping and recovery of the entire sample N_2O in the pre-concentration system is critical to ensure an accurate isotopic measurement, as incomplete recovery would likely produce fractionation effects. During assessment the quadrupole mass spectrometer could be placed in constant scanning mode to capture any potential N_2O sample lost beyond the traps. Complete trapping and full recovery of N_2O was also assessed with linearity tests to determine break-through sample size and break-through parameter set-points where the N_2O response began to decrease indicating incomplete trapping. Linearity tests were conducted with the Niwot Ridge air standard tank. Figure 2.5 displays the sample size linearity validation for the final Stheno configuration and parameter set-points in which the air standard aliquot was drawn over T1 at the same 30 ml/min sampling flow rate for variable amounts of time to simulate a range of N_2O quantities. The instrument response linearity holds for both the N_2O^+ molecular ion (m/z 44, 45, 46) as shown and the NO^+ fragment ion (m/z 30, 31) as well. Scaled to the air standard tank calibrated mole fraction peak size for the 420 ml volume of Stheno air samples, the air standard aliquot volumes equate mole fractions in the Stheno 420 ml air sample size from approximately 300 to 430 ppb, well spanning the mole fractions encountered in observations and indicating full recovery of N_2O.

The parameters tested for cryo-trapping loading and unloading are also critical for the resulting N_2O peak shape, particularly the smaller focusing T2. The addition of a needle valve downstream of T2 during the T1-to-T2 transfer more finely regulates the transfer flow and pressure on T2 and was set in the optimal position for sharp collection of N_2O. The T2 desorption technique of isolated static heating prior to entering helium carrier gas flow, possible with the specially engraved rotor of the multi-port valve, was key for obtaining a concentrated release of N_2O from the trap, and was optimized with flow rate and heating temperature to achieve a sharp chromatographic peak. Testing with a fully dynamic desorption without static heating resulted in poorer peak resolution.

Figure 2.5 Quantitative trapping and recovery was checked by following the linearity of peak response over a range of Niwot Ridge air standard sample sizes. The plotted volumes correspond to approximately 300 ppb to 430 ppb of N_2O in a typical 420 ml sample.

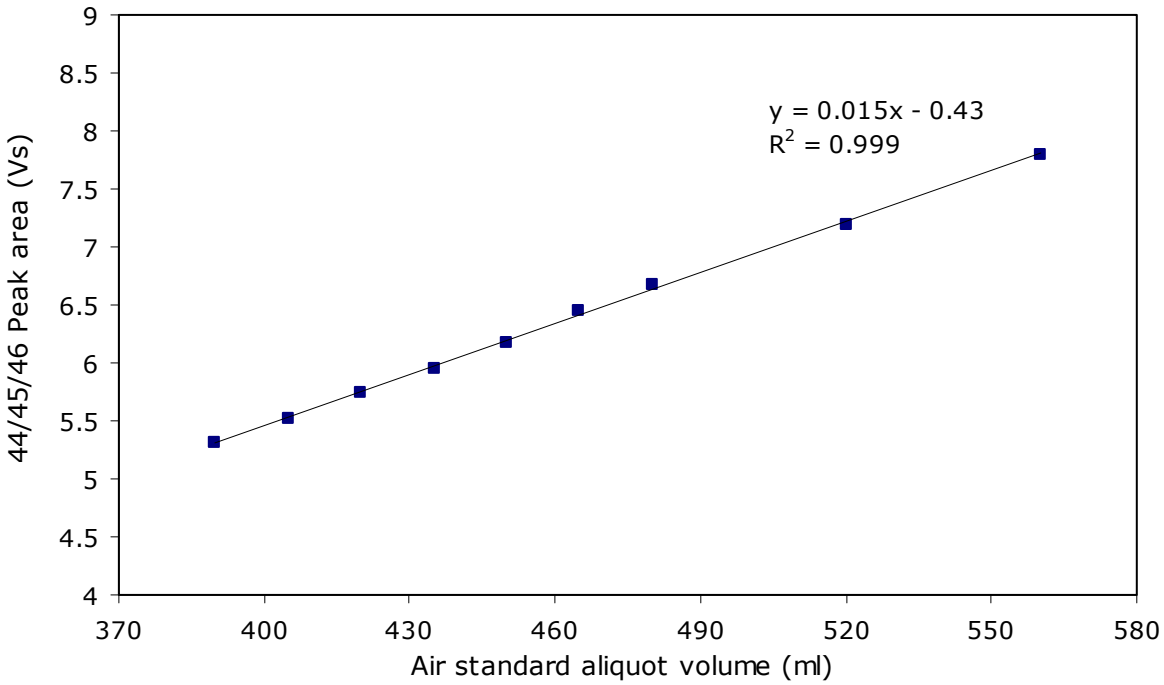

iii) Gas chromatography

GC separation is critical in IRMS analysis for compounds producing coincident molecular or fragment ions as N_2O, particularly the isotopologues of CO_2 (m/z 44, 45, 46), certain hydrocarbons (e.g. ethanol m/z 46; propane m/z 44, 45, 46; larger hydrocarbons with C_2H_6+ m/z 30, 31 or C_3H_8+ m/z 44, 45, 46 fragments), and fluorocarbons with CF^+ m/z 31 fragments. CO_2 is largely removed by the Ascarite II trap, but typically elutes immediately prior to the N_2O peak. Hydrocarbons and fluorocarbons are present in the ambient atmosphere, and can off-gas from analytical materials during sample processing.

Multiple column types were tested or investigated prior to selection of CP-PoraBOND Q fused silica PLOT GC column (0.32mmID, Agilent) of 10 m and 25 m lengths for the pre- and main columns, including HiSiv-3000 (micropacked, 450 mg, 0.43 inID, 1.8 m) pre-column, CP-PoraPLOT Q, Porapak Q, Porasil C, and molecular sieve 5A.

These alternative columns have been used for N_2O separation for mole fraction measurements, but many were eliminated because of questionable fractionation effects or insufficient N_2O separation. CP-PoraPLOT Q is commonly used in the few measurements of atmospheric N_2O isotopes (e.g. Kaiser et al 2006, Rockmann et al 2003, 2005, Yoshida & Toyoda 2000, Park et al 2004, Perez et al 2006, Croteau et al 2010) often because it is the column for the prevalent Thermofinnigan PreCon (Brand 1995) and IsoPrime TraceGas system. Porapak Q was used for offline N_2O isotope analysis (Kaiser et al 2003). The selected CP-PoraBOND Q is a more stable bonded PLOT column than these alternatives which can last for longer term and has no loose particles to cause detector anomalies, and has virtually no catalytic activity.

Chromatographic parameters for GC oven temperature (30 °C isothermal) and flow rate to desorb T2 and pass through columns (~2 ml/min) were stepwise tested to achieve the best separation and sharp peak shape.

2.2.3 Maximization of Signal-to-Noise ratio

The good separation resulting in a sharp N_2O peak that resulted from the efforts described above contributes significantly to maximizing the signal-to-noise ratio.

i) Carrier gas purity

High carrier gas purity is vital to minimize background noise and prevent contamination. Ultra high purity helium (>99.999%, Airgas) plumbed to all components of the Stheno+CF-IRMS system (Stheno carrier gas, multi-port valve purge, open split) passes through centrally located hydrocarbon, water, and oxygen high-capacity gas purifiers (Supelco). Immediately prior to the Stheno system, helium was regulated with a high purity regulator (Tescom, 64-2600 series) equipped with Vespel (polyimide) seat to avoid fluorocarbon contamination. As the final step before entering the system, was further purified with a VICI Helium Purifier with heated getter alloy chemisorbing all non-noble gases (documented outlet impurities <10 ppb H_2O, H_2, O_2, N_2, NO, NH_3, CO, CO_2, CF_4, CCl_4, SiH_4, CH_4, and other hydrocarbons).

He carrier gas purity was assessed by adding a He line connection directly to one of the Stheno inlet ports and admitting approximately 0.5 L, 1 L, and 2 L STP helium samples. No N_2O contamination was detectable in the helium carrier gas. The carrier gas integrity entering Stheno through the three EPCs was also checked by "sampling" gas via these system inlets. Again, helium carrier gas and the EPC connections were free of detectable interferences.

ii) Contamination

Aside from the carrier gas, system contamination can occur through minute leaks at component junctions imperceptible with common soap bubble checks. Thorough leak tests were conducted with helium carrier gas flowing through the system and a He leak checker along the entire flow path. Additionally, closed system pressure holds were performed and high pressure (~30 psi) was able to be maintained for several hours. Around the pre- and main column fittings and associated multi-port valves, leaks were checked for by spraying Ar gas with quadrupole MS monitoring m/z 40.

Throughout the use of Stheno, regular blank runs were performed to ensure a clean system, particularly following system changes and chemical trap replacement. Different blank methods were used to test various aspects of the system: sampling of an helium aliquot through the entire system, using no sample flow but with T1 inline, using no sample just desorption of traps, and testing previous sample volume dependency. Typical blank run chromatograms are included in Appendix 2.II.

iii) Sample size and IRMS peak size response

Signal-to-noise is generally improved with a larger N_2O peak size and the precision of an isotope ratio measurement by IRMS depends upon this peak area. Rockmann et al (2003) found for N_2O isotope analysis of air samples, standard deviations (a proxy for precisions) increased up to 3 Vs but remained relatively flat for >3 Vs peak areas. The sample aliquot size for each N_2O^+ or NO^+ analysis was tested and selected as 420 mL STP. For N_2O^+ ion analyses sample peak sizes are approximately 5.5-5.8 Vs. For NO^+ fragment ion analyses this was a compromise between the low yield of fragment ions and wanting to avoid overly long sample admission times and sample consumption, leading to peak areas at around 2.5 Vs.

iv) *Open split*

Background noise can amplify from open split entrainment in which pressure variations in the laboratory environment affect the above ambient pressure in the open split. The closed bottom open split design minimizes entrainment and contamination compared to a flow through open-ended open split.

2.2.4 Fractionation avoidance

A foremost requirement for accurate isotopic analysis is the minimization of any potential isotopic fractionation which could occur during sample processing prior to detector analysis. A substantial aspect of minimizing sample fractionation is ensuring full recovery of N_2O from Stheno and careful selection of trapping procedures, which was addressed in the optimization of Stheno above. Deserving particular attention is unintended isotopic fractionation during pre-concentration from differential diffusion, chemisorption (when gas reacts with the host), or isotopic exchange with host lattice or other molecules as the N_2O is processed in the traps and GC column, thus there was careful consideration of phase partitioning for the trap material and GC columns. A main criteria for the trap absorbent in respect to minimizing potential fractionation is to have the minimal absorptive surface which will still quantitatively trap all of the N_2O sample, which was found to be ideally achieved using glass beads (DMCS-treated, 100/120 mesh). Though HayeSepD can be used for trapping N_2O (e.g. Mohn et al 2009), the strong absorbent properties leave a large possibility for preferential desorption from the trap between N_2O isotopologues and thus fractionating the sample. The chemical reaction of the sample in the chemical trap might also fractionate N_2O unintentionally. Ascarite used for CO_2 removal was reported not to fractionate N_2O in air samples by Kaiser et al (2003). To limit differential diffusion, throughout Stheno dead-volumes, unions, and changes in tubing diameter were minimized to create as smooth a flow path as possible. The sample inlet manifold and any reference gas transfer lines are constructed with electropolished ¼" stainless steel tubing. All air sample flasks are internally electropolished.

The selection of gas regulators controlling any N_2O to be analyzed (air samples, air standard, pure standards) has much potential to interfere with the accurate analysis of N_2O isotopic composition, particularly potential fractionation, thus regulator specifications were purposefully chosen for robust analysis. For the Niwot Ridge standard air tank (Tescom 74-2400 series), pure N_2O reference tanks (Tescom 74-2400 series), and sample flask manifold (Tescom 64-3600 series) single-stage regulators were chosen because this design employs fewer wetted parts and the simpler design leaves less room for isotopic fractionation as the gas travels through the regulator. Precise outlet pressure is not needed because of downstream flow controllers and pressure gauges. Additionally, to reduce the chance of fractionation the regulators are threadless and internally treated by Precision ElectroPolish to 5 Ra microinch internal surfaces. All regulators are equipped with stainless steel electropolished high purity pressure gauges (WISE), accuracy +/- 1% full range.

The degree of pre-concentration fractionation which might occur with respect to the precision of measurements made here by CF-IRMS is uncertain. However, particularly as detector capabilities progress towards significantly better precision than achievable by IRMS any minute fractionation effects will be consequential.

2.2.5 Fluorocarbon m/z 31 interference prevention

A specific challenge unique to N_2O isotopic analysis for IRMS measurement in addition to usual separation needs is the noted interference with the $^{15}N^{16}O^+$ fragment ion m/z 31 by $^{12}C^{17}F^+$ ion fragment (m/z 31) produced form fluorocarbons. These fluorocarbons are present in the atmosphere from both natural and anthropogenic origins as well as being introduced from the

analysis system itself. Nitrous oxide isotopomer measurements by fragment ion analysis are known to be plagued by interferences in the m/z 31 ion signal. Kaiser et al. (2003) identified CHF_3 in atmospheric samples as the source of m/z 31 interference via the production of CF^+ fragment ions. Röckmann et al. (2003) hypothesized the presence of sundry other fluorinated hydrocarbons that create an array of peaks that appear in the m/z 31 trace, the most troubling being slow moving, late-eluting compounds that can co-elute with nitrous oxide during a subsequent run. Viton is a common and useful material for o-rings, diaphragms, and other flexible or sealing purposes, but has been repeatedly found as a significant m/z 31 source from off-gassing within the analytical system ($CHF_3 \rightarrow CF^+$) (e.g. Rockmann et al 2003, Kaiser et al 2003, Miller et al 2008). Kaiser et al (2003) eliminated most Viton o-rings from their system and removed much of the m/z 31 interference, however other m/z 31 contaminants remained.

As mentioned several times during the earlier Stheno system description, avoidance of all fluorocarbon materials which might off-gas CF^+ m/z 31 ion generating compounds, particularly Viton (fluoropolymer), was rigorously applied to the entire measurement system. This effort entails specially chosen and/or constructed regulators, chemical trap fittings, valves, pumps, etc. Stheno is a predominately stainless steel system with limited fluorocarbons of any type. Connections were made with Swagelok or VCR all-metal fittings and there are no o-rings in the Stheno system, including for the glass chemical trap which was attached and sealed with nylon ferrules. All tubing is stainless steel. Manual valves external to Stheno for the flask sample manifold and related to the pure N_2O reference tanks are Swagelok 4H SS bellows valves. Connections with the IRMS dual inlet interface for the reference gas were made with UltraTorr fittings with butyl rubber o-rings in place of the standard Viton. Pump hose connections were likewise made with butyl rubber, and CFC-based grease was avoided using silicone grease instead. Placement of the Nafion dryer is prior to the GC columns so any off-gassing fluorocarbons from the fluoropolymer/Teflon membrane can be separated from N_2O. The diaphragm pump used for flask air sampling (KNF UN86-SNI) was customized with a 316SS head, EPDM (ethylene propylene diene monomer rubber) diaphragm, and Neoprene (chloropolymer) valves in place of typical Viton materials contamination. Miller et al (2008) found this pump with the original Viton diaphragm and valve plate contaminated air samples with CHF_3 by ~25 – 130% above ambient atmospheric levels. Compromises were necessary for the NPT fittings utilizing Teflon tape on the few spherical flasks used for air sampling, and the multi-port Valco valves were equipped with Valcon E (polyaryletherketone/PTFE composite) rotors, but these are prior to the GC column allowing for peak separation. Post-Stheno and GC, where there are no more separation capabilities, the open split leading to the CF interface uses helium controlled by a Porter pressure regulator (Model 8286) with only non-fluorocarbon materials (aluminum, music wire, Buna-N (nitrile rubber) o-ring, stainless steel diaphragm) and the CF interface is a Swagelok 4H bellows valve attached with SS Swagelok fittings.

In addition to the quality features of the regulators mentioned previously, all regulators are stainless steel and customized with Vespel (polyimide) seats. In atmospheric analyses a number of problems have been encountered for regulators that employ Viton seals, and manufacturers' tests for analytical contamination are insufficient (White et al 2002, IAEA-TECDOC-1268). The Viton seals which have the propensity to offgas are critical to avoid for the regulators in this IRMS analysis which are handling all He carrier gas, air samples, and air standard, and particularly for the pure N_2O standards which will not undergo separation prior to IRMS measurement.

Vital to addressing the m/z 31 issue is the addition of a short GC pre-column with backflush after N_2O has passed to flush out the heavier fluorocarbon species, a feature now incorporated into many N_2O isotope CF-IRMS systems (e.g. Rockmann et al 2003, McIlvin & Casciotti 2011). In Stheno the backflush is the default mode for the pre-column so that it is always backflushing except

for the short analysis time when sample is passing from T2 through the pre-column to the main column. Additionally, the pre- and main columns are ramped to 200 °C and held for 5 minutes after each analysis to help move the slow-eluting compounds out of the system.

Some m/z 31 producing fluorocarbons are not slow-eluting and have peaks at nearby retention times to N_2O, and are thus unaffected by the backflushing efforts. The GC column types and optimal peak separation parameters as described earlier were selected for their ability to clearly define the N_2O peak apart from other compounds, including the full range of fluorocarbon diagnostic ions provided by the quadrupole MS during the initial development phase and later in parallel with the IRMS. Analysis of the fluorocarbon diagnostic masses (chromatograms in Appendix 2.III) confirms a small fluorocarbon compound following N_2O but sufficiently small and separated from the N_2O peak as to not interfere with the m/z 31 measurement (Figure 2.6). The diagnostic masses support that there are no other fluorocarbons underlying N_2O or close enough to affect the N_2O measurement.

2.2.6 Minimize analysis time

For continuous, high-frequency, in situ observations to be possible the pre-concentration unit must be as streamlined as possible since this component will be the limiting factor for measurements by CF-IRMS or optical detector. The fully automated nature of Stheno means that all valves, flow and pressure controllers, trap temperatures, and chromatography are controlled with the GCWerks software allowing for air samples to be pre-concentrated continuously without a need to restart the system or, notably, restock liquid nitrogen between runs. A pre-concentration cycle by Stheno (Figure 2.2) is 34 minutes. Much of this time is due to the required cool down of the traps and GC oven between cycles. The GCWerks software used to control all internal components of Stheno was designed by P. Salameh (UCSD-SIO) specifically for high-frequency in situ measurements by the instruments in the AGAGE network. The multiple inlet ports connected to the multi-port, multi-position valve (V1) also allow for automatic switching between any connected air sources as programmed (e.g. air standard, in situ air inlet, flask air sample, or helium line for blank analysis). Sample admission and analysis flow rates were maximized while still maintaining full N_2O recovery and good separation, and unnecessary dead-volumes and flow path lengths in the system were minimized. During the measurement procedure the system can perform a number of operations simultaneously to improve time efficiency, so that as one sample is being measured by the IRMS the next air aliquot can start the pre-concentration process and the sample inlet manifold is evacuated in preparation for the next sample.

The required manual replacement of Ascarite II/$Mg(ClO_4)_2$ is an unfortunate repercussion of the chemical trap. However, its installation with an additional valve to avoid the entire system being exposed during chemical exchange is important for minimizing the delay to resuming air sample measurements since instrument flush-out time is greatly reduced. This is a feature not seen in other pre-concentration systems that have needed to incorporate a chemical trap.

2.3 Performance

2.3.1 N_2O peak separation

The final Stheno CF-IRMS configuration chromatograms for the molecular (m/z 44,45,46) and fragment (m/z 30,31) ions of a typical Mace Head flask air sample display good peak shape and separation from neighboring interfering compounds (Figure 2.6). In the m/z 44,45,46 chromatogram, the first small peak preceding the large N_2O peak is CO_2 which has been

significantly minimized from the initial ~1000:1 CO_2:N_2O ratio in air by the Ascarite II chemical trap and successfully fully separated from the N_2O peak to baseline. The fragment ion analysis shows one m/z 31 peak following the N_2O peak with sufficient separation. Close inspection of the chromatogram baseline shows two other m/z peaks further after, both slightly visible in Figure 2.6. Diagnostic fluorocarbon ions as monitored by the quadrupole MS (Appendix 2.III) confirm that these are the only fluorocarbon m/z 31 peaks in the vicinity of N_2O and there are no underlying interferences.

Figure 2.6 Ion current intensity (mV) traces of a typical N_2O air sample peak for a) the molecular ion N_2O^+ monitoring mode m/z 44, 45, 46, 47, and b) the fragment ion monitoring mode m/z 30, 31, 32.

a)

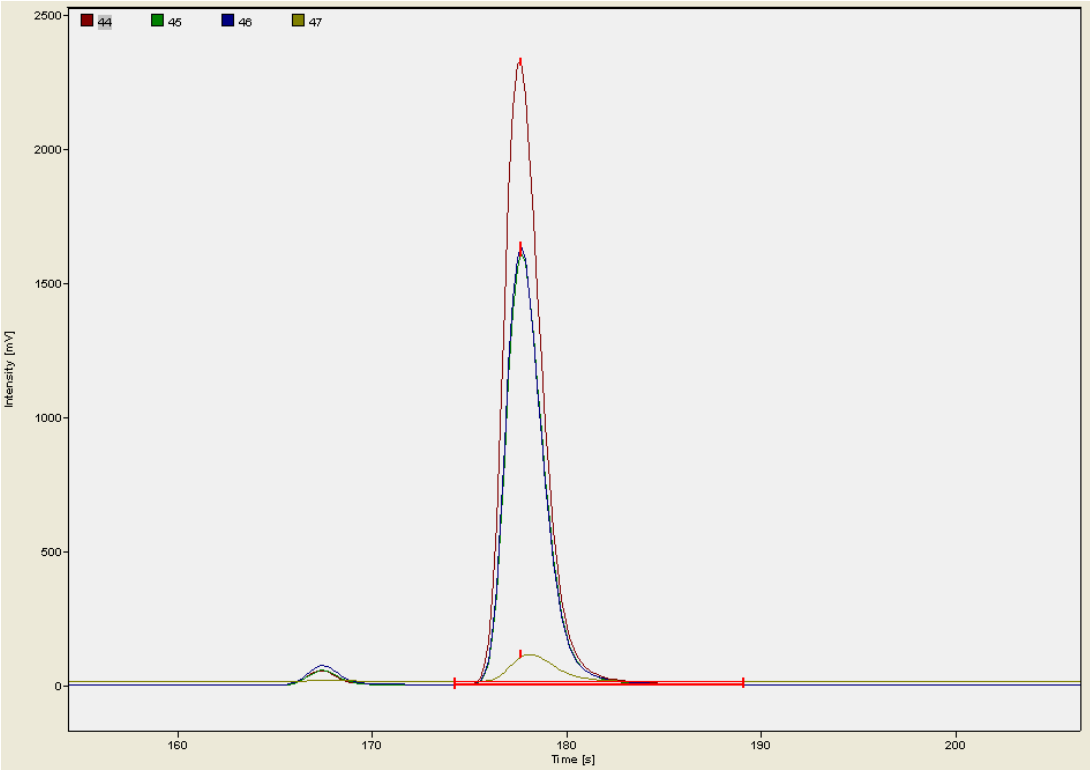

b)

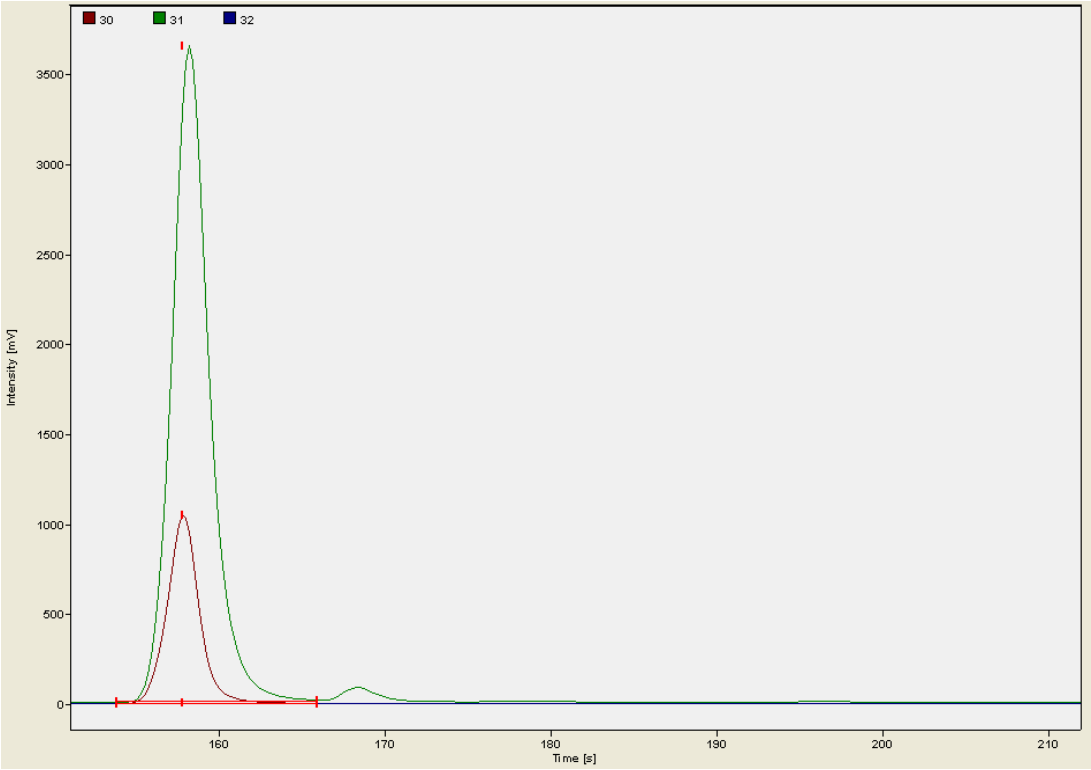

2.3.2 Precision

Measurement precision is estimated as the repeatability of the measured isotopic values for a given air sample determined as the standard deviation of the isotopic ratios from the sample series of 3-5 pairs of 44/45/46 and 30/31 Stheno+CF-IRMS runs. Long-term precision was evaluated by the stability of the measured Niwot Ridge air standard tank isotopic composition over the course of the measurement period (approximately 1 year).

The attention to maximizing precision and addressing the N_2O IRMS measurement challenges resulted in improved precisions in comparison to other measurement systems precisions for atmospheric N_2O, particularly for the site-specific ^{15}N isotopomers for which the Stheno+CF-IRMS system has higher precision than all other systems (Table 2.1). The offline analysis by Kaiser et al (2003) reports slightly better $\delta^{18}O$ precision. The optimization measures discussed in section 2.2 all contribute to some extent to the superior precision in Stheno+CF-IRMS. A significant reason for this improvement is likely due to the fully automated capacity which allows exactly repeatable measurements. The Stheno+CF-IRMS system is software controlled in all aspects so that there is consistency between every measurement cycle performed for a single air sample (3-5 pairs of N_2O^+ and NO^+ IRMS monitoring, in total 6-10 Stheno+CF-IRMS cycles per flask observation) from withdrawl of the sub-sample aliquot from the flask through Stheno pre-concentration, importantly including cryotrapping timing, temperatures, and heating rates; open split interface; and IRMS measurement sequence. The exact repeatability aids in consistency between repeated measurements of a single sample and thus reduces the standard deviation between results. Most notably, though, is the improvement in precision specifically for the ^{15}N site-specific isotopomers. The measured $\delta^{15}N^{\alpha}$ and $\delta^{15}N^{\beta}$ rely upon the less abundant and troublesome monitoring of the m/z 30,31 NO^+ ion fragment. The extreme attention to minimizing the m/z 31

contamination interference throughout the entire Stheno+CF-IRMS system as detailed above is likely a strong factor in this marked precision improvement. Contamination and poor peak separation strongly affects the ability to properly integrate the N_2O peak areas for determination of the isotope ratios, and the presence of m/z 31 fluorocarbon interference is encountered in all of these measurement systems with noted difficulties. The minimization efforts incorporated into Stheno+CF-IRMS successfully lessened the m/z 31 presence and any potential overlap or underlying of the N_2O sample peak, and successfully resulted in a distinct improvement in ^{15}N isotopomers precision.

Table 2.1 Precisions (‰, 1σ) achieved with the Stheno+CF-IRMS system alongside the mean and standard deviation in the baseline air samples measurements by the system. Reported precisions in other N_2O isotopic analysis systems are listed for comparison.

	$\Delta^{15}N^{bulk}$	$\delta^{15}N^{\alpha}$	$\delta^{15}N^{\beta}$	SP	$\delta^{18}O$
Stheno+CF-IRMS precisions (1σ)					
Individual flask sample precision (mean, typical)	*0.05*	*0.11*	*0.14*	*0.21*	*0.10*
Long-term air std stability/precision	*0.06*	*0.17*	*0.22*	*0.38*	*0.14*
MH baseline observations mean (n = 30)	6.60	16.61	-3.41	20.02	44.13
SD	*0.12*	*0.17*	*0.34*	*0.47*	*0.14*
Other measurement systems precisions					
Offline extraction dual inlet analysis (Kaiser et al 2003)	*0.05*	*0.18*	*0.19*		*0.04*
CF-IRMS Max Planck Institute (Rockmann et al 2003, 2005)	*0.06*	*0.3*	*0.3*		*0.09*
CF-IRMS UC Berkeley (e.g. Park et al 2004, Perez et al 2006, Croteau et al 2010)	*0.2*	*0.8*	*0.9*		*0.3*
CF-IRMS Tokyo Institute of Technology (Yoshida & Toyoda 2000, Toyoda et al 2004, 2008, 2009)	*0.1 - 0.5*	*0.5 - 1*	*0.5 - 1*		*0.1 - 0.5*

Tropospheric observations of Mace Head air flask samples show variability larger than the measurement precision, both individual and long-term, for all isotope values, indicating that this system is indeed able to discern subtle signals in the tropospheric composition. Air sample observations categorized as baseline background air originating from the Atlantic or Arctic (n = 30, see Chapter 4 for full criteria) have a standard deviation slightly larger than the precision, possibly capturing seasonal variation or subtle changes in N_2O influences of background air. The non-baseline categorized samples (n = 18) included a few observations significantly removed from the baseline mean isotopic composition by as much as 0.5 to 0.6 ‰, appearing to capture strong influences from surface sources and potentially a stratospheric direct impact. Detailed analysis and assessment of the Mace Head flask air samples are provided in Chapter 4.

Conclusion

The first fully-automated, liquid-cryogen-free pre-concentration device optimized specifically for N_2O isotopic analysis has been successfully coupled to a CF-IRMS system and demonstrates higher-precision and higher-frequency capabilities than other systems for the isotopic analysis of atmospheric N_2O. Making measurements of the tropospheric isotopic composition of N_2O to detect informative signals is a challenge. High-precision capabilities are required to detect subtle signals on long-term, seasonal, and short-term timescales, necessitating an N_2O-tailored isotopic analysis system. The precision needs to be paired with high-frequency capabilities as well to interpret these signals, thereby needing a fully automated, liquid-cryogen-free system to be potentially non-laboratory-bound. The Stheno pre-concentration system uniquely meets these needs, additionally with the careful optimization for N_2O and isotopic analysis thus putting greater confidence in the measured values. Most importantly, the system succeeded in detecting the subtle variation in tropospheric composition at a remote research station.

Stheno measurement precision is significantly superior for the ^{15}N site-specific $\delta^{15}N^{\alpha}$ and $\delta^{15}N^{\beta}$ compositions to that reported in other systems, and among the best for bulk ^{15}N and ^{18}O compositions. The ^{15}N site-specific precision is 2-3 fold better than the best achieved previously by CF-IRMS (Rockmann et al 2005) and with a marked improvement over offline IRMS as well (Kaiser et al 2003). Achieving sufficient precision for N_2O ^{15}N isotopomers has been a challenge for the research community, and the focused attention to maximizing precision and particularly avoiding m/z 31 contamination interference in Stheno+CF-IRMS allowed the system to show great improvement in the measurement capabilities for the very scientifically useful ^{15}N site-specific composition.

In use with tropospheric air flask sample analyses, Stheno+CF-IRMS was able to detect variations in tropospheric composition greater than analytical precision thus capturing the desired N_2O tropospheric signals. The variations existed in background air, and large deviations in non-background air observations were well-within measurement precision capabilities. The outlying observations appear to be capturing useful information about N_2O regional sources, which could yield insight into surface emissions quantification and distribution. Beyond demonstrating the utility of tropospheric observations of N_2O isotopic composition by showing that signals are detectable, the flask observations illustrated that a measurement program of collected air samples returned to the laboratory for analysis is too low-frequency for complete interpretation of the N_2O isotopic composition variation. High-frequency observations will be needed to validate source-receptor relationships in the detected signals, which is now possible with the fully automated in situ capabilities of Stheno.

Part II. Isotope ratio mass spectrometry of nitrous oxide

The Stheno pre-concentration device for isotopic measurements of N_2O in tropospheric air samples was run with an isotope ratio mass spectrometer in continuous flow mode. This sub-chapter gives the isotopic analysis details of the IRMS measurements. The lab had not previously made measurements of N_2O isotopic composition, thus part of this thesis work was to build the robust foundation for such measurements in this specific laboratory space. Given the high need for high-precision in these measurements, there was particular attention given to optimization of the IRMS measurement protocol, referencing, calibration, and additional challenging nuances of site-specific ^{15}N isotopic measurements, and thus it is valuable to provide this information.

2.4 Isotope ratio mass spectrometry of N_2O

In the technique simultaneously developed by Brenninkmeijer & Rockmann (1999) and Toyoda & Yoshida (1999), the molecular ion N_2O^+ is monitored at m/z 44, 45, 46 and the NO^+ fragment ion is monitored at m/z 30, 31 to determine not only $\delta^{15}N^{bulk}$ and $\delta^{18}O$, but also the ^{15}N site-specific isotopomers $\delta^{15}N^{\alpha}$ and $\delta^{15}N^{\beta}$ ($N^{\beta}N^{\alpha}O$). The technique stems from the idea that the NO^+ fragments will contain the N predominately from the central N^{α} ($N^{\alpha}O^+$). The fragmentation into NO^+ ions is only ~1/3 the abundance of the molecular ion N_2O^+ thus the m/z 30 and 31 ion currents are smaller and have lower precision. A small offset correction for the contribution of ^{17}O to masses 31 and 45 applies to atmospheric samples (Brenninkmeijer & Rockmann 1999, Toyoda & Yoshida 1999, Sutka et al 2003).

Fragment ion		m/z	Molecular ion		m/z
$^{14}N^{\beta}\,^{16}O^+$		30	$^{14}N^{14}N^{16}O^+$		44
$^{14}N^{\alpha}\,^{16}O^+$					
$^{15}N^{\beta}\,^{16}O^+$		31	$^{14}N^{15}N^{16}O^+$		45
$^{15}N^{\alpha}\,^{16}O^+$			$^{15}N^{14}N^{16}O^+$		
$^{14}N^{17}O^+$			$^{14}N^{14}N^{17}O^+$		
$^{14}N^{\beta}\,^{18}O^+$	$^{15}N^{17}O^+$	32	$^{14}N^{14}N^{18}O^+$	$^{15}N^{15}N^{16}O^+$	46
$^{14}N^{\alpha}\,^{18}O^+$				$^{14}N^{15}N^{17}O^+$	
				$^{15}N^{14}N^{17}O^+$	
	$^{15}N^{18}O^+$	33		$^{15}N^{15}N^{17}O^+$	47
				$^{14}N^{15}N^{18}O^+$	
				$^{15}N^{14}N^{18}O^+$	
				$^{15}N^{15}N^{18}O^+$	48

Table 2.2 N_2O stable isotope contributions to the IRMS monitored NO^+ and N_2O^+ ions. Ions in gray indicate ions containing two rare isotopes and thus not significantly contributing to that ion mass. m/z 32 is a major fragment ion but is not be utilized because of interference from O_2. Note that the N_2^+ fragment (m/z 28, 29) allows the determination of $\delta^{17}O$ but the achievable precision is only about 0.5 per mil. Conversion of N_2O to O_2 is preferred for $\delta^{17}O$ measurements and thus this continuous flow IRMS measurement scheme does not include $\delta^{17}O$ measurements.

An ion rearrangement process, or scrambling, can occur with the formation of the NO^+ fragment ions in the IRMS ion source which is characteristic of each individual mass spectrometer. The rearrangement causes that not all of the N in the NO^+ ion (m/z 30,31) is from the central (α) N, and instead a small percent of the NO^+ contains the terminal (β) N. This has been attributed to possibly the formation of triangular N_2O^+ within the IRMS source. The scrambling effect tends to be on the order of 8 to 10% in the IRMS systems tested. Rather than a single scrambling factor, here we use the two terms γ, ϰ to account for the difference in ionization of $^{14}N^{15}NO$ and $^{15}N^{14}NO$ in the fractionation and molecular rearrangement that occur during fragment ion formation in the ion source. Gamma (γ) is the relative production of m/z 30 ions from $^{14}N^{15}NO$ and kappa (ϰ) is the relative production of m/z 31 ions from $^{15}N^{14}NO$. When only one factor is used, the assumption is that the ionization of $N^{\beta}N^{\alpha}O$ will occur with the same small amount of $N^{\beta}O^+$ formation irregardless of the N^{β} and N^{α} compositions. The inclusion of two factors in place of the typically used one scrambling factor (e.g. Brenninkmeijer & Rockmann 1999, Yoshida & Toyoda 1999, Rockmann et al 2003a,b, Park et al 2004, etc) improves the accuracy of these measurements. These do not account for the full set of ionization differences between all of the isotopologues as in Westley et al (2007), however this simplification has no effect within the measurement precision.

Kappa and gamma rearrangement factors were determined using the known ^{15}N site specific isotopomer composition of three gases: one a pure N_2O tank calibrated by Tokyo Institute of Technology (S. Toyoda), and two generated from the thermal decomposition of labeled ammonium nitrate, with the NH_4^+ and NO_3^- compositions determined independently (see Part III). The three gases are measured against each other by traditional dual inlet IRMS in a series of analyses, and γ and ϰ are iteratively optimized in equation (3) below to best fit the measured values with the known values.

2.4.1 Calculation of isotopic ratios from raw 45/44, 46/44, and 31/30 ratios

Commonly, N_2O isotopic values are obtained from simplified calculations where $\delta^{18}O$ and $\delta^{15}N^{bulk}$ are obtained from the ratios 45:44 (^{45}R) and 46:44 (^{46}R), and these are used with the 31:30 (^{31}R) ion beam ratio to determine $\delta^{15}N^{\alpha}$, as in Toyoda and Yoshida (1999) and Brenninkmeijer and Rockmann (1999). The value of $\delta^{15}N^{\beta}$ is then calculated from the bulk and alpha compositions given that $\delta^{15}N$ is the average of $\delta^{15}N^{\alpha}$ and $\delta^{15}N^{\beta}$.

Several assumptions go into this simplified calculation about the nature of isotopes. As N_2O isotope research pushes for optimal precision and accuracy capabilities, these simplifications will start to be manifested in the data. Therefore here a more thorough set of relations is used which includes the 2 rearrangement factors and simultaneously calculates each isotope ratio (admittedly still holding some assumptions; see Westley et al (2007) for more thorough theory and calculation).

Laboratory standard cylinders of pure N_2O (section 2.6) with calibrated isotopic compositions are used as transfer references to correct for instrumental conditions and yield isotopic values relative to primary standards air-N_2 for ^{15}N isotopomers and VSMOW for ^{18}O. Sample raw ratios 45/44, 46/44, and 31/30 of integrated peak areas (mVs) are corrected for the exact channel resistor values and ionization/detection variability using the known composition of the reference standard to give *R* ratios of relative ion current signal intensities.

$$\text{raw}R = V45/V44$$
$$R = I45/I44$$
$$I = V/\Omega \rightarrow I45/I44 = [V45/V44] * [\Omega 44/\ \Omega 45]$$

$$R_{sample} = \text{raw}R_{sample} * [R_{standard\_know}/\text{raw}R_{standard}]$$

$R_{standard\_know}$ are the assigned actual ^{46}R, ^{45}R, ^{31}R values of the N_2O reference gas, back calculated from TITech calibrated $\delta^{15}N^{\alpha}$, $\delta^{15}N^{\beta}$, $\delta^{18}O$ values along with the rearrangement factors γ, $\varkappa$ particular to this IRMS.

With the convention designating the central nitrogen as alpha and the outer nitrogen as beta,

$$^{15}R^{\alpha} = [^{14}N^{15}NO]/[^{14}N^{14}NO]$$
$$^{15}R^{\beta} = [^{15}N^{14}NO]/[^{14}N^{14}NO]$$

$\delta^{15}N^{\alpha}$, $\delta^{15}N^{\beta}$, and $\delta^{18}O$ are solved using the following relations, followed with the conversion of $^{15}R^{\alpha}$, $^{15}R^{\beta}$, and ^{18}R ratios to delta values versus air-N_2 or VSMOW:

(1) $$^{45}R = {}^{15}R^{\alpha} + {}^{15}R^{\beta} + {}^{17}R$$

(2) $$^{46}R = ({}^{15}R^{\alpha} + {}^{15}R^{\beta}){}^{17}R + {}^{15}R^{\alpha}{}^{15}R^{\beta} + {}^{18}R$$

(3) $$^{31}R = \frac{{}^{15}R^{\alpha}(1-\gamma) + {}^{15}R^{\beta}(\varkappa) + {}^{15}R^{\alpha}{}^{15}R^{\beta} + {}^{17}R + {}^{17}R^{*}\gamma{}^{15}R^{\alpha} + {}^{17}R^{*}(1-\varkappa){}^{15}R^{\beta}}{1 + \gamma{}^{15}R^{\alpha} + (1-\varkappa){}^{15}R^{\beta}}$$

(4) $$^{17}R/0.0003799 = (^{18}R/0.0020052)^{0.516}$$
(Based on the isotopic ratios of VSMOW reference composition)

The traditional IRMS dual inlet mode was used with pure N_2O gas for the initial IRMS setup and testing, determination of the NO^+ fragmentation rearrangement coefficients specific to this IRMS instrument, referencing of pure N_2O lab standards, and calibration by thermal decomposition of ammonium nitrate. The dual inlet variable volume inlet (also referred to as "bellows") was also used for the reference of air samples admitted via continuous flow mode. Continuous flow mode was used for tropospheric air sample analysis with the Stheno system (Chapter 2, Part I).

Each dual inlet bellows volume is connected to the ion source via a capillary leak to allow slow flow between the bellows and the ion source of the mass spectrometer. Viscous flow through the capillary ensures that gas volumes are not fractionated during measurement because in this flow regime there is no preferential transport of the lighter isotope due to the bulk flow pushing along behind. In the design of modern isotope ratios mass spectrometers, molecular flow can occur below 20 mbar (Brand 1996) wherein mass 44 N_2O moves faster than heavier isotopologues. This results in the bellows getting enriched over time. Careful attention was placed to make sure that pressure in the bellows always remained above 20 mbar.

2.5 IRMS set-up and optimization

The IRMS detector for this study is a MAT253 magnetic sector with 10kV acceleration voltage from Thermo Scientific. In an IRMS, ions 30, 31, 44, 45, and 46 are collected in separate Faraday cups (conductive, metal vessels that neutralize ions which hit them and in response become charged) connected to feedback resistors to achieve sufficient precision at very low abundances. The MAT253 IRMS is equipped with collector cups that do not allow simultaneous monitoring of the 5 desired ions. The strong magnet in the 10 keV MAT253 instrument causes the 30 and 46 ions to separate beyond the ion collector width, thus only smaller 3keV IRMS instruments can allow simultaneous collection. For N_2O isotopic composition, analyses collect ions 44/45/46 followed by 30/31 in sequential IRMS measurements.

The Thermofinnigan MAT253 IRMS used in this work was not previously configured for isotopic measurements of N_2O therefore initial configuration was needed. Mass spectrometer

parameters for N_2O isotopic analysis modes were optimized for linearity, sensitivity, stability, and greatest degree of NO^+ fragmentation. To assess for maximum fragmentation, pure N_2O gas was analyzed over a range of electron energies alternating between monitoring ions m/z 44,45,46 and 30,31. Over the range of electron energies tested, 85 eV gave the highest ion beam intensity (mV) ratio of m/z 30 to 44 (Figure 2.7).

Figure 2.7 N_2O admitted via dual inlet to assess the IRMS electron energy (eV) at which the greatest m/z 30 fragment to m/z 44 ion ratio is attained. Fragment ratios are the mean of eight measurement pairs of successive 44/45/46 and 30/3 monitoring.

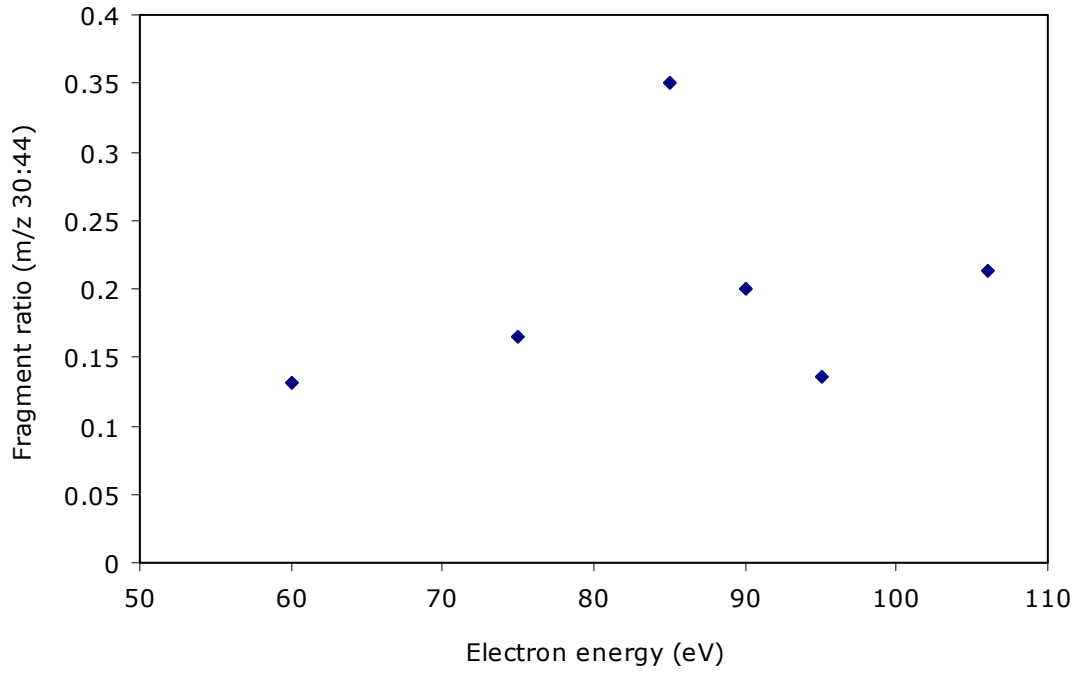

Final configuration parameters for the N_2O^+ and NO^+ monitoring modes are given in Table 2.3, along with the Faraday cup configuration for collection of the respective ions. The m/z 31 ion collection on cup 3 was set to use the amplified resistor channel available for that cup to increase the voltage signal since this corresponds to the rare ^{15}N isotope ion on the already lower abundance NO^+ fragment. Once the optimally tuned configuration for each ion monitoring mode was set it was not changed in case alterations would cause changes in the ion source affecting the NO^+ ion rearrangement factors.

Fragment ion m/z 32 is not used for N_2O isotope ratio analysis since this is the ion for molecular O_2 which is present in instrumental background noise. For this same reason m/z 32 was utilized to assess air leaks, in particular with the instrument in continuous flow mode for the detection of higher than expected levels of O_2 in the He to indicate an air leak in the Stheno+CF-IRMS interface or open split.

Table 2.3 IRMS parameters and cup configuration set for the measurement of N_2O isotopic composition in the two monitoring modes.

	N_2O^+ mode	NO^+ mode
High voltage accelerating potential	9.600KV	9.627 KV
Magnet	5810 steps	4212 steps
Emission	1.5 mA	1.5 mA
Trap	73.3 V	98.5 V
Electron energy	85.018 V	85.018 V

m/z	Cup configuration	Channel resistor (ohms)		m/z	Cup configuration	Channel resistor (ohms)
44	cup2 ch1	3.00E+08		**30**	cup1 ch1	3.00E+08
45	cup3 ch3	3.00E+10		**31**	cup3 ch3 + amplifier	3.00E+11
46	cup4 ch5	1.00E+11		**32**	cup5 ch5	1.00E+11
47	cup6 ch6 + amplifier	1.00E+12				

2.6 Standards

Two high-pressure cylinders of pure N_2O (Airgas, VLSI grade, >99.9999%) were used for IRMS setup and tests, and for reference for continuous flow air sample analyses (Ref I, Ref II). Ref I was calibrated by S. Toyoda on the Tokyo Institute of Technology ^{15}N site-specific scale, which has been accepted in the community as a temporary international reference until an official site-specific N_2O isotope calibration standard exists. Given calibration discrepancies, an independent isotopomer calibration was performed at MIT through the thermal decomposition of ammonium nitrate which matched TITech values within measurement precision (Chapter 2, Part III). For comparative consistency in the N_2O isotopomer community the TITech calibrated values are used rather than our own. Only N_2O Ref II was used during the air sample analyses thus maintaining Ref I as a stable reference source unaffected by fractionation caused by repeated aliquot removal. Ref I composition was calibrated as $\delta^{15}N^{\alpha}$ -0.44 ±0.02‰ (±1σ), $\delta^{15}N^{\beta}$ 1.50 ±0.06‰, $\delta^{15}N^{bulk}$ 0.53 ±0.04‰, $\delta^{18}O$ 40.14 ±0.10‰. N_2O Ref II was referenced to N_2O Ref I by means of 5 separate aliquot pairs taken from Ref II and Ref I cylinders. Each of these aliquot comparisons entailed 4 repeated pairs of 44/45/46 and 30/31 monitoring, and each of these measurement cycles involved 8 sets of paired measurements from the left and right bellows (sample and reference). The 5 independent aliquot pairs account for variation which might occur between cylinder aliquots and in transfer to the bellows. Ref II composition was determined as $\delta^{15}N^{\alpha}$ -0.78 ±0.037‰ (±1σ), $\delta^{15}N^{\beta}$ 0.30 ±0.041‰, $\delta^{15}N^{bulk}$ -0.24 ±0.010‰, $\delta^{18}O$ 40.43 ±0.040‰.

2.6.1 Transfer procedure

The precision and repeatability of isotopic measurements from the dual inlet bellows, whether for dual inlet analysis or for referencing during continuous flow analysis, are subject to error associated with transfer of the pure N_2O reference gas from cylinder to bellows. In dual inlet analysis there is no separation of N_2O from interfering compounds transferred to the bellows from the flasks, or directly to the ion source via other paths. Careful attention was given to the procedure to avoid contamination or isotopic fractionation. In particular contamination is a risk for ambient

air which has relatively high concentrations of CO_2 with nominal mass 44, 45, and 46, and fluorocarbon compounds which produce $^{12}C^{19}F^+$ m/z 31 fragments. These ions interfere with N_2O^+ and NO^+ analyses, respectively. Care was taken to minimize the background air blank for CO_2 before analyses, and avoid contact with Teflon or other common fluorocarbon laboratory materials.

Electropolished stainless steel 2.9L spherical flasks (Biospherics Research Corp, electropolished by Electromatic, Inc) equipped with a bellows valve (Nupro SS-4H) were used to load the pure N_2O reference gases into the bellows volumes. The transfer occurred via a vacuum manifold (Appendix 2.IV) of stainless steel ¼" electropolished tubing vacuumed with a rotary vane pump (ULVAC KIKO Inc) capable of reaching <5 mTorr (thermocouple vacuum gauge, 0-1000 mTorr, Kurt J. Lesker). The transfer flask was connected to the vacuum manifold to which the high pressure N_2O reference tank was permanently connected. The transfer fitting to attach the flask to the vacuum line and dual inlet interface was a stainless steel UltraTorr fitting with butyl o-rings (Marco Rubber) replacing the standard Viton rings to prevent known off-gassing of interfering fluorocarbons from Viton. The butyl material was selected and tested to create a vacuum seal. The ultra high purity regulator model with the pure N_2O reference cylinders (Tescom 74-2400 series) was specified to minimize chances for isotope fractionation and off-gassing of compounds into the pure N_2O stream (non-fluorocarbon Vespel seat, single stage, internally precision electropolished, 5 Ra microinch surface, internally springless, low internal volume).

Following and preceding gas transfer, the vacuum manifold is cleaned with 6 to 8 repetitions of evacuating to <5 mTorr and pressurizing to ~40 psi with Research Plus grade N_2 gas (Airgas, >99.9999%, <0.1 ppm CO_2) affixed to the manifold. The vacuum line between use remained at vacuum pressures to prevent accumulation or condensation on the tubing interior. After use for transfer, flasks are cleared by evacuating to <5 mTorr followed by 3 cycles of pressurizing to ~40 psi with Research Plus grade N_2 gas and evacuating to <5 mTorr, and a final evacuation to <5 mTorr. Evacuated flasks are left evacuated for the approximately 3-4 weeks between measurement sessions, aiding in desorption of any gas which had adsorbed onto the flask walls and was not removed with the "cleaning" procedure. Prior to a measurement session the cleaning procedure is again repeated before filling and equilibrating with the pure N_2O to approximately 200-300 Torr.

2.6.2 Transfer associated drift

During analyses the reference gas in the bellows needs to be periodically replaced due to the reservoir bleed effect (see 'Reference stability' in section 2.7). To minimize the fractionation that will occur with removal of aliquots of N_2O gas from the main reference gas cylinders, ideally the number of transfer flasks taken is minimized by filling the bellows multiple times from the same transfer flask. Likewise, removal of aliquots from the transfer flask into the bellows offers opportunity for fractionation and drift in the reference gas isotopic composition from that transfer flask. It was therefore valuable to assess the number of aliquots that could be taken from a 2.9L transfer flask without drift in the reference gas isotope ratio.

Stability in the isotopic composition of flasks aliquots was assessed with repeated dual inlet analyses of successive aliquots from the same pure N_2O transfer flask. In testing, a maximum of 7 aliquots were taken sequentially from the flask and analyzed by dual inlet in four sets of alternating six m/z 44,45,46 monitoring mode and six m/z 30,31 monitoring mode. Plotted in Figure 2.8 are the differences from the mean isotopic composition ($\Delta = \delta - \delta_{mean}$) for the 7 aliquots sequence. For all isotope ratios there was no drift in composition over 7 aliquots and minimal deviations from the mean isotopic composition. The standard deviation of the aliquot analyses was $\delta^{15}N^{\alpha}$ 0.034‰, $\delta^{15}N^{\beta}$ 0.034‰, $\delta^{15}N^{bulk}$ 0.007‰, $\delta^{18}O$ 0.010‰. This indicates that at least 7 aliquots can be taken from a single N_2O reference transfer flask without concern of the reference gas ratio changing, and

thus 7 aliquots maximum was adopted for all procedures throughout this IRMS research which all depend upon a pure N_2O reference gas from the bellows volume inlet, e.g. calibration, rearrangement coefficient determination, and air sample measurement.

Consistency in the isotopic composition between flasks transferred via this procedure was assessed with the calibration of Ref II to Ref I (above) giving 1σ uncertainties of $\delta^{15}N^{\alpha}$ 0.037‰, $\delta^{15}N^{\beta}$ 0.041‰, $\delta^{15}N^{bulk}$ 0.010‰, $\delta^{18}O$ 0.040‰.

Figure 2.8 Difference ($\Delta = \delta - \delta_{mean}$) from the mean isotopic composition following a series of 7 aliquots taken sequentially from the same flask. None of the isotopic values show the presence of drift towards a more enriched or depleted composition with aliquot removal up to 7.

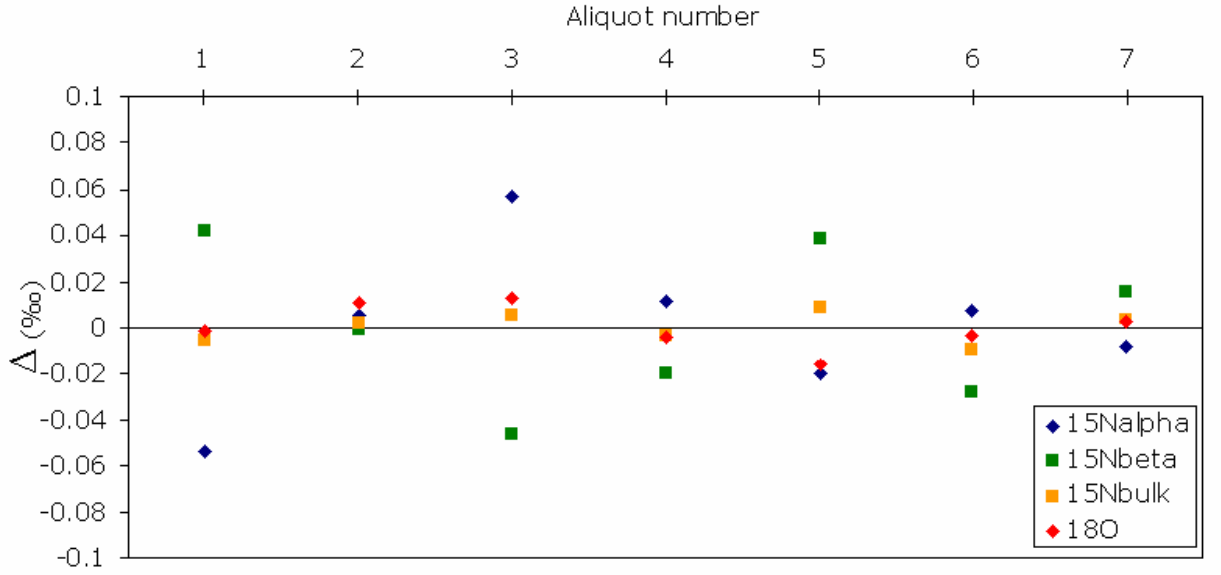

2.7 Continuous flow analysis and optimization

Whereas dual inlet analysis requires micromole quantities of N_2O gas (corresponding to hundreds of liters of ambient tropospheric air), continuous flow analysis allows nanomole quantities to be analyzed with similar precision. At tropospheric mole fractions (~320 ppb) there are approximately 13.1 nmol/L of N_2O at STP. The typical protocol for Stheno+CF-IRMS draws 420 mL of air sample per analysis, corresponding to ~5.5 nmol N_2O.

2.7.1 Reference method

Unlike the referencing procedure for dual inlet analysis, in continuous flow analysis it is impossible to reference the sample to a standard gas with a precisely known composition which has been processed and introduced in the same manner. For atmospheric samples a number of methods exist for referencing continuous flow analyses with precisely known pure gas, including admission from the bellows inlet or via a separate open split capillary onto the CF helium flow with or without diverting the sample stream effluent. In a detailed assessment of various referencing methods for CF analyses of CO_2, Merritt et al (1994) found no difference in the precisions between the methods which used pure reference gas. In the current study the dual inlet bellows were used to inject precisely controlled flows of pure N_2O reference gas resulting in square reference peaks onto the

helium stream preceding and following open split sample effluent admission. At the start of a measurement sequence reference gas is admitted from the bellows for peak centering. Two admissions of reference gas (Ref II) from the bellows onto the helium stream are admitted to the ion source for measurement to ensure reference gas values have stabilized. A third reference gas admission then occurs immediately prior to sample peak elution followed by a fourth reference gas measurement. The mean measurement of the third and fourth reference peaks which bracket the sample is used for reference.

The width of the square reference peak (determined by the length of time the valve to the bellows is open) was tested to determine the optimum time and if non-linearities existed related to peak width and therefore peak area. The choice of peak width is balanced between (a) wanting to shorten analysis time, minimize wasting of reference gas, and more closely match the narrow Gaussian transient sample peak width, and (b) countered by the desire to have an accurate and reproducible peak ratio reading. A variety of peak widths were tested in measurement series. Small but significant differences for ^{45}R, ^{46}R, and ^{31}R were found for short peak widths of 5 or 10 seconds as compared to the chosen 20 second reference gas admission, meaning the per mil difference between the 5 or 10 second peaks with the 20 second peaks was near or sometimes larger than the desired level of precision. At reference gas admission times of 15 seconds or greater this dependence of isotope ratios upon peak width became flat and yielded constant values. A reference gas admission time of 20 seconds was safely chosen for the continuous flow analyses.

The height of the square reference peak is determined by the pressure inside of the bellows. This was determined to optimally be 30.2 to 30.3 mbar, which was safely >20 mbar pressure to maintain viscous flow (and therefore non-fractionating flow) through the capillary to the IRMS ion source, but low enough to be at similar height as the Gaussian transient sample peaks, within 300 mV for the 44 and 30 ion peak heights (see Figure 2.4). For each continuous flow measurement, the bellows volume was manually adjusted so that the admission of the pure N_2O pulse was at 30.2 or 30.3 mbar (control was not fine enough to distinguish these pressures).

2.7.2 Reference stability (drift)

The reservoir bleed effect is the phenomena in which drift can occur as gas is repeatedly admitted from the bellows to the ion source, and has potential drift specific to the continuous flow reference procedure. To minimize the concern for drift, at the start of each day of air sample analyses a new reference gas aliquot was introduced into both the left and right bellows and mixed. Reference gas used for air samples was divided between both bellows.

To test the drift over the course of one day of continual air sample analyses, reference gas was admitted to both bellows and mixed. A single bellows was then used for an entire day of Stheno+CF-IRMS analyses equating to 14 continuous flow runs (7 N_2O^+ mode, 7 NO^+ mode). This represents the maximum usage since in practice those 14 runs would be shared by both bellows therefore each bellows would only be pulled from by half of this amount. At the end of the day of analyses the bleed effect drift for the used bellows was assessed by comparing the used "sample" bellows with the untouched "reference" bellows. Analysis comparing the two was necessarily done in continuous flow mode, and was achieved by alternating four 20 second pulses of gas from each bellows on the background CF helium stream. This was done once in N_2O^+ mode and once in NO^+ mode and was compared to the initial "zero" test performed in the same manner at the start of the day to account for random differences between the two bellows from the start.

The drift over one day of CF analyses for the measured values δ45, δ46, and δ31 were <+0.01‰, +0.01‰, and -0.04‰, respectively, negligible given continuous flow measurement precision.

2.7.3 Sample size linearity

IRMS instruments can have sample size non-linearities, whereby the measured isotope ratios are dependent upon the size of the sample vs. the reference peak, particularly at smaller voltages and of concern for the fragment 30/31 ion (Rockmann et al 2003a). The effect most likely originates in mixing of the sample and reference gas in the ion source (IAEA Tecdoc 825, Allison & Francey), but could also be related to non-linearities in the IRMS electronics or, specific for N_2O fragment analysis, due to slight constant baseline contamination for m/z 31 (CF^+). The relationships between sample size and measured δ values were checked through a series of analyses of the Niwot Ridge (NR) reference air drawing different volumes through Stheno, thus resulting in variable peak sizes measured by the IRMS and a range of "effective mole fractions". This analysis is shown in Figure 2.9. The upper plot illustrates the compositions relative to total 44,45,46 or 30,31 peak area (Vs) and shows comparison of the relative peak area sizes for N_2O^+ and NO^+ analyses. The lower plot is the same analysis composition data but in terms of effective mole fractions to align the N_2O^+ and NO^+ analyses for the same sampled air together and to put this analysis in the context of performance with tropospheric air samples of variable mole fractions. The effective mole fractions were determined by defining the 420 ml sampling volume from Stheno at the calibrated NR mole fraction and scaling other peak sizes. Over the range 298 to 439 ppb the isotope ratios show no sign of non-linearity, much exceeding the linearity requirements for tropospheric samples collected at Mace Head with N_2O mole fractions ranging 322.5 to 325.1 ppb. No linearity correction is therefore required over the small mole fraction range of tropospheric air N_2O. The small variations in δ45, δ46, and δ31 are similar to the variation between repeated measurements of tropospheric air in constant 420 ml volumes, showing a slightly higher standard deviation in δ31 than the mean air sample repeated analyses (1σ = 0.16 ‰ in variable volumes, 1σ = 0.11‰ in constant volume).

Figure 2.9 IRMS isotope ratios over a range of air standard sample sizes to assess for a sample size dependent non-linearity in the measured isotopic composition. Same analysis runs in both upper and lower plots.
Effective mole fraction = scaled to peak size of known NR air standard mole fraction in the Stheno 420ml air aliquot volume.

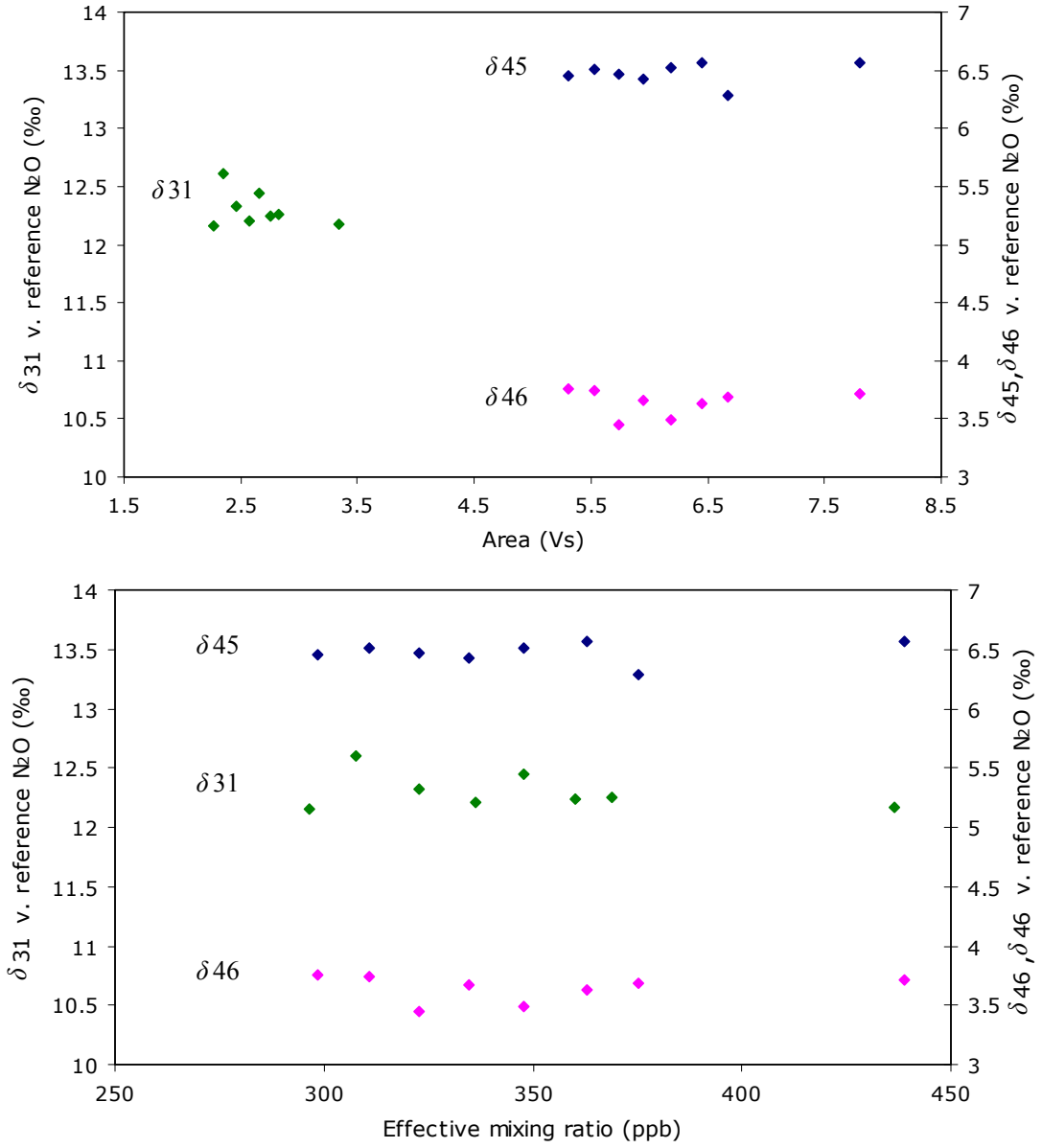

2.8 Precision

2.8.1 Dual inlet analysis

A bellows "zero" test, in which the same gas is introduced into both dual inlet bellows and measured against each other, accounts for contributions to variability and precision in the IRMS instrument itself, but does not include external variability in use of the dual inlet. A thorough assessment of dual inlet mode precision for the regular use of a reference gas includes the variations involved in the transfer of the reference N_2O gas from the cylinders to the IRMS; both the small differences which will exist between samples of the cylinder and variations in transfer conditions

which may affect the actual aliquot introduced into the IRMS. For the referencing of Ref II to Ref I, the five independent cylinder aliquot pairs account for this transfer variation as well, and thus the standard deviation of this suite of dual inlet analyses serves as a more thorough and appropriate proxy for dual inlet referencing precision.

$\delta^{15}N^{\alpha}$ 1σ = 0.037‰
$\delta^{15}N^{\beta}$ 1σ = 0.041‰
$\delta^{15}N^{bulk}$ 1σ = 0.010‰
$\delta^{18}O$ 1σ = 0.040‰

These precisions correspond to variation in the measured values of δ45-N_2O 1σ = 0.010‰, δ46-N_2O 1σ = 0.039‰, δ31-N_2O 1σ = 0.022‰. Despite expectations that the 31/30 measurement should be less precise than the 46/44 measurement because of the ~1/3 abundance of the NO^+ fragment ion, there tends to be actually worse precision for δ46-N_2O than δ31-N_2O in this instrument. This lower δ46 precision is carried over to the continuous flow measurements as well indicating a central IRMS cause. For the tropospheric air sample analyses, for all flask observations the mean individual 1σ precisions were δ45-N_2O 1σ = 0.081‰, δ46-N_2O 1σ = 0.130‰, δ31-N_2O 1σ = 0.115‰. The 46/44 value primarily reflects the ^{18}O composition (Table 2.2). The lower than expected 46/44 precision for this IRMS instrument is likely what is causing to the relatively low $\delta^{18}O$ precision in the Stheno+CF-IRMS continuous flow analyses compared to that achieved for $\delta^{15}N^{bulk}$ (0.10 and 0.05‰, respectively, for individual flask measurement, 0.14 and 0.06‰ for long-term air standard), which in other IRMS systems have similar precisions (Table 2.1). This is possibly related to the fundamental ion collector cup arrangement on this IRMS which is configured for m/z 46 ion collection with a resistor nominally one-third smaller than the m/z 31 amplified channel (Table 2.3).

2.8.2 Continuous flow analysis

In Part I of this chapter the precision of the continuous flow mode for tropospheric air analyses via Stheno was assessed and discussed in terms of the variation in repeated measurements of the air samples and air standard long-term. A component of that variability in the measured air sample values is due to the precision of the referencing method. The repeatability and precision of the pure N_2O reference for sample measurements via the dual inlet bellows can be partially proxied by the dual inlet precision. However, this does not include the effects of the reference entering the ion source alongside the CF helium stream. To assess the CF referencing technique precision, the same 20 second reference gas pulse sequences as in the continuous flow procedure were alternated between the left and right bellows in four cycles of four left/right sets in both N_2O^+ and NO^+ modes. Each left bellows pulse was referenced to the following right bellows pulse. The standard deviation is taken to represent the uncertainty in the continuous flow reference pulse composition administered from the dual inlet bellows. Standard deviations were well below the variation seen in repeated sample analyses (δ45 1σ <0.01‰, δ46 1σ = 0.02‰, δ31 1σ = 0.02‰) indicating that referencing variation is not contributing significantly to the uncertainty in air sample measurements and supporting the proper functionality of the IRMS instrument while in continuous flow mode with a steady stream of helium.

2.8.3 Theoretical shot-noise-limit precision

The shot-noise-limit is the theoretical maximum attainable performance for a measurement by mass spectrometer which based upon ion collection statistics is the precision which would be obtained if the ion beam was the only source of noise, thus limited only by electronic noise (Merritt & Hayes 1994, Hayes 2002)

If it is assumed that the reference isotopic ratio is about the same as the sample ratio, then

σ^2 (shot-noise-limit) = $2\text{x}10^6\ (1+R)^2/(EMR)$ (Merritt & Hayes 1994)
where R = ion current (isotope) ratio,
E = IRMS efficiency (=molecular ions at collector/molecules introduced),
M = number of molecules introduced

Here the product EM is the number of ions collected, which would be the peak integrated ion current divided by the electronic charge of an electron ($q_e = 1.6\text{x}10^{-19}$ C). The integrated peak signal output by IRMS in units Vs (A) divided by the feedback resistor of the ion channel on the IRMS ($R_f = 3\text{x}10^8\ \Omega$) gives the integrated ion current. Substituting $EM = A/(R_f q_e)$ and using $R = 0.00774$ from the N_2O reference 45/44 ratio

$$\sigma^2 = 9.6\text{x}10^{-5}\,(1+R)^2/(AR) = 0.0126\ /\ A$$

For a typical sample m/z 44 peak area of 5.7 Vs this results in a shot noise limit precision of 0.047‰. Accounting for signal-to-noise characteristics of typical ion-current-amplifier systems, the maximum theoretical attainable precision is 84% of the shot-noise-limit for ^{15}N (Hayes 2002). This results in a theoretical maximum precision of 0.056‰. If the sample and reference peak areas are not assumed to be equivalent, then the above equation becomes

$$\sigma^2 = \tfrac{1}{2}\,(0.0126)\ /\ ((1/A_{\text{sample}}) + (1/A_{\text{reference}}))$$

Because of the larger peak area of the reference peak, this improves the theoretical maximum precision (accounting for signal-to-noise) to 0.042‰ for the isotopic composition based upon the molecular ion m/z 44,45,46.

For $\delta^{15}N^{bulk}$, this is not significantly below the achieved precision with Stheno+CF-IRMS, typically near 0.05‰ for an individual sample, and thus we cannot expect this precision to improve significantly by CF-IRMS techniques.

Substituting $R = 0.004316$ for the N_2O reference 31/30 ratio, and using the typical smaller sample peak area of 2.4 Vs, the theoretical maximum precision is 0.085‰. The typical $\delta^{15}N^{\alpha}$ standard deviation for repeated measurements of an individual sample is 0.11‰, which is fairly close to the theoretical maximum. $\delta^{15}N^{\beta}$ typical standard deviation is 0.14‰ and holds more room for improvement.

Overall, the comparison between the precisions achieved with Stheno+CF-IRMS (Table 2.1) and the theoretical maximum point to the success of Stheno+CF-IRMS. Any pre-concentration and sample processing system will inherently contribute sources of noise and it is generally assumed that the actual precision of the CF-IRMS will be within a factor of 2 of the shot noise limit. The proximity of the achieved precision of Stheno+CF-IRMS to the theoretical maximum is much better than a factor of 2 and suggests that little further improvement using CF-IRMS technology without substantially increasing the sample size.

Part III. Nitrous oxide (N_2O) isotopomer calibration by the ^{15}N site-specific synthesis of N_2O from ammonium nitrate (NH_4NO_3)

Note that these works on calibration and the resultant data are not finalized and are in progress in a joint collaboration project with S. Toyoda at the Tokyo Institute of Technology (TITech). It is included in this thesis for completeness as the accuracy of the calibration scale is an important issue for any use of N_2O site-specific isotopic composition data in the community, and considerable research has gone into these issues. This section summarizes the motivation and studies conducted thus far.

2.9 N_2O isotopomer calibration

Currently there is no international reference standard for N_2O isotopic composition. For calibration of bulk $\delta^{15}N$ and $\delta^{18}O$ compositions, references can be traced to primary standards by chemical conversion of N_2O to N_2 and CO_2, but all ^{15}N site-specific information is lost. Thus, the calibration of $\delta^{15}N^{\alpha}$ and $\delta^{15}N^{\beta}$ has proven problematic. The two groups that originally established the IRMS method to determine the site-specific ^{15}N use two different calibration scales, with largely different results. In site-specific analysis, Kaiser et al (2004) report tropospheric composition as $\delta^{15}N^{\beta}$ = -15.8 ±0.6‰ and $\delta^{15}N^{\alpha}$ = 29.2 ±0.6‰. Toyoda and Yoshida (1999) (T&Y1999) measured $\delta^{15}N^{\beta}$ = -2.35‰ and $\delta^{15}N^{\alpha}$ = 16.35‰. This wide discrepancy (corresponding to a site preference difference of over 25‰) is due to their different approaches to calibration: Kaiser et al through use of mixtures of the reference gas with trace additions of isotopically labeled N_2O, and Toyoda & Yoshida by synthesis of N_2O via thermal decomposition of isotopically labeled ammonium nitrate (NH_4NO_3).

Subsequent analysis of these techniques has garnered support for the thermal decomposition of NH_4NO_3, despite the drawback of messy wet chemistry and potential for fractionation during the thermal decomposition to N_2O (Westley et al 2007, Griffith et al 2009). The calibration discrepancy stems from isotope effects associated with the formation of the NO^+ fragment ion in the IRMS ion source. The different N_2O isotopomers form fragments at slightly different rates which are affected by the specific ion source conditions, thus making the gas tracer addition calibration technique impossible to replicate on a different IRMS. In the thermal decomposition approach, information on the relative abundance of N_2O gas isotopomers is obtained independently through the measurement of the isotopic composition of the NH_4NO_3 starting material.

Support for the T&Y1999 site-specific calibration was gained with a study using IRMS-independent optical Fourier-Transform-Infrared (FT-IR) spectroscopy methods (Griffith et al 2009), however considerations of the accuracy and precision of the procedures and FT-IR capabilities suggest the conclusion may be premature. For determining calibration, it is the absolute *accuracy* which is most important rather than the precision of the number returned. Optical methods in general are able to quantify isotopologue amounts precisely, however absolute accuracy is uncertain and relies upon external calibration. In the above FT-IR analysis of N_2O, the reported precision for the site preference is high at 0.1‰, however the analysis has an absolute accuracy of only 3%, or 30‰, due to inaccuracies in the line parameters, instrumental effects, and difficulties in fitting spectra, which is insufficient to distinguish the <30‰ calibration discrepancy between T&Y1999 and Kaiser et al (2004). Uncertainty is also brought into the approach which uses similar manometric mixing to that of Kaiser et al (2004) to create the needed external calibration source which then hinges upon inexact manometric mixing abilities. Additionally, a "significant calibration offset" is

applied to the site preference of -20 to -28‰ because of systematic instrument errors which were quantified in admittedly non-ideal ways, quite significant relative to the T&Y1999 and Kaiser et al (2004) discrepancy and without which would have resulted in a calibration matching Kaiser et al (2004). The order of magnitudes of these uncertainties in the accuracy warrant questioning whether there is a conclusive answer to the calibration of N_2O isotopomers.

An independent calibration test by the ammonium nitrate thermal decomposition reaction was performed as a part of this thesis for a number of reasons.

- *Validation of the T&Y1999 scale.* Repeating the process of NH_4NO_3 thermal decomposition-based N_2O calibration provides an important inter-laboratory check on the validity and accuracy of this calibration method given its potential for error. It has only been repeated once by Westley et al (2007). Only after such verifications of the calibration procedure occur can it be accepted as an international community standard, which is a necessary foundation for use of any N_2O isotopomer data, including N_2O isotopic composition in the troposphere not only for this short-term thesis pilot study but also for the long-term aim of continuous in situ observations into the future.
- *Assessment of the absolute accuracy and robustness of the method.* The method of ammonium nitrate calibration technique for N_2O is contingent upon the often cited but not recently verified assumption that there is not site-specific fractionation in the thermal decomposition reaction and the relative positions of the N atoms in NH_4NO_3 are preserved in the formation of NNO (Friedman & Bigeleisen 1950). The Griffith et al (2009) FTIR review of the calibration only concludes to say that the T&Y1999 calibration is more accurate than that method by Kaiser et al (2004), but as discussed above, there are large absolute accuracy uncertainties in the FTIR analysis of significant magnitude and no insight into the true accuracy of N_2O calibration. For the long-term use of this calibration for N_2O isotopomer research, a through evaluation of isotope fractionation in the decomposition of NH_4NO_3 is required.
- *Calibration across a wider range of N_2O isotopic ratios.* The original T&Y1999 site-specific calibration is tied to only one ammonium nitrate isotopic composition: $\delta^{15}NH_4^+$ = -5.54 ±0.23‰ (N^β-N_2O product), $\delta^{15}NO_3^-$ = -3.55 ±0.04‰ (N^α-N_2O product). To have an adequate calibration scale for use in varied applications of N_2O isotopes as will be needed for future progress on, e.g., source signature characterization, it is necessary to perform the calibration procedure across a range of compositions. A range is also needed to adequately assess for any fractionation in the decomposition reaction and to fully account for the specific instrument non-linearities and performance.

Any reference gas value provided by the T&Y1999 scale is essentially normalized to the original NH_4NO_3 composition in T&Y1999. Repeating the ammonium nitrate technique with approximately the same reactant NH_4NO_3 composition to calibrate a reference gas would then yield the same calibration result as T&Y1999, regardless of the presence of any fractionation effects that could be occurring. When comparing the thermal decomposition results to an N_2O reference calibration by T&Y1999, isotopic composition at the T&Y1999 value is then defined as having zero fractionation in the N_2O gas product.

Westley et al (2007) repeated the ammonium nitrate calibration across a range of five isotopic compositions. Any fractionation or other artifact in the calibration procedure would likely be small, though important, and it is not clear whether there was potentially any fractionation across the individual compositions in the results of Westley et al 2007 as only the mean of the five was reported. The associated standard deviation (Table 2.5) is fairly significant relative to the magnitude of the composition and leaves uncertainty in the exact distribution of calibration results for each separate original isotopic ratio.

- *Building capacity at the MIT lab to produce N_2O of different isotopic compositions.* MIT is continuing with N_2O isotopic analysis research and this is a useful skill to have for use isotopically distinct N_2O in, e.g., comparisons between instruments or tests of instrument performance, particularly for those in development.
- *Building capacity at the MIT lab to monitor the long term stability of the N_2O calibration scale.*
- *Supporting and furthering calibration rooted in a physical solid material which can be preserved and verified with a different means of isotope measurement.*

2.10 Methods

The thermal decomposition of ammonium nitrate to produce N_2O occurs by the reaction:

$$NH_4NO_3 \rightarrow NNO + 2H_2O$$

With the side reaction (Shah and Oza 1932):

$$5\ NH_4NO_3 \rightarrow 4N_2 + 9H_2O + 2HNO_3$$
$$4HNO_3 \rightarrow 2H_2O + 2NO_2 + O_2$$

The explosive reaction results in products different than thermal decomposition, with very little N_2O (Saunders 1921).

$$8NH_4NO_3 \rightarrow 16H_2O + 2NO_2 + 4NO + 5N_2$$

The principle according to Friedman and Bigeleisen (1950) is that the relative position of the N atoms with respect to O does not change, thus NO_3^- composition determines N^α and NH_4^+ composition determines N^β. For the calibration of N_2O, the isotopic composition of the NH_4NO_3 salt reactant is determined by independent methods giving the advantage of the N_2O gas being characterized separately from N_2O gas measurements and rooted in a physical material.

A range of six isotopically labeled NH_4NO_3 batches are created following the recrystallization procedure of Westley et al (2007) using tracer additions of ^{15}N-ammonium chloride or ^{15}N-sodium nitrate to produce reactants with a range of $^{15}NH_4$ (N^α) and $^{15}NO_3$ (N^β) compositions spanning N_2O analysis needs to give site preferences ranging -43‰ to 23‰ (Table 2.4).

The isotopic compositions of the NH_4NO_3 salts are determined by several methods. Initially this was performed at MIT through an online elemental carbon-nitrogen analyzer (EA) coupled with IRMS (Delta V, Thermofinnigan) for batches A-E. To determine the site-specific composition, the ammonium nitrate is precipitated with sodium tetraphenylborate (tpb) as in Westley et al (2007) to form NH_4-tbp. The NO_3^- composition of NH_4NO_3 is calculated using the EA results for NH_4NO_3 bulk ^{15}N and NH_4-tpb. Each batch of NH_4NO_3 and NH_4-tetraphenylborate is analyzed by EA in five replicates alongside primary standards NH_4SO_3 (IAEA-N-2) (20.41‰ v. air-N_2), KNO_3 (IAEA-NO-3) (4.72‰ v. air-N_2), and Acetanilide (Costech) (-7.0‰ v. air-N_2). The amount weighed for each EA sample (including standard materials) was adjusted according to the number of nitrogens and molecular weight of the compound to obtain approximately equivalent peak sizes (32 Vs, range 27 to 37 Vs). Within this range replicate samples were checked that there was no delta value dependence on sample size. All samples and standards were measured on the EA-IRMS referenced to pure gas N_2. A linear calibration correction curve was generated with the IAEA standard materials, which was then applied to the NH_4NO_3 and NH_4-tpb. Acetanilide is an in-house standard to check instrument functioning and consistency throughout all EA runs (including both N_2 and

CO_2), but not used in the calibration curve. EA-IRMS analysis has high accuracy with the direct comparison to primary standards. Precisions are somewhat poor, ~0.1 to 0.4 ‰.

The six NH_4NO_3 batches additionally were analyzed by the traditional distillation/combustion method by first separating the NH_4^+ by base/acid distillation, and then using Devarda's alloy to reduce the NO_3^- to ammonium ion (Toyoda & Yoshida 1999, Mariotti et al 1978, Mulvaney et al 1993). Ammonium ion solutions are oxidized to N_2 on a vacuum manifold and the N_2 is collected on molecular sieve 5A with liquid nitrogen for $\delta^{15}N$ analysis by IRMS to determine $\delta^{15}N\text{-}NH_4^+$ and $\delta^{15}N\text{-}NO_3^-$. For the nitrate ion converted to ammonium samples, m/z 32 (O_2) and 40 (Ar) signals on the IRMS suggested contamination by air for samples A-E and thus these $\delta^{15}N\text{-}NO_3$ results were discarded. Similarly, the F batch in the NH_4^+ analysis showed suspected air contamination and was discarded. Courtesy T. Yamazaki at TITech, the $\delta^{15}N\text{-}NO_3$ compositions were measured by the denitrifier method. Subsequent analysis at TITech was done to check bulk NH_4NO_3 composition by EA.

Ammonium nitrate thermal decomposition

Multiple procedures and variations for the thermal decomposition of NH_4NO_3 were attempted prior to the final optimized procedure, with input from Saunders (1922), Shah & Oza (1932), Friedman & Bigeleisen (1950), Feick & Hainer (1954), Rosser et al (1963), Brower et al (1989), Toyoda & Yoshida (1999), Westley et al (2007), M. Westley (personal communication), and S. Toyoda (personal communication). Variables adjusted to obtain complete decomposition and good N_2O yield included oven temperature, reaction time, heating rate, cooling rate, performed in sealed tubes or directly on a vacuum line, and with or without addition of water to initiate the reaction.

The optimized thermal decomposition procedure followed:

- Pre-combust Pyrex tubes at 250 °C overnight.
- Weigh approximately 200-700 μmol (~15-50 mg) of each batch of NH_4NO_3 in 9 mm Pyrex tubes
- Affix tube to a custom-made vacuum manifold (rotary vane pump, ULVAC) with an UltraTorr fitting and evacuate gas phase to < 5mTorr
- Seal glass tubes by torch to create a reaction tube ~10-15 cm long, 5 mmID.
- Place the tubes in a 25 °C oven and slowly ramp heat 1.3 °C/min to 270 °C (approximately 3 hours). Hold oven temperature at 270 °C for 10 hours for the thermal decomposition reaction, then use a slow controlled cooling 1.3 °C/min to 25 °C.

Results of this optimized procedure yielded complete elimination of the NH_4NO_3 solid and a colorless gas of 82-90% yield N_2O.

Ideally all of the NH_4NO_3 would proceed by the first reaction above yielding only nitrous oxide and water, however possible products are N_2 (boiling point -195.8 °C), O_2 (-182.3 °C), NO (-151.8 °C), N_2O (-88.6 °C), H_2O, NO_2 (21.3 °C), HNO_3 (83 °C). N_2O was separated from other products on a vacuum manifold (Appendix 2.IV). A "tube cracker" was designed using Swagelok flexible tubing, on one end welded to ¼" SS tube to attach to the vacuum line via an UltraTorr fitting, the other end fitted with a 3/8" bored-through UltraTorr fitting to accommodate the reaction tubes. Notched Pyrex reaction tubes were inserted halfway and following evacuation of the dead air space, the flexible tubing was bent to crack the tubes. Contents are released first into a loop submersed in a dry-ice/ethanol bath (~-72 °C) to trap H_2O, NO_2, and HNO_3. N_2O was then trapped in a liquid nitrogen (LN_2) loop. Remaining incondensable gas (N_2, O_2) was approximated with a calibrated electronic manometer. Incondensable gas was then pumped from the system. Of the likely possible byproducts, NO is possibly trapped in the liquid nitrogen with N_2O. Toyoda &

Yoshida (1999) examined for the presence of NO following similar reaction conditions and found that the amount of NO formed is negligible. Trapped N_2O was heated and double distilled over the dry ice/ethanol loop to purify of H_2O, NO_2, and HNO_3 which may have migrated to the LN2 trap from the warmer dry-ice/ethanol trap. The purified N_2O was quantified using the manometer and known volumes of the vacuum line. N_2O was then trapped using LN_2 in a 15 cm electropolished ¼" stainless steel close-ended tube equipped with a bellows valve (SS-4H).

Two to four successful N_2O decomposition products resulted for each NH_4NO_3 batch. Batches A-E were analyzed at MIT, batch F at TITech. Separated N_2O gas was analyzed by dual inlet on the MAT253 IRMS (see Chapter 2, Part II) measured against N_2O Ref I, which isotopic composition was determined directly by S. Toyoda on their calibration scale but all calibration analyses are done using no prior site-specific isotopomer information of the N_2O reference gas.

2.11 Results & Discussion

Yield of N_2O was calculated using the molar amount of NH_4NO_3 starting material and the manometrically determined molar amount of resulting N_2O gas after separation on the vacuum manifold (MKS Baratron manometer). Yields of N_2O spanned 82 to 90%, but most were essentially equivalent within precision in the range of 86-88%. Within the range of reactant amounts and vessel volumes, no relation was found between the yield and 1) amount of NH_4NO_3, 2) vessel size, or 3) the combined effects of these on interior compression/expansion.

Table 2.4 Ammonium nitrate batches ^{15}N-labeling preparations and compositions (‰). Site-specific values determined by the distillation/combustion method ($\delta^{15}N$-NH_4^+,-NO_3^-), denitrifier method ($\delta^{15}N$-NO_3^-), and EA at TITech with those taken for each sample as noted in text and table notes. "SP" calculated from site-specific values in the table as NO_3 – NH_4 composition difference. Bulk values given for TITech EA and derived average NH_4, NO_3 composition.

Ammonium nitrate batch	Preparation	$\delta^{15}N$-NH_4 (N^β) (dist/comb)	$\delta^{15}N$-NO_3 (N^α) (denitrifier)	$\delta^{15}N$-NH_4NO_3 EA	derived	"Site preference"
A	NH_4NO_3	-1.92	1.49	-0.70	-0.22	3.41
B	NH_4NO_3 + $^{15}NO_3$	-2.27	21.09	9.21	9.41	23.36
C	NH_4NO_3 + $^{15}NO_3$	-2.36	14.04[b]	5.84	NA	16.40
D	NH_4NO_3 + $^{15}NH_4$	17.22	1.63	9.77	9.43	-15.59
E	NH_4NO_3 + $^{15}NH_4$	8.34	3.27	5.96	5.81	-5.07
F	NH_4NO_3 + $^{15}NH_4$	39.56[a]	-3.50	18.03	NA	-43.06

a. Derived from dist/comb $\delta^{15}N$-NO_3^- results and TITech EA bulk composition
b. Derived from dist/comb $\delta^{15}N$-NH_4^+ results and TITech EA bulk composition

The $\delta^{15}N^{bulk}$-N_2O and $\delta^{15}N$-NH_4NO_3 compositions are not dependent upon the site-specific calibration and therefore provide a check of experimental and instrumental performance and potential fractionation. $\delta^{15}N$-NH_4NO_3 was measured directly by EA at both MIT and TITech, and is also calculated as the mean NH_4- and NO_3^- compositions from the distillation/combustion (dist/comb) and denitrifier methods. The results across the 6 different isotopic compositions are generally described by a straight line (Figure 2.10), but some do not fall on a 1:1 line for $\delta^{15}N^{bulk}$ in the resultant N_2O gas vs. $\delta^{15}N$-NH_4NO_3 which suggests some aspect of the process for those samples there was fractionation. The fractionation could be possibly related to the thermal

decomposition reaction itself, N_2O product processing and measurement, or NH_4NO_3 sample processing and composition analysis.

Figure 2.10 Comparison of initial ammonium nitrate reactant bulk ^{15}N compositions as determined by various methods with that in the product N_2O gas. The line in the plot marks 1:1 correspondence. See Table 2.4 for A through F batch descriptions.

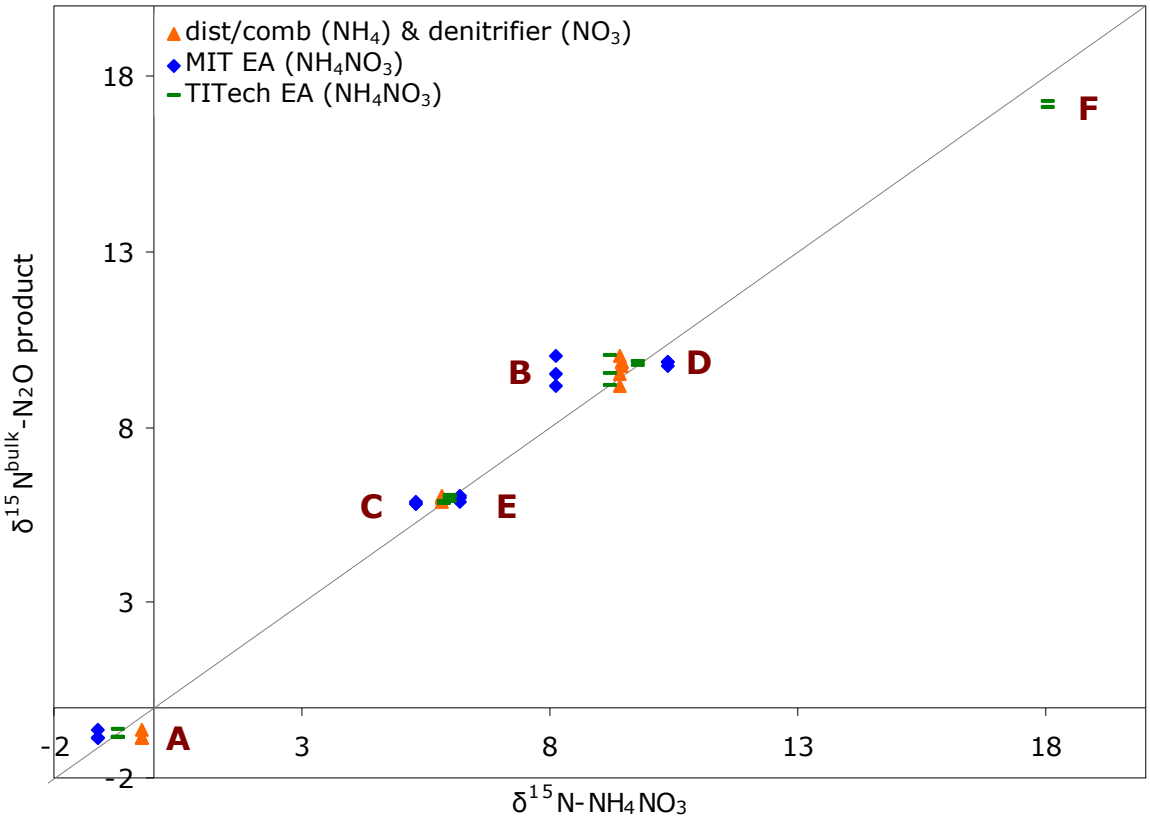

The discrepancy between ammonium nitrate compositions determined by the various methods suggests that the NH_4NO_3 composition analysis aspect of the calibration procedure is fractionating, at least. It does not rule out potential fractionation also occurring within a common procedural aspect including the thermal decomposition reaction itself. The combination of the dist/comb and denitrifier methods yields results which fit the 1:1 line well for all except for the outlying C batch (not plotted), suggesting that there was some procedural error with this C sample analysis by the denitrifier method. The samples analyzed by combustion on the MIT EA seem to follow diverging lines with the $^{15}NH_4$-labeled D and E (resulting in a negative ammonium nitrate "site preference" = $\delta^{15}NO_3$ - $\delta^{15}NH_4$) showing different behavior than the $^{15}NO_3$-labeled B and C (resulting in a positive "SP") (Table 2.4). A is unlabeled and has a slightly positive "SP" and could be seen to follow either behavior. The results for these corresponding batches with the TITech EA fit the 1:1 line quite well, except for the relatively ^{15}N bulk-enriched and extremely negative "SP" batch F. Westley et al (2007) found different results with their thermal decomposition using the online carbon-nitrogen analyzer (e.g. EA) approach to measure bulk NH_4NO_3 composition. The $\delta^{15}N^{bulk}$-N_2O and $\delta^{15}N$-NH_4NO_3 relationship well-followed a straight line with a slope close to 1 and only a small y-axis offset (slope = 0.992, offset = -0.793, R2 = 0.996). Given the good bulk ^{15}N correspondence between NH_4NO_3 and product N_2O by TITech EA for the same batches, and the

match of the EA analysis procedure used in Westley et al (2007), and likewise for the combined dist/comb and denitrifier results, the MIT EA analysis results are set aside due to suspected EA combustion reactor problems at the time of measurement. Resulting site-specific compositions of batches A-F are presented in Table 2.4 using the likely valid data from the dist/comb method for δ^{15}N-NH_4^+ for A-E and δ^{15}N-NO_3^- for F, and denitrifier method for δ^{15}N-NO_3^-, with noted alternatives for samples C and F. The accurate and confident determination of the site-specific NH_4NO_3 composition has proven to be a significant cause of uncertainty in this calibration procedure. Values presented are pending and will be confirmed by follow-up analyses.

For completeness of this effort towards N_2O isotopomer calibration, the composition of MIT Ref I was assessed using the NH_4NO_3 site-specific composition values given in Table 2.4 for batches A-E. These N_2O thermal decomposition products were measured at MIT by IRMS dual inlet analysis versus MIT Ref I giving oxygen ^{17}R, ^{18}R compositions for each batch N_2O product. It was assumed no fractionation in the thermal decomposition reaction and the site-specific $^{15}R^{\alpha}$ and $^{15}R^{\beta}$ compositions were determined with knowledge of the starting δ^{15}N-NO_3^- and δ^{15}N-NH_4^+ compositions. To perform the ^{15}N isotopomer calibration of MIT Ref I, using the ^{31}R equation in Part II of this chapter a "known" ^{31}R value for each batch and IRMS analysis is calculated and used as the reference gas composition with the raw measured ^{31}R of MIT Ref I. This ^{31}R for Ref I is used with the previously known non-site-specific ^{45}R and ^{46}R compositions and the $^{15}R^{\alpha}$ and $^{15}R^{\beta}$ are iteratively calculated as described in Part II.

The mean calibrated isotopomer composition determined from 40 synthesized N_2O products from five (A-E) ammonium nitrate batches covering a range of compositions is $\delta^{15}N^{\alpha}$ = 0.71‰ and $\delta^{15}N^{\beta}$ = 0.35‰ with 1σ uncertainty of 0.88‰, corresponding to a site preference of 0.35‰ (Table 2.5).

The resulting calibration does not align with the values determined on the T&Y1999 scale within the estimated standard deviation uncertainty. The values are close in distance to the uncertainty estimate, however distinctively having opposite signs for alpha and site preference. This is quite different than the results in the re-calibration by Westley et al (2007) (Table 2.5). The derived composition for their reference N_2O gas was quite close to the T&Y1999 determined value. However, the standard deviations here and in that study are essentially the same and we do not know how the derived compositions were spread amongst their five isotopically different NH_4NO_3 batches.

Table 2.5 Comparison of isotopomer calibration of two references gases determined by the thermal decomposition of NH_4NO_3 method. Left side are the results of this study for MIT N_2O Ref I (±1σ) as compared with the values determined by S. Toyoda at the Tokyo Institute of Technology. For comparison, on the right side are the results for the calibration by NH_4NO_3 study by Westley et al (2007).

	MIT Ref I composition		***Westley et al (2007) reference composition***	
	This study	**T&Y value**	***Westley***	***T&Y value***
$\delta^{15}N^{\alpha}$	0.71 ±0.88‰	-0.44 ±0.02‰	*2.82 ±0.92‰*	*3.01 ‰*
$\delta^{15}N^{\beta}$	0.35 ±0.88‰	1.50 ±0.06‰	*0.25 ±0.92‰*	*0.77 ‰*
SP	0.35 ‰	-1.95 ‰	*2.57 ‰*	*2.24 ‰*

In this study, within the mean calibrated Ref I composition the calibration values determined separately by each NH_4NO_3 starting batch show a range of results in relation to the T&Y1999 Ref I value (Table 2.6). Though the standard deviation across all samples is relatively large (0.88‰), within each NH_4NO_3 batch there is little deviation. The ammonium nitrate batch calibrations appear to follow 2 paths: The A, D, and E results are generally consistent with each other having positive

$\delta^{15}N^{\alpha}$, negative $\delta^{15}N^{\beta}$, and positive SP, all on similar orders of magnitude; and the B and C batches have similar negative alpha, positive beta, and negative site preference. Interestingly, this is the same delineation between batches as observed with the MIT EA results comparing the ^{15}N bulk compositions between NH_4NO_3 reactant and N_2O product (Figure 2.10) where B and C have distinctively positive site preferences, even though the MIT EA results were put aside and not used for any analysis. B and C determined isotopomer calibration for MIT Ref I are much in line with the S. Toyoda measured calibration value of the Ref I.

Table 2.6 Isotopomer calibration results for MIT Ref I showing the separate results for each ammonium nitrate batch. n refers to the number of successful thermal decomposition reactions and N_2O product isotopic analyses on the IRMS comparing MIT Ref I.

	MIT Ref I $\delta^{15}N^{\alpha}$-N_2O	MIT Ref I $\delta^{15}N^{\beta}$-N_2O	MIT Ref I SP
A (n = 4)	1.11 ±0.02 (1σ)	-0.05 ±0.02	1.15
B (n = 3)	-0.31 ±0.10	1.37 ±0.10	-1.69
C (n = 3)	-0.14 ±0.02	1.20 ±0.02	-1.34
D (n = 3)	1.62 ±0.04	-0.56 ±0.04	2.19
E (n = 3)	1.26 ± 0.02	-0.20 ±0.02	1.46
T&Y value	-0.44 ±0.02	1.50 ±0.06	-1.95

For use in the present research the MIT Ref I calibration by S. Toyoda on the T&Y1999 scale were adopted for consistent comparisons within the research community. However, the confounding results warrant further investigation.

2.12 Future work

In collaboration with S. Toyoda, work is continuing into the robustness of N_2O isotopomer calibration by the thermal decomposition of ammonia nitrate. The goals of this collaboration include answering the accuracy and precision of isotope measurements in NH_4 and NO_3, evaluation of isotope fractionation (and other artifact, if any) in the decomposition of NH_4NO_3, and improving the accuracy and precision of the calibration over a span of isotopic compositions. It is important to verify that there is not site-specific dependent fractionation occurring that would cause isotopic ratios to become progressively more off-scale as they have a more distinct composition from the original ammonium nitrate calibration.

Many analyses of the NH_4NO_3 starting material have been conducted by various methods, however there is still uncertainty in the site-specific compositions of the six ammonium nitrate batches and they should be reanalyzed. For the long term needs of this scientific community for N_2O isotopomer calibration, as exists for other standard materials, ideally several NH_4NO_3 official samples of differing compositions would be analyzed by several separate laboratories by different methods. The ability to accurately determine the isotopic composition of NH_4NO_3 is not trivial and current methods leave room for fractionation and experimental error.

Additional work towards understanding and improving the N_2O site-specific calibration should include repeated thermal decomposition reactions from the batches and analysis of both the N_2O and the smaller fraction of N_2 compositions in the resulting gas, as the original thermal decomposition and N_2O product analyses have not been checked and repeated yet. The N_2O gases

prepared from these several isotopically-distinct NH_4NO_3 batches should also be used to calibrate several working N_2O standards with variable isotopic compositions themselves.

In further investigation of composition-dependent isotopic fractionation, it would be worthwhile to inquire with M. Westley about the calibration results specific to each original isotopically distinct batch in her study. The standard deviation for the mean across all five batches in her result is the same as achieved here (Table 2.5), and indeed in this study there is question of site-specific fractionation in the thermal decomposition from the results between different batches—batches B and C with highly positive "site preferences" having a distinct calibration result from samples A, D, and E with negative or positive "site preference" near zero.

With the ongoing development of optical methods for N_2O isotopic measurements at MIT (in collaboration with Aerodyne, Inc), there is potential for utilization of the alternative measurement techniques to assist with the site-specific isotopomer calibration of N_2O. However, the absolute accuracy of optical methods is limited and N_2O isotopomer research must rely upon a strong calibration anchor, such as the physical material of NH_4NO_3 salts.

Chapter 2 References

Brand WA (1995). PreCon: a fully automated interface for the pre-GC concentration of trace gases in air for isotopic analysis. *Isotopes Environ Health Stud* 31: 277-284.

Brand W (1996). High precision isotope ratio monitoring techniques in mass spectrometry. *J Mass Spectrom* 31: 225-235.

Brenninkmeijer CAM & Rockmann T (1999). Mass spectrometry of the intra-molecular nitrogen isotope distribution of environmental nitrous oxide using fragment-ion analysis. *Rap Commun Mass Spectrom* 13: 2028-2033.

Brower KR, Oxley JC & Tewari M (1989). Evidence for homolytic decomposition of ammonium nitrate at high temperature. *J Phys Chem* 93(10): 4029-4033.

Cliff SS & Thiemens MH (1994). High-precision isotopic determination of the $^{18}O/^{16}O$ and $^{17}O/^{16}O$ ratios in nitrous oxide. *Anal Chem* 66: 2791-2793.

Coplen TB, Bohlke JK & Casciotti KL (2004). Using dual-bacterial denitrification to improve $d^{15}N$ determinations of nitrates containing mass-independent ^{17}O. *Rapid Commun Mass Spectrom* 18: 245-250.

Croteau P, Atlas EL, Schauffler SM, Blake DR, Diskin S & Boering KA (2010). Effect of local and regional sources on the isotopic composition of nitrous oxide in the tropical free troposphere and tropopause layer. *J Geophys Res* 115: D00J11.

Feick G and Hainer RM (1954). A Temperature-limiting mechanism in the thermal decomposition of ammonium nitrate. *Nature* 173: 4416.

Ferretti DF, Lowe DC, Martin RJ & Brailsford GW (2000). A new gas chromatograph–isotope ratio mass spectrometry technique for high-precision, N_2O-free analysis of $\delta^{13}C$ and $\delta^{18}O$ in atmospheric CO_2 from small air samples. *J Geophys Res* 105: 6709-6718.

Fisher R, Lowry D, Wilkin O, Sriskantharajah S & Nisbet EG (2006). High-precision, automated stable isotope analysis of atmospheric methane and carbon dioxide using continuous-flow isotope-ratio mass spectrometry. *Rapid Commun Mass Spectrom* 20: 200-208.

Friedman L & Bigeleisen J (1950). Oxygen and nitrogen isotope effects in the decomposition of ammonium nitrate. *J Chemical Physics* 18: 1325-1331.

Griffith DWT, Parkes SD, Haverd V, Paton-Walsh C & Wilson SR (2009). Absolute calibration of the intramolecular site preference of ^{15}N fractionation in tropospheric N_2O by FT-IR spectroscopy. *Anal Chem* 81(6): 2227-2234.

Kaiser J, Park S, Boering KA, Brenninkmeijer CAM, Hilkert A & Rockmann T (2004). Mass spectrometric method for the absolute calibration of the intramolecular nitrogen isotope distribution in nitrous oxide. *Anal Bioanal Chem* 378: 256-269.

Kaiser J, Rockmann T & Brenninkmeijer CAM (2003). Complete and accurate mass-spectrometric isotope analysis of tropospheric nitrous oxide. *J Geophys Res* 108 (D15): 4476.

Kaiser J, Engel A, Borchers R & Rockmann T (2006). Probing stratospheric transport and chemistry with new balloon and aircraft observations of the meridional and vertical N_2O isotope distribution. *Atmospheric Chemistry and Physics* 6: 3535-3556.

Kim KR & Craig H (1990). Nitrogen-15 and oxygen-18 characteristics of nitrous oxide: A global perspective. *Science* 262: 1855-1857.

Mariotti A, Letolle R & Guillemot J (1978). Analyse isotopique de l'azote au niveau des abondances naturelles. *Analusis* 6: 421-425.

McIlvin MR & Casciotti KL (2011). Fully automated system for stable isotopic analyses of dissolved nitrous oxide at natural abundance levels. *Limnol Oceanogr: Methods* 8: 54-66.

Meier-Augenstein W, Brans W, Hoffmann GF & Rating D (1994). Bridging the information gap between isotope ratio mass spectrometry and conventional mass spectrometry. *Biological Mass Spectrometry* 23: 376-378.

Merritt DA, Brand WA & Hayes JM (1994). Isotope-ratio-monitoring gas chromatography-mass spectrometry: methods for isotopic calibration. *Org Geochem* 21(6/7): 573-583.

Merritt DA, Hayes JM & Marias DJD (1995). Carbon isotopic analysis of atmospheric methane by isotope-ratio-monitoring gas-chromatography mass-spectrometry. *J Geophys Res* 100: 1317-1326.

Miller JB, Mack KA, Dissly R, White JWC, Dlugokencky EJ & Tans PP (2002). Development of analytical methods and measurements of $^{13}C/^{12}C$ in atmospheric CH_4 from the NOAA/CMDL global air sampling network. *J Geophys Res* 107(D13): 4178.

Miller BR, Weiss RF, Salameh PK, Tanhua T, Greally BR, Muhle J & Simmonds PG (2008). Medusa: A sample preconcentration and GC/MS detector system for in situ measurements of atmospheric trace halocarbons, hydrocarbons and sulfur compounds. *Anal Chem* 80: 1536 -1545.

Mohn J, Wachter H, Tuzson B, Sigrist MW & Emmenegger L (2008). Nitrous oxide isotopomer determination with a quantum cascade laser based spectrometer. Workshop on eddy covariance flux measurements of CH_4 and N_2O exchanges, Hyytiälä, Finland, 8-11th April 2008.

Mohn J, Guggenheim C, Tuzson B, Vollmer MK & Emmenegger L (2009). A liquid nitrogen-free preconcentration unit for measurements of ambient N_2O isotopomers by QCLAS. *Atmos Meas Tech Discuss* 2: 3099-3126.

Mulvaney RL. Mass Spectrometry. *In* Nitrogen Isotope Techniques, Knowles R & Blackburn TH, Editors. Academic Press: San Diego, 1993; pp 11-57.

Nevison CD, Kinnison DE & Weiss RF (2004). Stratospheric influence on the tropospheric seasonal cycles of nitrous oxide and chlorofluorocarbons. *Geophys Res Lett* 31: L20103.

Park SY, Atlas EL, Boering KA (2004). Measurements of N_2O isotopologues in the stratosphere: Influence of transport on the apparent enrichment factors and the isotopologue fluxes to the troposphere, *J Geophys Res* 109: 462-464.

Perez T, Garcia-Montiel D, Trumbore S, Tyler S, De Camargo P, Moreira M & Piccolo M & Cerri C (2006). Nitrous oxide nitrification and denitrification N-15 enrichment factors from Amazon forest soils. *Ecological Applications* 16: 2153-2167.

Prinn, R *et al.* (2000). A history of chemically and radiatively important gases in air deducted from ALE/GAGE/AGAGE. *J Geophys Res* 105: 17751-17792.

Rockmann T, Kaiser J, Brennickmeijer CAM & Brand WA (2003a). Gas chromatography/isotope-ratio mass spectrometry method for high-precision position-dependent ^{15}N and ^{18}O measurements of atmospheric nitrous oxide. *Rapid Commun Mass Spectrom* 17: 1897-1908.

Rockmann T, Kaiser J & Brennickmeijer CAM (2003b). The isotopic fingerprint of the pre-industrial and the anthropogenic N_2O source. *Atmospheric Chemistry and Physics* 3: 315-323.

Rockmann T, Kaiser J, Brennickmeijer CAM & Brand WA (2003c). Gas chromatography/isotope-ratio mass spectrometry method for high-precision position-dependent ^{15}N and ^{18}O measurements of atmospheric nitrous oxide. *Rapid Commun Mass Spectrom* 17: 1897-1908.

Rockmann T & Levin I (2005). High-precision determination of the changing isotopic composition of atmospheric N_2O from 1990 to 2002. *J Geophys Res* 110: D21304.

Rosser WA, Inami SH & Wise H (1963). The kinetics of decomposition of liquid ammonium nitrate. *J Phys Chem* 67: 1753.

Ryall DB & Maryon RH (1998). Validation of the UK Met Office's NAME model against the ETEX dataset. *Atmospheric Environment* 32: 4265-4276.

Saunders HL (1922). The decomposition of ammonium nitrate by heat. *J Chem Soc* 698: 121.

Schnyder H, Schäufele R & Wenzel R (2004). Mobile, outdoor continuous-flow isotope-ratio mass spectrometer system for automated high-frequency ^{13}C- and ^{18}O-CO_2 analysis for Keeling plot applications. *Rapid Commun Mass Spectrom* 18: 3068-3074.

Shah MS & Oza TM (1932). The decomposition of ammonium nitrate. *J Chem Soc*: 725- 736.

Sutka RL, Ostrom NE, Ostrom PH, Breznak JA & Gandhi H (2003). Nitrogen isotopomer site preference of N_2O produced by *Nitrosomonas europaea* and *Methylococcus capsulatus* Bath. *Rapid Commun Mass Spectrom* 17: 738-745.

Tanaka N, Rye DM, Rye R, Avak H & Yoshinari T (1995). High precision mass spectrometric analysis of isotopic abundance ratios in nitrous oxide by direct injection of N_2O. *International Journal of Mass Spectrometry and Ion Processes* 142: 163-175.

Toyoda S & Yoshida N (1999). Determination of nitrogen isotopomers of nitrous oxide on a modified isotope ratio mass spectrometer. *Anal Chem* 71: 4711-4718.

Toyoda S *et al.* (2004). Temporal and latitudinal distributions of stratospheric N_2O isotopomers. *J Geophys Res* 109: D08308.

Toyoda S, Yamamoto S, Arai S, Nara H, Yoshida N, Kashiwakura K & Akiyama K (2008). Isotopomeric characterization of N_2O produced, consumed, and emitted by automobiles. *Rapid Commun Mass Spectrom* 22: 603-612.

Toyoda S, Iwai H, Koba K & Yoshida N (2009). Isotopomeric analysis of N_2O dissolved in a river in the Tokyo metropolitan area. *Rapid Commun Mass Spectrom* 23: 809-821.

Turatti F (2001). Isotopic characterisation of atmospheric nitrous oxide fourier transform infrared spectroscopy, Ph.D thesis, Dept of Chemistry, University of Wollongong, (http://ro.uow.edu.au/theses/1160).

Westley MB, Popp BN & Rust TM (2007). The calibration of the intramolecular nitrogen isotope distribution in nitrous oxide measured by isotope ratio mass spectrometry. *Rapid Commun Mass Spectrom* 21: 391-405.

White JWC, Ferretti DF, Vaughn BH, Francey RJ, Allison CE (2002). Stable isotope measurements of atmospheric CO_2. *In*: Stable isotope measurement techniques for atmospheric greenhouse gases, IAEA-TECDOC-1268.

Yoshida N & Toyoda S (2000). Constraining the atmospheric N_2O budget from intramolecular site preference in N_2O isotopomers. *Nature* 405: 330-334.

Chapter 3: Regional simulations of nitrous oxide isotopic composition at Mace Head

Introduction

Nitrous oxide is one of the major greenhouse gases and a significant contributor to the destruction of the ozone layer in the stratosphere, yet its global budget is currently not well-constrained. Sources are predominantly from microbial production in soils and less so the oceans, with natural microbial sources making up ~2/3 of the total source, balanced by loss in the stratosphere by photolysis and reaction with $O(^1D)$. Natural sources have been augmented by human agriculture, fertilization, and other fixed-nitrogen pollution and run-off, in addition to smaller but still significant industrial sources, which has caused an increase in tropospheric mole fractions from pre-industrial ~270 ppb to currently around 324 ppb. The growth rate in Mace Head, Ireland over the past ~15 years has held fairly consistently around 0.7 ppb/y (Nevison et al 2011, Manning et al 2011). Beyond general knowledge of the global budget and likely causes of increase, there is significant uncertainty in source magnitudes and distribution, even more so on a regional basis. Inverse modeling efforts using N_2O mole fraction data cite that much of this uncertainty is brought about from uncertainty in the mixing between the troposphere and stratosphere where N_2O loss occurs (Hirsch et al 2006, Huang et al 2008).

N_2O has a small observed seasonal cycle with an amplitude ranging from ~0.3 ppb to 0.9 ppb over the past 15 years (Nevison et al 2011). Seasonality in N_2O could be affected by a number of seasonally-varying controls such as biogeochemical surface sources, ocean thermal gas fluxes, tropospheric transport mechanisms, and stratosphere-to-troposphere mixing of N_2O-depleted air. Observations and modeling studies have supported different controls between the Northern and Southern Hemispheres as well as between specific locations within a hemisphere. In published analyses of N_2O tropospheric mole fractions in measurements and models, seasonal stratosphere-troposphere exchange has been found as a significant control on the small seasonal cycle of N_2O in the Northern Hemisphere mid-latitudes (Levin et al 2002, Liao et al 2004, Nevison et al 2004, 2007, 2011, Jiang et al 2007). The efficient quasi-horizontal STE by eddy motions in the NH mid-latitudes mean that 67-81% of the stratospheric air in the NH free troposphere originates from exchange between 30-70°N (Liang et al 2009). The importance of the seasonal downward flux of stratospheric air into the lower troposphere has been regarded as likely a major control particularly at Mace Head (Nevison et al 2004, Nevison et al 2007, Jiang et al 2007, Liang et al 2008, Ishijima et al 2010, Nevison et al 2011), but smaller contributions from other effects are likely playing a role as well. Specifically at Mace Head, model simulations of N_2O mole fractions without including stratospheric loss show the seasonal cycle in phase with both observations and the hypothesized stratospheric seasonal influence for both N_2O and CFCs, suggesting that tropospheric transport has seasonal effects which will be difficult to separate from the stratospheric seasonal signal (Nevison et al 2007). Discriminating the complete suite of controls on the seasonal cycle will yield significant insight into the budget of N_2O.

Acquisition of N_2O isotopic data to accompany the mole fractions have the potential to aid in distinguishing amongst sources, troposphere transport mechanisms, stratospheric mixing, and other N_2O-related processes by providing additional information to separate the controls in N_2O cycling which the mole fraction metric alone is too coarse to detect. Different sources bear different isotopic signatures on N_2O, and the major surface source, soil, tends to be ^{15}N and ^{18}O isotopically depleted compared to the troposphere. The isotopically light surface sources and are balanced by

^{15}N- and ^{18}O-enriched N_2O in the stratosphere. Generally the tropospheric composition has been regarded as constant in present-day (with a small long-term trend due to the anthropogenic source), and as such has been used as a transfer standard to compare measurements (e.g. Park et al 2004, Croteau et al 2010). The concept of balancing N_2O isotopic composition in the troposphere has been applied on a global level to confirm rough balance with sources magnitudes (e.g. Rahn & Wahlen 2000, Yoshida & Toyoda 2000, Toyoda et al 2002, Rockmann et al 2003, Park et al 2004), but no previous models exist which assess subtle variations in the tropospheric isotopic composition. The utilization of N_2O isotopes in the troposphere has never yet been fully applied to short-term variability, seasonal cycles, nor to variability on a more specific regional scale, which is needed to be able to specifically define N_2O emissions and anthropogenic influences spatially and to conduct emissions attribution exercises.

N_2O isotopologue measurements in the troposphere thus far are scarce, but suggest that the ability of current measurement precision is at the cusp of being able to interpret and distinguish isotopic signals. A detailed forward modeling effort is thus very desirable to determine the nature and magnitude of expected isotopic signals to indicate the required level of precision for instrumentation development. Additionally, quantitative interpretation of isotopic data is not straightforward and can be aided by the development of a companion forward model (Alexander et al 2005), thus construction of a base regional model will provide a valuable structure for future observation interpretation.

Measurement precisions (1σ) attainable for air sample analysis by isotope ratio mass spectrometry with the newly developed Stheno+CF-IRMS system (see Chapter 2) for the ^{15}N and ^{18}O mono-substituted isotopologues are approximately: $\delta^{15}N^{\alpha}$ 0.11‰, $\delta^{15}N^{\beta}$ 0.14‰, and $\delta^{18}O$ 0.10‰, and the derived $\delta^{15}N^{bulk}$ ($=(\delta^{15}N^{\alpha}+\delta^{15}N^{\beta})/2$) 0.05‰ and SP ($=\delta^{15}N^{\alpha}-\delta^{15}N^{\beta}$) 0.21‰. These precisions are better than or match those reported in other IRMS systems (e.g. Yoshida & Toyoda 2000, Kaiser et al 2003, Rockmann et al 2005, Park et al 2004, Croteau et al 2011), particularly with superior ^{15}N site-specific precision, and the Stheno+CF-IRMS optimized system may represent the limit of precision which can be achieved by IRMS technology for tropospheric air samples. Optical methods currently in development show promise of improved precision capabilities, with projected 1σ precisions for the Stheno+QCL (Quantum Cascade Laser with pre-concentration, MIT and Aerodyne Research, Inc) of ±0.025‰ for the individual isotopomers $\delta^{15}N^{\alpha}$ and $\delta^{15}N^{\beta}$, and ±0.05‰ for $\delta^{18}O$ (±1σ). The model results are thus examined in terms of current and projected measurement precision capabilities.

This chapter will address the potential for the isotopic composition of N_2O in the troposphere to inform the budget on a regional perspective through the development and application of a forward model of regional tropospheric N_2O isotopic composition centered at the Mace Head, Ireland Atmospheric Research Station (53.32°N, 9.90°W).

Mace Head provides a particularly useful location for interpreting N_2O budget and isotopic composition. Its synoptic situation on the Ireland west coast has it receiving westerly background air from across the Atlantic Ocean and from the Arctic ~50% of the time to allow assessment of the background NH troposphere, while also receiving influence from the east over the UK and Europe ~35%, with the remaining fraction being of local, mixed, or southern origin. Isotopic data would be particularly useful for regions such as Europe where strong agricultural soil, natural soil, and industrial sources are in close proximity and across national borders where emissions attribution is now of political interest. Mace Head is also situated in the Northern Hemisphere high latitudes where the stratospheric downward mixing into the troposphere is particularly strong, thus bringing a more prominent stratospheric loss isotopic signature. Correlations in N_2O mole fractions with CFCs in seasonal maxima and minima suggest shared controlling factors, and have been used to

deduce that the observed N_2O seasonal mole fraction cycle is largely controlled by the seasonal stratospheric downflux of N_2O- and CFC-depleted air (Nevison et al 2004, Nevison et al 2011). The Mace Head N_2O mole fraction seasonal cycle has a broad spring maxima (Feb-Mar) and sharp late summer minima (July-Aug-Sep). Data and global modeling analyses have pointed to stratospheric and tropospheric transport as both contributing to this cycle, but with considerable uncertainties in degree and the possible influence from other controls (Jiang et al 2007, Nevison et al 2007, Nevison et al 2011).

This regional isotopic model will examine a full annual cycle at time stamps (j = 56) corresponding to non-continuous flask air samples collected regularly from the Mace Head, Ireland monitoring station starting November 2009 through January 2011 (see Chapter 4). The model serves to assess N_2O isotopic composition expected variations and their magnitudes in response to different signals at Mace Head station by exploring parameter space in model scenarios. In this study, the model base is idealized and not intended to be accurate enough to interpret actual individual observations, particularly given the episodic nature of N_2O source emissions. The major influences on N_2O isotopic composition and mole fractions in the troposphere at Mace Head, which would cause significant variability or modulate a seasonal cycle, are (i) large-scale tropospheric transport affecting background air, (ii) stratosphere-troposphere exchange (STE) affecting background air, and (iii) regional surface source emissions. The main goal of this model is to simulate tropospheric N_2O isotopic composition resulting from the major controllers of N_2O in the atmosphere. These factors are addressed individually in the next sections.

3.1 Methods

3.1.1 Model framework

The (i) long-distance transport background, (ii) stratospheric influence, and (iii) surface source emissions are modeled to affect the troposphere through the mass balance and isotope mass balance of background and regional contributions,

$$C_{MH,j} = C_{bg,j} + C_{regional,j} \quad (1)$$

$$\delta_{MH,j}\, C_{MH,j} = \delta_{bg,m}\, C_{bg,j} + \delta_{regional,j}\, C_{regional,j} \quad (2)$$

where MH refers to the simulated observation at each time stamp j at Mace Head and 'regional' emissions are added to the background 'bg' composition which includes stratosphere seasonal effects. The following sections describe the determination of each of the variables. $C_{bg,j}$ is the individual time stamp background N_2O concentration (Section 3.1.2); $\delta_{bg,m}$ is a monthly varying background isotopic composition from the stratospheric seasonal mixing effect simulated by two end-member linear mixing between the background troposphere and lower stratosphere using CFC-12 as an STE proxy (Section 3.1.3); and $\delta_{regional,j}$ and $C_{regional,j}$ are determined using estimated constant source-specific isotopic signatures and monthly varying emission databases (Table 3.1) with 3D Lagrangian particle dispersion model air history fields calculated at each time stamp, treating each isotopologue as a separate tracer (Section 3.1.4). With this structure and inputs, the forward model is run to estimate the isotopic composition and N_2O mole fraction arriving at Mace Head at each time stamp (j = 56).

3.1.2 Baseline determination

Large-scale transport effects (e.g. convection, seasonal changes in boundary layer height, and interhemispheric transport) are materialized in background air variation. Baseline flask sampling time stamps are defined as meeting several criteria:

1) No increases in trace gases indicative of local soil sources (N_2O, CH_4, $CHCl_3$) or man-made polluted air (CO, CFC-11,-12,-113) in the simultaneous AGAGE instrumentation measurements defined as a pollution event by the AGAGE algorithm (O'Doherty et al 2001);

2) No meteorologically calm conditions with low wind speeds <4 ms^{-1} observed on the Mace Head tower at the sample time which could be capturing immediately local sources;

3) Boundary layer (BL) depth >300 m as calculated in the United Kingdom Meteorological Office's numerical weather prediction (NWP) model (Cullen 1993). Less than 300 m BL is often coincident with low wind, stable situations;

4) NAME 3D Lagrangian dispersion model air histories (see detailed NAME model description below) show minimal influence from local or European land sources as analyzed and classed according to Manning et al (2011) for significant contributions from local and European grid boxes (courtesy A. Manning, UKMO);

5) HYSPLIT back trajectory model shows no indication of high altitude direct stratospheric air intrusion with a 315 h back trajectory (see HYSPLIT description below).

Time stamps meeting these baseline criteria (n = 33) are interpreted to reflect general trends and seasonality in the background NH troposphere rather than containing any significant local or regional signals.

Background air N_2O mole fraction ($C_{bg,i}$) is determined from continuous in situ data of N_2O mole fractions (~40 min interval) at the Mace Head station collected by AGAGE by GC-ECD (Prinn et al 2000). Precision of each individual AGAGE measurement is about 0.03% (0.1 ppb), SIO 2005 absolute mole fraction calibration scale. Over the time frame of the model only small variations (<1 to a few ppb) are seen in the observed N_2O mole fractions at Mace Head. For 2010, monthly means of AGAGE high-frequency measurements of N_2O in non-polluted air (order 10^3 measurements) have a February maximum and August minimum with a detrended seasonal cycle peak-to-peak amplitude of 0.85 ppb. N_2O pollution events are defined by the AGAGE algorithm (O'Doherty et al 2001). This is inline with the mean observed N_2O seasonal cycle at Mace Head in the AGAGE data since 1994 which has an August minimum and slightly less pronounced amplitude of 0.66 ppb. Although the time stamps for this isotopic analysis are not regularly distributed throughout the year, Figure 3.1 displays how the point data fairly well represent N_2O mole fractions at Mace Head over the model time frame with both non-polluted and polluted observations. The background air N_2O mole fractions for each time stamp ($C_{bg,i}$) for input into the regional model system uses the 4-week running mean of the continuous AGAGE non-polluted mole fractions.

Figure 3.1 Observation time stamp mole fractions overlaid with AGAGE high-frequency N_2O mole fraction data from Mace Head. AGAGE pollution-flagged data is in purple, non-polluted in green. The 4-week running mean of non-polluted data is marked by the black curve.

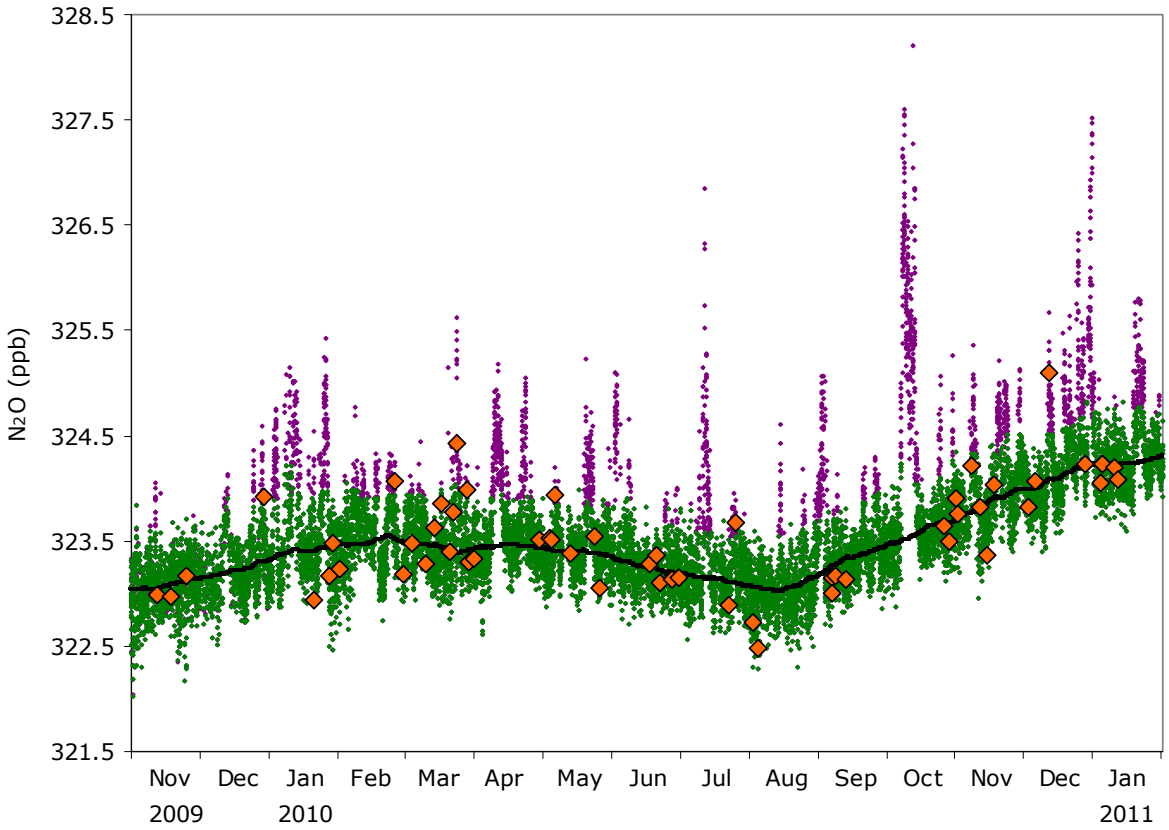

The model regional emissions scheme (see section 3.1.4) independently determines the regional contribution to N_2O mole fraction in air arriving at Mace Head including the small regional input to baseline air, which arise predominately from Atlantic Ocean and diffuse North American sources. The AGAGE running mean values are offset downward to account for the modeled regional emissions contribution to baseline samples by subtracting the mean baseline regional emissions contribution determined by the model regional emissions scheme as 0.23 ppb. These offset values are used as background mole fraction input for each modeled time stamp to compute the isotopic composition and to which regional mole fraction increments are added. By utilizing the continuous AGAGE data, the background N_2O mole fractions ($C_{bg,j}$) used in the model thus incorporates the observed mole fraction seasonal cycle and long-term secular trend.

3.1.3 Stratospheric influence

Loss of N_2O occurs in the stratosphere through photolysis and reaction with $O(^1D)$. These reactions cause significant isotopic fractionation by preferentially eliminating the lighter isotopologues and leaving a more ^{15}N- and ^{18}O-enriched N_2O isotopic composition and site preference. Through stratosphere-troposphere exchange (STE) the effect of this fractionating loss process impacts the tropospheric composition.

Deep STE intrusions have a distinct winter maximum rather than in the spring when the most mass flux occurs (James et al 2003). Though at 14 m above sea level Mace Head would be highly unlikely to experience deep direct stratospheric intrusions, these events have been observed down to the surface reaching as low as 20 m asl (Gerasopoulos et al 2006). The impact of direct intrusions on atmospheric composition is substantial as it is a rapid transfer of stratospheric composition into the troposphere rather than the slow process of diffusive downward mixing.

Stratospheric intrusion events reaching Mace Head were assessed with the HYbrid Single Particle Lagrangian Integrated Trajectory model (HYSPLIT) developed by Roland Draxler at the NOAA Air Resources Laboratory, using National Center for Environmental Prediction analyzed global grid of meteorological data (2.5°×2.5° latitude-longitude, 17 pressure levels; Draxler 1998). The single back trajectories from the HYSPLIT model give finer resolution information about origin of air in the vertical whereas the NAME 3D Lagrangian dispersion model (described in section 3.1.4) output only distinguishes 4 vertical levels, with the highest level as 3-20 km which is insufficient to distinguish direct stratospheric influence. No clear significant direct stratospheric intrusions for any of the time stamps were evident. Thus, for this model, only the impact of seasonal stratosphere-troposphere exchange mass flux propagating to the surface is simulated.

Downward cross-tropopause air movement in terms of total mass flux peaks in the NH spring (Mar-May), predominantly as shallow intrusions (James et al 2003, Stohl et al 2003, Liang et al 2009). Downward propagation from the lower stratosphere through the free troposphere to the surface occurs over ~3 months (Liang et al 2009). This slow descent of stratospheric air is consistent with the observed mole fraction seasonal minima of N_2O and CFCs at Mace Head occurring in July-August-September (Nevison et al 2004, Nevison et al 2007). Chlorofluorocarbons are complementary tracers to N_2O budget interpretation since they are similarly long-lived and well-mixed in the troposphere and are destroyed photochemically in the stratosphere. Due to the fact that there are no longer significant surface sources of CFCs, they have been successfully used as a proxy for STE. Using AGAGE high-frquency data at Mace Head, here the CFC-12 seasonal cycle is used to derive a reasonable estimate of the seasonal cycle of N_2O attributable to stratospheric exchange following Nevison et al (2005), which is then combined with estimated lower stratospheric composition (δ_{lstrat}, C_{lstrat}) to determine the stratosphere seasonal influence on background air N_2O isotopic composition ($\delta_{bg,m}$) end-product. This estimation of a monthly-varying background isotopic composition for input into the overall model isotopic mass balance is described in the following paragraphs.

Monthly mean non-polluted N_2O and CFC-12 data from March 2001 to February 2011 (10 years) were detrended by subtracting a 3rd-order polynomial fit to remove the increasing N_2O and decreasing CFC-12 long-term trends. The residuals reveal the seasonal cycles, and over the 10 years of data the seasonal maxima and minima of N_2O and CFC-12 are generally aligned. For 2010, around which this estimate is being made, N_2O and CFC-12 share a February maximum and August minimum. CFC-12 residuals (ppt) are converted to N_2O residual units (ppb) by multiplying by the ratio of their mean mole fractions in 2010 at Mace Head, N_2O(ppb)/CFC-12(ppt). The CFC-12 thermal ocean flux affecting its seasonal cycle is small and assumed to not greatly impact the observed cycle at Mace Head, thereby leaving the cycle as assumed driven by stratospheric down-mixing alone (Nevison et al 2005). Additionally the small thermal ocean signal is in the opposite phase as stratospheric effects and therefore would only cause the CFC-12 proxy to provide an underestimate of the stratospheric cycle.

The CFC-12 stratospheric influence is scaled for N_2O by the relative efficiency of stratospheric removal of the two species. This ratio can be determined based upon the general

stratospheric tracer correlation theory that long-lived tracers far from their sources show related variability (Plumb and McConalogue 1988, Plumb and Ko 1992) and is taken as 0.7 from the Volk et al (1996) slope of normalized N_2O vs. CFC-12 data measured near the tropopause with ~10% uncertainty. The resulting N_2O stratospheric cycle determined from CFC-12 has an amplitude of 0.66 ppb, ~78% of the total observed N_2O 2010 February to August amplitude of 0.85 ppb.

Figure 3.2 Time series of observed N_2O and CFC-12 monthly mean non-polluted mole fraction residuals from continuous AGAGE data after removal of long-term secular trends. N_2O_strat cycle is the N_2O monthly varying seasonal cycle in background air due to stratospheric influence ($C_{bg,m}$) derived from the CFC-12 observations as described in the text. CFC-12 observations have been converted to N_2O ppb units using the ratio of mean 2010 mole fractions.

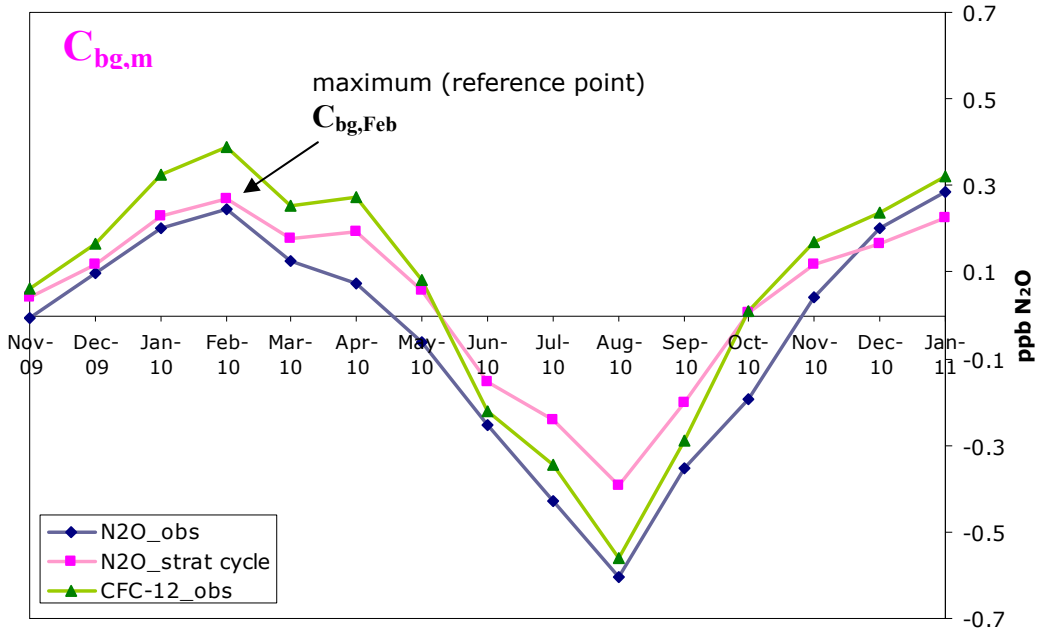

A monthly-varying N_2O isotopic composition cycle in the background troposphere ($\delta_{bg,m}$) from the derived seasonal influx of stratospheric air is made by representing the N_2O loss process as two end-member mixing between the background troposphere and the mid-latitude lower stratosphere in steady state. Stratospheric measurement campaigns consistently have found that in the lower stratosphere (where N_2O mole fractions >200ppb) isotopic composition and mole fractions show a compact relationship largely independent of latitude and season (Park et al 2004, Toyoda et al 2004, Kaiser et al 2006). Kaiser et al (2006) plotted the linear end-member mixing relationship with their stratospheric observations and discerned that mid-latitude N_2O isotope profiles could be described by a two end-member mixing relationship to a good approximation.

Figure 3.3 Diagram of the two end-member mixing scheme with the end product of estimating a monthly-varying background N_2O isotopic composition ($\delta_{bg,m}$), using CFC-12 as a proxy for the stratospheric seasonal N_2O cycle ($C_{bg,m}$) and estimated constant values for lower stratosphere composition (δ_{lstrat}, C_{lstrat}).

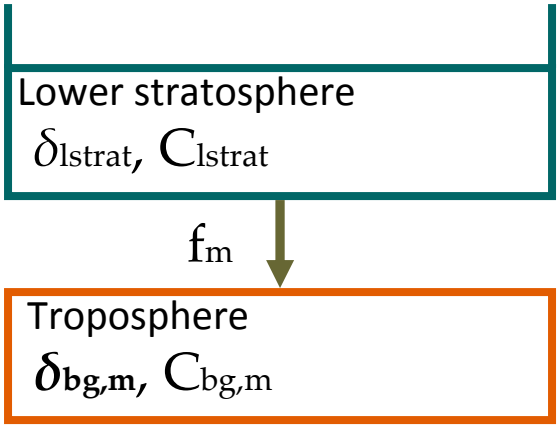

The February maximum mole fraction in the estimated background seasonal cycle due to the stratosphere ($C_{bg,Feb}$, labeled in Figure 3.2) is used as the reference point from which all other months have been depleted due to mixing with a different fraction (f_m) of the low N_2O mole fraction lower stratosphere. This linear two end-member mixing is described as:

$$C_{bg,m} = f_m\, C_{lstrat} + (1 - f_m)\, C_{bg,Feb} \qquad (3)$$

Here $C_{be,m}$ and $C_{bg,\,Feb}$ are the derived N_2O stratospheric cycle residuals as in Figure 3.2 for February 2010 and month m that have been added to the mean non-polluted mole fraction from the high-frequency AGAGE data for 2010 to give detrended N_2O values at 2010 tropospheric level mole fractions. C_{lstrat} is the estimated constant mole fraction in the lower stratosphere varied in different model scenarios as detailed below. f_m is the air mass fraction of lower stratospheric air (lstrat) which is mixed into the background troposphere (bg) to create the depletion from the February maximum mole fraction to that of the specific month m. Air masses will be at the same altitude and hence density when mixing, and therefore mole fraction units can be used in place of concentrations.

The monthly fraction f_m determined by the mole fraction end-member mixing is used in the corresponding isotope relationship:

$$\delta_{bg,m}\, C_{bg,m} = f_m\, \delta_{lstrat}\, C_{lstrat} + (1 - f_m)\, \delta_{bg,Feb}\, C_{bg,Feb} \qquad (4)$$

February 2010, bearing the mole fraction maximum and corresponding isotopic composition minimum, is again used as the reference point to which all other months are related. $\delta_{bg,m}$ and $\delta_{bg,Feb}$ represent the monthly-varying tropospheric background compositions for each month m and February 2010. To initially determine $\delta_{bg,Feb}$ it is assumed that the isotopic composition seasonal maxima and minima are symmetrical around the mean 2010 baseline composition such that ($\delta_{bg,Aug}$ + $\delta_{bg,Feb}$)/2 equals the 2010 mean. The mean 2010 isotopic composition is defined as the mean isotopic composition of the air sample measurements collected regularly from the Mace Head, Ireland monitoring station starting January 2010 through January 2011 (see Chapter 4) which meet the baseline criteria (n = 30) (Table 3.1). It is assumed that the distribution of these samples adequately represent the year within uncertainty and to contain no significant long-term trend over

the model time range November 2009 to January 2011. With the $\delta_{bg,Feb}$ value all of the other months can be solved individually according to the lower stratosphere air mass fraction, f_m, necessary to mix with the February maximum mole fraction to achieve the lower mole fraction for that month to achieve monthly-varying background isotopic composition for input into the overall model structure (section 3.1.1).

Lower stratosphere input variables, C_{lstrat} and δ_{lstrat}, are assumed constant with no monthly variation. Observations and theory have found a clear latitudinal dependence of the N_2O apparent fractionation constants and isotopic composition profiles in the middle and upper stratosphere, but less discernable differences in the lower stratosphere (Griffith et al 2000, Rockmann et al 2001, Morgan et al 2004, Park et al 2004, Toyoda et al 2004, Kaiser et al 2006). Recent stratospheric measurements by Kaiser et al (2006) covering parts of Europe point to the possibility of seasonality as well as longitudinal dependence in overall stratospheric profiles, but in the lower stratosphere the isotopic composition behavior is nearly constant. Temporally, Toyoda et al (2004) conclude that the average isotopic ratios in the lower stratosphere over Japan (39°N) were constant with no seasonal variation in May, June, August, and September observations.

Lower stratosphere air mass characteristic signature (δ_{lstrat}) and mole fraction (C_{lstrat}) are informed by stratospheric measurements at similar latitude to Mace Head (53.3°N). Mid-latitude observations and reported apparent fractionation constants over Japan (39°N; Toyoda et al 2004) and nearer to Ireland in France (Aire sur l'Adour 43.7°N; Gap 44.4°N; Kaiser et al 2006) at divergent longitudes and different months are equivalent in the lower stratosphere within uncertainty. Toyoda et al (2004) use their stratospheric profiles and apparent fractionation constants to estimate integrated isotopologue delta values and mole fractions in the lower stratosphere (upper boundary altitude of the lower stratosphere defined by analysis of isotopic data behavior change, their "Limit 1"). The Toyoda et al (2004) mean integrated composition of the "Limit 1" defined lower stratosphere in 5 stratospheric data sets over Japan is taken as the reference case δ_{lstrat} and C_{lstrat} (Table 3.1) in the lower stratosphere mixing with the background troposphere (Figure 3.3, equations 3 and 4). The lower stratosphere isotopic signature is depicted for ^{15}N isotopomers in Figure 3.4 relative to assigned source signatures and approximate tropospheric composition. Stratospheric values at higher altitudes would plot diagonally more ^{15}N and ^{18}O enriched, seen in upper stratosphere observations to reach extremely enriched composition near to or greater than 100‰ depending on isotopologue. Due to differences in the tropospheric composition reported by Toyoda et al (2004) and the mean 2010 tropospheric isotopic composition in this study, the lower stratosphere δ_{lstrat} is defined relative to the mean 2010 troposphere isotopic composition of this study to have the same absolute difference between the estimated lower stratosphere delta values of Toyoda et al (2004) and their reported troposphere composition.

Using these input values and the method outlined above, a step function of monthly varying $\delta_{bg,m}$ is created for each isotopic value which represents the seasonal influence of the stratosphere on background tropospheric composition. Figure 3.4 shows the resulting step function for bulk $\delta^{15}N$ in the reference case model scenario. Evident is the ^{15}N- (and ^{18}O-) enriched maximum in August, which coincides with the N_2O mole fraction seasonal minimum, resulting from the peak of stratospheric air influence at the surface in late summer at Mace Head.

Figure 3.4 Stratospheric influence seasonal cycle step function for $\delta^{15}N^{bulk}$, with a February minimum and August maximum. Step functions for $\delta^{15}N^{\alpha}$, $\delta^{15}N^{\beta}$, SP, and $\delta^{18}O$ are exactly mirrored in shape since they are all scaled to the CFC-12-determined stratosphere seasonal cycle with differing amplitudes as listed in text.

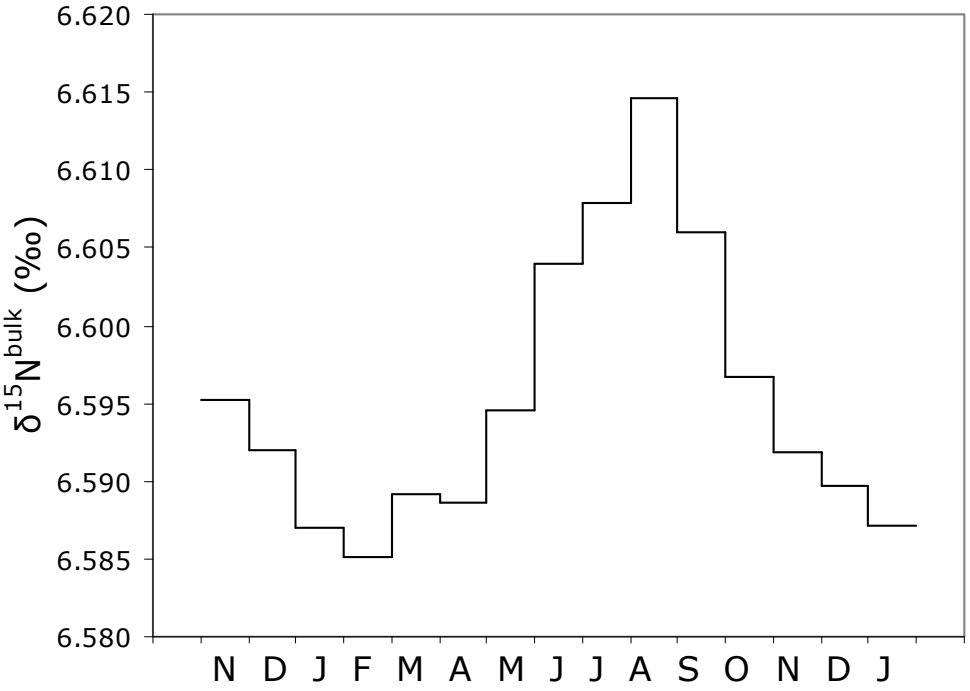

The stratospheric seasonal effect modeled here affects the background air arriving at Mace Head and will be most apparent in the baseline time stamps which receive little influence from regional emissions. Observation of this seasonal step function in actual air samples assumes high-frequency data collection since low-frequency flask observations have difficulty resolving subtle seasonal cycles in atmospheric trace gases.

For the reference case the resulting estimated seasonal peak-to-peak amplitudes are $\delta^{15}N^{bulk}$ 0.029‰, $\delta^{15}N^{\alpha}$ 0.039‰, $\delta^{15}N^{\beta}$ 0.020‰, SP 0.019‰, and $\delta^{18}O$ 0.026‰. Monthly steps for the reference case are near 0.005‰ or lower, below the order of feasible detection.

Stratospheric seasonal influence model scenarios

Alternative model scenarios examine a range of realistic input parameter values to assess possible magnitudes of the stratospheric seasonal influence on tropospheric isotopic composition. The model treatment of the stratospheric seasonal effect incorporates many simplifications and assumptions, and the reference case represents an attempt at a realistic but uncertain estimate. Because the stratosphere is suspected to play a large role in modulating the seasonal cycle in the N_2O mole fraction at Mace Head, it is valuable to assess the possible magnitudes of the seasonal cycle influence on isotopic composition and thus the desirable instrumentation precision for detection. In particular the assigned lower stratosphere composition values (C_{lstrat}, δ_{lstrat}) are a gross estimate and process simplification, and particularly the isotope ratios could range from these values by many per mil. Enrichment factors in the lower stratosphere are affected by myriad aspects including the relative contributions of photolysis and photooxidation in the N_2O loss process, sunlight and temperature effects on the photolysis fractionation factor, mixing of lower stratospheric

air with the upper stratosphere that has lower N_2O mole fractions and higher enrichment factors, horizontal mixing with polar or tropical air masses, and changes in the altitude of the upper boundary of air that undergoes significant mixing with the troposphere.

The alternative model scenarios help to determine the effects of modifying the lower stratospheric N_2O isotopic composition (δ_{lstrat}), lower stratospheric mole fraction (C_{lstrat}), tropospheric isotopic composition (mean $\delta_{bg,m}$), tropospheric mole fraction (mean $C_{bg,m}$), and amplitude of the tropospheric mole fraction stratospheric influence seasonal cycle ($C_{bg,Feb} - C_{bg,Aug}$), as listed in Table 3.1. The seasonal cycle scenarios are examined in terms of the resulting seasonal amplitude in the isotopic composition of the troposphere between the most ^{15}N- and ^{18}O-enriched month and the most depleted month, for 2010 and the behavior of CFC-12 determined as August and February, respectively.

Table 3.1 Listing of model scenarios regarding the stratospheric seasonal cycle and the modifications to the reference case input values. Scenario names correspond to abbreviated titles in Figure 3.11. Abbreviations: 'ls' lower stratosphere, 'bg' troposphere, 'δ' signature, 'C' mole fraction, 'S_amp' stratospheric seasonal amplitude. N_2O mole fraction (C) for the troposphere is the high-frequency AGAGE non-polluted data mean. The $C_{bg,m}$ used for each month in the stratospheric model is derived from this annual mean combined with the CFC-12 derived stratospheric seasonal component as described in text.

Scenario	**Input parameter**	**$\delta^{15}N$ ‰**	**$\delta^{15}N^{\alpha}$ ‰**	**$\delta^{15}N^{\beta}$ ‰**	**SP ‰**	**$\delta^{18}O$ ‰**	**C ppb**
Reference case	Troposphere mean $\delta_{bg,m}$, $C_{bg,m}$	6.60	16.61	-3.41	20.02	44.13	323.44
	Lower stratosphere δ_{lstrat}, C_{lstrat}	10.10	21.26	-1.06	22.32	47.23	260.0
	Troposphere $C_{bg,m}$ stratospheric seasonal amplitude = 0.66 ppb						
	Modification from reference case						
Toyoda2004 Limit 2	Toyoda et al 2004 "Limit 2" boundary for δ_{lstrat} and C_{lstrat}	8.50	18.96	-1.96	21.02	45.93	285
C_ls: 200ppb	Low C_{lstrat}						200
C_ls: 300ppb	High C_{lstrat}						300
δ_ls: med	Medium enriched δ_{lstrat}	18	30	6	24	50	
ls δ:high, C:260; C:225; C:200; C150	Highly enriched δ_{lstrat}, steps lower of C_{lstrat}	25	40	10	30	60	260; 225; 200; 150
C_bg: low	Low troposphere mean $C_{bg,m}$						322.0
C_bg: high	High troposphere mean $C_{bg,m}$						325.0
S_amp: 0.5ppb; 0.8ppb; 1ppb	Troposphere $C_{bg,m}$ stratospheric seasonal amplitude = 0.50; 0.80; 1.00 ppb						

The lower stratosphere has been simplified as a well-mixed box when in actuality there will be a gradient towards lower mole fractions and higher isotopic composition with altitude. Vertical profiles of the stratosphere show a steep drop in N_2O mole fractions and a corresponding steep

enrichment of the isotopic values approaching the middle and upper stratosphere (Rockmann et al 2001, Park et al 2004, Toyoda et al 2004, Kaiser et al 2006). The encroachment of higher altitude air into the lower stratosphere and the definition of the lower stratosphere "box" will have marked effects on the composition of air directly mixing with the troposphere. The first case regarding the lower stratosphere checks the slight difference when taking the stratospheric values derived by Toyoda et al (2004) using their "Limit 2" definition of the upper boundary of the lower stratosphere as the altitude at which the N_2O mole fraction is 250 ppb. The next set of scenarios examines the effect of the assumed mole fraction in the lower stratosphere with the same reference case isotopic signature to a lower value of 200 ppb and a higher value of 300 ppb, both reasonable values in line with observed stratospheric profiles. To assess the sensitivity of results to the prescribed isotopic composition of the lower stratosphere, a slightly more ^{15}N-, ^{18}O-enriched and then a highly enriched signature is used, both of which correspond to observed values in stratospheric measurement campaigns in the lower regions of the stratosphere, while holding the same reference case mole fraction. Realistically, more heavy-isotope enriched isotopic composition would result from more N_2O loss by photolysis and photooxidation, and would coincide with lower N_2O mole fractions. A series of cases with the highly heavy-isotope enriched isotopic composition thus steps through N_2O mole fractions from the reference case 260 ppb to lesser values 240 ppb, 200 ppb, 150 ppb. The well-mixed troposphere has a smaller range of possible associated compositions than the stratosphere. The mean tropospheric N_2O mole fraction for 2010 defines the center about which the CFC-12 derived stratospheric seasonal effect is imposed. The effect of small deviations in this central value is simulated with lower (322 ppb) and higher (325 ppb) mole fractions. The derivation of the stratospheric component of the 2010 N_2O seasonal cycle from CFC-12 data is examined through scenarios which have stratospheric component seasonal amplitudes of 0.50, 0.80, and 1.00 ppb (reference case = 0.66 ppb), while maintaining the same CFC-12 relation between the monthly steps.

3.1.4 Regional surface emissions: NAME Lagrangian particle model

A Lagrangian particle dispersion model is used to simulate regional surface source emissions affecting Mace Head and identify source-receptor relationships. The United Kingdom Meteorological Office (UKMO) Lagrangian numerical atmospheric-dispersion modeling environment (NAME) is a 3-D Lagrangian particle dispersion model (Ryall et al 1998, Manning et al 2003, Manning et al 2011), which uses full 3-D meteorology from the UKMO numerical weather prediction (NWP) model (Cullen et al 1997, Davies et al 2005). The model air parcels move in a three-dimensional space driven by either three-dimensional NWP meteorology or single-site observations with a turbulence parameterization scheme. In the work presented here the model schemes for representing chemistry, dry deposition, wet deposition and radioactive decay were not used since these are assumed to not significant apply to N_2O. The NAME model is run in backwards mode to estimate the recent pathways of air arriving at Mace Head (the receptor).

For the air histories stemming from Mace Head station, the computational domain covers 100.0° W to 45.125° E longitude and 10.0° N to 80.125° N latitude and 20 km vertically (31 vertical levels) with a horizontal resolution of 0.5625° longitude and 0.375° latitude (approx. 40 km horizontal resolution, 258×187 grid). The model is run for 3-hr periods over which particles are released from Mace Head at a rate of 1 g s^{-1}. Over the 3-hr period 33,000 inert particles record the dispersion in terms of time integrated air concentration from the backwards release of particles in units of g s m^{-3}, which is the output displayed in the air history maps. These particles are tracked backwards in time for 19 days, an appropriate amount of time to capture regional influence and

which by the end diffusion has reduced particle concentrations to negligible levels and many of the particles have left the computational domain. Occasionally synoptic scale analyzed meteorology can fail to capture local wind features such as land or seas breezes and adiabatic or katabatic winds. The accuracy of the NAME output capturing the proper local behavior was verified by a match between NWP output wind speed and direction for Mace Head and that measured directly on the Mace Head tower at the same time stamp. The vertical resolution divides the output into four levels recording particle dispersion for 0-100 m, 100-1000 m, 1000-3000 m, and 3000-20000 m, i.e. the 0-100 m surface level records the time and number of particles spent in each horizontal grid cell from 0 to 100 m altitude, thus focusing on the influence of air in close contact with the surface (and therefore surface sources) prior to reaching Mace Head. Example 0-100 m air histories are shown in Figure 3.9. An air parcel can travel back-and-forth between the vertical levels and will be recorded in each map for all moments spent in that vertical level. Thus for each of the sample observation collection times, the NAME model is able to represent the detailed transport from all possible source regions, responding to horizontal and vertical mixing, convection, and turbulence-- a marked improvement over single back trajectories.

The 0-100 m surface level output is used for the air history maps for the regional N_2O surface source modeling reference case simulations in this work. An alternative model sensitivity run uses an increased altitude of the air history to include the lowest 0-1000m surface layer (Appendix 2.I). The maps of time integrated air concentration of particles in each grid cell box (g m^{-3} · s) are divided by the total mass released (3 h × 1 g s^{-1} × 3600 s h^{-1} =10800 g) which determines a matrix of time integrated fraction of the total mass which was in each particular box (s m^{-3}). Each element of this matrix weights the prescribed estimated N_2O emission flux from that grid cell (g $m^{-2}s^{-1}$) multiplied by the surface area of each grid cell (m^2). Summation over all grid cells simulates the N_2O concentration received at Mace Head (g m^{-3}).

$$C_{regional,j} = \sum \text{air history j (g m}^{-3} \cdot \text{s)/(10800 g)} \times \text{grid surface area (m}^2\text{)} \times \text{emission flux (g m}^{-2}\text{ s}^{-1}\text{)} \quad (5)$$

where $C_{regional,j}$ is the amount of N_2O received at Mace Head for each observation time stamp and corresponding air history map, j. The concentration is converted to mole fractions (ppb) using the NWP pressure and temperature at Mace Head for that time stamp. Total N_2O emission fluxes are prescribed from emission inventories and source categories listed in Table 3.2.

To model the isotopes of N_2O, each isotopologue is represented as a separate tracer (the rare $^{14}N^{15}N^{16}O$, $^{15}N^{14}N^{16}O$, and $^{14}N^{14}N^{18}O$, and the abundant $^{14}N^{14}N^{16}O$). The emission flux (g m^{-2} s^{-1}) of each isotopologue emitted is calculated by converting the emission category specific isotope signature δ values (Table 3.2) to $^{\alpha}R$, $^{\beta}R$, and ^{18}R values, the ratio of rare isotopologue to the most abundant isotopologue $^{14}N^{14}N^{16}O$.

$$R = (\delta + 1)/R_{std} = [^{14}N^{15}N^{16}O]/[^{14}N^{14}N^{16}O],\ [^{15}N^{14}N^{16}O]/[^{14}N^{14}N^{16}O],\ [^{14}N^{14}N^{18}O]/[^{14}N^{14}N^{16}O]$$

(R_{std} = air-N_2 for ^{15}N isotopologues and VSMOW for ^{18}O).

The ratio is multiplied by the total N_2O emission flux field to derive separate emission fields for each isotopologue for each source category (monthly varying for some source categories), which is then summed with the isotopologue- and month-specific emission field for all categories to create monthly varying $^{15}N^{14}N^{16}O$, $^{14}N^{15}N^{16}O$, $^{14}N^{14}N^{18}O$, and $^{14}N^{14}N^{16}O$ emission flux matrices. Each of these is treated independently with equation (5) to determine the concentration (g m^{-3}) of each isotopologue reaching the Mace Head receptor. Concentration results ([$^{15}N^{14}N^{16}O$], [$^{14}N^{15}N^{16}O$],

[$^{14}N^{14}N^{18}O$], and [$^{14}N^{14}N^{16}O$]) are related as *R* ratios and reconverted to δ values giving $\delta_{regional,j}$, the isotope signature associated with the incremental increase of total N_2O mole fraction $C_{regional,j}$ received at Mace Head for that time stamp j.

The emission fields applied in the model fall into 13 categories as listed in Table 3.2 with the inventory database source. Natural soil emissions are taken from the NASA-CASA terrestrial biogeochemistry model with monthly varying emissions (Potter et al 1996). Ocean emissions use the Global Emissions Inventory Activity (GEIA) available with 1°x1° horizontal resolution as yearly average emissions (Bouwman et al 1995). These simulations will not account for any seasonality in ocean emissions. The regional ocean source affecting Mace Head in the northern Atlantic Ocean with low biological productivity is likely small (Walter et al 2006). Agricultural soil and livestock emissions are from the Emission Database for Global Atmospheric Research (EDGAR) v4.0 with monthly varying emissions (0.1°x0.1°). Anthropogenic industrial, combustion, and other emissions are from EDGAR 4.0. The Global Fire Emissions Database (GFED) provides monthly biomass burning emissions on a 1°x1° grid. Data for 2010 are not available and are taken for year 2005 which approximates an average biomass burning season from the GFED database. All emissions inventories are interpolated onto the NAME dispersion model horizontal resolution.

Data on isotopic signatures for the categories listed in Table 3.2 are limited, and thus for this model study the emission categories are aggregated into four isotopic signature categories: soil, ocean, biomass burning, and anthropogenic/industrial. The assigned ^{15}N isotopomer signatures in relation to each other and approximate tropospheric composition are depicted in Figure 3.5 for the reference case and depleted soil signature model scenario (see below). For the purposes of this model study these are rough estimates representing large scatters of signatures based upon emission measurements from soil (Kim & Craig 1993, Wada & Ueda 1996, Casciotti et al 1997, Perez et al 2000, 2001, Yamulki et al 2000, 2001, Tilsner et al 2003, Bol et al 2003, Van Groenigen et al 2005, Well et al 2005, Rock et al 2007, Zhu et al 2008, Opdyke et al 2009, Goldberg et al 2010, Ostrom et al 2010, Park et al 2011), ocean surface layer (Yoshinari et al 1997, Dore et al 1998, Naqvi et al 1998, Popp et al 2002, Yamagishi et al 2007), biomass burning (Ogawa & Yoshida 2005a), and industrial sources (Wahlen & Yoshinari 1985, Ogawa & Yoshida 2005b, Toyoda et al 2008). Fewer of these signature data offer ^{15}N site-specific isotopomer values since this measurement capability is relatively recent, with most signature information limited to only $^{15}N^{bulk}$ and ^{18}O. There are notably no direct measurements of signatures specific to the European domain, with most of the soil estimates from the tropics. No Atlantic Ocean data exists therefore the ocean signature estimate for this Mace Head centered study was informed by measurements in similarly low-productivity ocean regions.

Table 3.2
Input isotopic compositions (‰) of background air, lower stratosphere, and emissions for the reference case model. Values are compiled from studies and measurements as described in the text. Troposphere background and lower stratosphere values are input to produce the stratospheric influence $\delta_{bg,m}$ step functions. Seasonality column indicates which inputs are monthly varying. Emission categories list emission inventory source.

	$\delta^{15}N$	$\delta^{15}N^{\alpha}$	$\delta^{15}N^{\beta}$	SP	$\delta^{18}O$		
Troposphere background, δ_{bg} mean	6.60	16.61	-3.41	20.02	44.13		
Lower stratosphere (ref case), δ_{lstrat}	10.1	21.3	-1.1	22.3	47.2		
Emissions category						**Seasonality**	**Inventory**
Natural soil	-14.50	-12.00	-17.00	5.00	32.00	X	NASA-CASA
Agricultural soil	-14.50	-12.00	-17.00	5.00	32.00	X	EDGAR 4.0
Livestock	-14.50	-12.00	-17.00	5.00	32.00	X	EDGAR 4.0
Ocean	5.00	8.00	2.00	6.00	40.00		GEIA
Biomass burning	-1.50	0.00	-3.00	3.00	25.00	X	GFED
Agricultural burning	-1.50	0.00	-3.00	3.00	25.00		EDGAR 4.0
Industrial	0.00	6.00	-6.00	12.00	44.00		EDGAR 4.0
Energy manufacturing	0.00	6.00	-6.00	12.00	44.00	X	EDGAR 4.0
Residential	0.00	6.00	-6.00	12.00	44.00	X	EDGAR 4.0
Waste	0.00	6.00	-6.00	12.00	44.00		EDGAR 4.0
Transportation	0.00	6.00	-6.00	12.00	44.00		EDGAR 4.0
Oil & gas production	0.00	6.00	-6.00	12.00	44.00		EDGAR 4.0
Fossil fuel fires	0.00	6.00	-6.00	12.00	44.00		EDGAR 4.0

In the reference case scenario a less-divergent soil source signature close to tropospheric composition is used. Surface source effects on tropospheric isotopic composition are dominated by the soil source, the largest N_2O source, which encompasses both natural and agricultural soil emissions. The variation of isotopic signatures observed from soils and soil microbes is large, and values substantially depleted in ^{15}N and ^{18}O relative to atmospheric N_2O have been reached, most often associated with transient events of high N_2O emissions and therefore having a higher weighted effect. Measured N_2O soil emission compositions are quite scattered as indicated by the shaded oval in Figure 3.5, both between separate studies and locations and even temporally within single sites. It is unlikely that a single constant soil signature can adequately represent the dynamic nature of soil emissions both temporally and spatially, however current knowledge does not allow an informative dynamic distribution of signatures. A second model scenario with a ^{15}N- and ^{18}O-depleted soil signature addresses some of the uncertainty in the soil emissions isotopic signature. The depleted soil signature model scenario uses soil signature values of -50, -50, -50, 0, and 10 per mil for $\delta^{15}N$, $\delta^{15}N^{\alpha}$, $\delta^{15}N^{\beta}$, SP, and $\delta^{18}O$, respectively (Figure 3.5). It is not expected that soil emissions for every modeled time stamp would be properly represented by either the reference case emission signature or the depleted soil signature, but rather the computation of each of these model scenarios produces a possible range of regional soil source effects.

Figure 3.5 $\delta^{15}N^{\alpha}$ v. $\delta^{15}N^{\beta}$ input representative isotopic signatures for reference case and the ^{15}N-, ^{18}O- depleted soil signature case. Shaded regions represent the general areas where observations have been made for that signature. Note the stratospheric signature is specific to an estimate for the lower stratosphere effective signature and composition in the stratosphere becomes increasingly more enriched at higher altitudes.

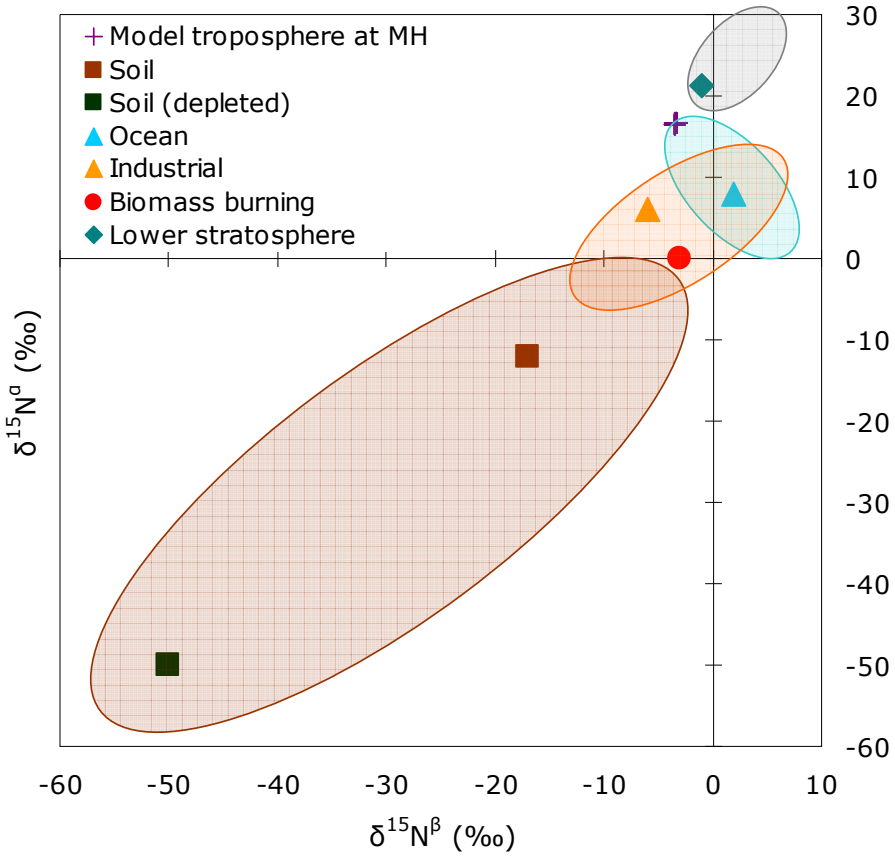

3.2 Results & Discussion

3.2.1 Mole fraction

The main purpose of this model is to simulate N_2O isotopic composition, but first the model output of whole N_2O mole fractions is compared to AGAGE observations at the corresponding observation time stamps. For assessment of isotopic composition and possible information contained in the variation, this comparison evaluates the general ability of the model's simplified regional sources to capture the observed variation created by the true episodic nature of N_2O emissions.

For the modeled time stamps (n = 56; 33 baseline, 23 non-baseline) the regional emissions model scheme adds between 0.09 ppb and 2.29 ppb to background mole fractions arriving at Mace Head, dependent upon the individual air history and monthly-varying emission field. There is generally good agreement between the modeled and observed mole fractions (Figure 3.4). There are a few model excursions which surpass the observed mole fraction, but likewise there are modeled time stamps when observed mole fractions higher than predicted by the model. This highlights the impact and importance of the extremely episodic nature of real N_2O soil emissions whereas the

model only uses a monthly-varying source field. With high-frequency data, these mismatches would be expected to statistically even out. Subtracting the seasonally varying 4-week running mean AGAGE baseline from the modeled and observed mole fractions gives similar standard deviations for the model (1σ = 0.39 ppb) and observations (1σ = 0.33 ppb), indicating that the model is well approximating the actual variation caused by regional source emissions.

The overall reasonable match between modeled and observed mole fractions suggests that the integrated magnitude, distribution, and timing of the emission fields are fairly realistic and in correspondence with the air history maps, and thus supports the general model framework for evaluating isotopic composition signals.

Figure 3.6 Time series from November 2009 to January 2011 of model simulated N_2O mole fractions and those measured at the corresponding observation time stamp at Mace Head by the AGAGE network. Filled data points are baseline time stamps, open data points are all other time stamps.

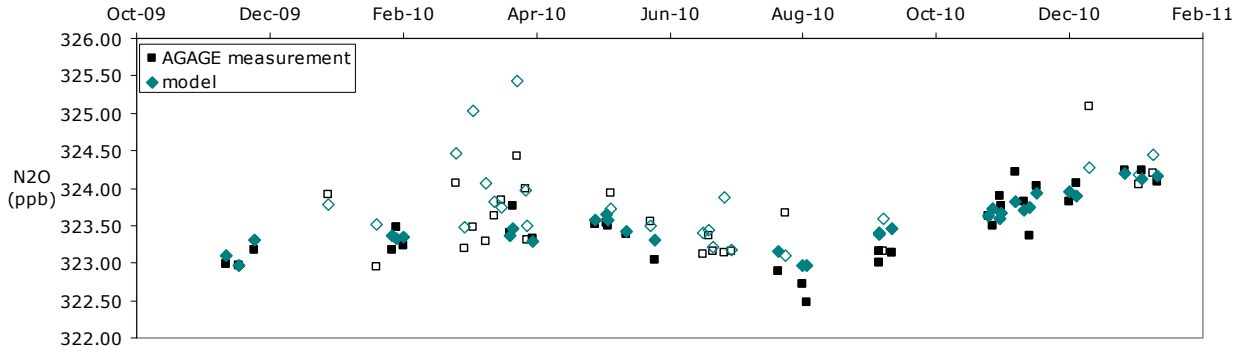

3.2.2 N_2O isotopic composition

In this model system the dominant control on the resulting isotopic composition is the balance between the stratospheric signature and soil source signature. This is shown in Figure 3.7a,b for the site specific isotopomers and bulk isotopic compositions, respectively. Variation in the modeled data is greatest for the $\delta^{15}N^{\alpha}$ and $\delta^{15}N^{bulk}$ compositions. Figure 3.7a can be related to Figure 3.5 which shows the model input isotopic signatures. The essentially stratosphere-soil mixing line is expected given that the soil microbial source is the largest emissions source globally and in this model system includes both natural and agricultural soil emissions. Soil also has the most divergent signature in the N isotopes compared to the tropospheric composition and thus its emissions will have a larger weighted effect on composition. The European domain also has significant hot spots of anthropogenic industrial sources and these emissions have estimated signatures in a similar direction as soil. Scatter perpendicular to the stratosphere-soil mixing line is predominantly caused by oceanic emissions in this model.

Figure 3.7 a) $\delta^{15}N^{\alpha}$ v $\delta^{15}N^{\beta}$ and b) $\delta^{18}O$ v $\delta^{15}N^{bulk}$ reference case model results. x- and y-axes in both plots are on the same scale.

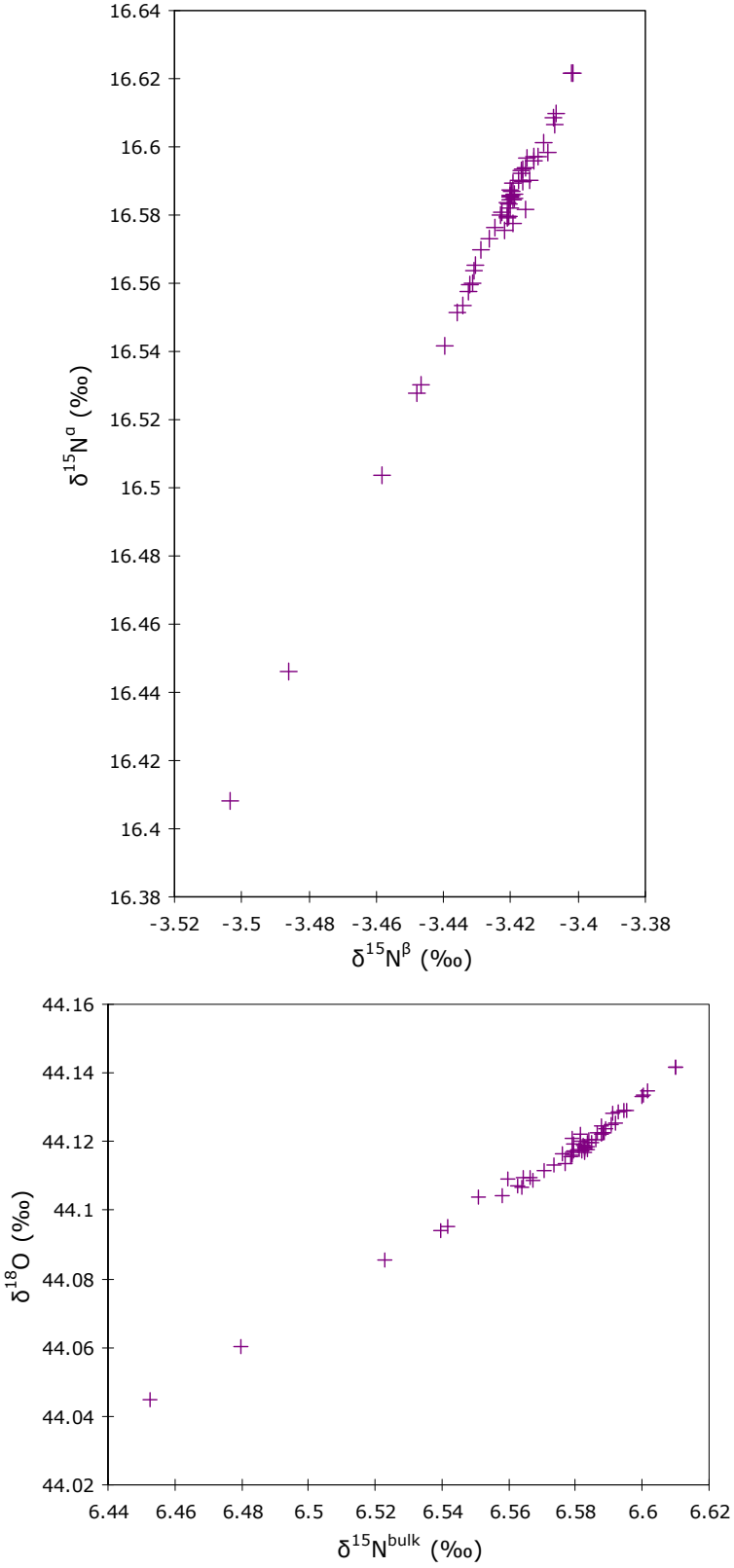

Figure 3.8 displays the time series of isotopic composition for the reference and depleted soil signature model cases. The cluster of larger departures from baseline in March results by chance due to the fact that there are more non-baseline time stamps in this time period and does not indicate a seasonal effect. Note that the y-axis tick marks for each isotopic value are at the same ‰ interval and spacing. Though they follow the same general pattern, it is significant that despite the small variability and seasonal amplitude that this simplified model simulates, the relative responses in the different isotopic values are different and hold information about the influencing process.

Model results must be considered in the context of current and projected measurement precision, as given in the Introduction to Chapter 3. Reference case results for the isotopic composition of N_2O at Mace Head station generally show only small variation, much of which would not be detected by Stheno+CF-IRMS measurement technology at the magnitudes predicted here. The reference case represents a minimum of the possible variation with static estimates of source signatures for only a limited number of aggregated source categories, simplified stratospheric influence, relatively static emissions field (only monthly-varying), and other model simplifications all which serve to dampen the output isotopic composition. The reference case paired with the depleted soil signature case simulates a potential range of variations driven by regional emissions which might be observed at Mace Head. The time series in Figure 3.8 use the reference case stratospheric seasonal cycle which is very small and its detection pushes the limits of precision for isotopic measurements. In the next two sections the model results are analyzed in terms of the short-term variation, mainly driven by the regional emissions aspect of the model, and the seasonal variation, which for the baseline time stamps is driven by the stratospheric influence simulation. The model scenarios explore potential magnitudes of isotopic variation, but still within the confines of this simplified model system.

Figure 3.8 Modeled time series from November 2009 to January 2011 of simulated N_2O isotopic ratios for $\delta^{15}N^{bulk}$, $\delta^{15}N^{\alpha}$, $\delta^{15}N^{\beta}$, SP,and $\delta^{18}O$ for the reference case and the depleted soil signature case. Darker data points are baseline time stamps, lighter data points are non-baseline time stamps. Note that the y-axis scale is the same for all isotopic values.

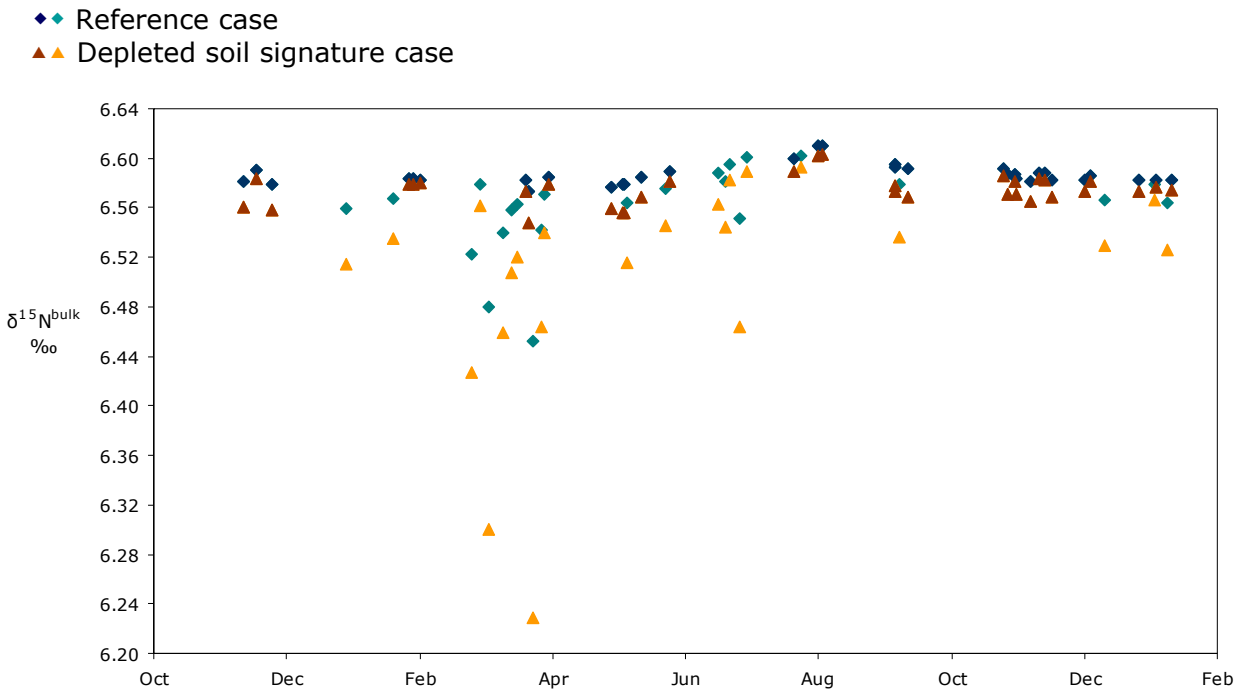

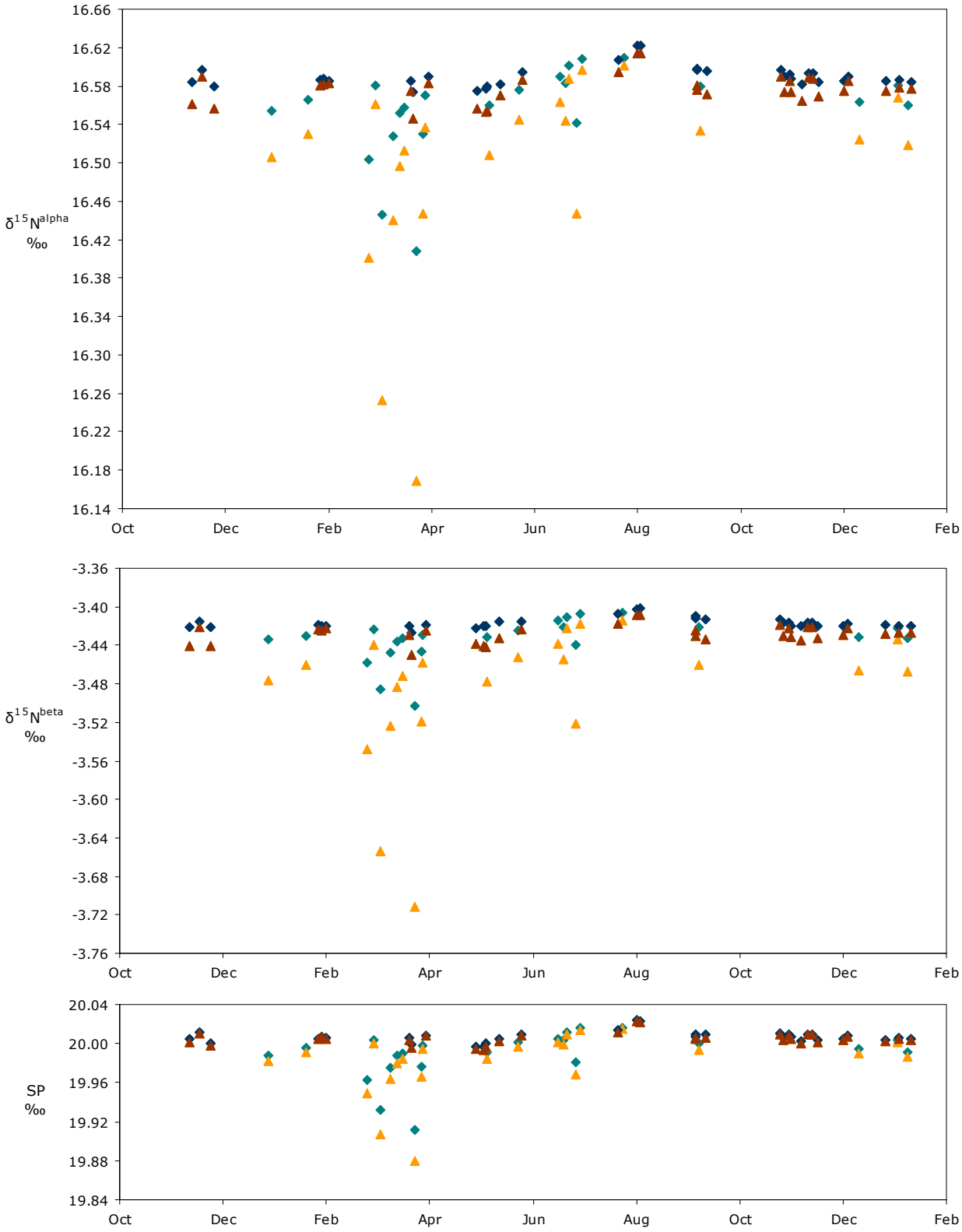
16.66
16.62
16.58
16.54
16.50
16.46
16.42
16.38
16.34
16.30
16.26
16.22
16.18
16.14
δ15Nalpha
‰
Oct
Dec
Feb
Apr
Jun
Aug
Oct
Dec
Feb
-3.36
-3.40
-3.44
-3.48
-3.52
-3.56
-3.60
-3.64
-3.68
-3.72
-3.76
δ15Nbeta
‰
Oct
Dec
Feb
Apr
Jun
Aug
Oct
Dec
Feb
20.04
20.00
19.96
19.92
19.88
19.84
SP
‰
Oct
Dec
Feb
Apr
Jun
Aug
Oct
Dec
Feb

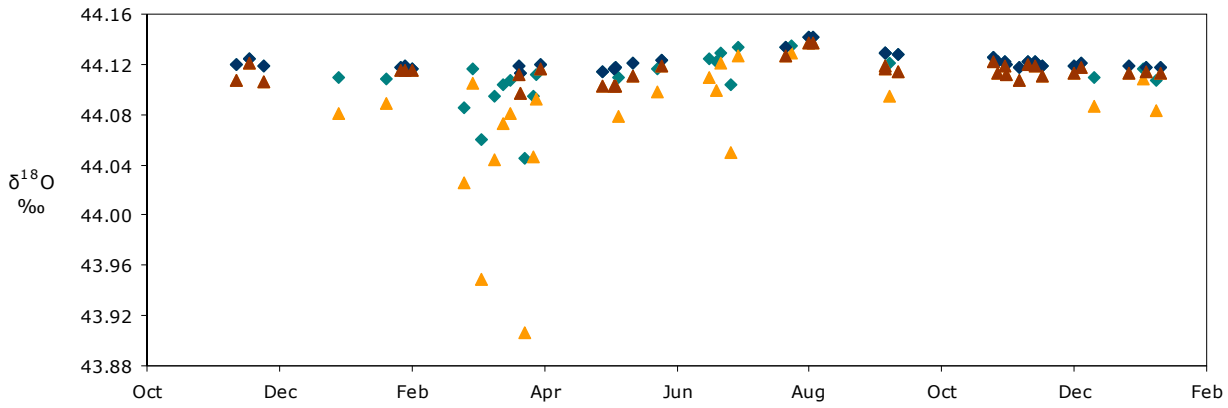

3.2.3 Short-term variability

Examination of the short-term variability in this model serves as an assessment of regional emissions and changing meteorology between different surface source footprints since there is no short-term variability imposed for neither transient stratospheric intrusions nor background troposphere fluctuations of isotopic composition. The reference and depleted soil signature cases span possible soil emissions signatures which an air parcel might encounter enroute to Mace Head station. Knowledge of the highly episodic nature of N_2O emissions from soil with both temporal and spatial heterogeneity suggests that the isotopic signature of N_2O from soils would be fluctuating as well. Monthly-varying N_2O emissions are a gross oversimplification since the bulk of N_2O emitted from soils arises during high flux events rather than a steady source, particularly after precipitation or irrigation, N fertilizer application, and freeze-thaw events among many other controlling influences. These high flux events arise in response to changing microbial processes between denitirification, nitrification, nitrifier denitrification, denitrifier N_2O consumption, etc., each which have been studied to have variable N_2O isotopic signatures dependent upon the fractionating enzymatic process as well as the original N substrate material in the soil and any oxygen exchange occurring in the substrate (Stein & Yung 2003, Toyoda et al 2005, 2011, Bateman et al 2005, Perez et al 2006, Kool et al 2009, Sutka et al 2006, Ostrom et al 2007, Casciotti et al 2009, Snider et al 2009, Well et al 2009). Recent reports of the possible prevalence of soil sinks in some European soils would further increase the scatter of net signature from soils (Goldberg & Gebauer 2008). Each model case imposes a single representative soil signature, but undoubtedly this varies on short-term time scales and likely seasonally as well. The results for both of these cases combined in Figure 3.8 thus encompass potential degrees of deviation in isotopic composition from baseline composition, attempting to capture the behavior of real observations which might produce a spectrum between these two scenarios.

The largest short-term variations occur in the n = 23 non-baseline time stamps. Table 3.3 reports the greatest degree of deviations from the annual mean baseline composition (mean $\delta_{bg,m}$) for each of the rare isotopologues in the two model cases, summarized as the range of the six largest modeled deivations. Reference case deviations from baseline composition reach the order of 0.05 up to 0.2‰ for the different isotopic δ values, but many subtle variations are <0.05‰ which would be undetectable by Stheno+CF-IRMS capabities. The depleted soil signature case expands the spectrum of variation to a realistic range of deviations with more on the order of 0.1‰, detectable by Stheno+CF-IRMS, possibly extending to >0.4‰ departures from baseline. The highly depleted soil signature also highlights additional time stamps which in the reference case are indistinguishable from baseline and places them within measurement precision of projected instrumentation abilities,

with acknowledgment that the highly depleted soil source and these magnitudes of deviations would not be expected to affect every time stamp.

Table 3.3 Modeled largest magnitudes of short-term deviations from the mean baseline isotopic composition resulting from the reference and depleted soil signature cases. Ranges are for the six largest modeled deviations.

	Reference case	Depleted soil signature case
$\delta^{15}N^{bulk}$	0.05 – 0.15 ‰	0.14 – 0.37 ‰
$\delta^{15}N^{\alpha}$	0.07 – 0.20 ‰	0.16 – 0.44 ‰
$\delta^{15}N^{\beta}$	0.03 – 0.09 ‰	0.11 – 0.30 ‰
SP	0.04 – 0.11 ‰	0.05 – 0.14 ‰
$\delta^{18}O$	0.03 – 0.09 ‰	0.08 – 0.23 ‰

Evident from this modeled time series is the likely potential utility of high-frequency measurements which capture short-term variations, reflecting changing meteorological patterns and surface source influences. Even the small data set used here captures non-baseline observation time stamps significantly influenced by emissions over land with deviations from baseline composition detectable with Stheno+CF-IRMS measurement precision. The likelihood of detecting variation is additionally aided with acknowledgment that the model scenarios use constant signature estimates of only a few aggregated categories and dampened N_2O emissions variation. Actual dynamic N_2O emissions with many dynamic signatures would likely bring higher variation and deviation in the isotopic composition. A more complete sample set with higher-frequency data would likely encounter many such data points holding useful information about regional surface sources.

Shown in Figure 3.7 are example air histories for a baseline and non-baseline categorized time stamps. The simulated observation with the greatest deviation from baseline composition showing extremely ^{15}N- and ^{18}O-depleted values is for the 25 March 2010 12:00h GMT time stamp. The air history shows significant influence from over the UK and western Europe.

Figure 3.9 Air histories (0-100m) for the a) 25 March 2010 12:00GMT non-baseline time stamp, and b) 3 August 2010 16:30GMT baseline categorized time stamp. The maps show the regions of the lowest surface layer influencing an observation at Mace Head for the particular time stamp 3-hour window.

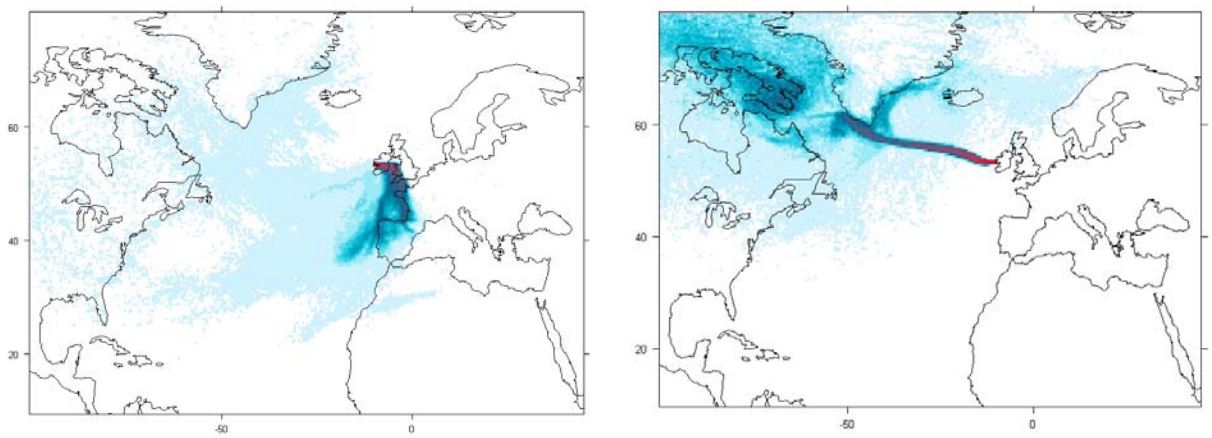

The seven simulated observations most isotopically lighter than baseline have common air history features which have passed over Ireland or the UK prior to reaching Mace Head, highlighting the weight held by proximal land sources. Recent work by Manning et al (2011) successfully applied a novel inverse modeling approach with regional land-influenced N_2O mole

fraction data at Mace Head to estimate total N_2O emissions and verify emission inventories from the UK and northwest Europe, both proximal land sources. The short-term variation in N_2O isotopic composition in this model with changing regional emissions influences suggests that incorporation of isotopic data alongside the mole fraction data in inversion methodologies such as that of Manning et al (2011) could aid emissions verification by adding the ability to distinguish between regional source categories (tied to signatures) rather than just total emissions which the mole fraction data are limited to.

In future modeling and measurement efforts the erratic soil emissions and signature could be better mediated with the statistical advantage of having a large collection of observation data points. With more than the current sparse data set it would be possible to apply a likely distribution of soil source signatures which might then statistically represent the net response of true variable soil signatures. The surface source signature distributions could also be better tailored to the specific region of study, which for Mace Head would be specific to temperate regions of Europe and ideally include signatures from regionally prominent N_2O sources such as peat. Because of the lack of certainty in soil signatures at the current time, the model made no distinction between agricultural and natural soil isotope signatures and their different spatial distributions. Recent measurements of N_2O emitted from agricultural and natural soils add to the small pool of information about emission signatures and suggest that fertilized agricultural soils are notably more depleted in $\delta^{15}N^{bulk}$ from natural soils, whereas the ^{15}N-site specific composition reflects different microbial processes (Park et al 2011). With more source signature data the N_2O isotopic composition in the troposphere will be valuable in separating the anthropogenic agricultural sources from the total emissions arriving at Mace Head.

3.2.4 Seasonal cycle

The modeled reference case time series (Figure 3.8) shows the isotopic composition of baseline time stamps following the seasonal influx of isotopically enriched stratospheric air so that isotopic values peak in August and have a February minimum, counter to the minimum mole fraction in August and maximum mole fraction in February (Figure 3.6). In this model system the baseline seasonal cycle modulation in the isotopologues are small and the detectable cycle results only from the effects of the stratospheric signal model component of monthly varying $\delta_{bg,m}$ step-functions. This model does not simulate any seasonal cycle in the background troposphere and therefore in the baseline data the seasonal cycle is examined through the model scenarios of the stratospheric component. The reference case plotted in Figure 3.8 illustrates baseline seasonal cycles of the same magnitudes as the amplitudes reported in Section 3.1.3 (peak-to-peak $\delta^{15}N^{bulk}$ 0.029‰, $\delta^{15}N^{\alpha}$ 0.039‰, $\delta^{15}N^{\beta}$ 0.020‰, SP 0.019‰, and $\delta^{18}O$ 0.026‰). The ability to resolve the stratospheric seasonal influence assumes high-frequency data collection since low-frequency flask observations have noted difficulty in resolving subtle signals with statistical significance.

The reference case stratospheric results in Figure 3.8 are highly uncertain and symbolize only one possible scenario. Multiple model scenarios explore input parameters and apply realistic alternative scenarios to assess possible magnitudes of the stratospheric seasonal signal. Results are illustrated by seasonal amplitudes for given cases in Figure 3.11 for $\delta^{15}N^{bulk}$ and $\delta^{15}N^{\alpha}$. Other isotopic values have slightly scaled resulting amplitudes, similar to the relative reference case amplitudes. Akin to the varied magnitudes of responses in the isotopologues to regional source signals, the isotopic values respond in different magnitudes to stratospheric influence and hold different information which is important in the ability to distinguish N_2O influences. In this model structure $\delta^{15}N^{\alpha}$ has the largest seasonal amplitude response to the stratospheric signal.

For the many of the model scenarios, peak-to-peak amplitudes are predicted to be <0.05‰. However, some realistic scenarios give amplitudes up to ~0.10 to 0.15‰, which are in the realm of detectability by current achievable precision in Stheno+CF-IRMS.

Figure 3.11 Stratospheric seasonal influence amplitudes (August maximum – February minimum) for $\delta^{15}N^{bulk}$ and $\delta^{15}N^{\alpha}$ for the cases listed in Table 3.1 and described in the text.

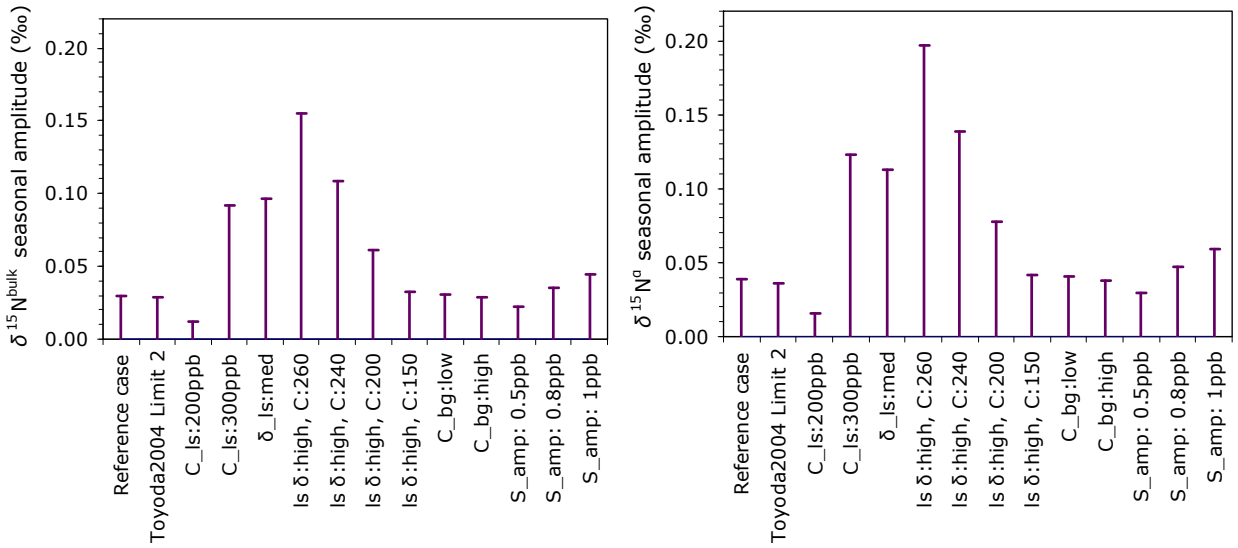

Uncertainty in the estimate of N_2O isotopic seasonal cycle driven by stratospheric mixing is due to uncertainty in the lower stratosphere conditions. In general, in these cases the most sensitive changes are associated with the prescribed lower stratosphere N_2O mole fraction and isotopic composition, with little effect by changes in tropospheric conditions.

The modified tropospheric mole fractions (C_bg:low, C_bg:high) have negligible effects compared to the reference case. Not intuitively, the amplitude of the tropospheric mole fraction seasonal cycle from the stratospheric effect (S_amp) has only a marginal impact on the isotopic seasonal amplitude. The relative effects scale linearly with the magnitude of the mole fraction seasonal amplitude. Though not displayed here, within uncertainty and potential variation in the tropospheric mean isotopic composition, which centers the derived seasonal step-function, there is no effect on the estimated amplitude of the stratospheric effect.

In contrast, modifying the highly uncertain conditions of the lower stratosphere causes significant changes in the tropospheric isotope seasonal amplitude.

Adjusting the mole fraction in the lower stratosphere greatly affects the weight given to the distinctive ^{15}N- and ^{18}O- enriched signature of the stratosphere and thus the isotopic signal in the troposphere is greatly modulated. Increasing the lower stratospheric mole fraction to 300 ppb causes substantial increases in amplitudes to within current IRMS precision capabilities (Stheno+CF-IRMS) for $\delta^{15}N^{bulk}$ and $\delta^{15}N^{\alpha}$ with values $\delta^{15}N^{bulk}$ 0.092‰, $\delta^{15}N^{\alpha}$ 0.123‰, $\delta^{15}N^{\beta}$ 0.062‰, SP 0.061‰, and $\delta^{18}O$ 0.082‰. Based upon observations in the stratosphere, a slight shifting of the definition of the lower stratosphere to lower altitudes could result in the integrated mole fraction to be the higher 300 ppb value. Conversely, the reduced mole fraction scenario (200 ppb) drops the amplitude by a little over half. The slight change in the chosen definition of the lower stratosphere from Toyoda et al (2004) is shown to have a negligible impact.

The prescribed isotopic composition in the lower stratosphere is highly uncertain considering observations of the steep change in composition with altitude, higher stratospheric composition which additionally varies between measurement locations laterally, and the limited temporal coverage of observations (Rockmann et al 2001, Park et al 2004, Toyoda et al 2004, Kaiser et al 2006). Slightly increasing the enrichment (δ_ls:med) to values measured in the upper portion of the lower stratosphere by Toyoda et al (2004) has a drastic impact on the amplitude of the signal in the troposphere. This realistic measurement-based case has seasonal amplitudes of $\delta^{15}N^{bulk}$ 0.096‰, $\delta^{15}N^{\alpha}$ 0.113‰, $\delta^{15}N^{\beta}$ 0.079‰, SP 0.034‰, and $\delta^{18}O$ 0.134‰, within detection limits by current IRMS precision for $\delta^{15}N^{bulk}$, $\delta^{15}N^{\alpha}$, and $\delta^{18}O$. Further enrichment of stratospheric isotopic composition as exists in higher levels of the stratosphere has not surprisingly a large impact of increasing the signal amplitude in the troposphere. The highly enriched lower stratosphere case with the equivalent mole fraction to the reference case (δ_ls:high, C:260) shows the greatest amplitude for all isotopic values but is not fully realistic because any greater fractionation in the stratosphere to cause a more highly enriched signature would be accompanied by a decrease in mole fraction. The scenarios with lowered mole fractions to 240 ppb and 200 ppb are reasonable and result in amplitudes resolvable by current IRMS capabilities for $\delta^{15}N^{bulk}$, $\delta^{15}N^{\alpha}$, and at the cusp for $\delta^{18}O$, and for $\delta^{15}N^{bulk}$, respectively. These realistic cases suggest that detection of the seasonal signal from the stratosphere in the isotopic composition of the troposphere is quite likely and supports the ability of tropospheric isotopic observations to interpret the N_2O mole fraction seasonal cycle.

The scenarios using this model design generally show that detection of the seasonal stratospheric isotopic signal with high-frequency data would be at the border with current measurement precision capabiities by IRMS (Stheno+CF-IRMS), with realistic scenarios resulting in both detectable and undetectable amplitudes. The stratospheric seasonal signal is modeled to be the strongest, and therefore the most likely to be detected, in $\delta^{15}N^{\alpha}$ and $\delta^{15}N^{bulk}$ for most scenarios. Projected improved precision by instrumentation in development (Stheno+QCL) would likely be able to detect seasonal cycles for the majority of scenarios. The fundamental assumption of the two-box mixing between the lower stratosphere and troposphere is supported in the general sense by other studies of observations and dynamics, but could be a false representation of the STE process and effect on the surface troposphere. Therefore, although this model suggests a potentially weak cycle, the possibility for the seasonal STE effect to manifest itself differently in actual observations is open.

This model focused on the stratospheric seasonal signal at Mace Head since the seasonal downward flux of stratospheric air has been put forward as the dominant cause of the N_2O mole fraction seasonal cycle. However, there are other potential seasonal influences on N_2O that could be manifested in the isotopic signal which were not found due to model limitations or not included this model.

Seasonality in the non-baseline data isotopic compositions could have resulted from seasonality in regional sources. Calculated results for the model system without the stratosphere, which would then only be taking into account regional emissions seasonality, yield no significant seasonal cycle in the non-baseline samples despite the fact that the other major influence on composition, soil emissions, does vary seasonally. The inability to detect a soil source seasonal cycle in this model is largely due to the low-frequency, uneven distribution non-baseline data points.

Likely corresponding to the seasonality and episodic nature of soil emissions there will be mirrored changes in the soil emissions isotopic signature which this model is not including. Environmentally changing factors with season such as precipitation and temperature, and for agriculture the yearly timings of irrigation, fertilizer application, harvest, and tilling, modify the

distribution of soil microbes and N_2O production processes. Freeze/thaw cycles in winter and early spring have been observed in multiple studies in Germany to induce large N_2O fluxes which account for the majority of total annual emissions (Flessa et al 1995, Guckland et al 2010, Wu et al 2010). In a study of N_2O agricultural emissions in Ireland, which will have a large impact on any easterly air at Mace Head, the large fluxes in spring associated with fertilizer application accounted for ~63% of annual emissions (Abdalla et al 2009). Studies of N_2O isotopic composition from soil emissions have found extremely depleted values associated with high release rates (Perez et al 2000, 2006). Most predominately this has been studied between nitrification and denitrification which can yield very divergent isotope signatures in released N_2O. Recent observations suggest an isotopic difference between natural and fertilized agricultural soil emissions (Park et al 2011). Current knowledge of source signatures, however, precludes the assignment of an informed distribution of soil signatures to the limited number of available data points. A likelihood of a variable soil isotope signature in addition to seasonally-varying whole N_2O emissions therefore might enable isotopic composition observations to detect a seasonal effect in the tropospheric isotope composition at Mace Head due to soil emissions. The detection of such a signal in the isotopic composition would be of great use to the study of the N_2O budget given that the extensive mole fraction data has not yet been able to accurately separate the soil signal, in either short-term, seasonal or interannual time frames.

Actual isotopic observations of baseline air with Mace Head as the receptor location might be able to capture northern hemisphere seasonal 'breathing' of the seasonally varying N_2O sources, which is not included in the background component of this model. The setup of this model prevents surface emissions from imposing any seasonal effect on the baseline samples which do not, by definition, have air histories with significant time spent over land and thus are predominantly capturing the assigned constant non-seasonally-varying ocean emissions. Analyses of the seasonal cycle of N_2O mole fractions have yielded insight into the main drivers of the N_2O budget at Mace Head and suggest the late summer minimum results largely from seasonality in the STE stratospheric signal of N_2O-depleted air and leave open the possibility of also tropospheric transport mechanisms (e.g. seasonal changes in boundary layer height, convection) and circulation controls (Jiang et al 2007, Nevison et al 2007). The constant isotopic background of this model therefore does not discount the possibility of a seasonal signal resulting from seasonality in surface emissions as manifested in the background troposphere or seasonal tropospheric transport effects. Actual isotopic observations would undoubtedly assist greatly in distinguishing these varying effects on the N_2O mole fraction seasonal cycle due to the separate isotopic fractionation patterns.

Conclusion

An idealized model of the isotopic composition of N_2O in the troposphere was developed utilizing the primary tools of UKMO NAME 3D Lagrangian air history estimates and AGAGE network in situ observations. The main aim of this model study was to simulate the transport of N_2O and its isotopic signatures to Mace Head from regional sources and the stratosphere to determine expected isotopic signals and identify source-receptor relationships, and furthermore the estimated ranges of short-term and seasonal variation inform the instrument precision needed to detect coherent signals. A second benefit of the creation of this model was the development of a forward model framework for future interpretation of tropospheric isotopic data, which could also be applied to locations other than Mace Head. Variations between air parcels and seasonality were

assessed though model scenarios in an attempt to provide a realistic picture of variation in isotopic composition at Mace Head station.

Synoptic scale, regional variations in the N_2O isotopic composition predicted by the model simulation driven by meteorology and regional emissions created modeled short-term variation detectable given current measurement precision capabilities. Soil emissions hold the greatest control over the simulated tropospheric isotopic composition over other emissions sources and balance the isotopically enriched stratospheric signal. The reference case scenario, having a soil signature closer to tropospheric composition, and highly depleted soil signature case together provided a range of potential deviations from baseline which may occur with air parcels influenced by regional soil emissions. Both cases predicted variability of magnitudes measureable by current instrumentation precision (Stheno+CF-IRMS, 1σ precisions $\delta^{15}N^{bulk}$ 0.05‰, $\delta^{15}N^{\alpha}$ 0.11‰, $\delta^{15}N^{\beta}$ 0.14‰, SP 0.21‰, $\delta^{18}O$ 0.10‰). The ^{15}N- and ^{18}O-depleted soil signature scenario illustrated particularly large departures from baseline isotopic composition at Mace Head. These large variations would not exist in all observations but would likely be captured in a portion of observations, particularly with increased data collection frequency. Coherent, valuable short-term isotopic variations in N_2O at Mace Head responding to changing air histories and regional emissions would be extractable by current instrumentation, and even finer scale information could be attained with projected improved future instrument precision by Stheno+QCL (±0.025‰ (±1σ) for ^{15}N isotopomers, ±0.05‰ for ^{18}O).

The seasonal cycle of isotopic composition in this model system driven by the stratosphere is small, as might be expected given the small amplitude of the mole fraction seasonal cycle. The stratospheric seasonal simulations within the simplified 2-box framework yield results suggesting the seasonal cycle would be at the border of detection for current measurement capabilities depending upon assumed values of uncertain input parameters. The stratospheric seasonal signal is modeled to be the strongest, and therefore the most likely to be detected, in $\delta^{15}N^{\alpha}$ and $\delta^{15}N^{bulk}$ for most scenarios. The magnitude of the seasonal signal is found to be only marginally responsive to the CFC-12 proxy based estimation of the N_2O mole fraction seasonal amplitude and very unresponsive to tropospheric input values. The signal at Mace Head is highly sensitive to the composition assigned to the lower stratosphere. The assumed constant mole fraction and isotopic composition input values for the lower stratosphere within the 2-box framework are highly uncertain due to limited stratospheric measurements and unknown degree to which the more extreme middle and upper stratospheric compositions would impact the troposphere. Realistic alternatives to the reference case values give markedly increased seasonal signals and encourage the ability of instrumentation to detect the stratospheric seasonal signal. Projected precisions for optical instrumentation in development (Stheno+QCL) would likely be able to detect seasonal cycles for the majority of scenarios.

Additional variation not captured by these simulations may reside in a number of model simplifications which could be expanded and improved upon. Input emissions fields are overly homogeneous to capture the true often sporadic nature of N_2O emissions from soil, both temporally and spatially, which would impact each individual air parcel differently depending upon the specific conditions and footprint. The simulations are thus missing variations from the episodic emissions and/or emissions signatures with higher frequency than the monthly-varying soil emissions and imposed constant isotopic signature. Another model feature masking potential variation is the sparse collection of data points which cannot capture the many fluctuations which would result from high-frequency data. This is clearly evident in the high-frequency continuous AGAGE data for the N_2O mole fractions which is able to capture alternating synoptic patterns and changing air parcels arriving at Mace Head thus covering a broad number of air origins. Stratospheric effects in this model system only include a monthly varying step function of the slowly propagating seasonal influence.

However, actual transient dynamics of stratosphere-troposphere exchange processes might lead to influence on shorter timescales. Tropopause folds can bring stratospheric air directly towards the surface with a more significant impact on surface composition, particularly at the latitudes near Mace Head on the North Atlantic storm track which aids in transporting stratospheric mixing down to lower altitudes. The exclusion of tropospheric transport from the background isotopic signal masks effects of emissions from regions outside the computational domain. For regions just outside the domain these emissions would contribute to short-term variation. Seasonal effects in tropospheric transport have been implicated as contributing to the observed N_2O seasonal cycle at Mace Head (Nevison et al 2007). Fluctuating background conditions could therefore augment the model stratospheric seasonal signal.

The additional sources of variation not simulated in this study mean that the modeled short-term and seasonal isotopic deviations estimated here represent a lower limit. This further supports the ability of measurements of tropospheric N_2O isotopic composition to detect N_2O influences with valuable information beyond that from mole fractions alone. The importance is emphasized for N_2O for which the distinction between influences-- specific source type, stratospheric loss and mixing, and transport effects-- has proven difficult to determine with only mole fraction data in inverse top-down schemes and data analyses. Bottom-up models and inventories attempting to quantify and delineate between emission types exhibit large uncertainty given the complicated nature of N_2O emissions. Also, the desire for emissions quantification and verification for individual emitting sectors is high in the current policy environment, and isotopic composition information in the troposphere lends itself to the distinction among various N_2O governing processes. A primary insight provided by this simulation study is the likely efficacy of N_2O isotopic composition observations for quantification and characterization of regional surface emissions using the measurable short-term variability between air masses with spatially and temporally different origins. With an increased knowledge base of isotopic signatures and sufficient precision and frequency of measurements, there is potential to distinguish between anthropogenic agricultural soil N_2O emissions and natural soil emissions. Manning et al (2011) recently employed a novel inverse modeling technique with the NAME air histories stemming from Mace Head mole fraction observations to verify and quantify N_2O emissions in the UK and northwest Europe. The results presented here encourage the incorporation of isotopic data into this framework which would provide additional information to be able to separate the emission sources between sectors.

By having the isotopic data alongside the N_2O concentrations, there are 4 independent pieces of information (N_2O, $\delta^{15}N^{\alpha}$, $\delta^{15}N^{\beta}$, $\delta^{18}O$), and the derived quantities $\delta^{15}N^{bulk}$ and SP, to inform emission distributions, stratospheric influences, and troposphere transport effects on N_2O. This information would ideally occur with more extensive use of the model and air histories with a continuous high-frequency time series, such as by Manning et al (2011), as well as be paired with complementary research into source emission signatures approximating the region under analysis (i.e. temperate European soil emissions signatures, whereas the majority of existent signature estimates are based in the tropics, and European industry-type-specific source signatures).

This study highlights the need for high-frequency data to be able to capture subtle informative variations. This is particularly true for detection of seasonal signals which these simulations demonstrated to be on the edge of detection, even with the improved projected precision and frequency. Pulling apart the controls on N_2O seasonality would greatly enhance the understanding of the N_2O global budget. Analogous to how the progression of N_2O mole fraction measurement precision capabilities and high-frequency data enabled detection of the mole fraction seasonal cycle in the mid-1990s, the modeling results obtained here imply that the detection of the seasonal cycle in N_2O isotopic composition may require improvement from current measurement precision capabilities and initiation of high-frequency data collection. Looking to the future with

long-term data, these results illustrating coherent detectable source-receptor relationships point to the further usefulness of isotopic composition in separating of the causes of the long-term trends in N_2O, including the diagnoses of interannual and inter-seasonal variability in growth for a more complete understanding of N_2O regional and global controls. These utilities hinge on, however, a research community jointly working on this task to provide the emissions and stratospheric signatures, inter-calibration accuracy, modeling and meteorology, and high-precision high-frequency observations.

Chapter 3 References

Abdalla M, Wattenbach M, Smith P, Ambus P, Jones M &Williams M (2009). Application of the DNDC model to predict emissions of N_2O from Irish agriculture. *Geoderma* 151: 327-337.

Alexander B, Park RJ, Jacob DJ, Li QB, Yantosca RM, Savarino J, Lee CCW & Thiemens MH (2005). Sulfate formation in sea salt aerosols: Constraints from oxygen isotopes. *J Geophys Res* 110: D10307.

Bateman AS, Kelly SD & Jickells TJ (2005). Nitrogen isotope relationships between crops and fertilizer: implications for using nitrogen isotope analysis as an indicator of agricultural regime. *J Agric Food Chem* 53: 5760-5765.

Bol R, Toyoda S, Yamulki S, Hawkins JMB, Cardenas LM & Yoshida N (2003). Dual isotope and isotopomer ratios of N_2O emitted from a temperate grassland soil after fertiliser application. *Rapid Commun Mass Spectrom* 17: 2550-2556.

Bouwman AF (1995). Direct emission of nitrous oxide from agricultural soils. *Nutrient Cycling in Agroecosystems* 46(1): 53-70.

Butchart N & Coauthors (2006). Simulations of anthropogenic change in the strength of the Brewer–Dobson circulation. *Climate Dyn* 27: 727-741.

Butchart N & Coauthors (2010). Chemistry-climate model simulations of twenty-first century stratospheric climate and circulation changes. *J Climate* 23: 5349-5374.

Casciotti K, Rahn T & Wahlen M (1997). Stable isotopes of N and O in nitrous oxide emissions from fertilized soils. *EOS Trans Am Geophys Union* 78: F58 (Fall Meet Suppl).

Casciotti KL (2009). Inverse kinetic isotope fractionation during bacterial nitrite oxidation. *Geochim Cosmochim Acta* 73: 2061-2076.

Croteau P, Atlas EL, Schauffler SM, Blake DR, Diskin GS & Boering KA (2010). Effect of local and regional sources on the isotopic composition of nitrous oxide in the tropical free troposphere and tropopause layer. *J Geophys Res* 115: D00J11.

Cullen MJP (1993). The Unified Forecast/Climate Model. *Meteorol Mag* 1449: 81-94.

Cullen MJP, Davies T, Mawson MH, James JA, Coulter SC & Malcolm A. An overview of numerical methods for the next generation UK NWP and climate model. *In*: Lin CA, Laprise R & Ritchie H, Editors, Numerical Methods in Atmospheric and Ocean Modelling. Canadian Meteorological & Oceanographic Society, Ottowa, Canada, 1997.

Davies T, Cullen MJP, Malcolm AJ, Mawson MH, Staniforth A, White AA & Wood N (2005). A new dynamical core for the Met Office's global and regional modelling of the atmosphere. *Q J R Meteorol Soc* 131: 1759-1782.

Dore JE, Popp BN, Karl DM & Sansone FJ (1998). A large source of atmospheric nitrous oxide from subtropical North Pacific surface waters. *Nature* 396: 63-66.

Draxler RR & Hess GD (1998). An overview of the HYSPLIT_4 modelling system for trajectories, dispersion, and deposition. *Australian Meteorol Mag* 47: 295-308.

Flessa H, Dorsch P & Beese F (1995). Seasonal variation of N_2O and CH_4 fluxes in differently managed arable soils in southern Germany. *J Geophys Res* 100: 23115–23124.

Garcia R, Randel WJ (2008). Acceleration of the Brewer-Dobson circulation due to increases in greenhouse gases. *J Atmos Sci* 65: 2731-2739.

Gerasopoulos E, Zanis P, Papastefanou C,. Zerefos CS, Ioannidou A, Wernli H (2006). A complex case study of down to the surface intrusions of persistent stratospheric air over the Eastern Mediterranean. *Atmospheric Environment* 40: 4113-4125.

Goldberg SD & Gebauer G (2009). Drought turns a Central European Norway spruce forest soil from an N_2O source to a transient N_2 sink. *Global Change Biology* 15: 850-860.

Goldberg SD, Borken W & Gebauer G (2010). N_2O emission in a Norway spruce forest due to soil frost: concentration and isotope profiles shed a new light on an old story. *Biogeochemistry* 97: 21-30.

Griffith DWT, Toon GC, Sen B, Blavier J-F & Toth RA (2000). Vertical profiles of nitrous oxide isotopomer fractionation measured in the stratosphere. *Geophys Res Lett* 27: 2485-2488.

Guckland A, Corre M & Flessa H (2010). Variability of soil N cycling and N_2O emission in a mixed deciduous forest with different abundance of beech. *Plant Soil* 336: 25-38.

Hirsch AI, Michalak AM, Bruhwiler LM, Peters W, Dlugokencky EJ & Coauthors (2006). Inverse modeling estimates of the global nitrous oxide surface flux from 1998-2001. *Global Biogeochem Cycles* 20: GB1008.

Huang J, Golombek A, Prinn R, Weiss R, Fraser P, Simmonds P, Dlugokencky EJ, Hall B, Elkins J, Steele P, Langenfelds R, Krummel P, Dutton G & Porter L (2008). Estimation of regional emissions of nitrous oxide from 1997 to 2005 using multi-network measurements, a chemical transport model, and a Kalman Filter. *J Geophys Res* 113: D17313.

Ishijima K *et al.* (2010). Stratospheric influence on the seasonal cycle of nitrous oxide in the troposphere as deduced from aircraft observations and model simulations, *J Geophys Res* 115: D20308.

James P, Stohl A, Forster C, Eckhardt S, Seibert P & Frank A (2003a). A 15-year climatology of stratosphere-troposphere exchange with a Lagrangian particle dispersion model: 2, Mean climate and seasonal variability. *J Geophys Res* 108(D12): 8522.

James P, Stohl A, Forster C & Eckhardt S (2003b). A 15-year climatology of stratosphere-troposphere exchange with a Lagrangian particle dispersion model: 1. Methodology and validation. *J Geophys Res* 108(D12): 8519.

Jiang X, Ku WL, Shia R-L, Li Q, Elkins JW, Prinn RG & Yung YL (2007). Seasonal cycle of N_2O: Analysis of data. *Global Biogeochem Cycles* 21: GB1006.

Kaiser J, Engel A, Borchers R & Rockmann T (2006). Probing stratospheric transport and chemistry with new balloon and aircraft observations of the meridional and vertical N_2O isotope distribution. *Atmospheric Chemistry and Physics* 6: 3535-3556.

Kim K-R & Craig H (1993). Nitrogen-15 and oxygen-18 characteristics of nitrous oxide: A global perspective. *Science* 262: 1855-1857.

Kool DM, Wrage N, Oenema O, Harris D & van Groenigen JW (2009). The ^{18}O signature of biogenic nitrous oxide is determined by O exchange with water, *Rapid Commun Mass Spectrom* 23: 104-108.

Levin *et al.* (2002). Three years of trace gas observations over the EuroSiberian domain derived from aircraft sampling: a concerted action. *Tellus* 54: 696-712.

Liang Q, Stolarski RS, Douglass AR, Newman PA & Nielsen JE (2008). Evaluation of emissions and transport of CFCs using surface observations and their seasonal cycles and the GEOS CCM simulation with emissions-based forcing. *J Geophys Res* 113: D14302.

Liang Q, Douglass AR, Duncan BN, Stolarski RS & Witte JC (2009). The governing processes and timescales of stratosphere-to-troposphere transport and its contribution to ozone in the Arctic troposphere. *Atmos Chem Phys* 9: 3011-3025.

Liao T, Camp CD, & Yung YL (2004). The seasonal cycle of N_2O. *Geophys Res Letters* 31: L17108.

Manning AJ, Ryall DB, Derwent RG, Simmonds PG & O'Doherty S (2003). Estimating European emissions of ozone-depleting and greenhouse gases using observations and a modelling back-attribution technique. *J Geophys Res* 108: 4405.

Manning AJ, O'Doherty S, Jones AR, Simmonds PG & Derwent RG (2011). Estimating UK methane and nitrous oxide emissions from 1990 to 2007 using an inversion modeling approach. *J Geophys Res* 116: D02305.

Morgan CG, Allen M, Liang MC, Shia RL, Blake GA & Yung YL (2004). Isotopic fractionation of nitrous oxide in the stratosphere: Comparison between model and observations. *J Geophys Res* 109: D04305.

Naqvi SWA, Yoshinari T, Jayakumar DA, Altabet MA, Narvekar PV, Devol AH, Brandes JA & Codispoti LA (1998). Budgetary and biogeochemical implications of N_2O isotope signatures in the Arabian Sea. *Nature* 394: 462-464.

Nevison CD, Keeling RF, Weiss RF, Popp BN, Jin X, Fraser PJ, Porter LW & Hess PG (2005). Southern Ocean ventilation inferred from seasonal cycles of atmospheric N_2O and O_2/N_2 at Cape Grim, Tasmania. *Tellus Ser. B* 57: 218-229.

Nevison CD, Kinnison DE & Weiss RF (2004). Stratospheric influence on the tropospheric seasonal cycles of nitrous oxide and chlorofluorocarbons. *Geophys Res Lett* 31: L20103.

Nevison CD, Mahowald NM, Weiss RF & Prinn RG (2007). Interannual and seasonal variability in atmospheric N_2O. *Global Biogeochem Cycles* 21: GB3017.

Nevison CD, Dlugokencky E, Dutton G, Elkins JW, Fraser P, Hall B, Krummel PB & Langenfelds RL (2011). Exploring causes of interannual variability in the seasonal cycles of tropospheric nitrous oxide. *Atmos Chem Phys* 11: 3713-3730.

O'Doherty S *et al.* (2001). In situ chloroform measurements at Advanced Global Atmospheric Gases Experiment atmospheric research stations from 1994 to 1998. *J Geophys Res* 106: 20429–20444.

Ogawa M & Yoshida N (2005a). Nitrous oxide emission from the burning of agricultural residue. *Atmospheric Environment* 39: 3421-3429.

Ogawa M & Yoshida N (2005b). Intramolecular distribution of stable nitrogen and oxygen isotopes of nitrous oxide emitted during coal combustion. *Chemosphere* 61: 877-887.

Opdyke MR, Ostrom NE & Ostrom PH (2009). Evidence for the predominance of denitrification as a source of N_2O in temperate agricultural soils based on isotopologue measurements. *Global Biogeochem Cycles* 23: GB4018.

Ostrom NE, Pitt A, Sutka R, Ostrom PH, Grandy As, Huizinga KM, Robertson GP (2007). Isotopologue effects during N_2O reduction in soils and in pure cultures of denitrifiers. *J Geophys Res* 112: G02005.

Ostrom NE, Pitt A, Sutka RL, Ostrom PH, Grandy AS, Huizinga KM, Gandhi H, von Fischer JC & Robertson GP (2010). Isotopologue data reveal bacterial denitrification as the primary source of N_2O during a high flux event following cultivation of a native temperate grassland. *Soil Biology and Biochemistry* 42: 499-506.

Park SY, Atlas EL, Boering KA (2004). Measurements of N_2O isotopologues in the stratosphere: Influence of transport on the apparent enrichment factors and the isotopologue fluxes to the troposphere, *J Geophys Res* 109: 462-464.

Park S, Perez T, Boering KA, Trumbore SE, Gil J, Marquina S & Tyler SC (2011). Can N_2O stable isotopes and isotopomers be useful tools to characterize sources and microbial pathways of N_2O production and consumption in tropical soils? *Global Biogeochem Cycles* 25: GB1001.

Pataki DE, Ehleringer JR, Flannagan LB, Yakir D, Bowling DR, Still CJ, Buchmann N, Kaplan JO & Berry JA (2003). The application and interpretation of Keeling plots in terrestrial carbon cycle research. *Global Biogeochem Cycles* 17: 1022.

Perez T, Trumbore SE, Tyler SC, Davidson EA, Keller M & DeCarmargo PB (2000). Isotopic variability of N_2O emissions from tropical forest soils. *Global Biogeochem Cycles* 14: 525-535.

Perez T, Trumbore SE, Tyler SC, Matson PA, Ortiz-Monasterio I, Rahn T & DWT Griffith (2001). Identifying the agricultural imprint on the global N_2O budget using stable isotopes. *J Geophys Res* 106: 9869-9878.

Perez T, Garcia-Montiel D, Trumbore S, Tyler S, De Camargo P, Moreira M & Piccolo M & Cerri C (2006). Nitrous oxide nitrification and denitrification N-15 enrichment factors from Amazon forest soils. *Ecological Applications* 16: 2153-2167.

Plumb RA & Ko MRK (1992). Interrelationships between mole fractions of long-lived stratospheric constituents. *J Geophys Res* 97: 10145-10156.

Plumb RA & McConalogue DD (1988). On the meridional structure of long-lived tropospheric constituents. *J Geophys Res* 93: 15897-15913.

Popp BN, Westley MB, Toyoda S, Miwa T, Dore JE & coauthors (2002). Nitrogen and oxygen isotopomeric constraints on the origins and sea-to-air flux of N_2O in the oligotrophic subtropical North Pacific gyre. *Global Biogeochem Cycles* 16: doi:2001GB001806.

Potter CS, Matson PA, Vitousek PM & Davidson EA (1996). Process modeling of controls on nitrogen trace gas emissions from soils worldwide. *J Geophys Res* 101: 1361-1377.

Prinn, R *et al.* (2000). A history of chemically and radiatively important gases in air deducted from ALE/GAGE/AGAGE. *J Geophys Res* 105: 17751-17792.

Rahn T & Wahlen M (2000). A reassessment of the global isotopic budget of atmospheric nitrous oxide. *Global Biogeochem Cycles* 14: 537-543.

Rock L, Ellert BH, Mayer B & Norman AL (2007). Isotopic composition of tropospheric and soil N_2O from successive depths of agricultural plots with contrasting crops and nitrogen amendments. *J Geophys Res* 112: D18303.

Rockmann T, Kaiser J, Brenninkmeijer CAM, Crowley J, Borchers R, Brand W & Crutzen P (2001). Isotopic enrichment of nitrous oxide ($^{15}N^{14}NO$, $^{14}N^{15}NO$, $^{14}N^{14}N^{18}O$) in the stratosphere and in the laboratory. *J Geophys Res* 106: 10403.

Rockmann T, Kaiser J & Brennickmeijer CAM (2003b). The isotopic fingerprint of the pre-industrial and the anthropogenic N_2O source. *Atmospheric Chemistry and Physics* 3: 315-323

Simmonds PG, Derwent RG, Manning AJ, O'Doherty S & Spain G (2010). Natural chloroform emissions from the blanket peat bogs in the vicinity of Mace Head, Ireland over a 14-year period. *Atmospheric Environment* 44: 1284-1291.

Snider DM, Schiff SL & Spoelstra J (2009). $^{15}N/^{14}N$ and $^{18}O/^{16}O$ stable isotope ratios of nitrous oxide produced during denitrification in temperate forest soils. *Geochimica et Cosmochimica*

Acta 73: 877-888.

Stein L & Yung Y (2003). Production, isotopic composition, and atmospheric fate of biologically produced nitrous oxide. *Ann Rev Earth Planetary Sci* 31: 329-356.

Stohl A *et al.* (2003). Stratosphere-troposphere exchange: A review, and what we have learned from STACCATO. *J Geophys Res* 108: 8516.

Sutka RL, Ostrom NE, Ostrom PH, Breznak JA, Gandhi H, Pitt AJ & Li F (2006). Distinguishing nitrous oxide production from nitrification, and denitrification on the basis of isotopomer abundances. *Appl Exp Microbiol* 72: 638-644.

Tilsner J, Wrage N, Lauf J & Gebauer G (2003). Emission of gaseous nitrogen oxides from an extensively managed grassland in NE Bavaria, Germany: II. Stable isotope natural abundance of N_2O. *Biogeochemistry* 63: 249-267.

Toyoda S, Yoshida N, Miwa T, Matsui Y, Yamagishi H, Tsunogai U, Nojiri Y & Tsurushima N (2002). Production mechanism and global budget of N_2O inferred from its isotopomers in the western North Pacific. *Geophys Res Lett* 29(3): 1037.

Toyoda S *et al.* (2004). Temporal and latitudinal distributions of stratospheric N_2O isotopomers. *J Geophys Res* 109: D08308.

Toyoda S, Mutobe H, Yamagishi H, Yoshida N & Tanji Y (2005). Fractionation of N_2O isotopomers during production by denitrifier. *Soil Biology and Biochemistry* 37(8): 1535-1545.

Toyoda S, Yamamoto S, Arai S, Nara H, Yoshida N, Kashiwakura K & Akiyama K (2008). Isotopomeric characterization of N_2O produced, consumed, and emitted by automobiles. *Rapid Commun Mass Spectrom* 22: 603-612.

Toyoda S *et al.* (2011). Characterization and production and consumption processes of N_2O emitted from temperate agricultural soils determined via isotopomer ratio analysis. *Global Biogeochem Cycles* 25: GB2008.

Van Groenigen JW, Zwart KB, Harris D & van Kessel C (2005). Vertical gradients of $d^{15}N$ and $d^{18}O$ in soil atmospheric N_2O—temporal dynamics in a sandy soil. *Rapid Commun Mass Spectrom* 19: 1289-1295.

Volk CM et al. (1996). Quantifying transport between the tropical and mid-latitude lower stratosphere. *Science* 272: 1763-1768.

Wada E & Ueda S. Carbon, nitrogen, and oxygen isotope ratios of CH_4 and N_2O in soil ecosystems. *In* Mass Spectrometry of Soils, Boutton TB & Yamasaki S, Editors, CRC Press, Boca Raton, Florida, 1996, 517 pp.

Wahlen M & Yoshinari T (1985). Oxygen isotope ratios in N_2O from different environments, *Nature* 313: 780-782.

Walter S, Bange HW, Breitenbach U & Wallace DWR (2006). Nitrous oxide in the North Atlantic Ocean. *Biogeosciences* 3: 607-619.

Well R, Flessa H, Jaradat F, Toyoda S & Yoshida N (2005). Measurement of isotopomer signatures of N_2O in groundwater. *J Geophys Res* 110: G02006.

Well R & Flessa H (2009). Isotopologue signatures of N_2O produced by denitrification in soils, *J Geophys Res* 114: G02020.

Westley MB, Popp BN & Rust TM (2007). The calibration of the intramolecular nitrogen isotope distribution in nitrous oxide measured by isotope ratio mass spectrometry. *Rapid Commun Mass Spectrom* 21: 391-405.

Wofsy SC, the Hippo Science Team and cooperating modellers and satellite teams (2011). HIAPER Pole-to-Pole Observations (HIPPO): fine-grained, global-scale measurements of climatically important atmospheric gases and aerosols. *Phil Trans R Soc A* 369: 2073-2086.

Wu X, Bruggemann N, Gasche R, Shen Z, Wolf B & Butterbach-Bahl K (2010). Environmental controls over soil-atmosphere exchange of N_2O, NO, and CO_2 in a temperate Norway spruce forest. *Global Biogeochem Cycles* 24: GB2012.

Yamagishi H, Westley MB, Popp BN, Toyoda S, Yoshida N, Watanabe S, Koba K & Yamanaka Y (2007). Role of nitrification and denitrification on the nitrous oxide cycle in the eastern tropical North Pacific and Gulf of California. *J Geophys Res - Biogeosci* 112: G02015.

Yamulki S, Wolf I, Bol R, Grant B, Brumme R, Veldkamp E & Jarvis SC (2000). Effects of dung and urine amendments on the isotope content of N_2O released from grasslands. *Rapid Commun Mass Spectrom* 14: 1356-1360.

Yamulki S, Toyoda S, Yoshida N, Veldkamp E, Grant B & Bol R (2001). Diurnal fluxes and the isotopomer ratios of N_2O in a temperate grassland following urine amendment. *Rapid Commun Mass Spectrom* 15: 1263-1269.

Yoshinari T, Altabet MA, Naqvi SWA, Codispoti L, Jayakumar A, *et al.* (1997). Nitrogen and oxygen isotopic compositions of N_2O from suboxic waters of the eastern tropical North Pacific and the Arabian Sea-- Measurement by continuous-flow isotope ratio monitoring. *Mar Chem* 56: 253-264.

Zhu R, Liu Y, Li X, Sun J, Xu H & Sun L (2008), Stable isotope natural abundance of nitrous oxide emitted from Antarctic tundra soils: effects of sea animal excrement depositions. *Rapid Commun Mass Spectrom* 22: 3570-3578.

Chapter 4: Tropospheric N_2O isotopic composition at Mace Head over 2010

Introduction

Nitrous oxide is an important greenhouse gas and a major contributor to the destruction of the ozone layer, and its concentrations in the atmosphere have been on a steady rise coinciding with the industrial era from ~270 ppb to presently ~323 ppb. There is much uncertainty in the global and regional budgets, and the isotopic composition of N_2O in the troposphere is an underutilized tool which carries information about N_2O sources, sinks, and other influences not captured in mole fraction observations.

Sources and sinks affecting N_2O in the troposphere are tied to characteristic isotopic signatures which will cause distinctive signals in the tropospheric isotopic composition. Figure 1.3a-c in Chapter 1 illustrates the $\delta^{15}N^{bulk}$, $\delta^{15}N^{\alpha}$, $\delta^{15}N^{\beta}$, $\delta^{18}O$, and site preference (SP = $\delta^{15}N^{\alpha}$ - $\delta^{15}N^{\beta}$) signatures of the major sources and sinks in relation to the tropospheric composition. Soil emissions from microbial production are estimated to be roughly 50% of the global source (Denman et al 2007), which has a ^{15}N- and ^{18}O- isotopically depleted signature relative to the atmosphere largely due to fractionation by enzymatic activity. Measurements of the isotopic composition in soil emissions have yielded a large array of isotopically depleted signatures because of the episodic nature of N_2O soil emissions and multiple competing microbial sources. Pulses of N_2O which account for the majority of total emissions are associated with extremely low δ values relative to tropospheric composition. Much of the soil source is natural, but it has been intensified by agriculture and fertilizer input so that now the anthropogenic contribution to atmospheric N_2O is approximately 1/3 of the total source, and attributed as the main cause of rising N_2O concentrations in the atmosphere. Recent measurements have suggested that the agricultural source may have a distinctively more-depleted $\delta^{15}N^{bulk}$ composition than the natural soil source, possibly allowing for valuable separation of these two sources (Perez et al 2001, Yamulki et al 2001, Park et al 2011). Anthropogenic influences on N_2O also include industrial and combustion sources. To date there have been very few measurements of the associated N_2O signatures, with the few data plotted in Figure 1.3a-c. However the fractionating processes will each have a distinct isotopic composition. The oceans provide a microbial source as well, tending to patchy with hot spots of production such as the eastern tropical north Pacific. Measurements in the ocean surface layer suggest that the isotopic signature is slightly depleted in bulk isotopic composition ($^{15}N^{bulk}$ and ^{18}O) and site-specific $^{15}N^{\alpha}$ relative to the troposphere, but with slight relative enrichment in $^{15}N^{\beta}$ (Yoshinari et al 1997, Dore et al 1998, Naqvi et al 1998, Popp et al 2002, Yamagishi et al 2007). These major sources of N_2O which tend to be isotopically lighter are balanced in the troposphere by N_2O loss in the stratosphere through UV photolysis and reaction with $O(^1D)$. The stratospheric loss reactions preferentially react with isotopically-light N_2O leaving a characteristic enriched composition in bulk and ^{15}N site-specific composition, which then mixes down into the troposphere through stratosphere-troposphere exchange (STE). Plotted in Figure 1.3a-c are estimates of the effective isotopically-enriched signature in the lower stratosphere which would mix with the troposphere. The fractionation and signatures of the stratospheric loss processes are relatively well understood (Yung & Miller 1997, Toyoda et al 2001, Rockmann et al 2001, Kaiser et al 2002a,b, Kaiser et al 2003b, McLinden et al 2003, Park et al 2004, Kaiser et al 2006), though the estimates for the effective signature mixing down to the troposphere has some uncertainty. Higher altitudes in the stratosphere become increasingly more enriched in bulk and site-specific ^{15}N and ^{18}O, measured to reach

extremely values in the upper levels of the stratosphere close to or over 100‰ dependent upon isotopologue (Toyoda et al 2004). With observations of N_2O isotopic composition in the troposphere, these signatures can be interpreted and relieve much uncertainty in N_2O global and regional budgets.

Despite this utility, observations of N_2O isotopic composition in the troposphere are limited, much due to the belief that current measurement techniques are not precise enough to detect the subtle yet valuable variations in isotopic composition. Kaiser et al (2003a) conducted the only focused tropospheric N_2O isotopic composition study with a dataset that spans ~2 years at sites spread throughout Europe and they were unable to discern temporal or spatial patterns related to N_2O processes. However, there was no information about distinguishing background air from regionally polluted air nor attribution of individual collected air samples to specific air mass origins, particularly a concern for these European sites surrounded by many regional influences. Their study also did not produce a consistent time series of all major isotopologues at a fixed site, which would be important to build a steady characterization of the N_2O regional European influences felt at that location.

Here this study produces the first observations of tropospheric N_2O isotopic composition with regular data covering a full annual cycle at one location. Crucially, these isotopic observations are uniquely paired with information about air sample histories and concurrent atmospheric data to inform the specific air mass origins, which is found to be vital for illustrating the consistency of isotopic signals with source and sink effects.

Observations span January 2010 to January 2011 at the Mace Head, Ireland Atmospheric Research Station (53.32N, 9.90W). Mace Head is a particularly well-suited location for assessment of N_2O influences and isotopic observations. On the west coast of Ireland it has a balanced synoptic situation with short-term (daily-weekly) fluctuations between westerly clean background air from across the Atlantic and Arctic ~50% of the time and air masses from local and/or European origin ~50%. The background air provides a broader picture of global scale variations and budget, while the European-influenced air carries the signals of land surface emissions from soil and industrial sources. N_2O isotopic data is especially useful tied to air history information in regions such as Europe where natural and anthropogenic emissions are in close proximity and across national borders, since mole fraction data alone is insufficient to distinguish between emission types and locations. Stratospheric influence on N_2O is also strong in the NH at the higher latitude location of Mace Head where the downward arm of the Brewer-Dobson circulation causes down-welling of stratospheric air into the troposphere. The seasonal July/August mole fraction minima at Mace Head is consistent with stratospheric down-welling of low concentration N_2O air during winter/spring and a 3-month delay in propagation to the surface. This notion is supported by correlated minima with complementary tracers such as CFC-11, CFC-12, CFC-113 which have the shared feature of having their primary sink in the stratosphere but no longer significant surface sources (Nevison et al 2004, 2007, 2011, Jiang et al 2007). Late summer minima in N_2O and CFC-12 possibly also reflect seasonal tropospheric transport mechanisms (e.g. convection, boundary layer height variations, interhemispheric transport) (Nevison et al 2007) but mole fraction data is unable to resolve stratospheric influence from other effects. Carried with the stratospheric air will be the characteristic ^{15}N- and ^{18}O-enriched N_2O isotopic signal which can be distinguished from surface emissions or synoptic influences. The stratospheric influence is currently the most pressing source of uncertainty in the N_2O budget (Hirsch et al 2006, Huang et al 2008).

N_2O has a long atmospheric lifetime of ~120 years which causes its tropospheric mole fraction to have very little variation in response to perturbations. The amplitude of the seasonal cycle of N_2O mole fraction is small; at Mace Head the mean detrended seasonal amplitude from AGAGE data from 1994 to 2010 is only 0.66 ppb relative to ~320 ppb atmospheric levels. Isotopic

signals similarly would be small. Improved mole fraction measurement techniques and high-frequency observations have allowed the detection of the small seasonal cycle (Fraser et al 1997, Prinn et al 2000, Nevison et al 2004) and likewise only with high-precision and high-frequency N_2O isotopic measurement techniques will we expect isotopic signals emerge. The Mace Head flask air sample observations are analyzed at MIT with the fully-automated Stheno pre-concentration system online with continuous flow isotope ratio mass spectrometry (Stheno+CF-IRMS), a system developed and optimized specifically to achieve the highest precision N_2O isotopic measurements which current technology will allow (Chapter 2).

The current dataset of N_2O isotopic composition over one annual cycle at Mace Head station serves as a preliminary assessment of N_2O isotopic variability in the troposphere on short-term, seasonal, and annual timescales, and explores the utilities of N_2O isotopic composition data in the troposphere for detection and interpretation of the aforementioned major controls on N_2O. Paired with detailed air history estimates and concurrent atmospheric data, isotopic composition is indeed found to vary in ways consistent with air mass origin and atmospheric tracer data. The resolvable source-receptor relationships are consistent with the observations data, but more measurements at high-frequency are needed for validation. This demonstrates the potential applicability of isotopic data, with an increased frequency of measurements, to a regional emissions inverse assessment such as that by Manning et al (2011). Isotopic observations at Mace Head also potentially capture an annual signal related to anonymously strong stratospheric activity in 2010. The ^{15}N site-specific isotopic composition shows an unexpected negative correlation, and considerations suggest that this is consistent with the air masses affecting Mace Head in the Northern Hemisphere higher latitudes which are balanced more towards aquatic emissions and far from the dominant soil source in the tropics. As no seasonal cycle could be clearly discerned from the low-frequency data, this study also informs the measurement precision and frequency required for future N_2O isotopic composition data to yield information about N_2O processes on short-term, seasonal, and annual timeframes. Continued observations of N_2O isotopic composition in the troposphere are shown to be warranted with abilities to discern stratospheric influence, disparate surface emissions, and synoptic mechanisms when tied to air mass origin information.

4.1 Methods

4.1.1 Tropospheric air samples

Air samples were collected regularly at the Mace Head Atmospheric Research Station, situated on the Atlantic coast of Ireland starting January 2010 through January 2011 with variable sampling interval; n = 48 flask samples. Mace Head is one of the primary Advanced Global Atmospheric Gases Experiment (AGAGE, http://agage.eas.gatech.edu/) stations making high-precision, continuous measurements of N_2O mole fraction and other trace gases since 1978 (Prinn et al 2000). Correspondence of the sample collection times with the AGAGE measured N_2O mole fraction data is shown in Figure 4.1 illustrating how the observations are representative of both baseline and non-baseline air masses as well as roughly capturing the mole fraction seasonal cycle.

Air collected from Mace Head enters through an inlet at 10 m on the Mace Head tower, 14 m above sea level situated 90 m from the shoreline and 50 m from high water. The flask sampling inlet is immediately adjacent to the AGAGE in situ instrumentation inlet. Air is pulled through a 7 μm filter and 1/4" stainless steel line dedicated to the sample flasks. Prior to sampling the line is flushed for ~30 minutes using a diaphragm pump (KNF UN86SNI, 316SS head, EPDM diaphragm, Neoprene valves). This pump used for air sampling is customized to avoid typical Viton materials

that are known to off-gas contamination (e.g. Rockmann et al 2003, Kaiser et al 2003, Miller et al 2008). Two types of sample flasks are used: 2.9L spherical stainless steel flasks (Biospherics Research Corp) electropolished by Electromatic, Inc. with a single inlet with a bellows valve (Nupro SS-4H), or 3L cylindrical stainless steel flasks (Lab Commerce, Santa Clara, CA, X23L-2N) with two inlets each with bellows valves (Nupro SS-4H). No bias in the results was evident between the 2 sampling canister models. Between air collections, all sampling flasks are cleaned and evacuated to <5 mtorr prior to shipment to Mace Head. Flask "cleaning" entails vacuuming flasks to <5 mTorr (rotary vacuum pump, ULVAC KIKO Inc), followed by 3 cycles of pressurizing to ~40 psi with Research Plus grade N_2 gas (Airgas, >99.9999%, <0.1 ppm CO_2) and evacuating to <5 mTorr, and a final evacuation to <5 mTorr. Flasks (both single and double inlet) are processed in the same manner before shipment to Mace Head. For the double inlet flasks one of the valves is attached to a dip tube to the bottom of the canister and is the preferred inlet for inputting sample and withdrawing sample for analysis. At Mace Head the double inlet flasks are simultaneously flushed for 30 minutes prior to closing the second valve and pressurizing with the KNF pump to ~3-4 bar a for about 10-15 minutes. Pre-evacuated single inlet flasks are filled through the flushed sample line and pressurized to ~3-4 bar a for about 10-15 minutes. See Appendix 4.III for additional information and images on air sampling at Mace Head. Air samples were shipped regularly to MIT for N_2O isotopic analysis.

Figure 4.1 Flask observation collection times overlaid with AGAGE high-frequency N_2O mole fraction data from Mace Head (0.1 ppb precision). AGAGE pollution-flagged data is in purple, non-polluted in green. The 4-week running mean of non-polluted data is marked by the black curve.

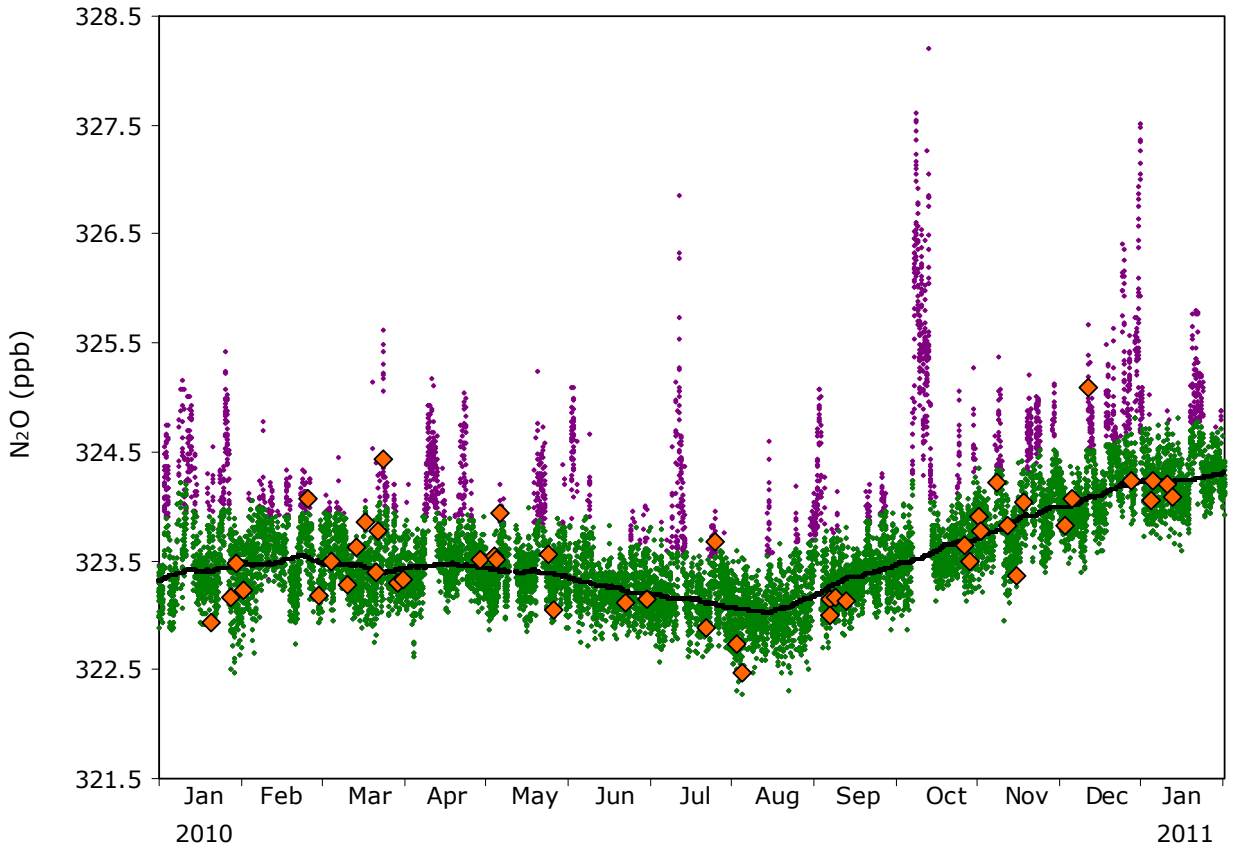

4.1.2 Measurements of isotopic composition

N_2O isotopologue measurements ($^{15}N^{\beta}$, $^{15}N^{\alpha}$, ^{18}O, where beta and alpha refer to the outer and central nitrogen positions, respectively) were made at MIT using an in-house designed automated liquid-cryogen-free pre-concentration device ('Stheno') coupled to a Thermofinnigan MAT 253 isotope ratio mass spectrometer in continuous helium flow mode via a custom-made open split interface (see Chapter 2). Isotopologue ratios are determined through the successive air sample aliquots monitoring the N_2O^+ molecular ion (m/z 44,45,46) and NO^+ fragment ion (m/z 30,31). On the Stheno+CF-IRMS system the number of repeated analyses of a single air sample is limited by Mace Head air sample size. A single flask sample is about 9 to 12 L STP (3-4 bar a in 2.9 or 3.0 L canisters), however sample canisters are not drawn to lower than ambient pressure to lessen the possibility of fractionation, leaving 6 to 9 L STP for analysis per air sample. This is ample sample to allow for 3-5 repetitions of IRMS analysis pairs 44/45/46 and 30/31 using 420ml STP a piece. Having this many repeated analyses of isotope composition for each sample gives confidence in the reported values, provides a good estimate of individual measurement uncertainty in the standard deviation, and alerts potential analytical problems if the measured values are not stable. Ratios for a single air sample were taken as the mean of 4 or 5 repeated pairs of measurements. Isotopic compositions are reported in terms of the site-specific $\delta^{15}N^{\alpha}$ and $\delta^{15}N^{\beta}$, $\delta^{18}O$, and the derived quantities $\delta^{15}N^{bulk}$ ($\delta^{15}N^{\alpha}+\delta^{15}N^{\beta}$ / 2) and site preference (SP = $\delta^{15}N^{\alpha}$ - $\delta^{15}N^{\beta}$). The common delta notation is used in units of per mil (‰) where $\delta = (R/R_{std}-1)$ with $\delta^{18}O$ and $\delta^{15}N$ values referenced to VSMOW and atmospheric N_2, respectively. Air samples are referenced to pure N_2O (Airgas, VLSI grade 99.9999%) calibrated on the common Tokyo Institute of Technology scale, which has been accepted in the community as a temporary international reference until an official site-specific N_2O isotope calibration standard exists. Further details of instrumentation and measurements can be found in Chapter 2 of this thesis.

Data of raw m/z 44,45,46 and 30,31 ion currents from the IRMS are collected using the Thermofinnigan Isodat software. Molecular ion ratios of rare to abundant (45/44, 46/44) versus the pure N_2O standard (δ45, δ46) are calculated using the background-corrected ion currents integrated under the square reference peak and eluting sample peak by Isodat software. Ratio 31/30 for the sample N_2O peak was obtained using the background-corrected Isodat integrated ion currents. Due to concerns of interfering m/z 31 peaks eluting from the GC under the square reference peaks for the samples measured prior to July 2010, fragment ion ratio 31/30 for the pure N_2O standard square peaks were determined by producing probability density functions using the raw ion current 30 and 31 signals from the IRMS. The detailed methodology of handling Isodat reference peak integration errors and its verification is detailed in Appendix 4.II.

Day-to-day variation and long-term instrumental drift were checked and corrected for with the concurrent daily analyses of an air standard tank (NOAA, Niwot Ridge, Colorado, N_2O = 322.72 ppb, NOAA-2006 scale). Raw 45/44, 46/44, or 31/30 ratios were scaled in sample values if the daily air standard showed significant deviation outside of analytical precision. Corrections to the raw sample data for variations were needed on only a few occasions. See Appendix 4.I and 4.II for details of data handling and corrections.

All trend analyses applying linear least squares regressions to the data use the linear model (lm) of R statistical software incorporating the error in the measurements.

4.1.3 Precision

Measurement precision is estimated as the repeatability of the measured isotopic values for a given air sample determined as the standard deviation (SD) of the isotopologue values from the sample series of 3-5 pairs of 44/45/46 and 30/31 Stheno+CF-IRMS runs. Long-term precision was

evaluated by the stability of the Niwot Ridge air standard tank isotopologue values over the course of the measurement period. Achieved precisions are reported in Table 4.1. Error bars on the isotopic composition results reflect the individual measurement standard error (SE = SD/√n; n = 3-5 measurements).

The precision of an isotope ratio measurement depends upon peak area. Rockmann et al (2003) found for N_2O isotope analysis of air samples, standard deviations increased at peak areas below 3 Vs but remained relatively flat for larger peak areas. Using the same air aliquot size (420 mL STP) for both molecular and fragment ion monitoring, for the NO^+ fragment ion analyses this is a compromise between the low yield of fragment ions and the desire to avoid overly long sample admission times and sample consumption, and optimized the peak areas at around 2.5 Vs. For N_2O^+ ion analyses sample peak sizes are approximately 5.5-5.8 Vs.

The precision achieved here of air samples by continuous flow-IRMS is superior for ^{15}N site-specific isotopomers and the same or slightly better for bulk ^{15}N and ^{18}O composition as that reported for other optimized CF-IRMS systems (Yoshida & Toyoda 2000, Rockmann et al 2005) and similar to precision by offline analysis (Kaiser et al 2003) (see Table 2.1). Systems based upon off-the-shelf universal pre-concentration units report lower precision (e.g. Croteau et al 2010, Park et al 2004) which is insufficient for detection of isotopic signals in tropospheric air. Some improvement in the continuous flow Stheno+CF-IRMS system could occur in the ^{15}N site-specific measurement precision in particular with a five collector-cup IRMS configuration to allow the simultaneous monitoring of all m/z 44, 45, 46, 30, and 31 ions. Otherwise, the precision for a single sample with this study's highly optimized and automated CF-IRMS measurement methodology appears to be near the limit for N_2O isotopologue measurement in tropospheric air by IRMS technology, and thus this study is very informative regarding the ability of IRMS measurement technology to analyze and resolve tropospheric N_2O isotopic composition.

4.1.4 Companion data

Reported N_2O mole fractions correspond to the simultaneously measured high-frequency (~40 min interval) in situ AGAGE multi-detector GC-ECD value at the time of sample collection (Prinn et al 2000). Precision of each individual measurement is about 0.03% (0.1 ppb), SIO 2005 calibration scale. Although this arrangement does not measure N_2O mole fraction in the same flask as that analyzed for isotopic composition, the AGAGE instrument sampling inlet and flask sampling inlet on the Mace Head tower are located immediately adjacent (see Appendix 4.III) and the relatively uniform concentration of the long-lived N_2O especially over such short time and space scales strongly support the use of this approximation. The mole fraction was confirmed during isotope IRMS analysis using the Niwot Ridge air standard tank with calibrated mole fraction 322.72 ppb (NOAA-2006 scale). Over the isotopic analysis measurement period only small variations are seen in the observed N_2O mole fractions at Mace Head. For 2010, monthly means of AGAGE Mace Head non-polluted N_2O mole fractions (definition of 'polluted' and 'non-polluted' by the AGAGE algorithm, O'Doherty et al 2001) have a February maximum and August minimum with a detrended seasonal cycle amplitude of 0.85 ppb. This is inline with the mean observed N_2O seasonal cycle at Mace Head in the AGAGE data since 1994 which has an August minimum and slightly less pronounced amplitude of 0.66 ppb. N_2O isotopic composition results are also analyzed in conjunction with the simultaneously measured high-frequency mole fraction data from AGAGE instrumentation at Mace Head of over 40 trace gas species in addition to N_2O, including the major chlorofluorocarbons (CFC-11, -12, -113), chloroform ($CHCl_3$), H_2, CO, and methane (CH_4).

Air mass characterization for each flask air sample is informed with air histories estimated with the UK Meteorological Office (UKMO) Numerical Atmospheric-dispersion Model Environment (NAME). The estimated air histories corresponding to each observation time are the

same as used in for regional modeling in Chapter 3. In summary, NAME is a 3-D Lagrangian particle dispersion model (Ryall et al 1998, Manning et al 2003, Manning et al 2011), which uses full 3-D meteorology from the UKMO numerical weather prediction (NWP) model (Cullen et al 1997, Davies et al 2005). The model is run for 3-hr periods, over which particles are released from Mace Head at a rate of 1 g/s, and over the 3-hr period 33,000 inert particles record the dispersion backwards in time for 19 days. The accuracy of the NAME output capturing the proper local behavior was verified by a match between NWP output wind speed and direction for Mace Head and that measured directly on the Mace Head tower at the same time stamp. The computational domain covers 100.0° W to 45.125° E longitude and 10.0°N to 80.125°N latitude with a resolution of 0.5625° longitude and 0.375° latitude (approx. 40 km horizontal resolution, 258x187 grid). Particles are recorded vertically in four levels of 0-100 m, 100-1000 m, 1000-3000 m, and 3000-20000 m to produce four maps of the time integrated air concentration of the particles thus recording the horizontally dispersed influence at each level. The 0-100 m air history map then represents air that has been in close contact with the surface prior to arriving at Mace Head is used to assess the influence of surface sources affecting Mace Head.

The vertical resolution of four NAME air history levels is too coarse for proper assessment of the possibility of direct stratospheric intrusions affecting Mace Head. Though at 14 m above sea level Mace Head would be highly unlikely to experience deep direct stratospheric intrusions, these events have been observed down to the surface reaching as low as 20 m asl (e.g. Gerasopoulos et al 2006) and Mace Head lies on a prominent stratospheric exchange latitudinal track. Higher vertical resolution air origins were checked with 315-hour back trajectories calculated with the HYbrid Single Particle Lagrangian Integrated Trajectory model (HYSPLIT) developed by Roland Draxler at the NOAA Air Resources Laboratory, using National Center for Environmental Prediction analyzed global grid of meteorological data (2.5°x2.5° latitude-longitude, 17 pressure levels; Draxler 1998). Though there is uncertainty as single back trajectories, HYSPLIT has been previously used to assess for stratospheric intrusions (e.g. Trickl et al 2010) and are able to signal high altitude originations particularly in the polar regions where the tropopause is low. The back trajectories verified the NAME air history maps as well, both having independent meteorological model algorithms and input meteorological data.

4.1.5 Baseline definition

Independent of isotopic composition the air samples are screened and sorted as to their air mass origin. 'Baseline' air masses arriving at Mace Head are aimed to give information about the background Northern Hemisphere nitrous oxide, rather than containing any local or European signals.

Baseline samples are defined equivalently to the definition used in regional modeling efforts (Chapter 3). In brief, baseline samples contain no pollution events in simultaneous AGAGE trace gases indicative of local surface sources (N_2O, CH_4, $CHCl_3$) or man-made polluted air (CO, CFC-11,-12,-113); wind speeds >4 ms^{-1} observed on the Mace Head tower; UKMO NWP model boundary layer depth >300 m; NAME Lagrangian dispersion model air histories classed according to Manning et al (2011) do not contain significant air concentration contributions from local and European grid boxes (courtesy A. Manning); HYSPLIT back trajectory model shows no indication of high altitude direct stratospheric air intrusion.

Air sampling times meeting these baseline criteria (n = 30) are interpreted to reflect general trends and seasonality in the background NH troposphere rather than containing any significant local or regional signals.

4.2 Results: 1-year of N_2O isotopologue observations

Following the definition of baseline observations, 30 samples are categorized as baseline and 18 samples as non-baseline. The collection of observations then sample the meteorological situation at Mace Head which sees both relatively clean tropospheric air in the baseline samples from the Atlantic and Arctic as well as more direct surface source influences in air masses traveling over the UK and Europe. No resolvable seasonal cycle in the baseline samples for any isotopic ratio was apparent. However, it was not expected to be able to resolve subtle seasonal cycles in the low-frequency data. Low-frequency weekly to biweekly flask sampling observations at Mace Head make interpretation of a tropospheric seasonal signal difficult because of the confluence of both baseline and complicating non-baseline air, even if that signal is clearly present in high-frequency AGAGE data (Nevison et al 2011). The signal in the seasonal cycle of the N_2O tropospheric baseline composition is small relative to the signal from pollution events. Additionally, baseline and non-baseline samples are not evenly distributed throughout the year, vulnerable to sampling biases, and given the current level of measurement precision do not permit effective analysis for seasonal cycles or the certainty of long-term trends. This is consistent with the inability to discern a seasonal cycle in the low-frequency data of Kaiser et al (2006) with n = 36 or fewer measurements of an individual isotopologue at a single location spanning 2 years, nor when including all locations throughout Europe in n = 90 or fewer data over 2 years.

Variation in the isotopic composition is small. Figure 4.3a-e shows the time series of observations of the isotopic composition. Mean composition of the baseline samples (n = 30) is $\delta^{15}N^{bulk}$ = 6.60 ±0.12, $\delta^{15}N^{\alpha}$ = 16.61 ±0.17, $\delta^{15}N^{\beta}$= -3.41 ±0.34, SP = 20.02 ±0.47, and $\delta^{18}O$ = 44.13 ±0.14 ‰ (1σ). Variations in the observations are greater than the estimated analytical error. Including all samples (n = 48) gives similar means and slightly larger standard deviations. These are tabulated with the instrumental precisions in Table 4.1. All observation compositions presented in this are tabulated in Appendix 4.IV with sample measurement date, time, and N_2O mole fraction.

Table 4.1 Precisions of the N_2O isotopic observations listed in relation to the mean composition and variability observed in the air samples. Precisions of this study as estimated by the standard deviation of 3-5 repeated measurements of a single air sample and the long-term standard deviation of the Niwot Ridge air standard composition.

	$\delta^{15}N^{bulk}$	$\delta^{15}N^{\alpha}$	$\delta^{15}N^{\beta}$	SP	$\delta^{18}O$
Individual measurement precision (typical)	*0.05*	*0.11*	*0.14*	*0.21*	*0.10*
Long-term air std stability/precision	*0.06*	*0.17*	*0.22*	*0.38*	*0.14*
Baseline observations mean (n = 30)	6.60	16.61	-3.41	20.02	44.13
SD	*0.12*	*0.17*	*0.34*	*0.47*	*0.14*
All observations mean (n = 48)	6.58	16.62	-3.45	20.07	44.16
SD	*0.14*	*0.20*	*0.33*	*0.48*	*0.15*

Though not causing a notable change in the overall standard deviation, even within this limited dataset a few non-baseline observations do exemplify isotopic compositions with significant measurable anomalies. Further analysis with air histories and other gas tracers suggestively link these anomalies to air origins and different N_2O influences in the next section.

Over the course of the year the collected baseline observations have significant trends in their isotopic compositions. Sample trends are assessed with the baseline categorized samples only

since these would reflect the steady measurement of background air at Mace Head while significant variation or potentially biasing outliers may be present in the non-baseline samples. Linear least squares regression fits (weighted with individual measurement errors) to the baseline data give statistically highly significant trends for $\delta^{15}N^{bulk}$: 0.25 ±0.06 ‰/y ($P < 0.001$, $R^2 = 0.38$), $\delta^{15}N^{\beta}$: 0.70 ±0.15 ‰/y ($P < 0.001$, $R^2 = 0.45$), and SP: -0.98 ±0.21 ‰/y ($P < 0.001$, $R^2 = 0.44$); significant trend for $\delta^{15}N^{\alpha}$: -0.27 ±0.09 ‰/y ($P < 0.005$, $R^2 = 0.25$); and no trend for $\delta^{18}O$ ($P > 0.05$, $R^2 = 0.11$). The first Stheno+CF-IRMS measurement session (corresponding to 3 baseline data points, 4 air samples total) produced anomalous results for the Niwot Ridge air standard tank. Though this instrumental effect was accounted for and a correction applied to the sample measurements (see Appendix 4.II), to ensure that a potential procedural error is not producing the suspected trends the linear model regression was recalculated removing the 3 affected baseline observations points. Still found are statistically significant trends but of slightly smaller magnitude in $\delta^{15}N^{bulk}$: 0.21 ±0.08 ‰/y ($P < 0.01$, $R^2 = 0.25$), $\delta^{15}N^{\beta}$: 0.61 ±0.18 ‰/y ($P < 0.005$, $R^2 = 0.31$), and SP: -0.88 ±0.26 ‰/y ($P < 0.005$, $R^2 = 0.31$); and borderline significant trend in $\delta^{15}N^{\alpha}$: -0.27 ±0.11 ‰/y ($P < 0.05$, $R^2 = 0.20$). Note that the commented significances of these trends are statistically supported by the derived P values for n = 30 data points, but the correlation coefficients (R^2 values) are still fairly low meaning that although the trend may be significant, it only accounts for a portion of the observed composition and there are other factors causing variation in the time series.

As mentioned above, low-frequency and possible sampling biases in the observation dates prevent certitude of the existence or magnitudes of these trends at Mace Head. The trends seen in $\delta^{15}N^{bulk}$ and particularly for the ^{15}N site-specific values $\delta^{15}N^{\beta}$ and SP are large compared to any anticipated trend and in the opposite direction of the long term trend derived from ice core and Antarctic firn air data or model analyses (Sowers et al 2002, McLinden et al 2003, Rockmann et al 2005, Ishijima et al 2007). The possibility of an analytical cause of the trends is thoroughly investigated here.

Raw data values $\delta45$, $\delta46$, and $\delta31$ versus the internal pure N_2O reference in the concurrently analyzed Niwot Ridge air standard data show no detectable instrumental drift over the measurement period. Individual measurement precisions (SD of 3-5 air sample measurements) for the raw delta measurements had mean values $\delta45$ $1\sigma = 0.08$‰, $\delta46$ $1\sigma = 0.13$‰, $\delta31$ $1\sigma = 0.12$‰. Figure 4.2 shows the raw $\delta45$ values versus date of analysis for the air standard and the samples, with each point corresponding to the mean of 3-5 repeated Stheno+CF-IRMS analyses. This comparison across analytical measurement time (rather than observation point time) allows detection of instrumental drift and variation in the standard to compare with that seen in the samples. Weighted linear least squares regression fits to the $\delta45$ data yield a statistically insignificant slope in the Niwot Ridge air standard (slope = 0.02 ±0.03 ‰/y) and a highly significant slope in the baseline sample data of 0.24 ±0.05 ‰/y ($P < 0.0005$, $R^2 = 0.41$). Though this is in measurement time and not air sample collection time, the analysis of flask samples occurred in order of sample collection and thus the trend in the sample $\delta45$, $\delta46$, and $\delta31$ raw data analyses are similarly mirrored in the calculated isotopic compositions in observation time, as in Figure 4.3. Raw $\delta45$ is primarily reflected in the $\delta^{15}N^{bulk}$ composition, $\delta46$ in the $\delta^{18}O$, and $\delta31$ into the ^{15}N site-specific alpha, beta, and site preference values. Raw values $\delta46$ and $\delta31$ for the air standard in measurement space similarly have no statistically significant temporal slope. The stability of the air standard measurement over time indicates that the IRMS response (including any possible trend in IRMS scrambling factors), pure N_2O reference gas, continuous flow interface, and pre-concentration device are not drifting significantly over the course of the year of measurements.

Figure 4.2 Air sample and Niwot Ridge air standard δ45-N_2O measurement values at the date of measurement. Lines show linear least squares regression fits to the respective data sets. Individual measurement precisions had a mean value of ±0.08‰ (1σ).

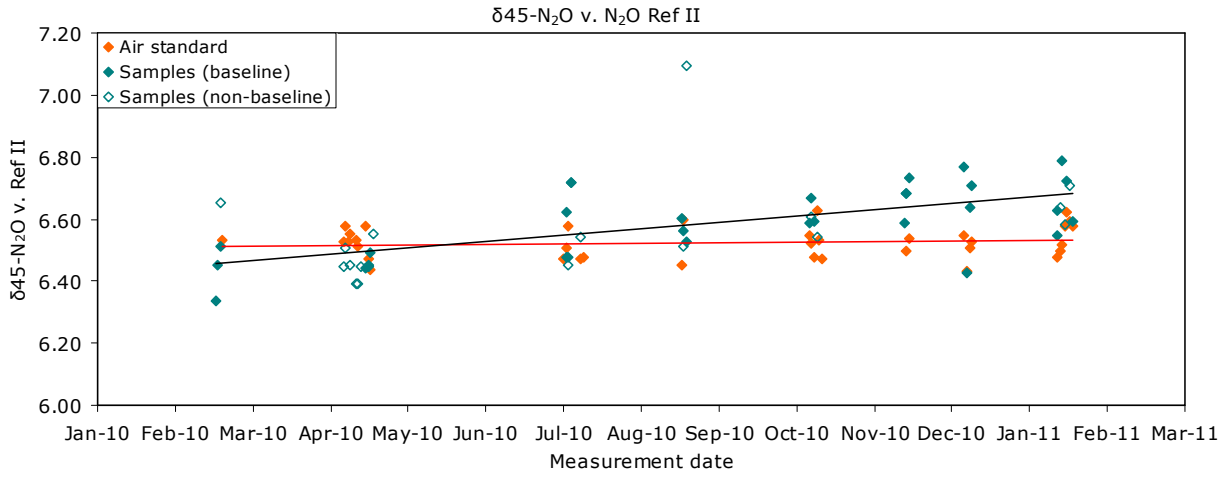

Although the air standard was used to mimic the air samples as much as possible, a few differences which could be the cause for sample trend were explored. Sample trends are not towards the isotope ratios of the two pure N_2O lab reference tanks which are near 0‰ for ^{15}N isotopologues and 40‰ for ^{18}O (Ref I: $\delta^{15}N^{\alpha}$ -0.4‰, $\delta^{15}N^{\beta}$ 1.5‰, $\delta^{15}N^{bulk}$ 0.5‰, $\delta^{18}O$ 40.1‰; Ref II: $\delta^{15}N^{\alpha}$ -0.8‰, $\delta^{15}N^{\beta}$ 0.3‰, $\delta^{15}N^{bulk}$ -0.2‰, $\delta^{18}O$ 40.4‰) indicating that the trends are not due to contamination which might have somehow influenced the flasks and not the air standard tank. Samples have variable mole fractions whereas the air standard is constant, however no relationship was found between slight mole fraction differences between samples and their measured δ45, δ46, and δ31.

The δ45 analysis is robust compared to δ46 and δ31 ratios on the IRMS (mean 1σ precisions 0.08‰, 0.13‰, 0.12‰, respectively) and largely indicates $\delta^{15}N^{bulk}$ with negligible contribution from $N_2{}^{17}O$. With the analytical stability checks performed, the trend in the $\delta^{15}N^{bulk}$ data is assumed valid. The 31/30 ratio measurement on the IRMS, which determines the site specific N isotopomer values, has less certainty. Instrumentally, the m/z 30 and 31 ions result from the fragmentation of N_2O into NO^+ and have about one-third abundances for detection than N_2O^+. Additionally this fragmentation is complicated by the N 'scrambling' which occurs between the alpha and beta positions, and possible fractionation associated with the fragmentation and scrambling. Major inconsistencies in the δ31 instrumental values should be seen equally in the air samples and air standard, and over the measurement period the air standard shows stable values.

Another cause of difficulty for the 31/30 ratio measurement is the potential contamination by fluorocarbon species which similarly form a m/z 31 fragment ion as CF^+, which has been observed and assessed in other N_2O isotopic studies (Rockmann et al 2003, Kaiser et al 2006). In the air standard tank this potential interference would be constant. However, the possible influence of an underlying CF^+ compound would vary between samples. Rigorous instrumental design and testing went into avoiding this contamination, including temporarily splitting the sample flow between the IRMS and a quadrupole mass spectrometer to simultaneously assess for hidden m/z 31 peaks underlying the N_2O peak at other masses indicative of fluorocarbon species (m/z 50, 51, 69, 85; see Chapter 2 Part I). No interfering fluorocarbon compounds were detected beneath the N_2O peak with the pre-concentration and separation method, however the sensitivity of the quadrupole MS may not have been high enough to detect a very small interfering peak which might affect sensitive isotopic ratios. Some atmospheric fluorocarbon species currently have a downward trend

since many are human-made and have been banned or are being phased out of production (AGAGE data; http://agage.eas.gatech.edu). If this is the case, then over the course of the year any underlying fluorocarbon associated m/z 31 augmentation would be decreasing and the N_2O measurement on the IRMS would reflect a decreasing 31/30 ratio. However, the identity(ies) of the specific fluorocarbon species which could possibly be underlying N_2O is uncertain, and there are many HFCs and other fluorocarbon compounds are still increasing exponentially in the atmosphere.

We therefore must leave open the possibility that for the $\delta 31$ measurement in air samples there is a fluorocarbon or some unknown cause which is interfering with the N_2O m/z 31 signal, which would have a consequence for the $\delta^{15}N^{\beta}$, $\delta^{15}N^{\alpha}$, and SP values. The relatively large and unexpected magnitude of the trend in the site specific isotopic composition suggests that this or some other interference or unaccounted instrumental effect could be contributing. The relatively robust $\delta 45$ and $\delta^{15}N^{bulk}$ data lack any mirrored trend in the air standard and no other conceived analytical causes. This trend in the robust $\delta^{15}N^{bulk}$ data is explored as a possibly true result. A possible real-world cause of this observation in the data towards more-enriched $\delta^{15}N$ could be stratospheric influence and will be discussed below.

Figure 4.3 Time series of N_2O isotopic observations at Mace Head from January 2010 to January 2011. Baseline air observation are in pink, non-baseline blue. Error bars are ±standard error of 3-5 repeated measurements. X-axis tick marks are at monthly intervals indicated by the bottom plot. Note y-axis tick marks are at the same 0.5‰ interval

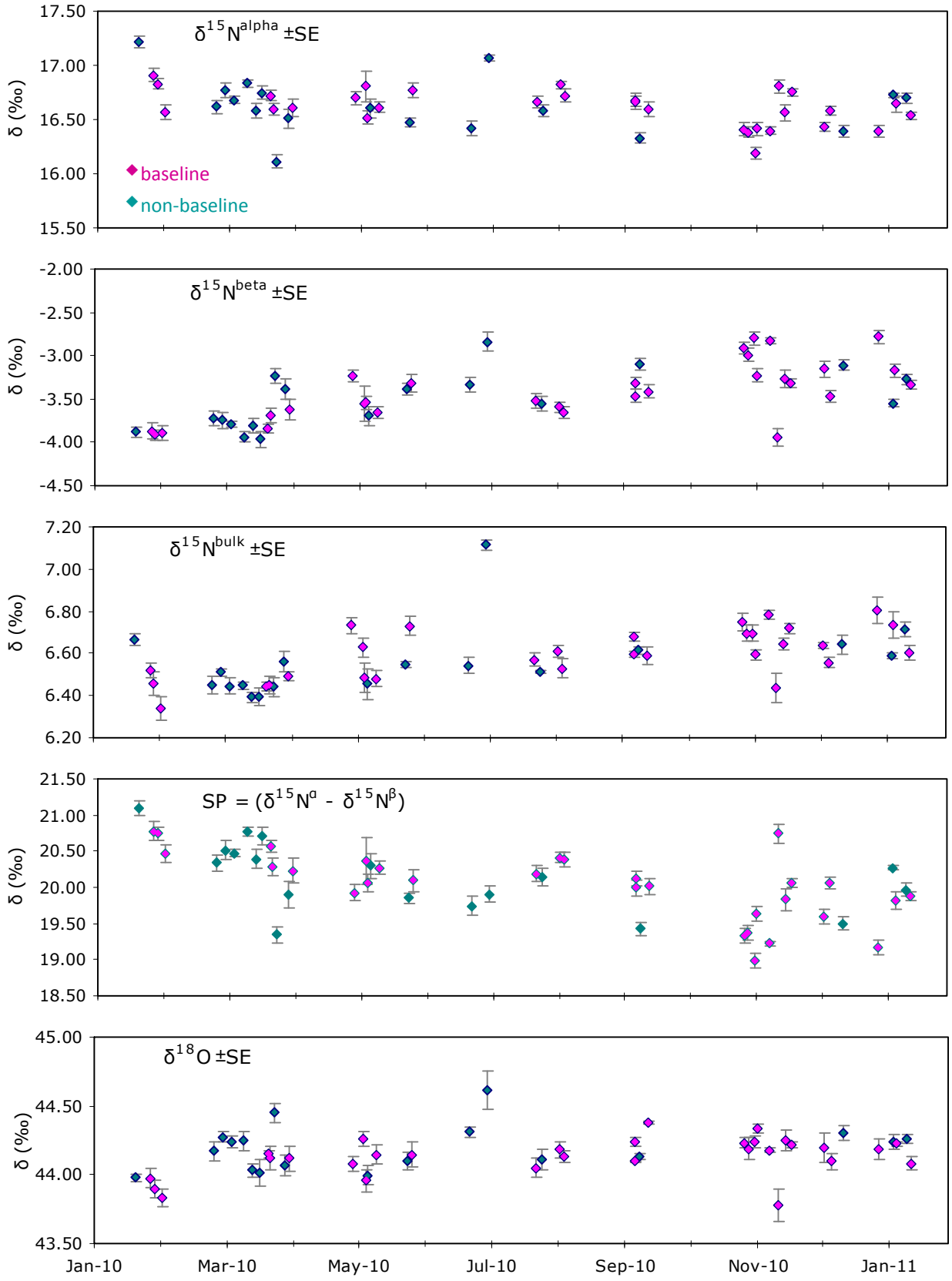
δ15Nalpha ±SE
δ15Nbeta ±SE
δ15Nbulk ±SE
SP = (δ15Nα - δ15Nβ)
δ18O ±SE
δ (‰)
baseline
non-baseline
17.50
17.00
16.50
16.00
15.50
-2.00
-2.50
-3.00
-3.50
-4.00
-4.50
7.20
7.00
6.80
6.60
6.40
6.20
21.50
21.00
20.50
20.00
19.50
19.00
18.50
45.00
44.50
44.00
43.50
Jan-10
Mar-10
May-10
Jul-10
Sep-10
Nov-10
Jan-11

4.3 Discussion

4.3.1 Annual trend

The slight positive trend seen in the $\delta^{15}N^{bulk}$ composition spanning 2010 at Mace Head is opposite to the negative long term trend derived in other studies and attributed to the increase of ^{15}N isotopically-depleted soil source from agriculture (Perez et al 2001, Sowers et al 2002, McLinden et al 2003, Rockmann et al 2005, Ishijima et al 2007). Presented is a discussion of consistencies with the observed trend, but high-frequency observations and data covering before and after 2010 would be required for more accurate detection and interpretation of any trend.

4.3.1(a) Anomalously large stratospheric inputs in 2010

The shift towards more isotopically enriched $\delta^{15}N^{bulk}$ composition at Mace Head over 2010 would be consistent with the stratosphere playing a larger role in that year either through increased downwelling of ^{15}N isotopically-enriched air or increased N_2O loss in the stratosphere leading to more enriched composition. Stratospheric N_2O is enriched in both ^{15}N and ^{18}O. However, an accompanying increase in $\delta^{18}O$ was not detected due to the larger error associated with $\delta^{18}O$ measurements. In support of an increased influence from the stratosphere, the observed N_2O mole fraction from continuous AGAGE data for 2010 at Mace Head has a seasonal cycle minimum in August which is more pronounced than the mean detrended seasonal cycle from 1994 to 2010. The mean detrended seasonal amplitude is 0.66 ppb whereas the seasonal cycle over 2010 has a greater 0.85 ppb amplitude, largely driven by the strong August minimum detrended anomaly of -0.60 ppb in 2010 balancing a more subtle February maximum. The late summer N_2O minimum at Mace Head has been well studied to result largely from the delayed downward propagation of stratospheric downwelling maximum in spring reaching the surface (Nevison et al 2007, Jiang et al 2007, Nevison et al 2011). Thus, this deeper August N_2O minimum suggests the stratospheric mixing or N_2O loss in the stratosphere was greater for 2010.

As further evidence of a stronger stratospheric influence, polar winter lower stratospheric temperature can be used as a proxy for the strength of the downward arm of the Brewer-Dobson circulation which forces upper stratospheric air into the lower stratosphere for exchange with the troposphere at midlatitudes (Newman et al 2001, Nevison et al 2007, Nevison et al 2011). Warmer temperatures in the lower stratosphere reflect stronger Brewer-Dobson circulation, of which the descending arm of stratospheric air brings the N_2O mole fraction-depleted and isotopically-enriched N_2O towards the troposphere. At Mace Head specifically, annual atmospheric growth rate anomalies are correlated to lower stratospheric temperature such that warmer years have lower growth of tropospheric N_2O mole fractions and CFCs (Nevison et al 2007), and correlations between seasonal N_2O minima and polar winter lower stratospheric temperatures explain much of the interannual variability in surface seasonal cycle with the late summer minima in N_2O and CFC-12 deeper in warmer years (Nevison et al 2011). NCEP Global Data Assimilation System-Climate Prediction Center reanalysis of polar (60°-90°N) zonal temperature anomalies (http://www.cpc.ncep.noaa.gov/) show that the lower stratospheric temperature (100 hPa) had a 4-12°C positive temperature anomaly during the February-March winter months of 2010 (Figure 4.4). These warmer winter temperatures point to a stronger NH stratospheric circulation and support the notion that the N_2O isotopic composition in the troposphere would be more influenced by the ^{15}N isotopically-enriched stratosphere in 2010, potentially contributing to a positive $\delta^{15}N$-N_2O trend.

Figure 4.4 Polar (60° - 90°N) zonal temperature anomalies for 2010, from the NCEP Global Data Assimilation System-Climate Prediction Center. The lower stratosphere is around 100 hPa, and shows a warm anomaly during February and March, indicative of strong stratospheric circulation.

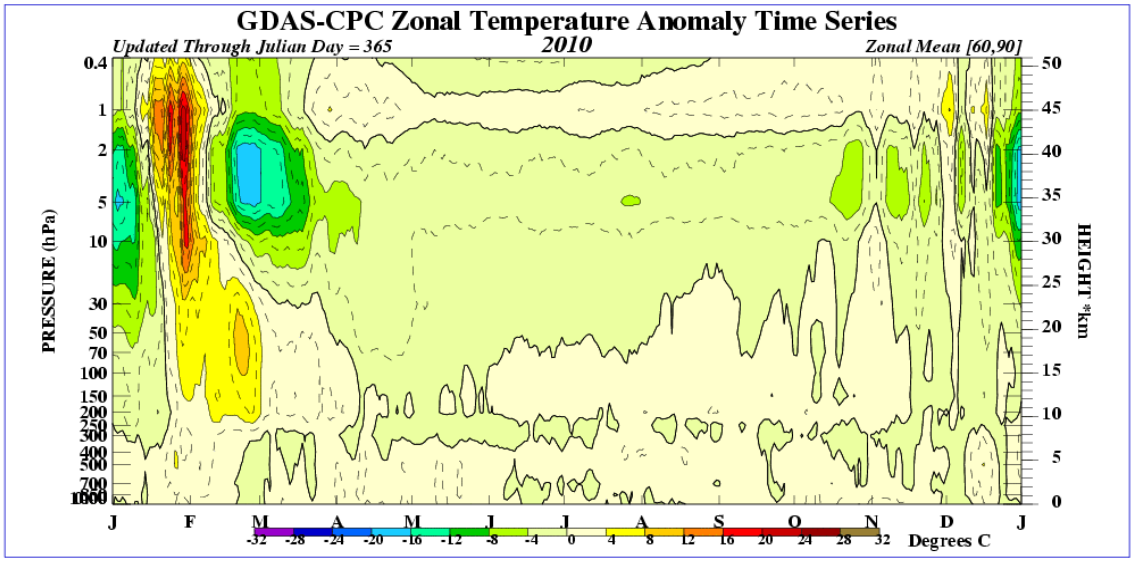

An increased strength of the Brewer-Dobson circulation in 2010 may have been contributed to by a long-term climate change trend of increased stratospheric circulation. Increasing temperatures in the troposphere have been accompanied by cooling temperatures in the stratosphere, which have been predicted to augment the stratospheric Brewer-Dobson circulation and consequently drive STE. In numerous atmospheric simulations of increased greenhouse gases the stratosphere responds with an enhanced Brewer-Dobson circulation, attributed to increased wave excitation in the warmed troposphere (Sigmond et al 2004, Butchart et al 2006, Olsen et al 2007, Garcia and Randel 2008, Butchart et al 2010). The year 2010 as having an anomalously strong stratospheric influence on surface N_2O is then following the trend towards enhanced stratospheric circulation, thus downwelling more ^{15}N isotopically-enriched N_2O from the upper stratosphere to the lower stratosphere and exchange with the troposphere.

Also potentially driving an enhanced stratospheric influence was the striking negative North Atlantic Oscillation (NAO) index in 2010. The North Atlantic Oscillation is a major source of interannual variability in atmospheric circulation, with the NAO index fundamentally a measure of the mean atmospheric pressure gradient between the Azores high and the Iceland low, and controls the strength and location of westerly winds and storm tracks across the North Atlantic. Compiling indices from the NOAA Climate Prediction Center from 1950 (http://www.cpc.ncep.noaa.gov/products/precip/CWlink/pna/nao.shtml) and prior to that from Jones et al (1997), the winter 2009/2010 (DJF) had the most negative value on record extending back to 1824 and considerably lower than the previous record low index winters. The negative phase of the index lasted strongly through to the end of the year in 3-month running mean data (NOAA CPC) instead of oscillating back to a positive phase. A similar sustained negative index only seen one other time (in 1968-1969). Negative NAO index years are associated with strong high latitude blocking of westerly flow, which cause low winter temperatures over Europe, and the 2009/2010 winter indeed had well-below average temperatures in the UK and Europe. By affecting the location and strength of the North Atlantic storm track, the NAO index is associated with changes in location and strength of stratosphere-troposphere exchange. During the negative NAO phase,

surface anticyclones are shifted to have a frequency maximum in the region centered on the UK between Iceland and Scandinavia, a phenomenon strongly anticorrelated with the NAO index in a 15-year climatological study (Sprenger and Wernli 2003). Stratospheric streamers form in association with anticyclones and could be the mechanism for the climatological stratosphere-to-troposphere maximum near Ireland and western Europe during the negative NAO phase (Sprenger and Wernli 2003). Additionally, tropopause height is high above regions of frequent anticyclones, which is linked to an increase in young PV > 2 stratospheric tracer in the upper troposphere (James et al 2003). The exceptional nature of the strongly negative sustained NAO index over 2010 suggests that its mechanism driving STE transfer of enriched $\delta^{15}N\text{-}N_2O$ could likely be contributing to the unexpected increasing trend observed in $\delta^{15}N^{bulk}$ at Mace Head.

4.3.1(b) Surface source contributions in 2010

An alternative or contributing factor to an increased stratospheric influence of ^{15}N-enriched N_2O in causing $\delta^{15}N^{bulk}$ to rise over 2010 would be if the ^{15}N-depleted surface sources had an anomalously low year, even with the excess contributed by human activities (predominately agriculture). This would tend to shift the natural balance between the enriched stratosphere and the depleted surface sources which would, without human added sources, keep N_2O isotopic composition in the troposphere constant. However, the climate in 2010 does not suggest this to be the case. Soils represent the highest source of N_2O and microbial productivity is largely regulated by temperature. Globally, the combined land and ocean surface temperature in the year 2010 was tied with 2005 as the warmest in the 1880-2010 record. This was likewise the case for the combined land and ocean surface temperature in the Northern Hemisphere, which had an annual temperature anomaly of +1.08 °C departure from the 1901-2000 average. Much of the warmest annual above-average temperatures were in the high latitude regions of the Northern Hemisphere, particularly North America (NOAA/National Climatic Data Center, State of the Climate, http://www.ncdc.noaa.gov/sotc/). Those soil emissions most affecting the baseline observations at Mace Head would arise from North America prior to transit across the Atlantic Ocean. Temperatures during the United States summer (JJA) were the fourth warmest in the 1895-2010 record (NOAA/NCDC), and Canada had its third warmest summer in its record since 1948 (Environment Canada, http://www.ec.gc.ca). This spread of warmer temperatures into the higher latitudes might cause an overall hemispheric increased soil source as well as causing N_2O producing soil to extend further into high latitude regions which are more directly upwind of Mace Head. Despite the record warm annual mean Northern Hemisphere temperature, the winter of 2009/2010 was markedly cold for the NH, particularly for Europe and the U.S., driven partly by the anomalous negative NAO index (UKMO). Episodic N_2O emissions have significant fluxes following freeze-thaw cycles, accounting for the major part of N_2O total annual emissions (Flessa et al 1995, Guckland et al 2010, Wu et al 2010). The exceptionally cold winter would cause the freeze-thaw N_2O emission pulses to include more southern latitudes than usual, thereby suggesting there might be higher N_2O emissions for the NH 2010 late winter/early spring. Combined with these temperature anomalies supporting microbial N_2O production from the soil, global precipitation in 2010 was the wettest on record since 1900 (NOAA/NCDC). Rainfall events and soil moisture conditions drive large pulses in N_2O episodic emissions therefore the higher precipitation might be expected to cause higher N_2O soil emissions.

These climatic soil conditions over 2010 suggest that the net production of N_2O from the soil in 2010 would not be reduced and in fact might be anomalously augmented. However, it is not clear whether a net 2010 reduction in soil emissions would be required to observe an increasing $\delta^{15}N$ signal in the troposphere, and possibly the trend could result from a large decrease between higher

spring emissions and lower fall emissions. This is a possibility given the theoretically augmented freeze-thaw emission pulses in the spring because of the anomalously cold 2009-2010 winter as discussed above. However, the overall warmer average temperature and increased precipitation spanning the growing season suggest that emissions after the winter/spring would not be markedly low in comparison.

Emissions from the northern Atlantic Ocean also would be affecting the baseline observations at Mace Head. However, N_2O productivity in the northern Atlantic has been measured to be very low and thus changes in production would not cause significant changes in the overall NH surface source of N_2O (Walter et al 2006). Additionally, the isotopic signature in open ocean surface waters is only slightly more ^{15}N-depleted than in the atmosphere, thus changes in the Atlantic Ocean source would not weight the $\delta^{15}N^{bulk}$ composition significantly (Popp et al 2002). Even if northern Atlantic Ocean N_2O emissions could affect Mace Head composition, the warmer sea-surface temperatures in the Northern Hemisphere over 2010 with +0.51 °C anomaly (NOAA/NCDC) would suggest that N_2O emissions would be higher in the northern Atlantic due to higher biological productivity as well as higher thermal flux out of the ocean into the atmosphere.

Climatic data suggests then that a reduction in ^{15}N isotopically-depleted surface emissions in 2010 is fairly unlikely and supports anomalous activity related to the stratosphere as a cause for the observed $\delta^{15}N^{bulk}$ increasing trend.

4.3.1(c) N_2O mole fraction

Notably though, the steady trend in $\delta^{15}N$ which may reflect an increase in the downflux of stratospheric $^{15}N_2O$-enriched and N_2O mole fraction-depleted air is not mirrored in the Mace Head surface mole fraction. The mole fraction exhibits a relatively deep seasonal dip in August but continues its usual seasonal cycle to return to higher levels which continue the long-term increasing trend in the N_2O mole fraction. A possible explanation for the discrepancy between the isotopic and mole fraction measures requires a mechanism which would affect mole fractions without significantly altering isotopic composition. Tropospheric transport mechanisms such as seasonal differences in boundary layer height, convection, and interhemispheric transport have been supported as a likely contributor to the observed N_2O mole fraction seasonal cycle at Mace Head, which is in phase with the stratospheric signal (Nevison et al 2007). These dynamic effects have been simulated to modulate a mole fraction seasonal cycle for both N_2O and CFCs at Mace Head without the presence of the stratospheric sink (Nevison et al 2007). For N_2O isotopic composition, however, certain dynamic effects might not affect isotopic composition and would not be expected to likewise create a seasonal cycle in $\delta^{15}N$, such as atmospheric compression or expansion phenomena. The seasonal pattern following N_2O mole fractions in 2010 may then largely be in response to seasonal changes in dynamical mechanisms. If this is the case then the isotopic composition data is shown to be valuable due to its ability to recover independent information about N_2O processes, particularly for its potential application to separate stratospheric and tropospheric transport controls on N_2O, as well as aid in interpretation of interannual variations in atmospheric N_2O.

4.3.2 Short-term variability

To inspect the day-to-day variability and anomalous deviations in N_2O isotopic composition at Mace Head, these data are treated as individual observations rather than a time series. Figure 4.5a-c displays isotopologue relationships for the observations (same data as the time series in Figure 2.3) similar to Figure 1.3a-c and Figure 3.5 but at a small scale focused on tropospheric composition and are therefore useful in identifying relationships between observations and fractionating processes or source compositions. Although the overall variation in composition is subtle, even from this low-

frequency time series of observations a few exemplary case studies demonstrate potential patterns of isotopic composition related to air origins consistent with expected source-receptor relationships. Observations with statistically distinguished isotopic compositions are associated with coherent patterns suggested here, but more measurements at high-frequency would be needed to verify the explanations. Because of the subtlety and uncertainty in the new field of N_2O isotopic composition in the troposphere, the source-receptor linkages can only be fully validated and exploited with more complete high-frequency data, which would allow categorization of air origins with air history estimates and other information to statistically find relationships and analyze correlations relevant to observed N_2O variations.

Figure 4.5 Isotopologue relationships plotted for the observations. a) $\delta^{15}N^{bulk}$ v $\delta^{18}O$, b) $\delta^{15}N^{\alpha}$ v $\delta^{15}N^{\beta}$, c) SP v $\delta^{15}N^{bulk}$. Note all three plots have the same ‰ axes interval. Baseline samples in pink, non-baseline in blue. Labeled date markers are referred to in the text. Error bars are ±SE (standard error) for each individual sample consisting of 3-5 repeated measurements.

a)

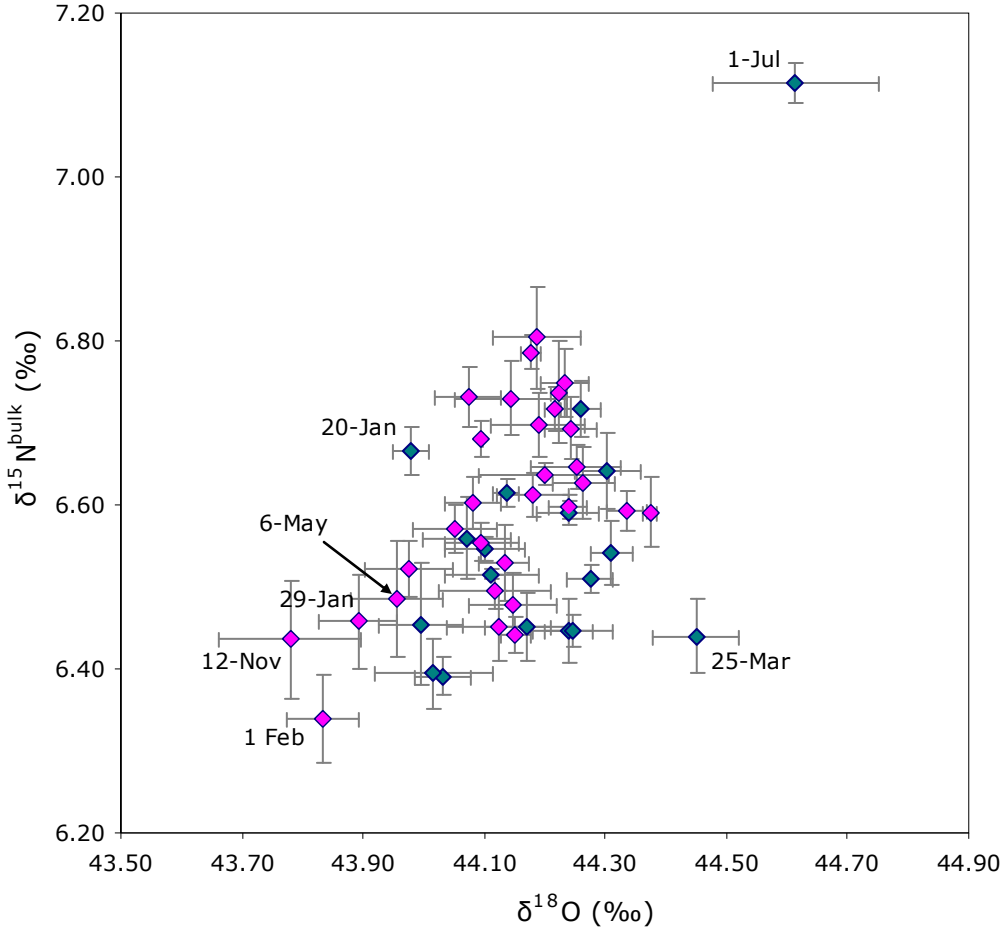

b)

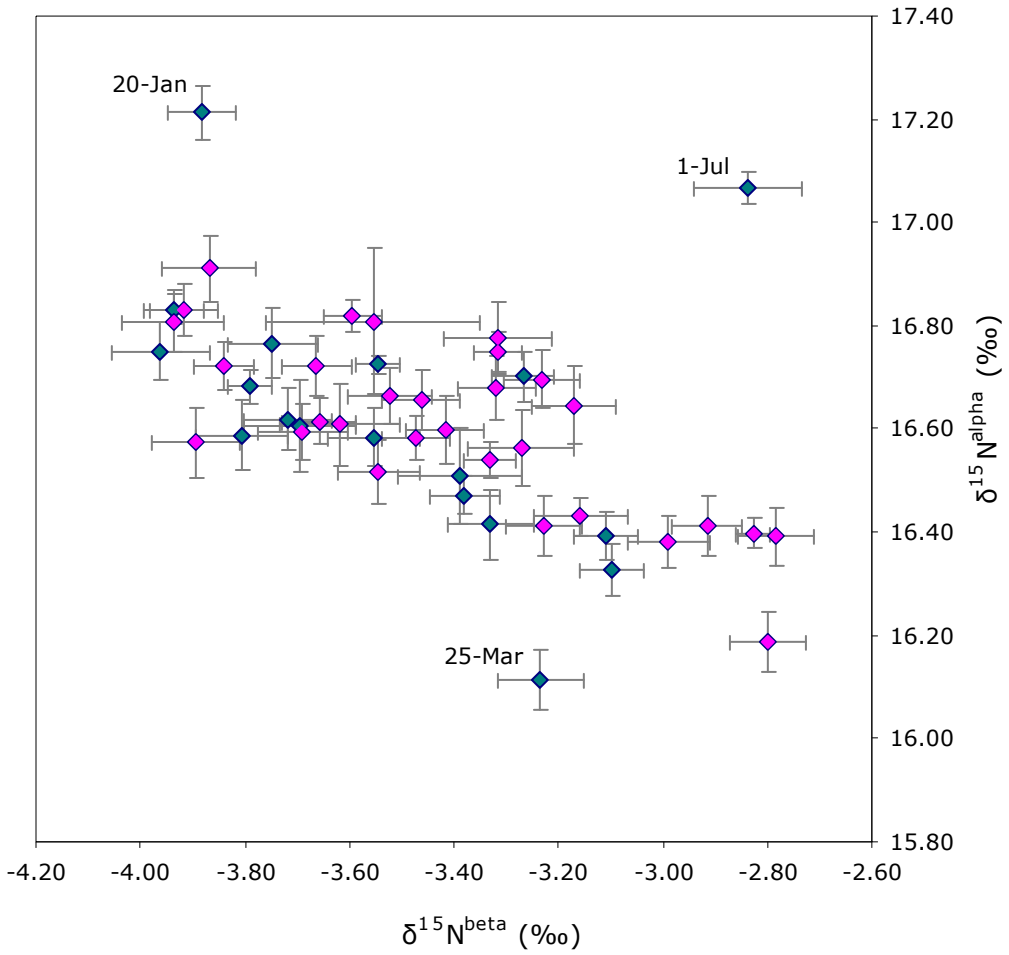
20-Jan
1-Jul
25-Mar
17.40
17.20
17.00
16.80
16.60
16.40
16.20
16.00
15.80
δ15Nalpha (‰)
-4.20
-4.00
-3.80
-3.60
-3.40
-3.20
-3.00
-2.80
-2.60
δ15Nbeta (‰)

c)

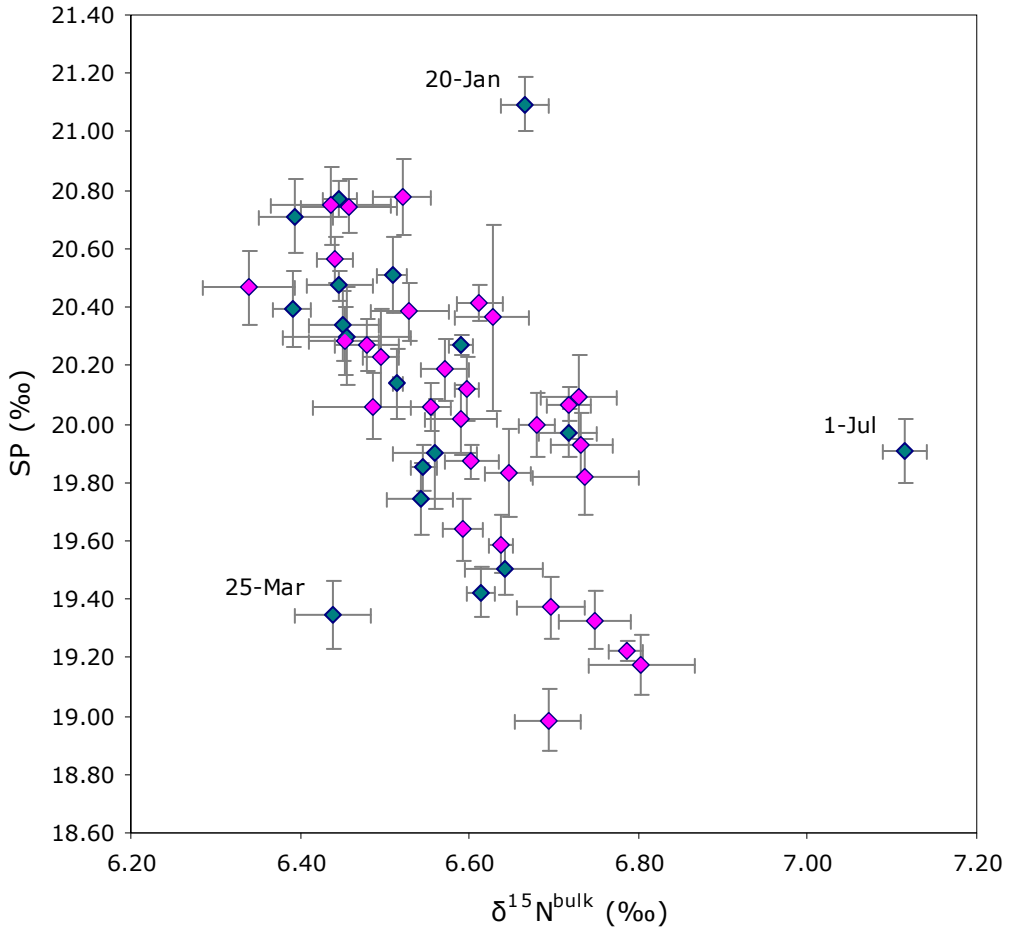

From the $\delta^{15}N^{bulk}$ and $\delta^{18}O$ information shown in Figure 4.5a, the air observation from 1 July 2010 is significantly removed and the 25 March 2010 observation also is somewhat notably distinct. The $\delta^{15}N$ site-specific information shown in Figures 4.5b and 4.5c also reveals the unique 1 July 2010 sample and the 25 March 2010 sample is more distinct with the site-specific information. Additionally the $\delta^{15}N$ site-specific information highlights the air sample from 20 January 2010 which is not as apparent in the bulk isotopic data. These specific unique observation points will be discussed individually below. Apart from individual samples with compositions significantly removed from the central cluster, preliminary inspection within the common grouping suggest that more subtle patterns may exist relating compositions to air origins and N_2O influences. One such pattern is exemplified in the baseline observations from 29 January, 1 February, 6 May, and 12 November 2010 that are grouped together with lighter compositions in the $^{15}N^{bulk}$ and ^{18}O information. This grouping is only revealed in the bulk isotopic data and not in the site-specific information, and will also be discussed below.

Discussions surrounding these cases offer tentative explanations for the isotopic patterns which are consistent with expectations of source-receptor relationships, but more measurements at high-frequency will be needed to validate the coherent patterns.

(i) 25 Mar 2010, 11:55h GMT

The observation collected on 25 March has a distinguished $^{15}N^{bulk}$-, $^{15}N^{\alpha}$- and ^{18}O-isotopically-depleted composition. The concurrent N_2O mole fraction value is significantly 1.1 ppb above baseline, and the high-frequency AGAGE data also flags the corresponding methane measurement as a pollution event. Assessment of the air history and meteorological situation make a clear connection with influence from a proximal regional surface source. The NAME air history (Figure 4.6a) shows the regional surface influence from Ireland, the UK and Western Europe. The analyzed UK NWP meteorology estimates a very shallow 204m boundary layer depth at the time of sampling, which would trap local surface emissions and allow N_2O mole fractions and proximal surface source signature to accumulate. Inspection of the full AGAGE high-frequency data reveals that the time of sampling is following a nighttime low boundary layer capping inversion indicated by hydrogen (which has a land sink) depletion and chloroform (which has a surface source) accumulation (Figure 4.6c), which occasionally can occur at Mace Head (Simmonds et al 2010). At the time of sampling the elevated levels of N_2O resulting from the capping inversion have not yet dissipated. The connection with prior H_2 depletion and $CHCl_3$ accumulation, and concurrent elevated N_2O (Figure 4.6b) and CH_4 levels is consistent with a soil source, potentially emanating from the nearby peat bogs at Mace Head. The specific isotopic composition shift in this sample therefore may hold important insights into the specific local peat bog N_2O emissions signature which could then be utilized to distinguish this influence from other N_2O governing processes. High-frequency sample collection, particularly during inversion accumulation and peak N_2O mole fractions , would be need for verification and more accurate interpretation of this potential surface source signal.

This observation time is interestingly also the most distinguished ^{15}N- and ^{18}O- depleted resulting data point obtained in the Chapter 3 regional modeling.

Figure 4.6 a) NAME air history for the 3-hr period spanning the 25 March 2010 air sample collection time. b) N_2O mole fraction time series of AGAGE high-frequency data for the 3 full days 24-26 March (00:00h 24 March to 23:59h 26 March). c) Same time period of AGAGE high-frequency data for chloroform and hydrogen, indicating a significant nighttime inversion. Exact flask collection time is indicated with the red line in both b and c.

a)

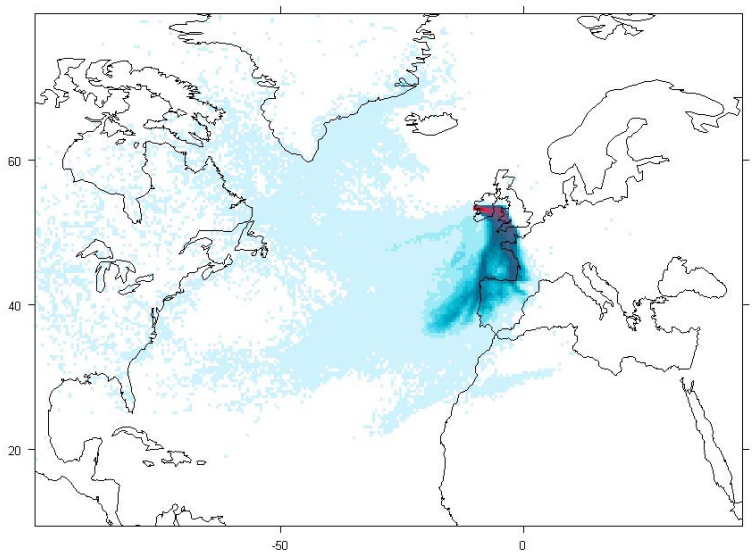

b,c)

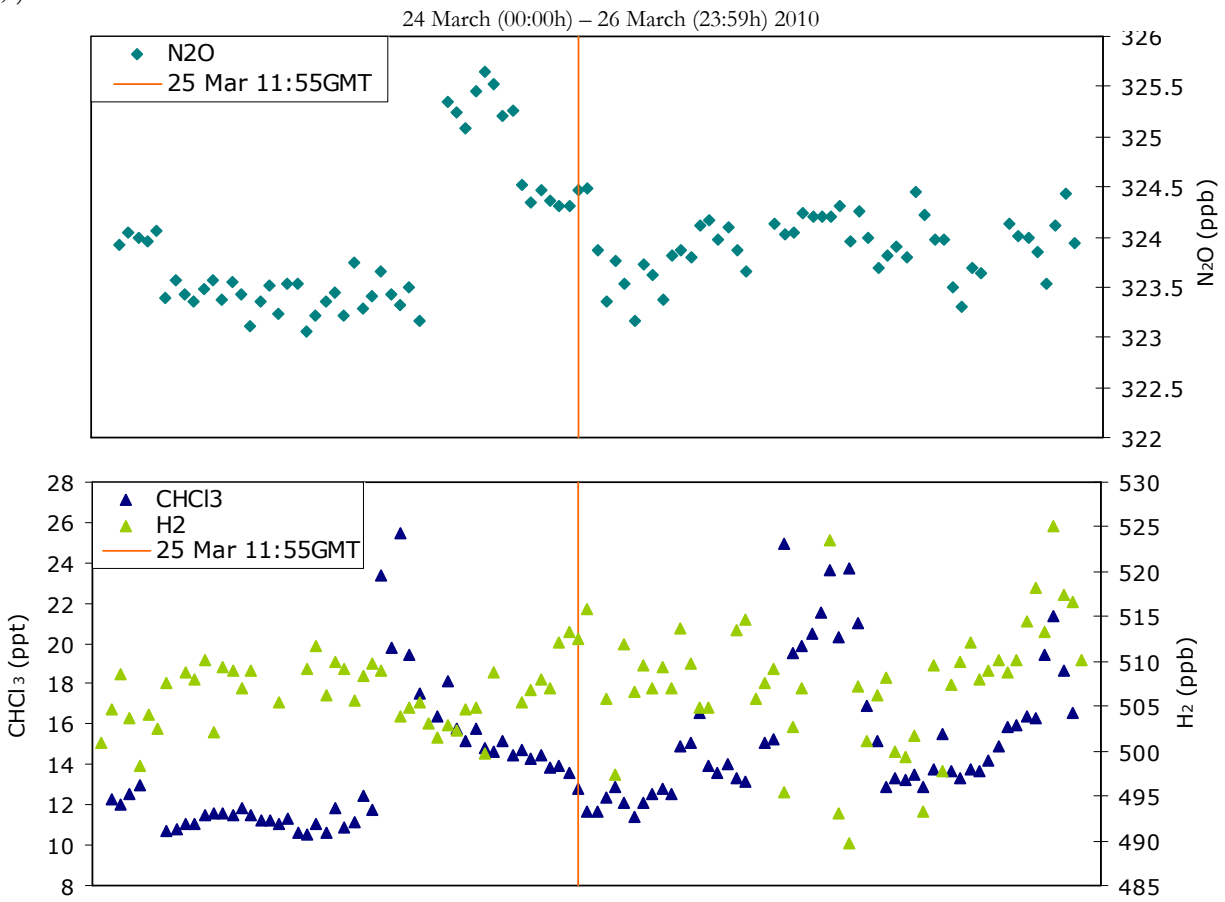

(ii) 20 January 2010, 15:20h GMT

The isotopic composition of the 20-January observation is marked in the ^{15}N site-specific information with a negatively correlated enriched $\delta^{15}N^{\alpha}$ and depleted $\delta^{15}N^{\beta}$, and resulting elevated site preference, relative to the other tropospheric samples. The N_2O mole fraction is at baseline levels and the NAME air history for the 3-hr 15:00-18:00h window (Figure 4.7a) shows baseline air originating from over the Atlantic Ocean. From observation at sample collection time there were slow 4 m/s winds on the Mace Head tower, also present in the corresponding UK-NWP meteorology which suggests that the slow winds were not completely localized to the tower and moment of record. AGAGE continuous high-frequency data (Figure 4.7b,c) from the adjacent inlet reported pollution-flagged CH_4 and $CHCl_3$ mole fractions. Though N_2O was at baseline, the air sample was collected immediately prior to a pollution event in which CH_4, $CHCl_3$, CO and N_2O are all elevated. The isotopic composition of N_2O thus informs N_2O controls that are not apparent in the NAME air history estimate alone, which is presumed reliable for discerning such information.

The isotopic signal in N_2O for the 20-January event is of an almost opposite and counterbalancing nature to that for the 25-March sample which also indicated surface source influence. Considering the simultaneous CO elevation, this observation could be capturing N_2O of a different origin associated with biomass burning or urban pollution. Specifically in the Mace Head region this could be the burning of peat for energy which is a common practice. Though impossible to validate with a single observation example, the ^{15}N site-specific composition shift observed in this sample may have insight into a specific N_2O emissions signature.

Figure 4.7 a) NAME air history for the 3-hr period spanning the 20 January 2010 air sample collection time. b) N_2O and CO mole fraction time series of AGAGE high-frequency data for 2 full days, 20-21 January (00:00h 20 January to 23:59h 21 January), indicating a pollution event following the sample collection. c) Same time period of AGAGE high-frequency data for chloroform and methane, indicating a pollution event. Exact flask collection time is indicated with the red line in both b and c. Tick marks are at the hour.

a)

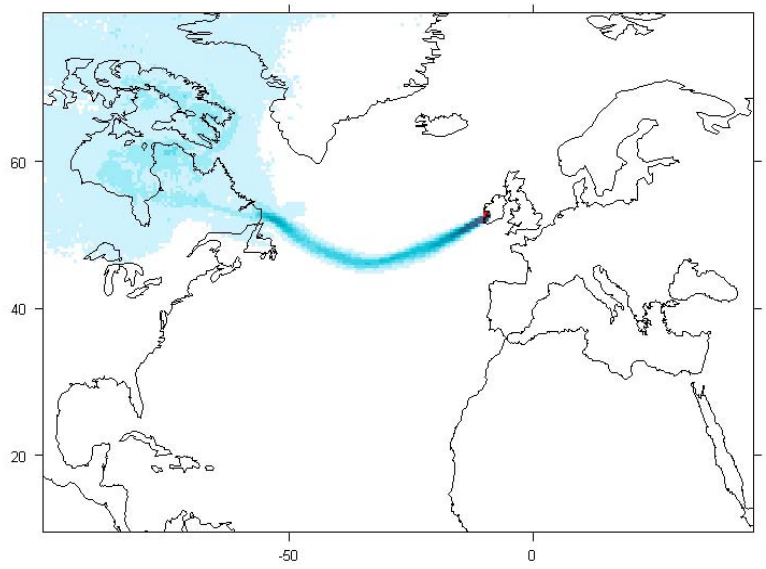

b,c)

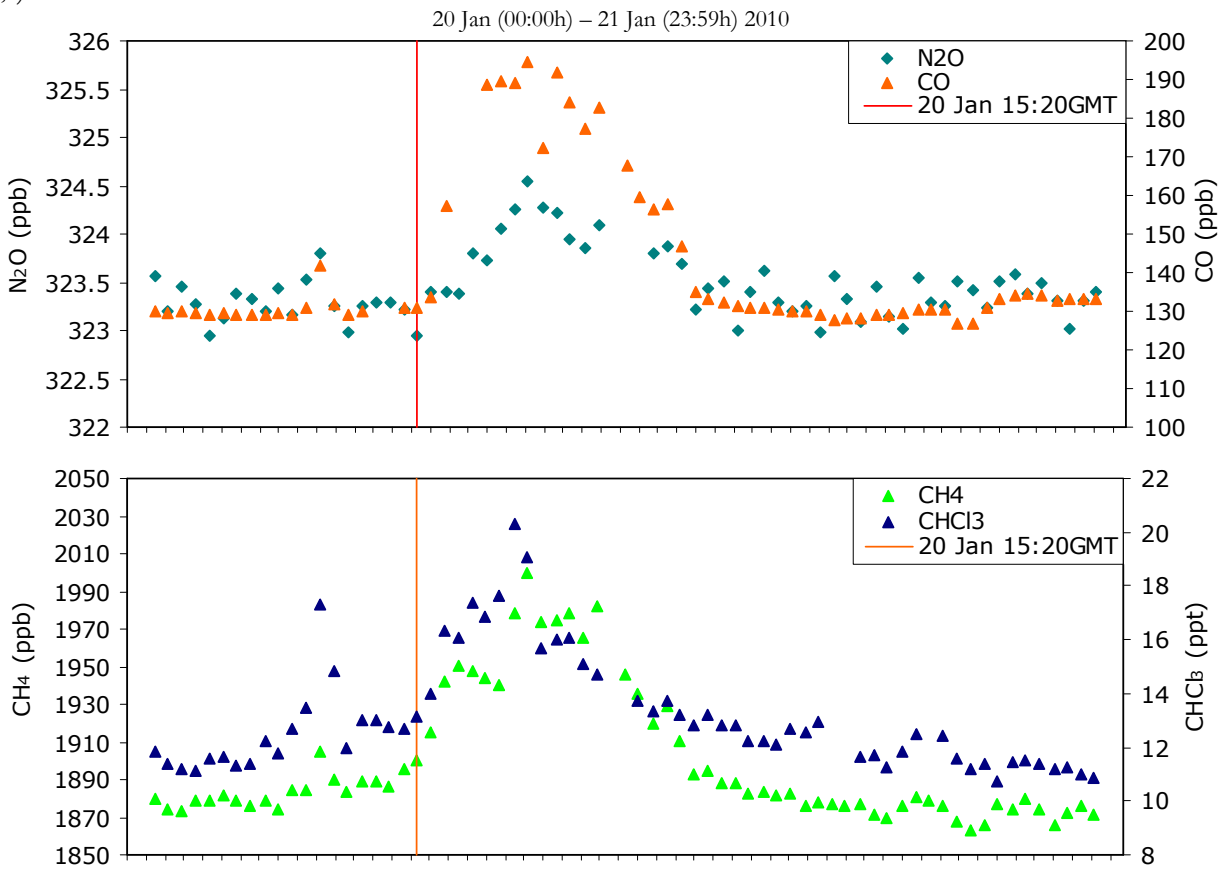

(iii) 1 July 2010, 9:20h GMT

From comparison between Figures 4.5a-c and 1.3a-c, the observation on 1 July has an isotopic composition significantly more enriched in $^{15}N^{bulk}$, $^{15}N^{\alpha}$, $^{15}N^{\beta}$ and ^{18}O than the majority observations in both the bulk and site-specific data in the direction of the stratospheric composition. HYSPLIT back trajectories were calculated for all of the observation points, and as expected very few indicated air origins at high altitudes in the polar region approaching tropopause height lending to possible direct influence from the stratosphere. The HYSPLIT back trajectory for the 1 July sample (Figure 4.8b) was unique in that it reaches >6 km in the polar region and gives the possibility of direct stratospheric air influence on Mace Head, which would be consistent with the observed enriched isotopic composition.

The corresponding AGAGE mole fraction measurement does not indicate a significant depletion, only 0.04 ppb below the 4-week running mean baseline, which is not consistent with a possible stratospheric influence. Apparent in AGAGE high-frequency mole fraction time series is the presence of minor elevated levels of N_2O and CO immediately prior to this sample collection (Figure 4.8c). Influence from stratospheric air with low concentrations of both N_2O and CO mixing with the boundary layer with above baseline mole fractions would offset each other and could conceivably explain the observed baseline mole fractions for these gases at the time of isotope sample collection. However, the N_2O mole fraction data is difficult to interpret in terms of the single isotopic composition observation, and only with high-frequency isotopic data could this stratospheric back trajectory consistency be validated.

If this stratospheric signal in the isotopic ccomposition were the case, then the information is uniquely reflected in the isotopic composition due to different process signatures but is not present in mole fraction data alone. The hypothesized consistency between the high altitude air history and the stratospheric signature could be demonstrating the responsiveness of N_2O isotopic composition to stratospheric air influence, and, if this were the case, then similar events could aid in determining the isotopic signal from stratospheric air downward mixing all the way to the surface. Numerous observations of stratospheric isotopic composition in the stratosphere and upper troposphere have been made, but there are only rough estimates of the stratospheric isotope signature which would be felt in the tropospheric composition. Clarification of the stratospheric signature reaching the troposphere would allow better interpretation of longer-term trends in N_2O resulting from the stratosphere, including the seasonal stratospheric effect known to impact the observed seasonal cycle particularly in the NH, interannual variability in STE and, eventually, decadal trends influencing tropospheric N_2O.

Figure 4.8 a) NAME air history for the 3-hr period spanning the 1 July 2010 air sample collection time. b) HYSPLIT back trajectory for 315h from the sample collection hour, indicating high altitude polar origins. c) N_2O and CO mole fraction time series of AGAGE high-frequency data for the 5 full days 28 June-2 July (00:00h 28 June to 23:59h 2 July). N_2O and CO baselines are 4-week running means of the high-frequency AGAGE non-polluted data. Exact flask collection time is indicated with the red line.

a)

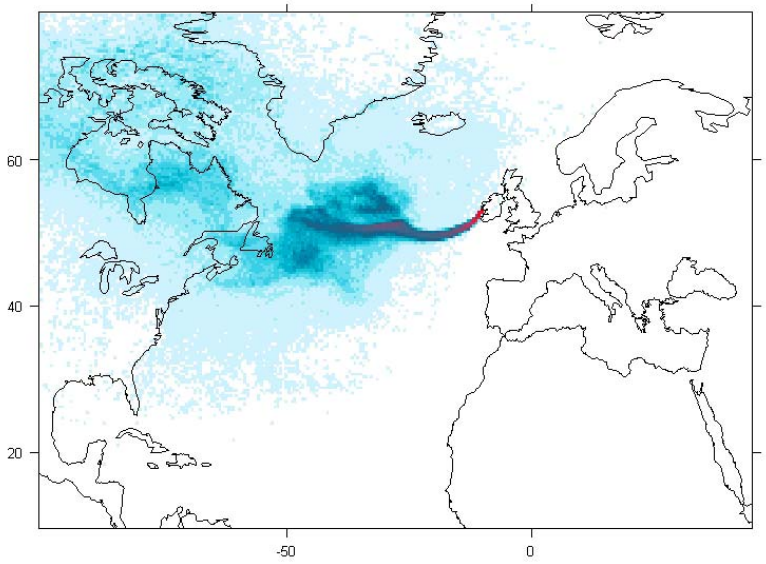

b)

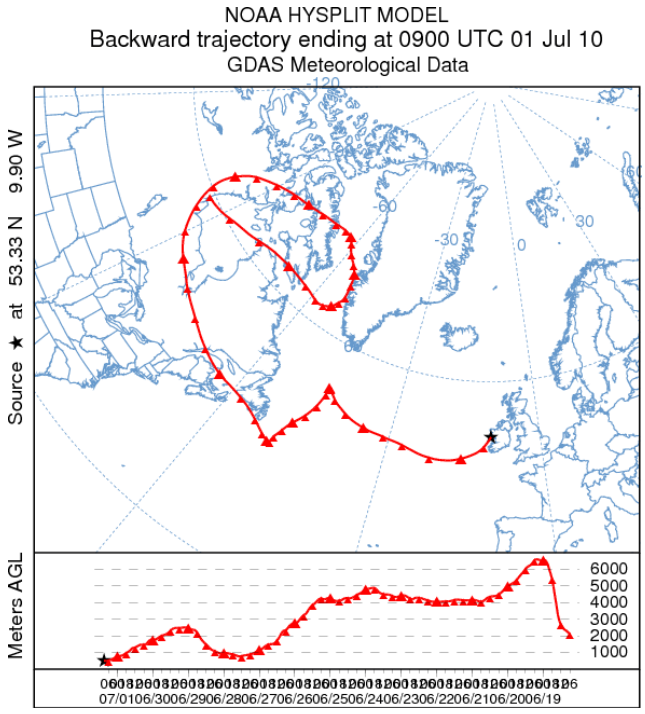

c)

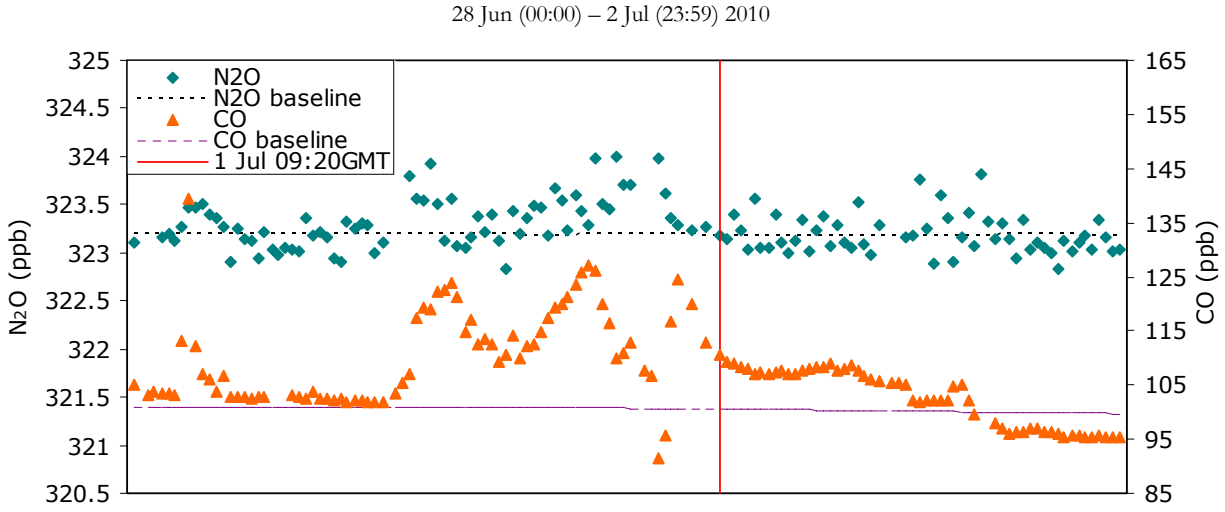

(iv) 29 Jan 11:30h, 1 Feb 11:07h, 6 May 12:30h, 12 Nov 11:08h GMT 2010

Although the majority of observations lie within a common isotopic composition cluster and thus appear essentially equivalent, particularly the baseline categorized observations, with sufficient measurement precision the positioning within this cluster may be important and may yield discernable information about N_2O influences. An example may exist with the four baseline categorized samples with the lightest $\delta^{15}N^{bulk}$ and $\delta^{18}O$ compositions (Figure 4.5a) with the stated observation dates throughout the year. Figure 4.9a-d shows the estimated NAME air histories all containing northerly origins, and the similarity suggests a possibility that the isotopic compositions have been influenced by a common northern signal. The dates of sample collection are also spread throughout the year removing the possibility that experimental error during a particular measurement session caused them to have similarly affected isotopic ratios. This similar isotopic composition is only apparent in the bulk isotopic composition $\delta^{15}N^{bulk}$ vs. $\delta^{18}O$ plot. The site-specific $\delta^{15}N^{\alpha}$, $\delta^{15}N^{\beta}$, and SP data for these samples do not follow a similar clear pattern, possibly interestingly showing that independent information may be obtained from the $^{15}N^{bulk}$ and ^{18}O isotope ratios and the ^{15}N site-specific isotope ratios. If the common isotopic compositions were validated to be significant, then the common northern signal could originate from higher latitudes towards the Arctic or simply encountering a more proximal northern Irelend enroute to Mace Head. Only with additional hogh-frequency data can this consistency be better interpreted and validated, but it illustrates the potential for information within baseline composition and not only within significantly anomalous individual deviations.

Figure 4.9 NAME air histories for the 3-hr period spanning each air sample collection time. a) 29 January 2010, b) 1 February 2010, c) 6 May 2010, d) 12 November 2010.

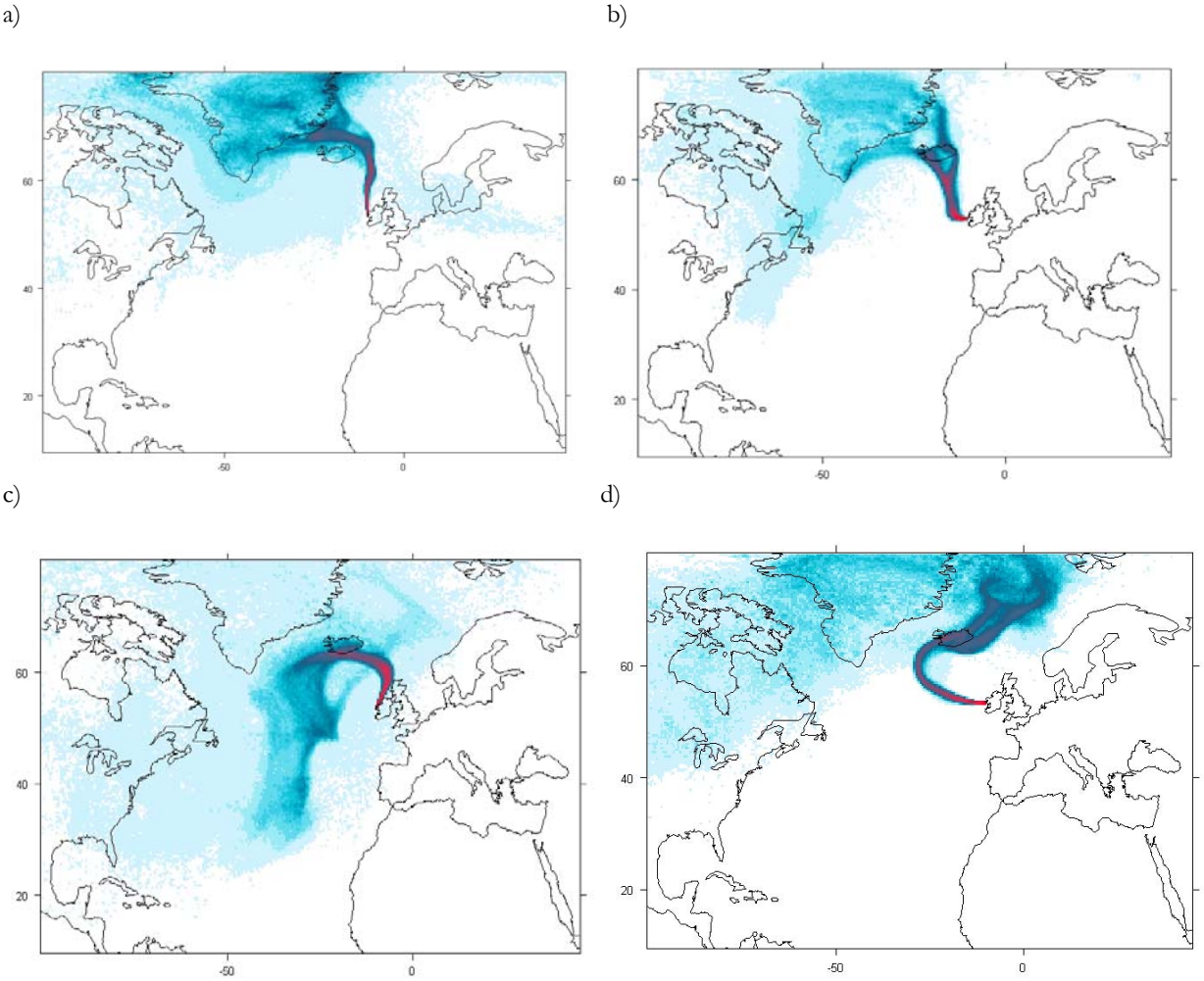

The above four case studies illustrated consistencies between tropospheric N_2O isotopic composition and air influences. While the coherent patterns are unable to be fully validated with only individual observations, they suggest a valuable discovery of previously unrecognized abilities of tropospheric measurements of N_2O isotopic composition. Beyond this recognition this low-frequency dataset is insufficient to apply thorough analysis, including source attribution. Attempts to apply "Keeling" analysis, which through isotope mixing mass balance provides an estimate of the sum source signature in δ vs. $1/[N_2O]$ plots, to the data and the individual case studies gave misdirected results (Keeling 1958). Keeling plot analysis cannot be accurately applied to these cases where there is only a small (around 1 ppb or less) difference in N_2O mole fraction between the outlier samples and the ~320 ppb mean background mole fraction (Pataki et al 2003). Non-linearities deviating from the ideal mixing model may be exacerbated by the small mole fraction range, and the small mole fraction variation increases the impact of measurement error. Diffusive environments have been shown to lead to non-linearities in isotope mixing analyses such as the

Keeling plot, studied on small scale soil chambers and potentially having far reaching effects on the much larger global diffusion scale (Risk & Kellman 2008, Nickerson & Risk 2009). The inapplicability of Keeling plot analysis to tropospheric N_2O isotopic variations has likewise been encountered for upper troposphere/lower stratosphere observations (Croteau et al 2010).

4.3.3 Isotopomer behavior

Apparent in the isotope relational plots in Figure 4.5, the majority of the samples form a negative correlation in their ^{15}N site-specific composition between $\delta^{15}N^{\alpha}$ and $\delta^{15}N^{\beta}$ and between $^{15}N^{bulk}$ and SP. The $^{15}N^{bulk}$ and ^{18}O data from Mace Head do not, however, have the same negative correlation. Expectations would be for observations to align in a stratosphere-soil mixing line because soils constitute the greatest source and the stratosphere the only major sink, as resulted from the simplified regional model in Figure 3.7. Though reality might not be as drastic as the simplified model relationships predict, a similar positive correlation would be expected. However, it should be noted that while there may be some expectations for N_2O isotopic composition behavior in the troposphere, these expectations are based upon intuition and simple models and there are so few actual observations of the troposphere that much could be possible in reality.

An analytical artifact causing this correlation was investigated. The most likely source of an analytical error regarding the ^{15}N site-specific data would be regarding the IRMS rearrangement coefficients, which accounts for the small fraction (~0.08) of $N\beta O^+$ that forms from $N\beta N\alpha O$ in the IRMS ion source. A change of the IRMS rearrangement coefficients kappa ($\varkappa$) and gamma (γ) for the calculation of $\delta^{15}N^{\alpha}$ and $\delta^{15}N^{\beta}$ results in distinct but essentially constant shifts in the alpha and beta compositions. For an incremental change in $\varkappa$ by 0.02, the composition of all of the observations were uniformly offset by -0.43 and +0.43‰ for $\delta^{15}N^{\alpha}$ and $\delta^{15}N^{\beta}$, respectively. The effect of a miscalculation in these IRMS parameters would then not affect any correlation between $\delta^{15}N^{\alpha}$ and $\delta^{15}N^{\beta}$ but rather displace the absolute location of the mean values. Similarly, alterations in the calibrated values of the reference gas to which $\delta45$, $\delta46$, and $\delta31$ are referenced for the calculation of $\delta^{15}N$ and $\delta^{18}O$ values results in a universal offset in all of the observation $\delta^{15}N^{\alpha}$ and $\delta^{15}N^{\beta}$ values. The contribution from another analytical cause is still possible, but further consideration could not find a clear source. Consequently, the negative correlation between $^{15}N^{\alpha}$ and $^{15}N^{\beta}$ is assumed real in further discussion.

Assuming that the observations and negative correlation are credible, then these observations at Mace Head may be reflecting atmospheric N_2O isotopic relations that do not match theoretical expectations for the composition to reflect mixing between the two most prominent end-members: stratospheric loss and soil emission (Figure 1.3a-c). The soil and stratospheric processes in themselves yield positive correlations. Both from signature measurements and consideration of enzymatic processes and isotope preference, it is expected that in N_2O processes there would be positive correlations between $^{15}N^{\alpha}$ and $^{15}N^{\beta}$, between bulk ^{15}N and either $^{15}N^{\alpha}$ or $^{15}N^{\beta}$, and between bulk ^{15}N and SP (Popp et al 2002, Stein & Yung 2003). Additionally, the mixing of the two compositions should result in a positive α and β correlation for the tropospheric reservoir.

Theoretical considerations of tropospheric N_2O isotopic composition, however, have been conducted through global scale balances which in total would expect a soil-stratosphere mixing line. Apparent from studies of N_2O mole fractions at various remote research stations around the globe, the seasonal cycle magnitudes and main drivers vary considerably between stations (Nevison et al 2004, 2005, 2007, 2011). This implies that although N_2O is generally a well-mixed trace gas, regionally N_2O is not homogeneous. Globally speaking, soils, both natural and agricultural, are estimated to be over 50% of the global source, however most of these emissions arise from the tropics (Denman et al 2007). In the northern hemisphere high latitudes, Mace Head is situated far from the large tropical soil N_2O flux and perhaps feels a weighted influence from oceanic, estuarial,

and other aquatic sources. Mace Head is located on the western coast of Ireland and all arriving air parcels have been influenced by oceanic, coastal, estuarial, and other aquatic environments, including baseline air masses across the Atlantic Ocean. Mace Head's location is especially distinctive in terms of N_2O emissions because of the prominent local peat and wet and boggy environment, and common local practice of burning peat for energy. Thus, far from the dominant tropical soil source and surrounded by aquatic microbial production of N_2O in the Northern Hemisphere high latitudes, the observations of tropospheric composition at Mace Head might actually not expect to demonstrate a stratosphere-soil mixing line.

A possible cause of the observed $^{15}N^{\alpha}$ and $^{15}N^{\beta}$ negative correlation could be a third significant end-member in addition to the soil-stratosphere mixing line. Kim & Craig (1993) propose three vectors to determine isotopic composition as soil, stratosphere, and ocean. Figure 1.3a-c illustrates signatures in relation to the tropospheric composition measurements in this thesis. The general pattern for the ^{15}N site-specific isotopomers is more clearly highlighted in Figure 3.5. A few comments are necessary regarding these plotted signature values. As mentioned previously, these are the collection of available data and are not fully representative of the variation in signature within each source type nor include all possible source type signatures. The signatures presented represent individual specific sets of conditions and cannot be taken as the representative composition of each of these sources. Additionally, variation in N_2O precursor molecules composition can vary considerable between locations and conditions. In the site-specific composition plots, the precursor composition tends to offset the particular site-specific composition while maintaining the same relationships between $^{15}N^{\alpha}$ and $^{15}N^{\beta}$. ^{15}N site-specific composition is indicative of enzymatic preference whereas bulk ^{15}N and ^{18}O isotopic composition tends to be more indicative of precursor molecule compositions (Toyoda et al 2002, Park et al 2011). For enzymatic processes from biological N_2O there has been observed constant effects on site-preference particular to nitrification (~30‰) and denitrification (~0‰), irregardless of precursor composition (Toyoda et al 2002, Toyoda et al 2005, Sutka et al 2006, Well et al 2009). Thus because of varying precursor molecules, the signatures in Figure 1.3 might not be perfectly aligned with the tropospheric composition measured at Mace Head. An additional contribution to the misalignment could be since no international N_2O isotopic standard exists, there is also possibly an interlaboratory calibration discrepancy. These reasons make the signatures in Figure 1.3 not necessarily directly comparable to the observations of tropospheric air at Mace Head measured in this study, but general patterns of signature effects can be surmised.

The ocean source signatures present in Figure 1.3a-c and Figure 3.5 have lighter $^{15}N^{\alpha}$ and heavier $^{15}N^{\beta}$ relative to the troposphere and show a negative slope between $\delta^{15}N^{\alpha}$ and $\delta^{15}N^{\beta}$, but no particular relationship in the bulk ^{15}N and ^{18}O signatures with composition near tropospheric. If these measurements are sufficient to represent the biological ocean surface source, then mixing model between tropospheric air and the ocean source could cause the observed isotopomer relationship in the Mace Head data. These signatures and mixing with the ocean do not fully answer the observed negative correlation at Mace Head. The site-specific signature data in Figure 1.3 are the mean representative surface ocean signatures from four separate studies, however these are only four with a fair amount of scatter, and none located in the Atlantic Ocean. Additionally the Atlantic Ocean has been measured to have low production of N_2O, and thus it would not be necessarily expected that there would be enough emissions from the Atlantic to affect the isotopic composition at Mace Head so drastically as to cause the strong negative ^{15}N site-specific correlation alone (Walter et al 2006).

Further contributions to the observed negative α and β correlation in addition to mixing with the oceanic source could stem from additional aquatic sources of N_2O affecting air masses arriving at Mace Head. Estuaries have been reported to produce a novel N_2O isotopic signal (Bol et al 2004),

and may be offering an unexplained enzymatic process producing the negative alpha-beta correlation. The Bol et al (2004) study incubates estuarine soil cores taken from intertidal zones in the UK, a temperate and relevant location to Mace Head. They measured N_2O emissions in flooded and non-flooded experimental set-ups. They report the flooded samples fell into a bimodal distribution in isotopic composition, and these two flooded subgroups have alpha and beta compositions which show a negative slope between the two modes. One flooded mode matches the non-flooded composition and is consistent with what others have measured for denitrification having relatively depleted $^{15}N^{\alpha}$ and enriched $^{15}N^{\beta}$ ($\delta^{15}N^{\alpha}$ ~ -15 to 10‰; $\delta^{15}N^{\beta}$ ~ -17 to -6 ‰). The other mode was unusually relatively enriched in $^{15}N^{\alpha}$ and depleted in $^{15}N^{\beta}$ ($\delta^{15}N^{\alpha}$ ~ 2 to 16‰; $\delta^{15}N^{\beta}$ ~ -52 to -37‰), and they suggest could be recording a previously unencountered N_2O isotopic signal. (Reported in Bol et al (2004) and plotted here in Figure 1.3a-c is the mean of the bimodally distributed flooded compositions thus only partially representing the distinctive new isotopic signal and which results in the negative correlation between $^{15}N^{\alpha}$ and $^{15}N^{\beta}$. The estuary data point with low $\delta^{15}N^{\beta}$ in Figure 1.3 is this reported average, and the separated unique mode carries a much more depleted $^{15}N^{\beta}$ and slightly more enriched $^{15}N^{\alpha}$.). In Figure 1.3 the negative correlations in the estuary source between $^{15}N^{\alpha}$ and $^{15}N^{\beta}$, and $\delta^{15}N^{bulk}$ and SP are apparent, but slightly misaligned for $\delta^{15}N^{\alpha}$ and $\delta^{15}N^{\beta}$ with the tropospheric air samples measured at Mace Head in this study to be able to produce the observed negative correlation between $\delta^{15}N^{\alpha}$ and $\delta^{15}N^{\beta}$ at Mace Head. This small discrepancy can be reconciled by the few considerations touched upon above regarding possible calibration misalignment the representativeness of the signature estimates. The Bol et al (2004) study only represents a small set of samples from the same soil source measured in a single experiment and cannot be taken as the representative composition of estuarine sources. The anomalous N_2O emissions mode actually did measure $\delta^{15}N^{\alpha}$ as high as ~16‰ which is essentially the tropospheric composition measured in this study. Because it is expected that the spread of variation in all estuarine source compositions would extend beyond that reported in this one study, it would follow to expect that estuary sources could have δ15α compositions greater than tropospheric air, while the $\delta^{15}N^{\beta}$ anomalous composition is extremely depleted relative to tropospheric composition. These considerations make the compositions measured by Bol et al (2004) not directly comparable to those measured in this study, but illustrative of the negative correlation in ^{15}N site-specific composition in emissions emitted from estuarine soils. The Bol et al (2004) estuary study, then, reveals a potential biological source mechanism which produces N_2O emissions with a relative composition which is negatively correlated in α and β, and could be contributing to an observed negative correlation between $\delta^{15}N^{\alpha}$ and $\delta^{15}N^{\beta}$ in air arriving at Mace Head.

The exact signatures reported for estuarine soils by Bol et al (2004) may actually be most relevant and striking for the possible discovery of a more widespread aquatic biological process which produces a range of N_2O emissions with a negative correlation between $^{15}N^{\alpha}$ and $^{15}N^{\beta}$, rather than being specific to only estuarial environments. The microbial N_2O production process causing emissions with negatively correlated α and β could possibly be present more broadly in aquatic environments, and therefore affecting observations at Mace Head by more than just entrainment of air from regional estuaries.

A kinetic or biological enzymatic mechanism to cause a negative slope between $\delta^{15}N^{\alpha}$ and $\delta^{15}N^{\beta}$ for either the proposed ocean or estuary is confounding since both kinetic and enzymatic processes suggest a positive correlation between alpha and beta, between bulk ^{15}N and alpha or beta, and between bulk ^{15}N and SP. Preferential reaction with the lighter ^{15}N isotopes for N_2O precursor molecules, or preferential reaction with light ^{15}N isotopologues for N_2O loss processes, would hold for both α and β nitrogens, often with more preference at the α position (see Popp et al 2002 and discussion therein). A very recent discovery may have found the previously unknown biological mechanism: N_2O produced by ammonia-oxidizing archaea (Santoro et al 2011). The isotopic

composition of surface ocean N_2O, as included in Figure 1.3, is somewhat inconsistent with the supposition that nitrification and nitrifier-denitrification are the main sources in the surface ocean affecting the atmosphere (Popp et al 2002, Dore et al 1998). Santoro et al (2011) show that cultures of marine archaea produce N_2O through ammonia oxidation, and that the produced N_2O has an isotopic composition similar to the reported ocean source composition. They suggest that these archaea may be the prominent ocean N_2O source rather than the previously supposed ammonia oxidizing bacteria. The recent discovery needs further investigation to fully assess the extent to which archaea may be an N_2O source. Perhaps this biological mechanism extends beyond oceans and into other aquatic environments, possibly explaining the unknown enzymatic process causing the negative correlation observed from the estuarial signatures by Bol et al (2004). The implications of this study on the Mace Head observations is a possible route by which negative correlations between alpha and beta could be produced enzymatically in aquatic environments, and legitimizes the reported signatures for ocean and estuary sources discussed above. If this mechanism is indeed more universal to aquatic environments, then Mace Head is certainly situated to feel the impact from local to regional to Atlantic Ocean aquatic sources of N_2O.

End-member mixing with the weighted impact of aquatic N_2O sources at Mace Head in Northern Hemisphere high latitiudes far from the strong tropical soil source is a feasible explanation for the observed negative correlation in the site-specific data at Mace Head. An additional relevant thought arises from the isotopic observations at Mace Head. The case studies on 25 March and 20 January 2010 capturing surfaces source more directly could possibly be highlighting two end-members mixing to to created the negative correlation between α and β positions. The composition of the 25 March sample (section 4.3.2*(i)*) has $^{15}N^{bulk}$-, $^{15}N^{\alpha}$- and ^{18}O- isotopically-depleted, but towards a $^{15}N^{\beta}$-enriched and low SP. In Figure 4.5 this observation is towards the lower right bound of the $^{15}N^{\alpha}$ vs. $\delta^{15}N^{\beta}$ site-specific composition of the observations. This air sample was collected during a low boundary layer which would be trapping a proximal local source signature. If this case identifies a surface source signature distinctive to the Mace Head region which is entrained into all air masses arriving at Mace Head, then it is consistent with the observed isotopic ratio correlations in all of the data (Figure 4.5) whereby the $^{15}N^{\beta}$ composition is uncorrelated or slightly negatively correlated to the $^{15}N^{\alpha}$ composition, and certainly not fitting the expected soil-stratosphere mixing line of positive correlation. The 20 January 2010 observation possibly offers a counterbalancing local signal in the isotopic ratios (section 4.3.2*(ii)*). The observation is measured to have a high SP resulting from an enriched $\delta^{15}N^{\alpha}$ composition and negatively correlated depleted $^{15}N^{\beta}$ composition, near the upper left bound of the $^{15}N^{\alpha}$ vs. $\delta^{15}N^{\beta}$ plot. This air sample was collected during slow 4 ms^{-1} winds which would similarly capture a locally originating signal as the 25 March observation, but coincident elevated trace gases are suggestive of a differing source associated with burning. In the Mace Head region, burning of peat is a common source of energy and would be a cause of local combustion with an unknown but characteristic N_2O isotopic signature. If these two regional sources were somewhat entrained into each air mass arriving at Mace Head, then the balance between these two sources mixing is consistent with causing a negative correlation. The extent to which that local source entrainment would impact the observations enough to cause the distinctive negative correlation is uncertain. If these sources were extremely localized then they likely would not be strong enough sources alone to cause the entire observed alpha-beta relationship, but they could be additive with the above discussed impact from oceanic, estuarial, and other aquatic microbial sources felt at Mace Head (and located distantly from the strong tropical soil source) to cause the negative correlation.

The negative correlation in the ^{15}N site-specific data observed in these measurements is initially unexpected, but with consideration is consistent with the balance of sources and signatures shifted more towards aquatic emissions rather than soil which would be affecting air masses at Mace Head. With the present low-frequency data set and single location, the discussion can only be speculation regarding the possible cause of the unexpected signal. High-frequency observations will better allow statistical interpretation with an added ability to categorized samples regarding surface influence from differing origins. More helpful to interpretation and validation of these suggested causes would be observations at a remote research station situated with a different balance of weighted surface influences on N_2O, ideally in the tropics.

Conclusion

Analysis of the first set of surface N_2O isotopic composition observations covering a full annual cycle in one location (Mace Head, Ireland) reveals non-constant composition with variability that is detectable with current instrument precision capabilities (Stheno+CF-IRMS, Chapter 2). Resolvable variation is clearly detected on the short-term between individual observations, as well as longer term possibly detecting an annual trend and suggestive of surface source isotopomer signals reaching Mace Head. The isotopic observations paired with air history information suggest the utility of tropospheric isotopic composition measurements by illustrating coherent patterns between isotopic composition and N_2O governing processes. N_2O isotopic values in the troposphere are possibly varying according to atmospheric mixing processes tied to surface source emissions, biomass burning pollution, and possibly the down-flux of stratospheric air, reflecting the differing source signatures and impact from stratospheric air. The current low-frequency flask data set is insufficient to validate the explanations but they do illustrate rational consistencies, which will require high-frequency measurements to better interpret and verify. By having isotopic composition data alongside the N_2O mole fractions, in the observed variation there is additional independent information to inform N_2O budget processes on regional and global scales.

The isotopic composition of $\delta^{15}N^{bulk}$ was seen to increase over the 2010 year. The presence of the trend in the $\delta^{15}N^{bulk}$ data is confidently found. However, a possibility remains for potential sampling biases resulting from the sparse and unevenly distributed observations which may not sufficiently represent the year. The presence of the $\delta^{15}N^{bulk}$ trend toward more ^{15}N-enriched values is consistent with a year of anomalously strong transfer of highly ^{15}N-enriched stratospheric air into the troposphere near Mace Head or of increased loss of N_2O in the stratosphere (or both). The notion of an increased stratospheric influence in 2010 is supported by N_2O mole fraction behavior, the lower stratosphere winter temperature proxy, the reported long-term trend of increasing stratospheric circulation, and notably a record NAO index having repercussions for STE near Mace Head. The yearly isotopic composition trend observed here suggests the utility of isotopic information to elucidate causes of interannual variability in atmospheric N_2O and N_2O growth rates. Future N_2O mole fraction data should be analyzed before assessing the growth rate of N_2O in 2010, but these isotopic data will hopefully help to clarify the main causes of observed N_2O mole fraction in 2010 variability.

The low-frequency flask observations are insufficient for detection of an isotopic seasonal cycle or finer isotopic composition variations at Mace Head, and it is unclear if current measurement precision capabilities are limiting as well. The presence of such a cycle at Mace Head is thus unrecognized, but the consistencies between variability and N_2O influences recognized here suggest that N_2O isotopic composition should carry a seasonal response to changing N_2O influences, and if

resolved allow better interpretation and separation of the various influences on the N_2O seasonal cycle. With adequate high-frequency data coverage of varied air histories it might even be possible to describe a seasonal cycle in the N_2O isotopic composition stemming from land-influenced air masses recording the soil source in addition to the background air seasonality.

The observations in this study illustrate examples of detectable short-term isotopic variability between observations with differing air origins and influences, which are suggestive of distinctive N_2O influences and contain information not found in the N_2O mole fraction. Each effect on tropospheric isotopic composition in the four cases presented here show consistencies with air origins linked to different N_2O influencing processes, supporting the ability to distinguish between surface sources of different origins (potentially resolving soil, urban, estuarine, and other disparate emissions). The isotopic signals do not necessarily have a clear corresponding N_2O mole fraction signal, which is similar to what has been also observed in tropical troposphere/lower stratosphere N_2O isotopic observations (Croteau et al 2010). Cases presented here also highlight that ^{15}N site-specific, $^{15}N^{bulk}$, and ^{18}O data can respond differently to changes in N_2O controls and provide unique information. The low-frequency data finds measurable and significant variations exists in N_2O isotopic composition in the troposphere, and is supportive of coherent, useful source-receptor relationships.

The observed variation in the non-baseline N_2O isotopic data at Mace Head have the potential to provide new constraints on European national emissions strengths. Specifically, this measurable isotopic variability tied to sources lends itself to potential application to back attribution techniques (e.g. Manning et al 2011 for UK/European N_2O emissions). Isotopic data brings additional information tied to characteristic source signatures allowing possible delineation of emissions between sectors, which is desirable knowledge as emissions regulations and attribution needs progress.

In addition to the cases of significant deviations from baseline composition in non-baseline air origins, information is potentially retained in the specific isotopic compositions within the more homogenous cluster given sufficient measurement precision. A case of baseline categorized samples was presented with four observations sharing common isotopic compositions and air origins, and potentially points to a common signal in these baseline observations. If this is the case, the typical categorization of 'baseline' samples may have to be further delineated to account for divergent N_2O influences within that grouping. This possibly includes high altitude origins potentially bearing stratospheric influence or northerly origins, or possibly even airmasses entraining surface sources over North America prior to crossing the Atlantic Ocean. Further improving instrumentation precision beyond the nearly peak IRMS capabilities achieved for these measurements (Chapter 2) will assist in extracting these subtle pieces of information. The data collected here also suggest that without full knowledge of air histories and potential N_2O influences, the practice of using tropospheric air as a constant for ^{15}N isotopomer standard is probably not valid with current measurement precision capabilities.

An unexpected negative correlation is observed in the ^{15}N site-specific composition over the year of observations at Mace Head. The possibility that this is an analytical artifact is still pending, but considerations of recent studies regarding N_2O emissions from aquatic sources suggest that observations at Mace Head are possibly recording the balance of N_2O surface sources in the northern hemisphere higher latitudes, which tends more towards aquatic emissions and far from the dominant soil source in the tropics.

These tropospheric observations imply that the isotopic composition variation does not correspond perfectly to currently estimated signatures of source origins. This reflects that these variations are showing effects from multiple influences combined, and/or that the current literature measurements of source signatures are insufficiently summarizing the full spectrum of signatures

and especially lack signature information specific to air masses affecting Mace Head. Observations capturing strong emissions signals could be valuable in assessing uncertain emissions signatures with a new top-down approach for source signature characterization. In situ flux measurements of N_2O isotope signatures directly from sources have yielded some insight; however the reported variability of isotope ratios is broad and there is difficultly in extrapolating these small scale measurements up to regional or global levels. N_2O isotopic data in the troposphere lends itself to top-down analysis of regional source signatures.

The present low-frequency data set collected over this year is insufficient for detailed emissions magnitude and distribution estimates, source signature attribution, or establishment of source-receptor relationships to N_2O controls. However, while it does not allow for more complete analysis of N_2O on short, seasonal, and annual timescales, it does demonstrate the potential for these utilities. These observations point strongly to the need and value of N_2O isotopic observations at higher frequency and more evenly distributed throughout the year, encompassing both baseline and non-baseline samples.

Chapter 4 References

Bol R, Rockmann T, Blackwell M & Yamulki S (2004). Influence of flooding on $d^{15}N$, $d^{18}O$, $1d^{15}N$ and $2d^{15}N$ signatures of N_2O released from estuarine soils—A laboratory experiment using tidal flooding chambers. *Rapid Commun Mass Spectrom* 18: 1561-1568.

Butchart N & Coauthors (2006). Simulations of anthropogenic change in the strength of the Brewer–Dobson circulation. *Climate Dyn* 27: 727-741.

Butchart N & Coauthors (2010). Chemistry-climate model simulations of twenty-first century stratospheric climate and circulation changes. *J Climate* 23: 5349-5374.

Croteau P, Atlas EL, Schauffler SM, Blake DR, Diskin S & Boering KA (2010). Effect of local and regional sources on the isotopic composition of nitrous oxide in the tropical free troposphere and tropopause layer. *J Geophys Res* 115: D00J11.

Cullen MJP (1993). The Unified Forecast/Climate Model. *Meteorol Mag* 1449: 81-94.

Cullen MJP, Davies T, Mawson MH, James JA, Coulter SC & Malcolm A. An overview of numerical methods for the next generation UK NWP and climate model. *In*: Lin CA, Laprise R & Ritchie H, Editors, Numerical Methods in Atmospheric and Ocean Modelling. Canadian Meteorological & Oceanographic Society, Ottowa, Canada, 1997.

Davies T, Cullen MJP, Malcolm AJ, Mawson MH, Staniforth A, White AA & Wood N (2005). A new dynamical core for the Met Office's global and regional modelling of the atmosphere. *Q J R Meteorol Soc* 131: 1759-1782.

Denman KL, Brasseur G, Chidthaisong A, Ciais P, Cox PM, Dickinson RE, Hauglustaine D, Heinze C, Holland E, Jacob D, Lohmann U, Ramachandran S, da Silva Dias PL, Wofsy SC & Zhang X (2007). Couplings Between Changes in the Climate System and Biogeochemistry. *In*: Climate Change 2007: The Physical Science Basis. Contribution of Working Group I to the Fourth Assessment Report of the Intergovernmental Panel on Climate Change [Solomon, S., D. Qin, M. Manning, Z. Chen, M. Marquis, K.B. Averyt, M.Tignor and H.L. Miller (eds.)]. Cambridge University Press, Cambridge, United Kingdom and New York, NY, USA.

Dore JE, Popp BN, Karl DM & Sansone FJ (1998). A large source of atmospheric nitrous oxide from subtropical North Pacific surface waters. *Nature* 396: 63-66.

Draxler RR & Hess GD (1998). An overview of the HYSPLIT_4 modelling system for trajectories, dispersion, and deposition. *Australian Meteorol Mag* 47: 295-308.

Flessa H, Dorsch P & Beese F (1995). Seasonal variation of N_2O and CH_4 fluxes in differently managed arable soils in southern Germany. *J Geophys Res* 100: 23115–23124.

Garcia R, Randel WJ (2008). Acceleration of the Brewer-Dobson circulation due to increases in greenhouse gases. *J Atmos Sci* 65: 2731-2739.

Gerasopoulos E, Zanis P, Papastefanou C,. Zerefos CS, Ioannidou A, Wernli H (2006). A complex case study of down to the surface intrusions of persistent stratospheric air over the Eastern Mediterranean. *Atmospheric Environment* 40: 4113-4125.

Guckland A, Corre M & Flessa H (2010). Variability of soil N cycling and N_2O emission in a mixed deciduous forest with different abundance of beech. *Plant Soil* 336: 25-38.

Hirsch AI, Michalak AM, Bruhwiler LM, Peters W, Dlugokencky EJ & Coauthors (2006). Inverse modeling estimates of the global nitrous oxide surface flux from 1998-2001. *Global Biogeochem Cycles* 20: GB1008.

Hodson E (2008). The municipal solid waste landfill as a source of Montreal Protocol-restricted halocarbons in the United States and United Kingdom. Ph.D. Thesis, Dept. of Earth, Atmospheric & Planetary Sciences, MIT.

Huang J, Golombek A, Prinn R, Weiss R, Fraser P, Simmonds P, Dlugokencky EJ, Hall B, Elkins J, Steele P, Langenfelds R, Krummel P, Dutton G & Porter L (2008). Estimation of regional emissions of nitrous oxide from 1997 to 2005 using multi-network measurements, a chemical transport model, and a Kalman Filter. *J Geophys Res* 113: D17313.

Ishijima, K., Sugawara, S., Kawamura, K., Hashida, G., Morimoto, S. and co-authors. 2007. Temporal variations of the atmospheric nitrous oxide concentration and its $d^{15}N$ and $d^{18}O$ for the latter half of the 20th century reconstructed from firn air analyses. *J. Geophys. Res.*

James P, Stohl A, Forster C, Eckhardt S, Seibert P & Frank A (2003a). A 15-year climatology of stratosphere-troposphere exchange with a Lagrangian particle dispersion model: 2, Mean climate and seasonal variability. *J Geophys Res* 108(D12): 8522.

Jiang X, Ku WL, Shia R-L, Li Q, Elkins JW, Prinn RG & Yung YL (2007). Seasonal cycle of N_2O: Analysis of data. *Global Biogeochem Cycles* 21: GB1006.

Jones PD*,* Jonsson T*,* Wheeler D. 1997. Extension to the North Atlantic Oscillation using early instrumental pressure observations from Gibraltar and South-West Iceland. Int. J. Climatol. 17*:* 1433–1450.

Kaiser J, Rockmann T & Brenninkmeijer CAM (2002a). Temperature dependence of isotope fractionation in N_2O photolysis. *Physical Chemistry Chemical Physics* 4 (18): 4220-4230.

Kaiser J, Brenninkmeijer CAM & Rockmann T (2002b). Intramolecular ^{15}N and ^{18}O fractionation in the reaction of N_2O with $O(^1D)$ and its implications for the stratospheric N_2O isotope signature. *J Geophys Res* 107 (D14): 4214.

Kaiser J, Rockmann T & Brenninkmeijer CAM (2003a). Complete and accurate mass-spectrometric isotope analysis of tropospheric nitrous oxide. *J Geophys Res* 108 (D15): 4476.

Kaiser J, Rockmann T, Brenninkmeijer CAM & Crutzen PJ (2003b). Wavelength dependence of isotope fractionation in N_2O photolysis. *Atmos Chem Phys* 3: 303-313.

Kaiser J, Engel A, Borchers R & Rockmann T (2006). Probing stratospheric transport and chemistry with new balloon and aircraft observations of the meridional and vertical N_2O isotope distribution. *Atmospheric Chemistry and Physics* 6: 3535-3556.

Keeling, CD (1958). The concentration and isotopic abundances of atmospheric carbon dioxide in rural areas. *Geochim. Cosmochim. Acta* 13: 322–334.

Manning AJ, O'Doherty S, Jones AR, Simmonds PG & Derwent RG (2011). Estimating UK methane and nitrous oxide emissions from 1990 to 2007 using an inversion modeling approach. *J Geophys Res* 116: D02305.

Manning AJ, Ryall DB, Derwent RG, Simmonds PG & O'Doherty S (2003). Estimating European emissions of ozone-depleting and greenhouse gases using observations and a modelling back-attribution technique. *J Geophys Res* 108: 4405.

McLinden CA *et al.* (2003). Global modeling of the isotopic analogues of N_2O: Stratospheric distributions, budgets, and the ^{17}O-^{18}O mass-independent anomaly, *J Geophys Res* 108(D8): 4233.

Merritt DA, Brand WA & Hayes JM (1994). Isotope-ratio-monitoring gas chromatography-mass spectrometry: methods for isotopic calibration. *Org Geochem* 21(6/7): 573-583.

Miller BR, Weiss RF, Salameh PK, Tanhua T, Greally BR, Muhle J & Simmonds PG (2008). Medusa: A sample preconcentration and GC/MS detector system for in situ measurements of atmospheric trace halocarbons, hydrocarbons and sulfur compounds. *Anal Chem* 80: 1536 -1545.

Naqvi SWA, Yoshinari T, Jayakumar DA, Altabet MA, Narvekar PV, Devol AH, Brandes JA & Codispoti LA (1998). Budgetary and biogeochemical implications of N_2O isotope signatures in the Arabian Sea. *Nature* 394: 462-464.

Nevison CD, Kinnison DE & Weiss RF (2004). Stratospheric influence on the tropospheric seasonal cycles of nitrous oxide and chlorofluorocarbons. *Geophys Res Lett* 31: L20103.

Nevison CD, Mahowald NM, Weiss RF & Prinn RG (2007). Interannual and seasonal variability in atmospheric N_2O. *Global Biogeochem Cycles* 21: GB3017.

Nevison CD, Dlugokencky E, Dutton G, Elkins JW, Fraser P, Hall B, Krummel PB & Langenfelds RL (2011). Exploring causes of interannual variability in the seasonal cycles of tropospheric nitrous oxide. *Atmos Chem Phys* 11: 3713-3730.

Newman PA, Nash ER & Rosenfield JE (2001). What controls the temperature of the Arctic stratosphere during the spring? *J Geophys Res* 106: 19999-20010.

Nickerson N & Risk D (2009). Keeling plots are non-linear in non-steady state diffusive environments. Geophys Res Lett 36: L08401.

O'Doherty S *et al.* (2001). *In situ* chloroform measurements at Advanced Global Atmospheric Gases Experiment atmospheric research stations from 1994 to 1998. *J Geophys Res* 106: 20429–20444.

Olsen MA, Schoeberl MR & Nielsen JE (2007). Response of stratospheric circulation and stratosphere-troposphere exchange to changing sea surface temperatures. *J Geophys Res* 112: D16104.

Park SY, Atlas EL, Boering KA (2004). Measurements of N_2O isotopologues in the stratosphere: Influence of transport on the apparent enrichment factors and the isotopologue fluxes to the troposphere, *J Geophys Res* 109: 462-464.

Park S, Perez T, Boering KA, Trumbore SE, Gil J, Marquina S & Tyler SC (2011). Can N_2O stable isotopes and isotopomers be useful tools to characterize sources and microbial pathways of N_2O production and consumption in tropical soils? *Global Biogeochem Cycles* 25: GB1001.

Pataki DE, Ehleringer JR, Flannagan LB, Yakir D, Bowling DR, Still CJ, Buchmann N, Kaplan JO & Berry JA (2003). The application and interpretation of Keeling plots in terrestrial carbon cycle research. *Global Biogeochem Cycles* 17: 1022.

Perez T, Trumbore SE, Tyler SC, Matson PA, Ortiz-Monasterio I, Rahn T & DWT Griffith (2001). Identifying the agricultural imprint on the global N_2O budget using stable isotopes. *J Geophys Res* 106: 9869-9878.

Popp BN, Westley MB, Toyoda S, Miwa T, Dore JE & coauthors (2002). Nitrogen and oxygen isotopomeric constraints on the origins and sea-to-air flux of N_2O in the oligotrophic subtropical North Pacific gyre. *Global Biogeochem Cycles* 16: doi:2001GB001806.

Prinn, R *et al.* (2000). A history of chemically and radiatively important gases in air deducted from ALE/GAGE/AGAGE. *J Geophys Res* 105: 17751-17792.

Risk, D., L. Kellman (2008) Isotopic fractionation in non-equilibrium diffusive environments. Geophysical Research Letters, 35, L02403, doi:10.1029/2007GL032374.

Rockmann T, Kaiser J, Brennickmeijer CAM & Brand WA (2003b). Gas chromatography/isotope-ratio mass spectrometry method for high-precision position-dependent ^{15}N and ^{18}O measurements of atmospheric nitrous oxide. *Rapid Commun Mass Spectrom* 17: 1897-1908.

Rockmann T, Kaiser J, Brenninkmeijer CAM, Crowley J, Borchers R, Brand W & Crutzen P (2001). Isotopic enrichment of nitrous oxide ($^{15}N^{14}NO$, $^{14}N^{15}NO$, $^{14}N^{14}N^{18}O$) in the stratosphere and in the laboratory. *J Geophys Res* 106: 10403.

Rockmann T & Levin I (2005). High-precision determination of the changing isotopic composition of atmospheric N_2O from 1990 to 2002. *J Geophys Res* 110: D21304.

Ryall DB & Maryon RH (1998). Validation of the UK Met Office's NAME model against the ETEX dataset. *Atmospheric Environment* 32: 4265-4276.

Santoro AE, Buchwald C, McIlvin MR, Casciotti KL (2011). Isotopic signature of N_2O produced by marine ammonia-oxidizing archaea. *Science* 28 July 2011: 1208239.

Sigmond M, Siegmund PC, Manzini E & Kelder H (2004). A simulation of the separate climate effects of middleatmospheric and tropospheric CO_2 doubling. *J Climate* 17: 2352-2367.

Simmonds PG, Derwent RG, Manning AJ, O'Doherty S & Spain G (2010). Natural chloroform emissions from the blanket peat bogs in the vicinity of Mace Head, Ireland over a 14-year period. *Atmospheric Environment* 44: 1284-1291.

Sowers T, Rodebaugh A, Yoshida N & Toyoda S (2002). Extending records of the isotopic composition of atmospheric N_2O back to 1800 A.D. from air trapped in snow at the South Pole and the Greenland Ice Sheet Project II ice core. *Global Biogeochem Cycles* 16(4): doi: 10.1029/2002GB001911. issn: 0886-6236.

Sprenger M & Wernli H (2003). A northern hemispheric climatology of cross- tropopause exchange for the ERA15 time period (1979-1993). *J Geophys Res* 108(D12): 8521.

Stein L & Yung Y (2003). Production, isotopic composition, and atmospheric fate of biologically produced nitrous oxide. *Ann Rev Earth Planetary Sci* 31: 329-356.

Sutka, RL, NE Ostrom, PH Ostrom, JA Breznak, H Gandhi, AJ Pitt, F Li (2006) Distinguishing nitrous oxide production from nitrification, and denitrification on the basis of isotopomer abundances. Appl. Exp. Microbiol. 72, 638– 644.

Toyoda S, Yoshida N, Urabe T, Aoki S, Nakazawa T, Sugawara S & Honda H (2001). Fractionation of N_2O isotopomers in the stratosphere. *J Geophys Res* 106: 7515-7522.

Toyoda, S, N Yoshida, T Miwa, Y Matsui, H Yamagishi, U Tsunogai, Y Nojiri, N Tsurushima (2002), Production mechanism and global budget of N_2O inferred from its isotopomers in the western North Pacific, Geophys. Res. Lett. 29(3), 1037.

Toyoda S *et al.* (2004). Temporal and latitudinal distributions of stratospheric N_2O isotopomers. *J Geophys Res* 109: D08308.

Toyoda, S, H Mutobe, H Yamagishi, N Yoshida, Y Tanji (2005) Fractionation of N_2O isotopomers during production by denitrifier Soil Biology and Biochemistry 37(8): 1535-1545.

Trickl T, Feldmann H, Kanter HJ, Scheel HE, Sprenger M, Stohl A & Wernli H (2010). Forecasted deep stratospheric intrusions over Central Europe: case studies and climatologies. *Atmos Chem Phys* 10: 499-524.

Walter S, Bange HW, Breitenbach U & Wallace DWR (2006). Nitrous oxide in the North Atlantic Ocean. *Biogeosciences* 3: 607-619.

Well, R, and Flessa H (2009). Isotopologue signatures of N_2O produced by denitrification in soils. J. Geophys. Res. 114, G02020

Wu X, Bruggemann N, Gasche R, Shen Z, Wolf B & Butterbach-Bahl K (2010). Environmental controls over soil-atmosphere exchange of N_2O, NO, and CO_2 in a temperate Norway spruce forest. *Global Biogeochem Cycles* 24: GB2012.

Yamagishi H, Westley MB, Popp BN, Toyoda S, Yoshida N, Watanabe S, Koba K & Yamanaka Y (2007). Role of nitrification and denitrification on the nitrous oxide cycle in the eastern tropical North Pacific and Gulf of California. *J Geophys Res* 112: G02015.

Yoshida N & Toyoda S (2000). Constraining the atmospheric N_2O budget from intramolecular site preference in N_2O isotopomers. *Nature* 405: 330-334.

Yoshinari T, Altabet MA, Naqvi SWA, Codispoti L, Jayakumar A, *et al.* (1997). Nitrogen and oxygen isotopic compositions of N_2O from suboxic waters of the eastern tropical North Pacific and the Arabian Sea-- Measurement by continuous-flow isotope ratio monitoring. *Mar Chem* 56: 253-264.

Yung YL, Miller CE (1997). Isotopic fractionation of stratospheric nitrous oxide. *Science* 278: 1778-80.

Chapter 5: Conclusions and looking ahead

This thesis has provided valuable progress on the utilization of nitrous oxide isotopic composition in the troposphere. The isotopic composition in the troposphere, when linked with air origin information and process isotopic signatures, illustrates consistencies with characteristic source-receptor relationships to potentially distinguish between N_2O influences which mole fractions alone are unable to do. The practical utility of N_2O isotopic composition in the troposphere has not been previously addressed beyond gross global budget models to ascertain consistency between estimates of global source strengths and their approximate signatures, stratospheric sink and fractionation, and assuming a *constant* present-day tropospheric isotopic composition. Scientific knowledge was previously limited by inadequate measurement precision capabilities and paucity of observations. This thesis developed an optimized high-precision fully-automated instrument system which was applied to make regular high-precision observations at a well-located remote research station. These observations of isotopic composition were importantly paired with detailed air mass origin information to reveal coherent source-receptor relationships detectable in the composition variations. Additionally this thesis has expanded the prior global budget models for N_2O isotopic composition with a detailed regional model approach to simulate the transport of air parcels containing N_2O isotopic signals, thus providing more thorough assessment of isotopic composition expected signals and laying the groundwork for future modeling applied N_2O isotopic composition observations in the troposphere.

The development of the Stheno pre-concentration device achieved significant progress for N_2O isotopic composition measurements enabling useful measurements to further scientific progress. The instrumentation system was uniquely optimized specifically for N_2O separation and isotope measurement, thereby enabling it to meet the precision challenge of detecting informative variation in tropospheric isotopic composition, and distinctively fully-automated, liquid-cryogen-free to allow for high-frequency measurements. Other online pre-concentration systems used for N_2O isotopic composition exist, but these systems are either based upon generalized trace gas concentrators (e.g. Rockmann et al 2003a, Park et al 2004, Perez et al 2006, Croteau et al 2010) or are not automated thus making consistent repeated measurements difficult (e.g. Yoshida & Toyoda 2000), and these systems therefore have noted lower precisions than that achieved here. Additionally all previous N_2O isotopic measurement systems rely upon liquid cryogen which inhibit fully-automated, high-frequency capabilities. Stheno was developed specifically for N_2O with tailored attention to specific needs of full N_2O recovery, separation from N_2O-specific interfering gases, and avoidance of isotopic fractionation—successfully resulting in superior precision for N_2O ^{15}N-resolved isotopomer compositions than reported for any other instrumentation system (1σ precisions of 0.11 and 0.14‰ for $\delta^{15}N^{\alpha}$ and $\delta^{15}N^{\beta}$, respectively) and better or matched precisions for N_2O bulk isotopic values (0.05 and 0.10‰ for $\delta^{15}N^{bulk}$ and $\delta^{18}O$, respectively). The site-specific ^{15}N composition is improved by 2-3 fold over the best achieved previously by an online CF-IRMS system (Rockmann et al 2005) and superior to offline IRMS as well (Kaiser et al 2003). The only significant limitation to higher precision in the current Stheno+CF-IRMS system is the IRMS collector cup configuration requiring two separate runs instead of being able to collect all needed ions in five cups simultaneously.

These precision numbers now have meaning following the observation campaign conducted as a central aspect of this thesis and marking the first set of N_2O isotopic composition observations capturing a full annual cycle at one site and paired with air origin modeling information. Previous tropospheric air measurements were sparsely conducted. A single more extensive measurement

campaign of tropospheric composition was pursued once before, concluding with the same commonly held belief that there is not useful variation in tropospheric N_2O isotopic composition (Kaiser et al 2003a). The air sample observations, however, were from multiple locations throughout Europe with no published connection with air mass origin information which would be of high importance at these inland sites surrounded by natural, agricultural, and industrial N_2O sources. The time series presented by Kaiser et al (2003a) with their quoted measurement precision suggests that they indeed detected useful variations. However, because the observations were not paired with air origin information, the likely meaningful variation was regarded as scatter. With no information of air history through any means, e.g. meteorological information, back trajectories/maps, or complementary measured tracers, any detected subtle variation will be interpreted as noise.

In contrast, these observations demonstrated that the tropospheric composition of N_2O has variations detectable by the measurement precision achieved here, and these variations are consistent with expected source and sink signals. The signals are admittedly subtle and require at least the high-precision optimized instrumentation developed for this work, but when used in combination with detailed air history information and complementary data these observations suggested relationships between N_2O isotopic variations and possibly air influenced by distinct surface sources or stratospheric sinks and downward mixing. These relationships are consistent with the data and air origins for the low-frequency flask observations, but more measurements at high frequency will be needed to better validate the explanations. Site-specific ^{15}N composition showed an unexpected overall negative correlation in the data, and though there is some possibility for uninvestigated analytical causes, the negative correlation is consistent with observations at Mace Head possibly recording the balance of N_2O surface sources in the northern hemisphere higher latitudes, which tends more towards aquatic emissions and far from the dominant soil source in the tropics. The observations pointed to the use of isotopic data for interpretation of longer-term changes and interannual variation as well. A slight increasing trend in $\delta^{15}N$ bulk is consistent with recording an anomalously extreme year (2010) for stratospheric influence in the troposphere. When mole fraction data has been fully assessed it will be interesting to see if N_2O indeed experienced lower growth rate than usual. No seasonal cycle could be detected, but such detection was limited by observation frequency with unclear implications for measurement precision. However, the coherent patterns discovered suggest that isotopic composition measurements have the potential to separate the competing seasonal influences including stratospheric loss and downward mixing, tropospheric transport, and biological source seasonality, which mole fraction data alone is unable to do.

The measurable isotopic variability tied to surface sources and stratospheric influence revealed in this thesis demonstrated potential to attribute variations to specific emission sources and interpret seasonal signals. These Mace Head observations showed how well isotopic data lends itself to potential application to back attribution techniques to assess regional emissions, e.g. Manning et al (2011). Specifically at Mace Head, N_2O isotopic data can provide new constraints on European national emissions strengths with the desirable ability to separate specific emission sectors. Mace Head station was strategically chosen for the pilot year of observations because of its situation at a confluence of N_2O influences: soil and anthropogenic sources from the east, clean background air from the west, and inline with strong stratospheric mixing. It proved to be an ideal location for future measurements of N_2O isotopic composition.

The continuous high-frequency mole fraction measurements of trace gases by the Advanced Global Atmospheric Gases Experiment (AGAGE) network of monitoring stations has demonstrated the drastic improvement in understanding obtained with high-frequency in situ data compared to low-frequency flask collection. Particularly for background variation, seasonality, and a

global picture, the in situ AGAGE data has proven superior for interpretation and quantification of the subtle signals of N_2O varations (Nevison et al 2011). Although in this thesis observations were lab-bound and relatively low-frequency, the development of Stheno using the core automation and liquid-cryogen-free technology of AGAGE network instrumentation (Miller et al 2008) allows the implementation of high-frequency, continuous data collection of N_2O isotopic composition in a remote research station to become feasible for the first time. Stheno additionally was constructed from the start with foresight for possible transition to other detector technologies and expansion of measurement capabilities.

Interpretation of isotopic observations is not straightforward. Understanding of observations can be facilitated with a companion forward model (e.g. Alexander et al 2005). To accompany the observations, a regional model system was developed here using combined techniques to gain further understanding of N_2O isotopic composition of the troposphere. Previous models with N_2O tropospheric isotopic composition have only been global budget estimates (e.g. Rahn & Wahlen 2000, Rockmann et al 2003b, Park et al 2004, Toyoda et al 2004) or for only the stratosphere (e.g. McLinden et al 2003, Morgan et al 2004). The model developed for this thesis utilizes as a primary tool a Lagrangian approach with high resolution NAME particle dispersion model air history estimates from the UK Met Office (A. Manning) which gives a more realistic distribution of air origins than individual back trajectories, thereby aiding insight into source-receptor relationships. Additionally, high-frequency AGAGE data were used to simulate realistic model scenarios of a seasonal stratospheric influence and its signal in tropospheric composition. The regional model approach of this thesis still maintained many assumptions and simplifications which could be improved upon to better interpret the true complexity of N_2O, but it has built a foundation and given insight into model structure for further development of N_2O isotopic composition modeling.

Variation in N_2O isotopic composition predicted by the regional model was subtle, however there were short-term variations between successive modeled air parcels surpassing the detection limit of current measurement precision achieved in this thesis. Additionally, assumptions and simplifications in the regional model meant that the potential variability of isotopic composition was likely underestimated. These isotopic signals at detectable levels corresponded to changing influence by European emissions and illustrated the coherent relationships between source influence and N_2O isotopic composition also seen in the observations. They likewise encourage the future use of back attribution techniques with N_2O isotopic observations for emissions quantification and separation between source types.

The regional model results specifically utilized the available NAME air history maps corresponding to the flask observations at Mace Head, and similar to the observations highlighted the importance of high-frequency data for better interpretation of N_2O isotopic signals. More extensive use of the model with a high-frequency time series in the future would allow better investigation into N_2O emissions. The episodic nature of N_2O emissions causes low-frequency data to not simulate reality well, but high-frequency resolution observations simulated by the model, and actual observations, would allow statistical treatment of the emission episodes to give a more realistic image of daily, monthly, seasonally, or annually changing emissions and emission signatures.

The regional model also allowed for further insight into expectations that the tropospheric observations from this thesis were not able to comment on—specifically the seasonal cycle of N_2O isotopic composition which will only be resolvable with high-frequency data. The simulation of the stratospheric seasonal influence, suggested to be the largest contributor to the observed seasonality in N_2O mole fraction at Mace Head, predicted its effect to be subtle and pushing the limits of detection. Model scenarios resulted in seasonal amplitudes spanning the cusp of detectability in N_2O isotopic composition measurements and it is uncertain whether the instrumentation development of

this thesis provided sufficient precision. Though not the pretty picture desired, this provides insight into the development of instrumentation and the goal for precision as well as expectations for the first suite of high-frequency isotopic data.

The observations and regional model together provided insight into the N_2O isotopic composition in the troposphere. The instrumental development of Stheno provided a new measuring capability to enable useful observations and a practical interpretation of precision and detectability by providing technology and design to make the achievement of high-precision, high-frequency in situ observations attainable for the first time. In total, a key insight is that a primary utility of N_2O isotopic data in the troposphere will be for analysis of regional surface emissions using the short-term variability between air samples with spatially and temporally different origins. Patterns of isotopic composition and air origin do exist with detectable variations pointing to the controls on N_2O in the troposphere. This information is attainable with the currently developed pre-concentration system capabilities, and would be aided tremendously with the onset of high-frequency data. This use for regional emissions characterization and quantification will undoubtedly require complementary research advances in characterizing source signatures. Further elucidation on the N_2O budget at the seasonal scale will be possible only with N_2O isotopic composition data at high-frequency and to create a distributed, unbiased, and full dataset, and at global scales with a widely distributed network of stations.

Chapter 5 References

Alexander B, Park RJ, Jacob DJ, Li QB, Yantosca RM, Savarino J, Lee CCW & Thiemens MH (2005). Sulfate formation in sea salt aerosols: Constraints from oxygen isotopes. *J Geophys Res* 110: D10307.

Croteau P, Atlas EL, Schauffler SM, Blake DR, Diskin S & Boering KA (2010). Effect of local and regional sources on the isotopic composition of nitrous oxide in the tropical free troposphere and tropopause layer. *J Geophys Res* 115: D00J11.

Kaiser J, Rockmann T & Brenninkmeijer CAM (2003a). Complete and accurate mass spectrometric isotope analysis of tropospheric nitrous oxide. *J Geophys Res*, 108(D15): 4476.

Manning AJ, O'Doherty S, Jones AR, Simmonds PG & Derwent RG (2011). Estimating UK methane and nitrous oxide emissions from 1990 to 2007 using an inversion modeling approach. *J Geophys Res* 116: D02305.

McLinden CA, Prather MJ & Johnson MS (2003). Global modeling of the isotopic analogues of N_2O: Stratospheric distributions, budgets, and the ^{17}O-^{18}O mass-independent anomaly. *J Geophys Res* 108(D8): 4233.

Miller BR, Weiss RF, Salameh PK, Tanhua T, Greally BR, Muhle J & Simmonds PG (2008). Medusa: A sample preconcentration and GC/MS detector system for in situ measurements of atmospheric trace halocarbons, hydrocarbons and sulfur compounds. *Anal Chem* 80: 1536 -1545.

Morgan CG, Allen M, Liang MC, Shia RL, Blake GA & Yung YL (2004). Isotopic fractionation of nitrous oxide in the stratosphere: Comparison between model and observations. *J Geophys Res* 109: D04305.

Nevison CD, Dlugokencky E, Dutton G, Elkins JW, Fraser P, Hall B, Krummel PB & Langenfelds RL (2011). Exploring causes of interannual variability in the seasonal cycles of tropospheric nitrous oxide. *Atmos Chem Phys* 11: 3713-3730.

Park SY, Atlas EL, Boering KA (2004). Measurements of N_2O isotopologues in the stratosphere: Influence of transport on the apparent enrichment factors and the isotopologue fluxes to the troposphere. *J Geophys Res* 109: 462-464.

Perez T, Garcia-Montiel D, Trumbore S, Tyler S, De Camargo P, Moreira M & Piccolo M & Cerri C (2006). Nitrous oxide nitrification and denitrification N-15 enrichment factors from Amazon forest soils. *Ecological Applications* 16: 2153-2167.

Rahn T & Wahlen M (2000). A reassessment of the global isotopic budget of atmospheric nitrous oxide. *Global Biogeochem Cycles* 14: 537-543.

Rockmann T, Kaiser J, Brenninkmeijer CAM & Brand WA (2003a). Gas chromatography/isotope-ratio mass spectrometry method for high-precision position-dependent ^{15}N and ^{18}O measurements of atmospheric nitrous oxide, *Rapid Commun Mass Spectrom* 17: 1897-1908.

Rockmann T, Kaiser J & Brennickmeijer CAM (2003b). The isotopic fingerprint of the pre-industrial and the anthropogenic N_2O source. *Atmospheric Chemistry and Physics* 3: 315-323

Toyoda S *et al.* (2004). Temporal and latitudinal distributions of stratospheric N_2O isotopomers. *J Geophys Res* 109: D08308.

Yoshida N & Toyoda S (2000). Constraining the atmospheric N_2O budget from intramolecular site preference in N_2O isotopomers. *Nature* 405: 330-334.

Appendix

Appendix 2

I. Pictures

Stheno system

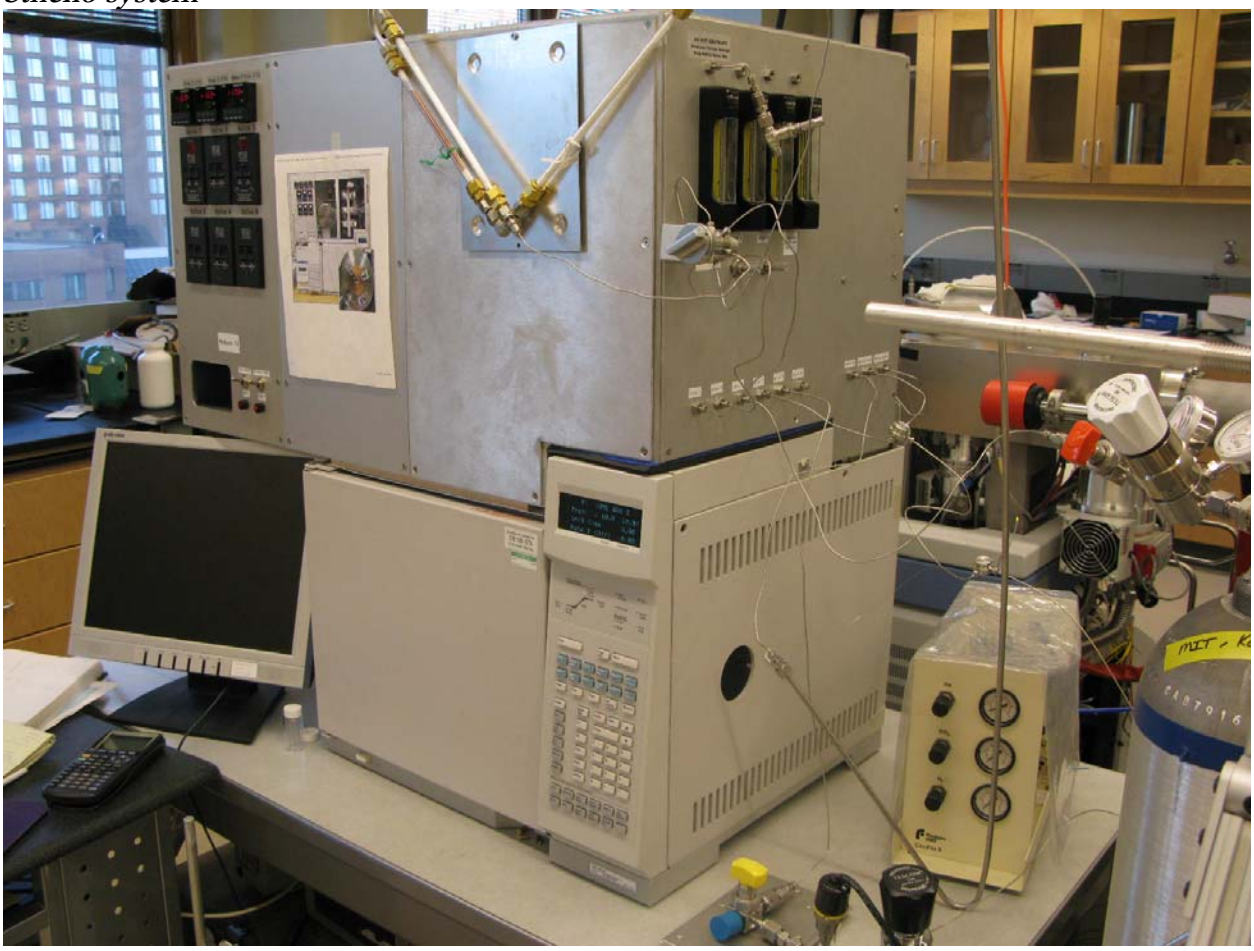

Overhead view inside Stheno housing

Left: Cryotiger coldhead with traps inside, electronic automated controls, Nafion dryer, Omega temperature controllers
Right: Stheno inlet, multiport valves, Red-Y flow controller

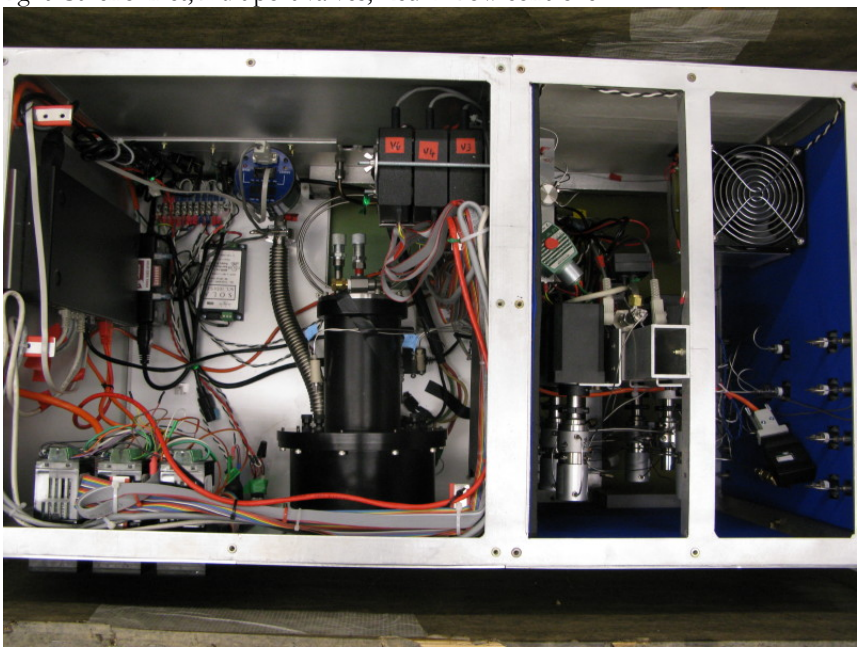

Multiport valves inside Stheno housing (clockwise from upper right: V1, V6, V5, V2)

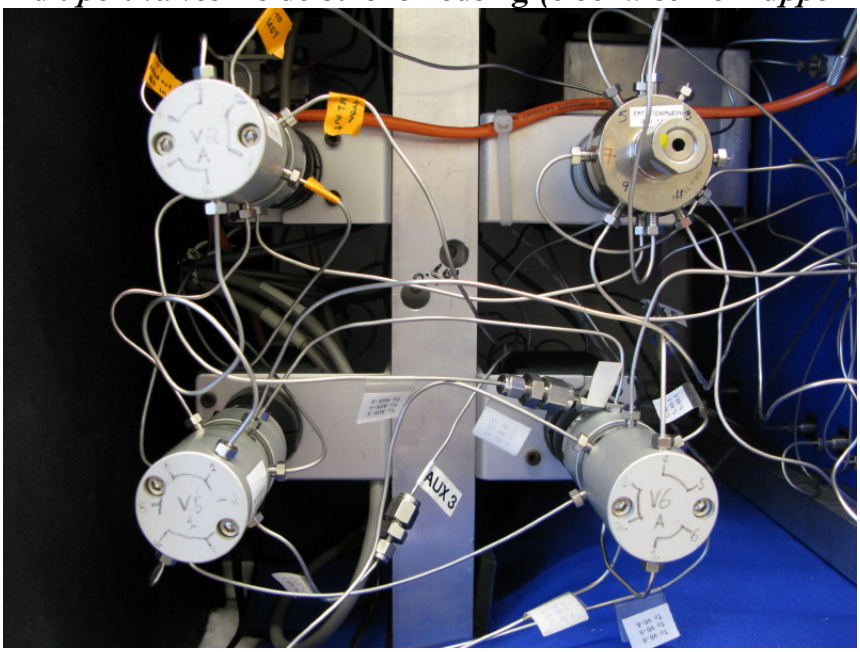

Cryotraps inside vacuumed Cryotiger coldhead shell

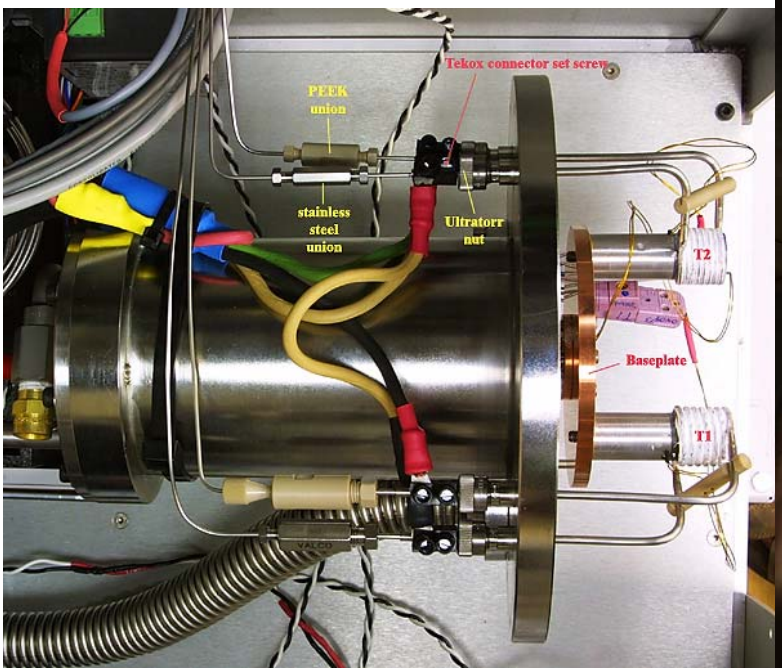

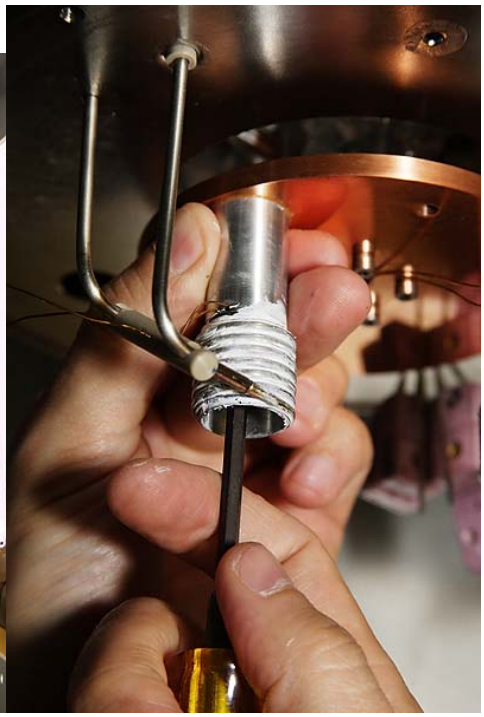

Open split

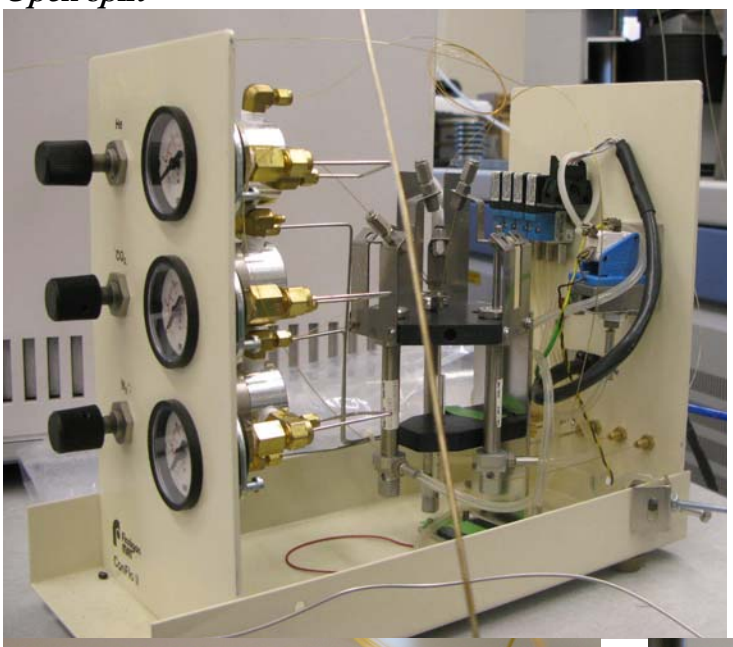

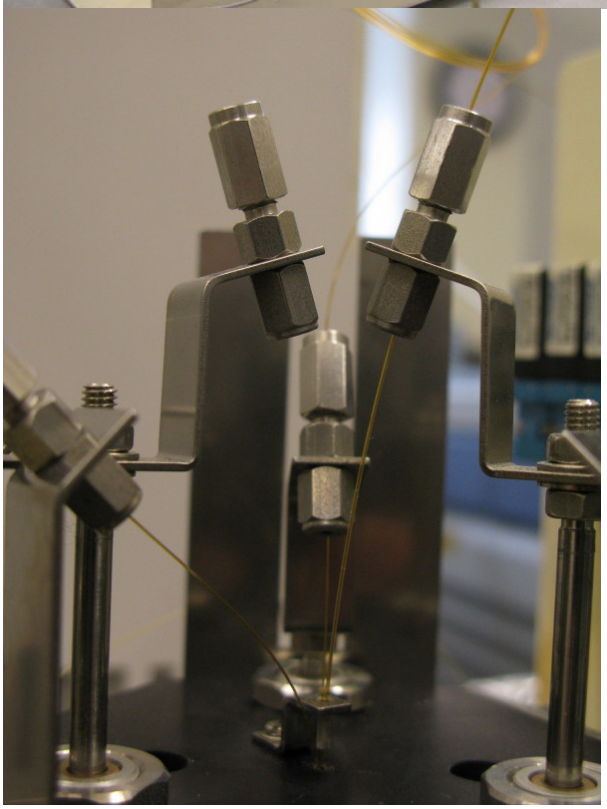

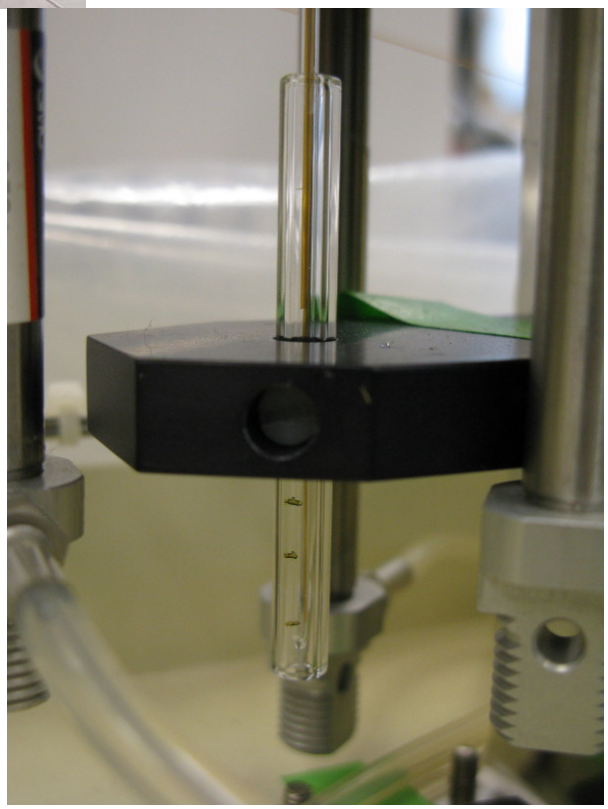

Continuous flow IRMS interface

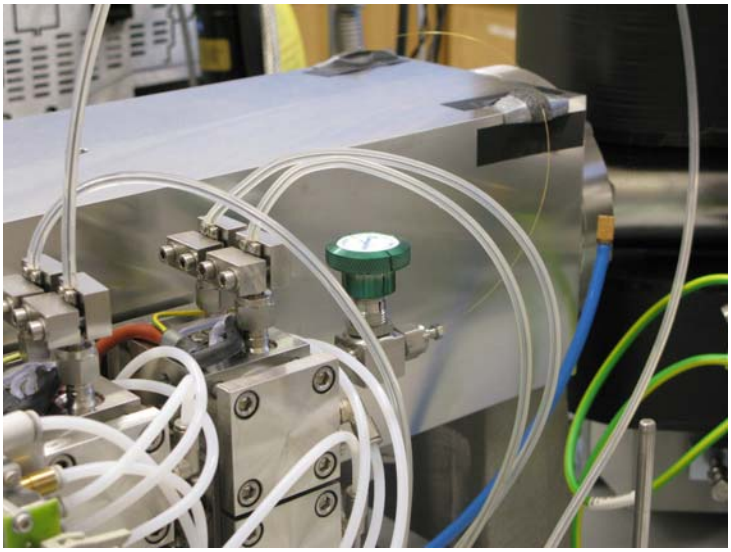

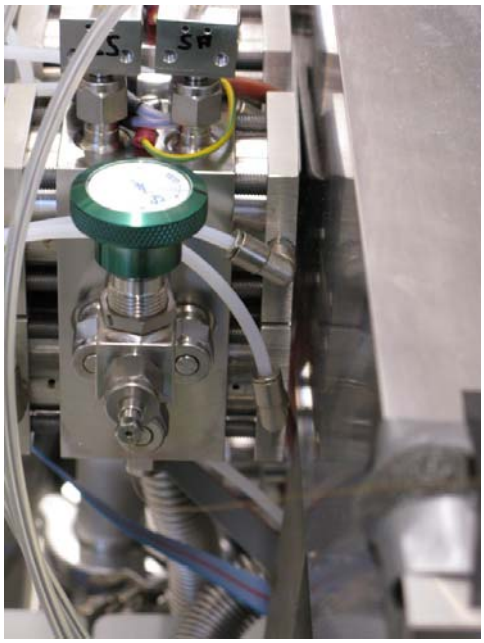

II. Blanks

Blank runs of Stheno+CF-IRMS pulling no air aliquot reveal no N_2O contamination from leaks or carry-over from previous sample not fully desorbed from a cryotrap. There is a small standing CO_2 peak which is typical of atmospheric pre-concentration systems. Shown are full chromatogram view and zoomed to the N_2O peak elution region.

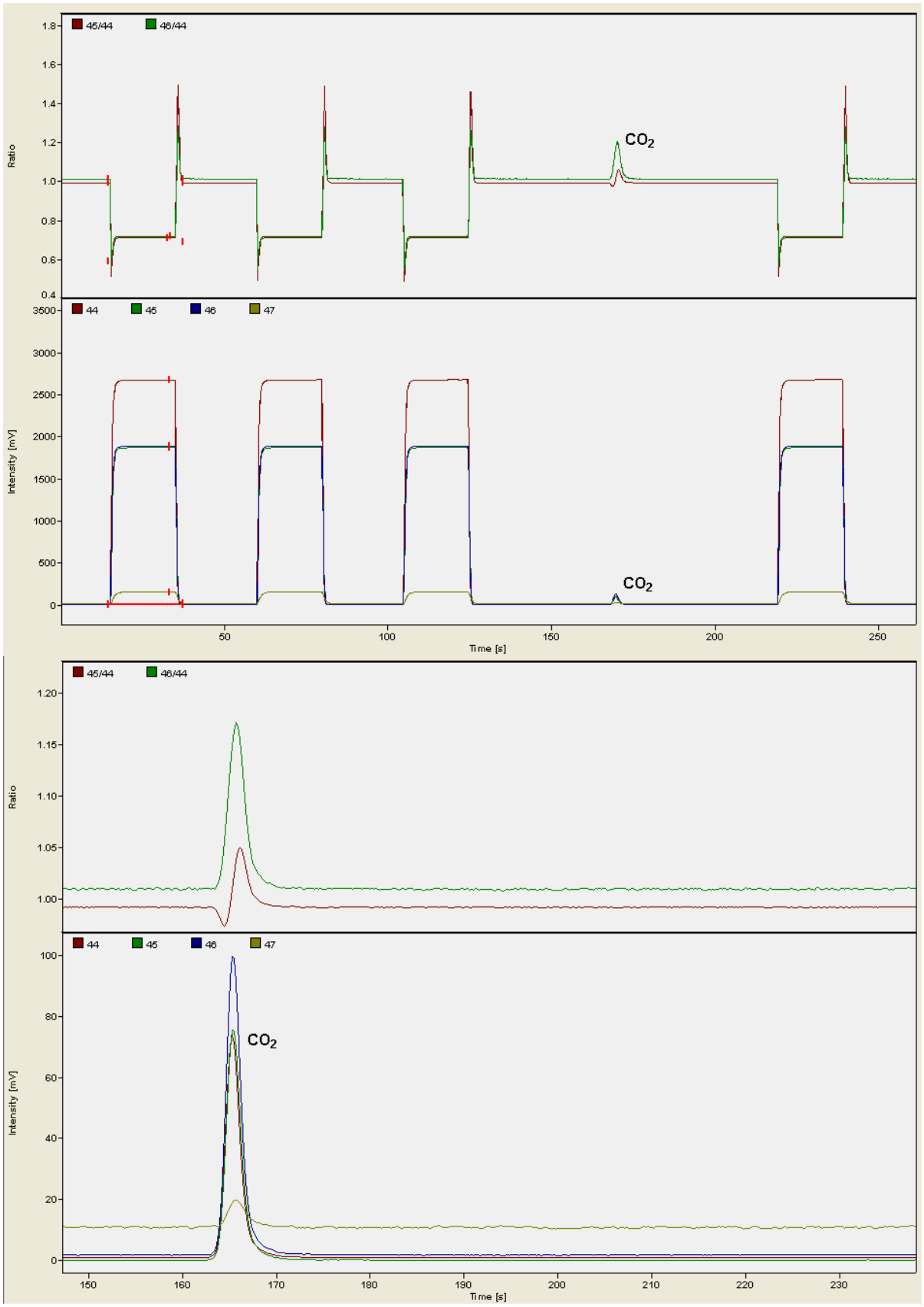
45/44
46/44
Ratio
CO2
44
45
46
47
Intensity [mV]
CO2
Time [s]
45/44
46/44
Ratio
44
45
46
47
CO2
Intensity [mV]
Time [s]

III. Quadrupole mass spectrometer fluorocarbon diagnostic SIM (select ion mass) chromatograms

Stheno sample run with AGAGE air standard tank collected at Mace Head, H-106, S/N 5310. Large peak at ~113 seconds retention time is N_2O. There is a small peak in the m/z 69 ion chromatogram indicative of a fluorocarbon compound and separated from N_2O at ~123 seconds retention time.

m/z 31 $^{12}C^{19}F^{+}$

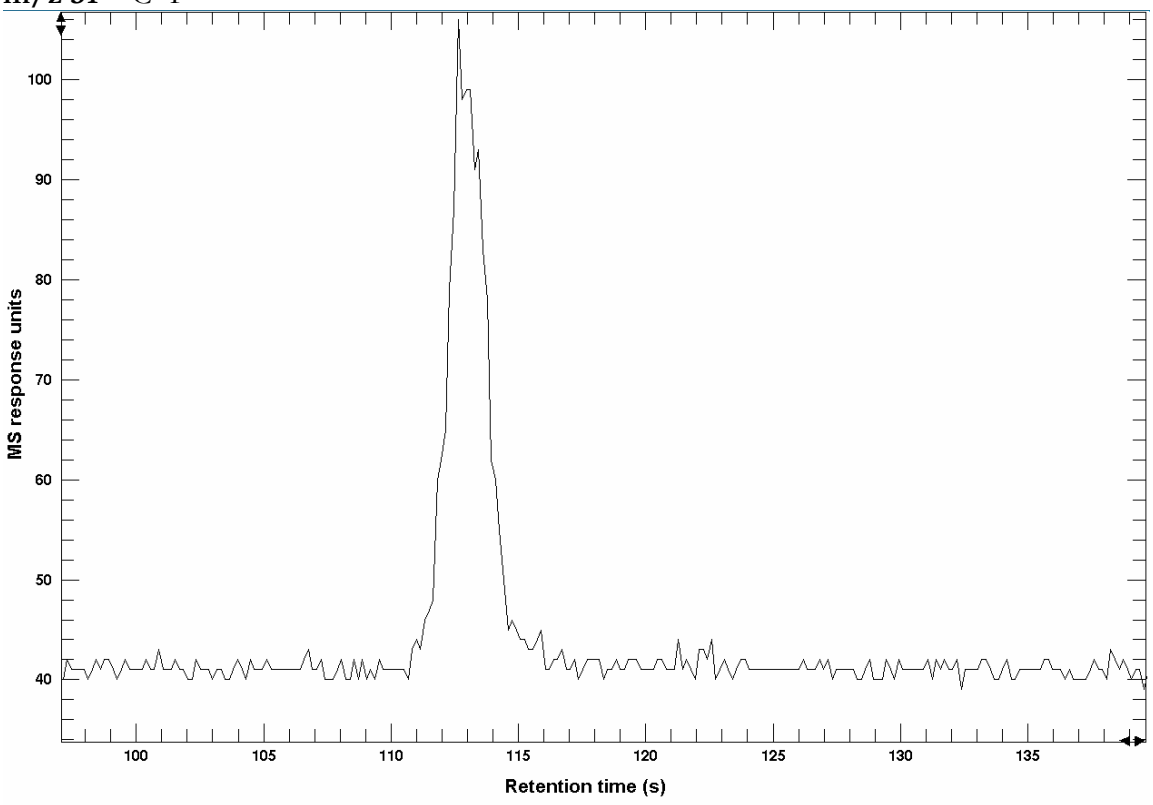

m/z 50 $^{12}C^{19}F_2^+$

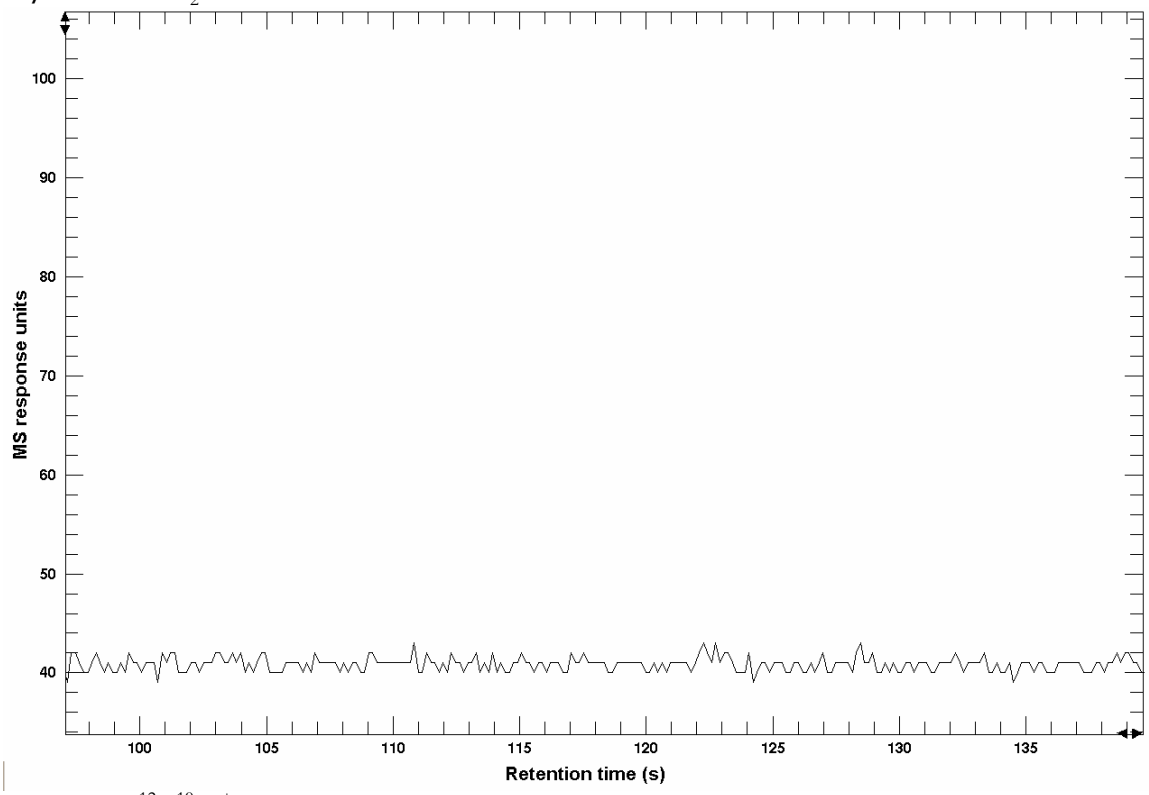

m/z 51 $H^{12}C^{19}F_2^+$

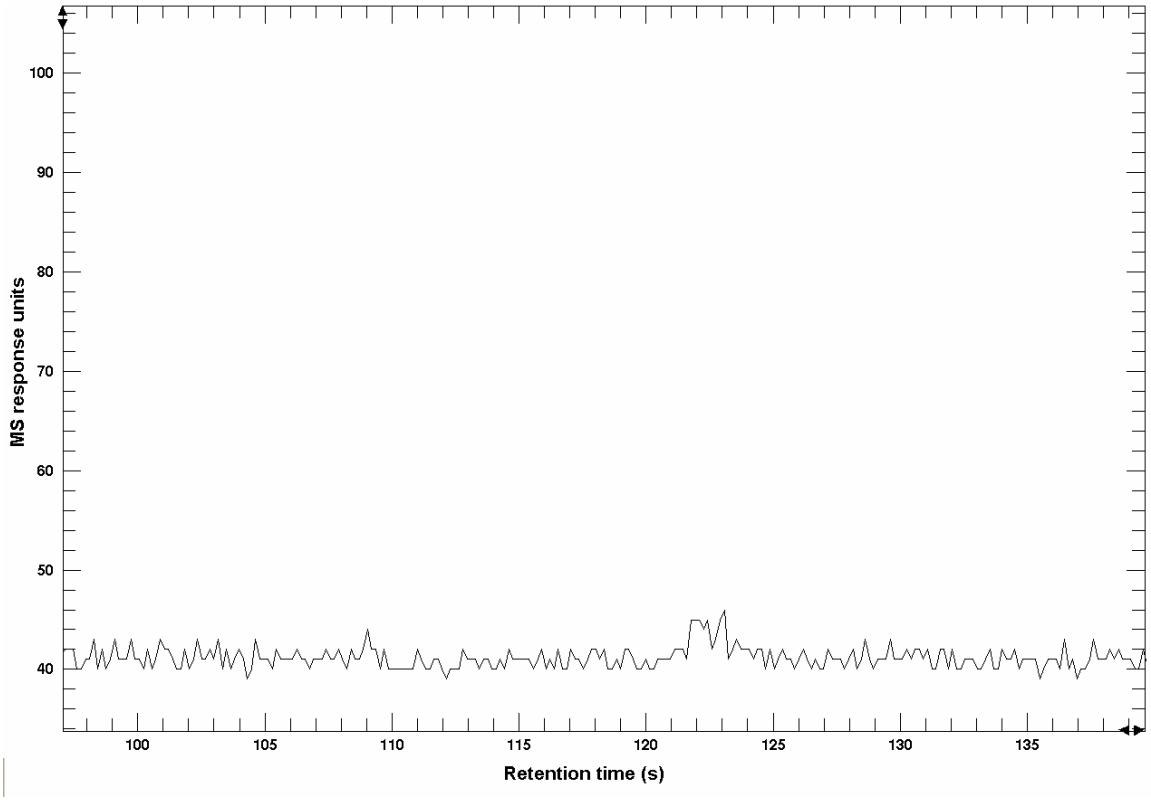

m/z 69 $^{12}C^{19}F_3^+$

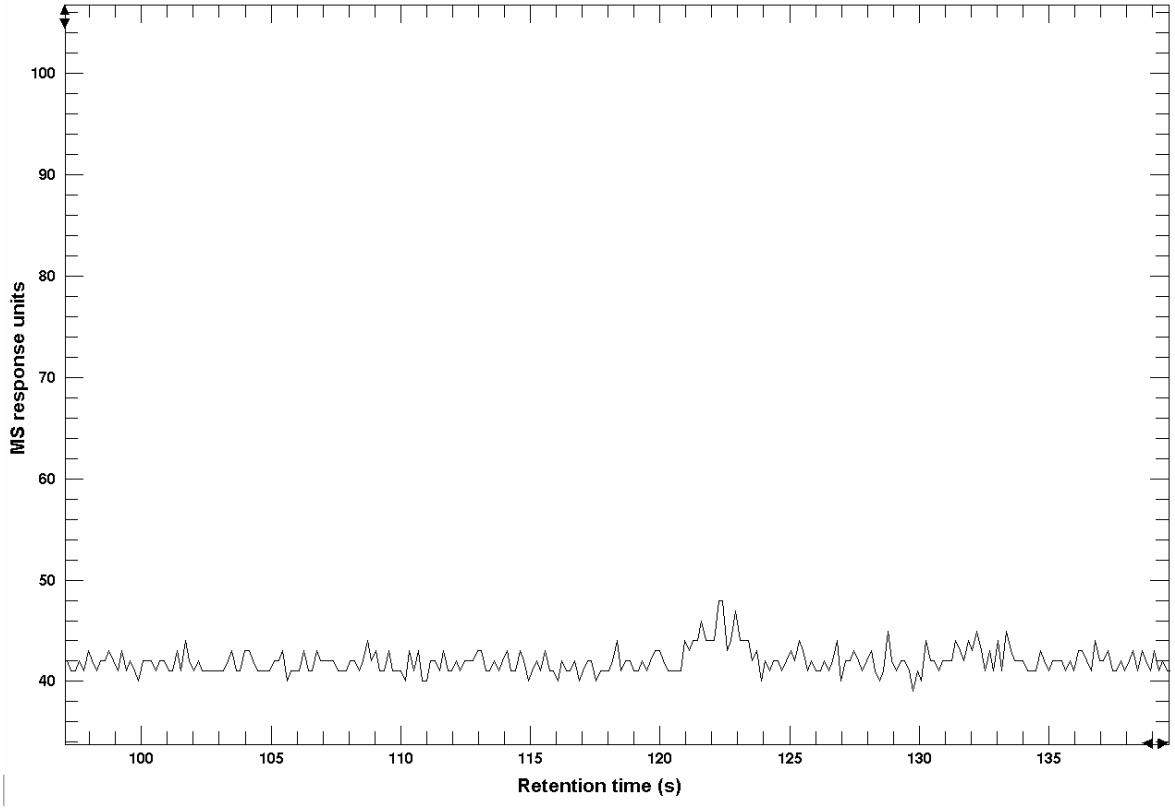

m/z 85

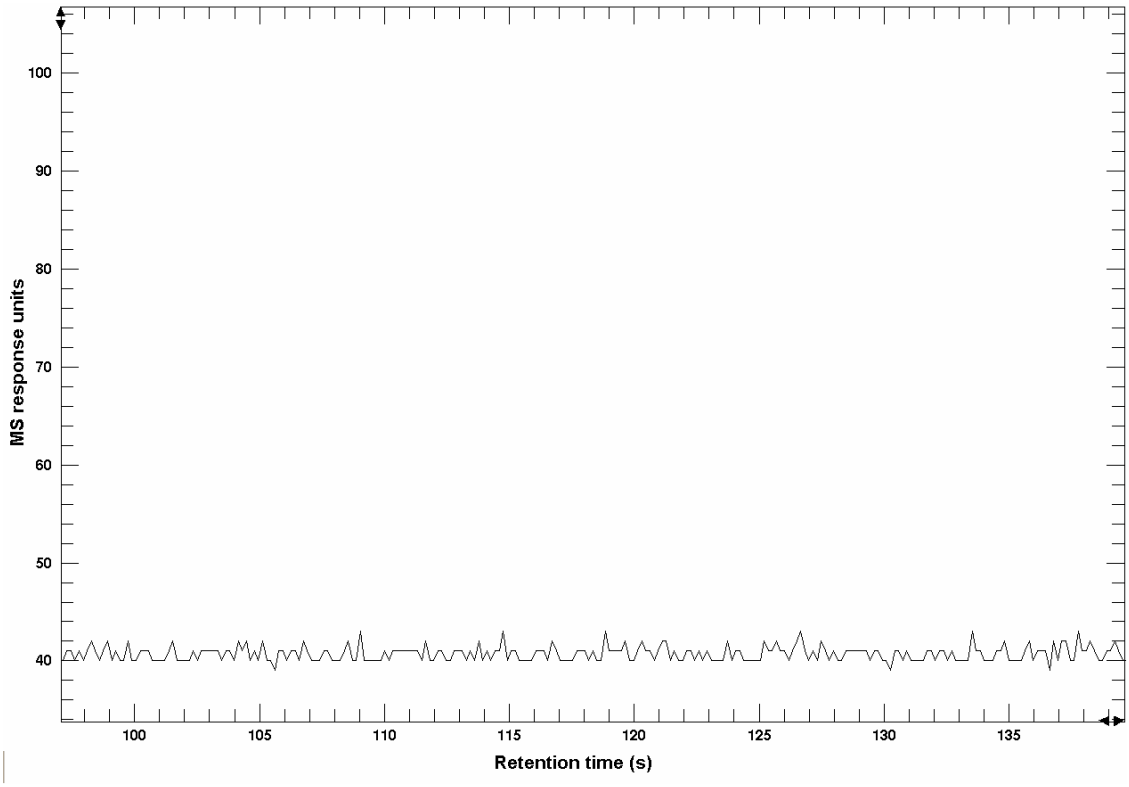

IV. Vacuum manifold

A custom built vacuum line manifold was utilized in many aspects of the analysis of the isotopic composition of N_2O related to the tropospheric air measurements and Stheno (Part I), IRMS use (Part II), and calibration (Part III).
Specifically: initial flask leak tests, flask cleaning and evacuation, calibration by NH_4NO_3 tube evacuation and sealing, calibration product tube cracking and separation, transfer of reference N_2O to transfer flask, and other transfer and evacuation uses.
Details are as follow:

- Direct-drive oil sealed rotary vacuum pump (ULVAC KIKO, Inc.)
- Molecular sieve 13X trap between vacuum pump and manifold to trap hydrocarbons released from the pump oil. Also serving to protect the pump from condensables being pumped out of the manifold.
- Liquid nitrogen trap (SS tubing loop immersed in liquid N_2) anytime pump line exposed to manifold
- SS-4H Nupro bellows-sealed valves (Swagelok)
- 1/4" electropolished stainless steel tubing (Swagelok)
- Thermocouple vacuum gauge tube and controller (0-1000 mTorr, Kurt J. Lesker). All metal construction. Series 205 controller accuracy +/- 1mTorr at 1-20 mTorr , +/- 5% of reading at 20-1000mTorr.
- Manifold capable of pressures down to 4 mTorr
- MKS Baratron absolute pressure transducer (0-1000 Torr, Type 722A). Accuracy 0.5% of reading. For this full-scale range, the lowest suggested pressure for reading 0.5 Torr, lowest suggested pressure for control 5 Torr. The sensor diaphragm is sensitive to temperature fluctuations. Zero 0.08 Torr/°C, Span 0.04% of reading/°C
- MKS PDR2000 capacitance diaphragm gauge controller display resolution 0.1 Torr.
- For all use of vacuum manifold, at the minimum initial "cleaning" entailed evacuation to <5mTorr, followed by 3-5 cycles of flushing with 40 psig UHP N_2 and evacuating to <5mTorr. More intensive use warranted extensive and prolonged "cleaning" procedures.
- Kept evacuated at all times to prevent condensation and desorb any gases from interior walls.

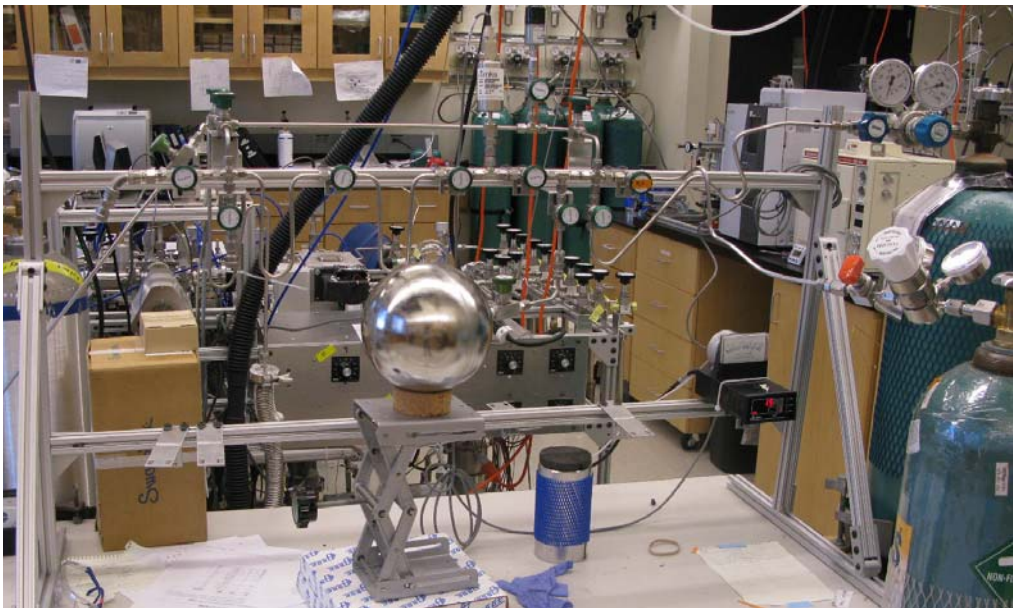

Appendix 3

I. Surface layer height

The reference case model uses the 0-100 m air history layer from the NAME model with the assumption that this boundary layer marks the layer of air influenced by surface emissions directly below. A model sensitivity test includes the next higher layer as well to give a 0-1000 m boundary. The planetary boundary layer of well-mixed air fluctuates with day-night transitions and meteorological conditions among other factors. The effect of increasing the boundary layer depth in the model is to weight each horizontal surface emission grid cell by the additional dispersion model output time integrated air concentration in the 100-1000 m layer. For this model sensitivity test the stratosphere is not included in order to isolate the effects of regional sources. NAME model output of >100m altitude layers are only available from the 11 March 2010 time stamp (n = 45).

For the 0-1000 m layer case, assessment of mole fractions (not pictured) shows that the model overestimates the variation from baseline (1σ = 0.52 ppb) compared to the observations (1σ = 0.33 ppb), suggesting that the reference case 0-100 m surface layer provides a better simulation of regional emissions and modeled deviations by the 0-1000 m case may be overestimated.

The increased emissions strength caused by weighting the higher layer is reflected in the isotopic compositions which are shifted to more ^{15}N- and ^{18}O-depleted values in the direction of the light soil signature and with greater deviation from baseline than in the reference case, shown in Figure 3.10 for $\delta^{15}N^{bulk}$ with similar phenomena for $\delta^{15}N^{\alpha}$, $\delta^{15}N^{\beta}$, SP, and $\delta^{18}O$. However, given the mole fraction overestimation, these larger isotopic deviations for the reference case, which would similarly increase the depleted soil signature case deviations, are likely unrealistic.

Figure 3.10 Time series of model output for $\delta^{15}N$ comparing using the air history 0-100m level or combined 0-1000m level to determine regional source emissions, no stratosphere included. Similar results for $\delta^{15}N^{\alpha}$, $\delta^{15}N^{\beta}$, SP, and $\delta^{18}O$. Filled data points are baseline time stamps, open data points are all other time stamps. Note that the y-axis scale is the same as in previous figures.

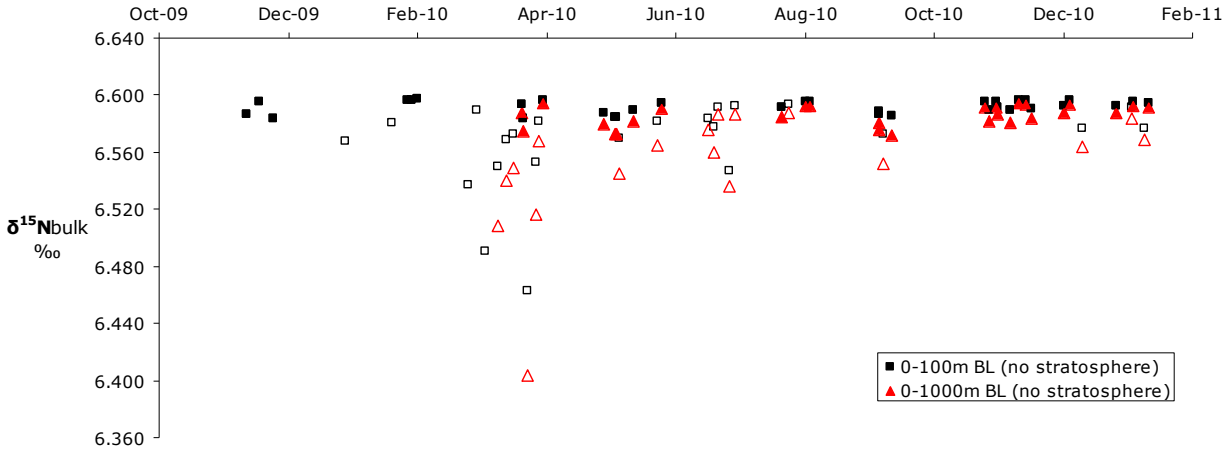

Appendix 4

I. Data integrity

Air sample contamination

Spherical flasks were screened for potential contamination due to prior use in other air-sampling measurement campaigns (Hodson 2008), and were subject to repeated flask evacuations <5 mtorr followed by pressurizing to ~40 psi with ultra high purity N_2 gas (Airgas) and left evacuated for 1-2 weeks to allow for desorbtion of any gas adhering to the internal walls. With any significant rise in pressure over that time the procedure was repeated.

All sample measurement results were additionally screened for potential contamination which is always a danger with pure N_2O present in a shared laboratory. Measured m/z 44 sample peak areas (Vs) were verified to vary only within the range observed in the Niwot Ridge air standard during that measurement session. Observations with large deviations in isotope compositions were verified that the composition was not deviating towards the isotope composition of the pure N_2O tanks in the lab in all of the results from the same individual flask.
Flasks which showed evidence of contamination were removed from use for air sampling and any results from these flasks were discarded.

Instrumental drift

Instrumental drift possibility was checked in the NR air standard for level response in δ45, δ46, δ31 within precision. The NR air standard showed no drift indicating that the IRMS response (including any possible trend in IRMS scrambling factor), pure N_2O standard, continuous flow interface, and Stheno pre-concentration device are not drifting significantly over the course of the year of measurements. Further discussion of Niwot Ridge air standard stability is in Chapter 2, Part II.

II. Data Corrections

Instrumental day-to-day conditions

Variations in the instrumental measurement conditions between each day of analysis (including all of the IRMS components and response; Stheno pre-concentration device functioning and components; possible effects of pressure, temperature, or moisture levels in the lab on instrumental functioning, particularly the continuous flow interface; and pure N_2O reference gas aliquots) were assessed with daily series of the Niwot Ridge (NR) air standard (3-5 pairs of molecular and fragment ions analyses). Because of the length of time to perform each run and the desire to maximize precision and particularly accuracy with a series of repeated measurements, a typical measurement day included an air standard series and 1 to 2 flask sample series. Significant variations in system functioning were noted by deviations in the air standard isotopic composition. Only two occasions necessitated corrections to the samples because of changes in the air standard response.

1) Measurement day 14 April 2010 the R45 and R46 for NR were significantly low in all runs, indicating a shift in instrumental conditions. The raw R45 and R46 values were scaled for the flask measured on that day prior to calculation of the isotopologue values, corresponding to the observation collected on 15 March 2010.

2) Starting with the November 2010 measurement session there was a substantial jump in site specific R31 in NR. The raw δ31 of NR air standard v. N_2O reference increased by approximately 0.3 ‰, corresponding to shifts in the site-specific isotopomer values of approximately

$\delta^{15}N^{\alpha}$ +0.44‰, $\delta^{15}N^{\beta}$ -0.42‰, and SP +0.87‰. Instrumental causes were investigated but did not resolve the cause of the jump in continuous flow sample gas v. N_2O reference relationship in the m/z 31/30 ratio. Affecting flasks measured in the November, December 2010 and January 2011 measurement sessions, these samples were scaled to raw R31 of NR. This correction was applied to observations collected after 27 Oct 2010 inclusive.

Reference peak 31/30 integration by probability density function

Sample N_2O peaks eluting from the Stheno GC onto the IRMS are referenced against pure N_2O standard gas admitted into the IRMS bracketing the sample peak (see Figure 2.3). For early measurements made in sessions July 2010 and earlier, the GC flow was run underneath the square reference peaks to have an accurate account for GC carrier gas background. Isotope calibration methods for continuous flow analyses that do not divert the analytical gas stream for the referencing give the highest performance with best precision (Merritt et al 1994). Rigorous initial testing and monitoring was conducted of the entire chromatogram for m/z 31 compounds surrounding the N_2O sample peak which would fall under the reference peaks (Chapter 2, Part I and II). Despite this, m/z 31 contaminating peaks barely distinguishable from noise were later discovered in the 31/30 trace which indeed influenced the square reference peak areas and disturbed the Isodat integrated reference value for 31/30. The m/z 31 interference manifested itself as a small hump atop the square reference peak 31/30 trace, and was only evident with extremely close inspection of the traces slightly above noise levels (Figure A4.1). After this discovery the referencing method was altered so that the GC flow was only in line with the IRMS at the time of N_2O sample peak elution. Chromatographic background levels subtracted for each peak integration were assigned individually for each reference or sample peak.

Figure A4.1 Example of three images of the same individual square reference peak from the IRMS exhibiting the m/z 31 interference. Upper plot in each image are the ion ratios, lower plot is the ion intensity IRMS output in mV. Only with inspection of the square reference peak at noise levels is the small m/z 31 interference apparent.

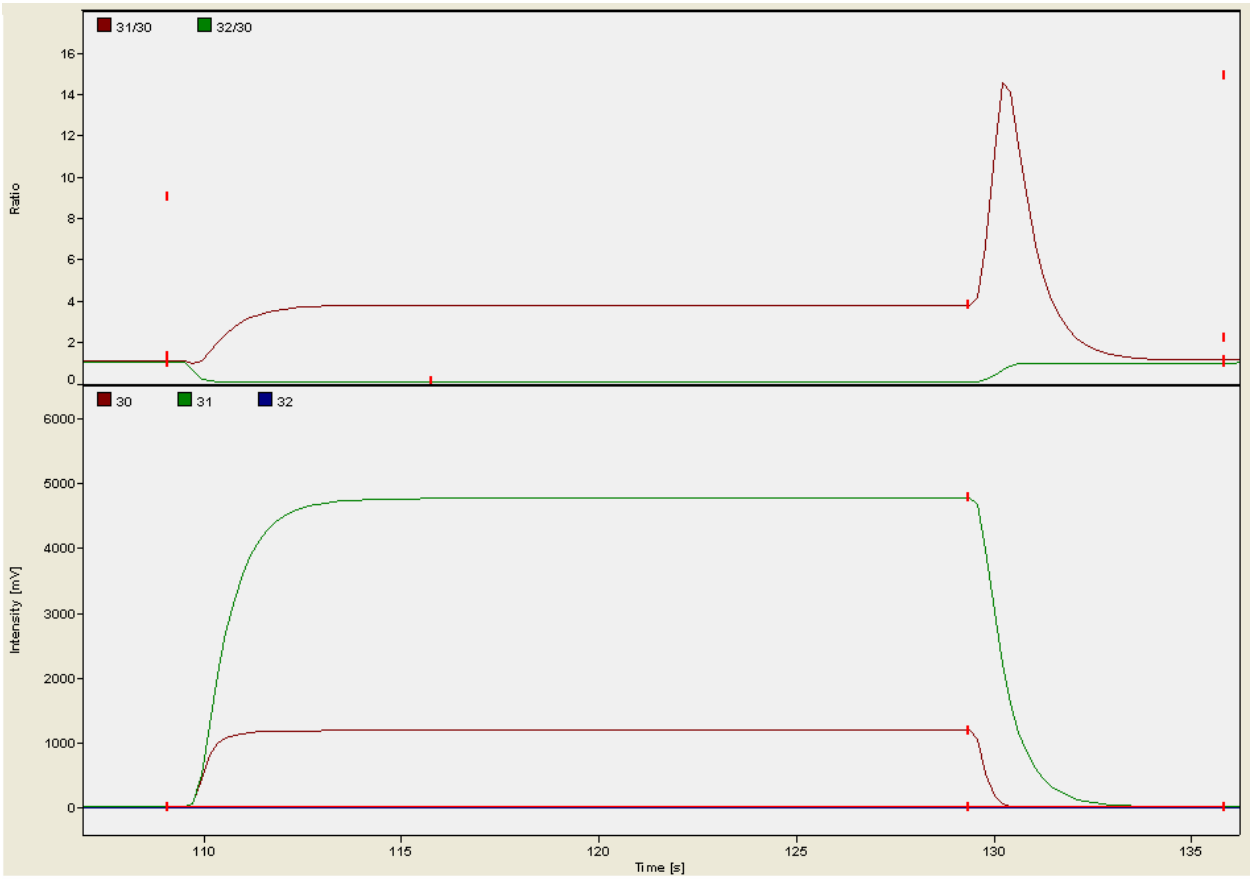
31/30
32/30
Ratio
16
14
12
10
8
6
4
2
0
30
31
32
Intensity [mV]
6000
5000
4000
3000
2000
1000
0
110
115
120
125
130
135
Time [s]

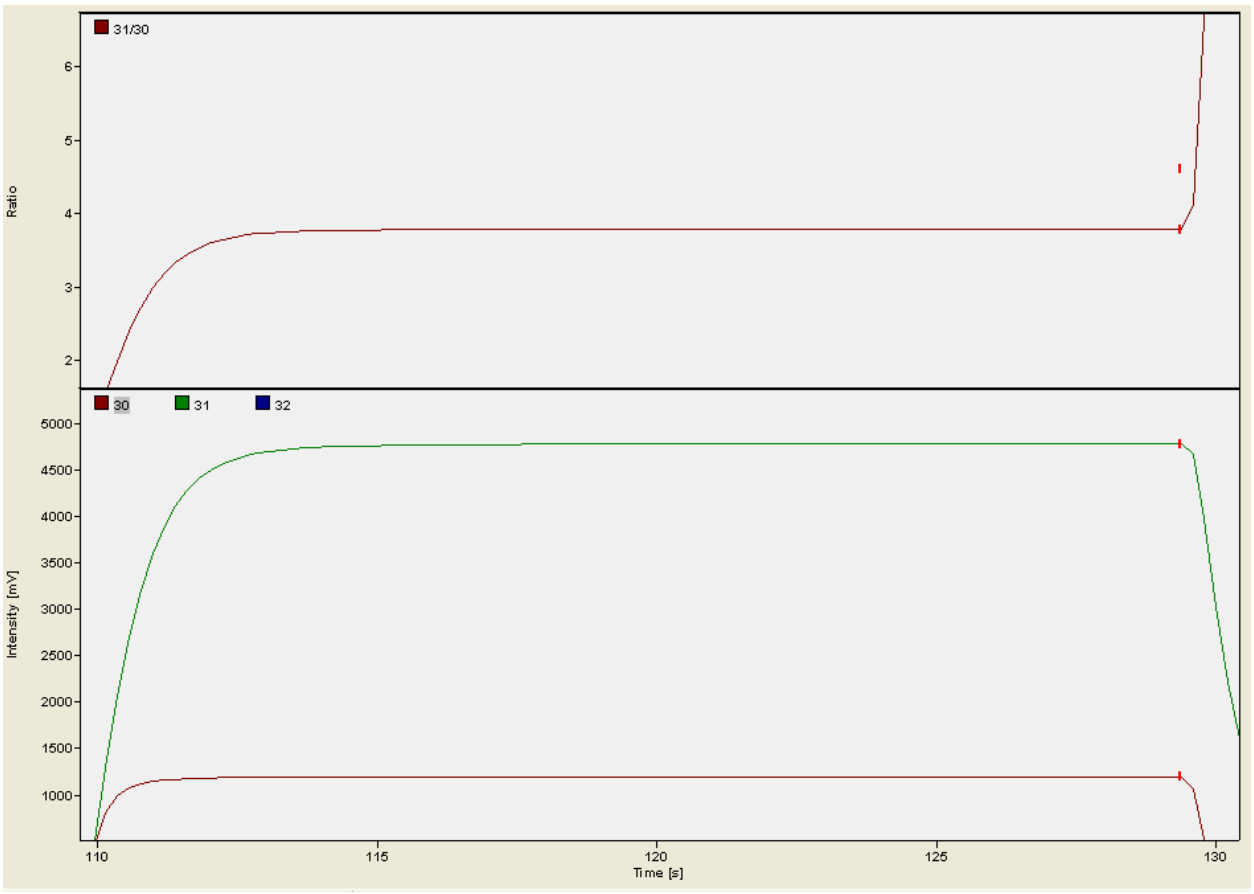
31/30
Ratio
6
5
4
3
2
30
31
32
Intensity [mV]
5000
4500
4000
3500
3000
2500
2000
1500
1000
110
115
120
125
130
Time [s]

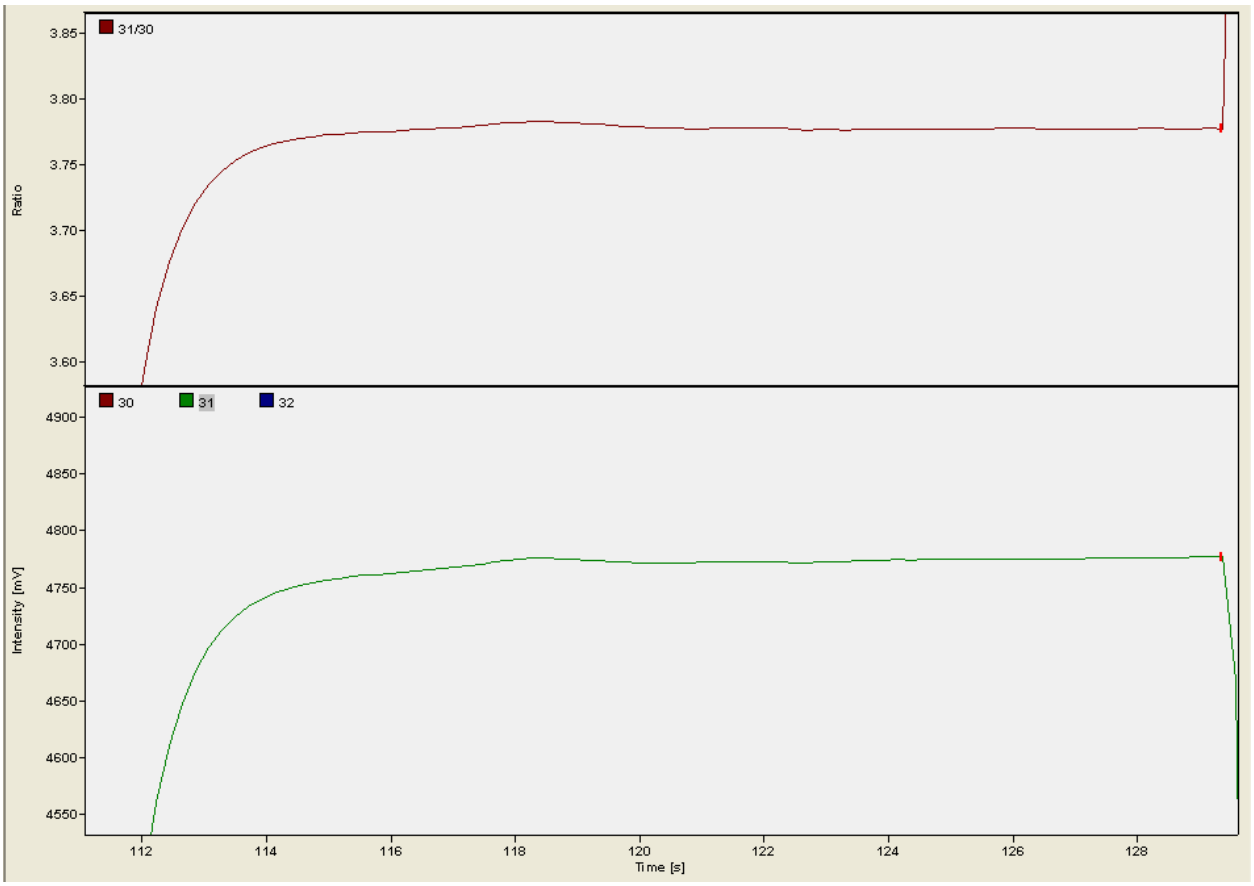

A new referencing method was developed to handle the Isodat reference peak integration error and avoid discarding the early measurements. Raw IRMS recorded data points (i.e. peak heights, ~4-5 per second) of m/z 30 and m/z 31 ion current intensities (mV) were used to generate a probability density function of the 31/30 ratio at each record point spanning the reference peak start and finish times. Bins of size 0.00005 for the raw 31/30 ratio were used. The maximum of the PDF is the 31/30 ratio which occurs most frequently along the square reference peak and thus does not include the small interfering hump. For each sample m/z 30,31 run a PDF is created and the maximum is taken as the reference peak 31/30 value. An example of the resulting PDF is shown in Figure A4.2 with the maximum clearly divergent from the Isodat IRMS software determined integration of the contaminated reference peak.

Figure A4.2 Example probability density function of raw 31/30 ratios of ion intensity peak height (mV) spanning a square reference peak which had an interfering m/z 31 tranisent peak underneath. Isodat software peak area determination of 31/30 ratio is marked in red, which includes integration of the interfering peak. PDF maximum coincides with the 31/30 ratio of peak heights most frequently occurring across the top of the square reference peak, and therefore coincides with the true reference peak 31/30 ratio.

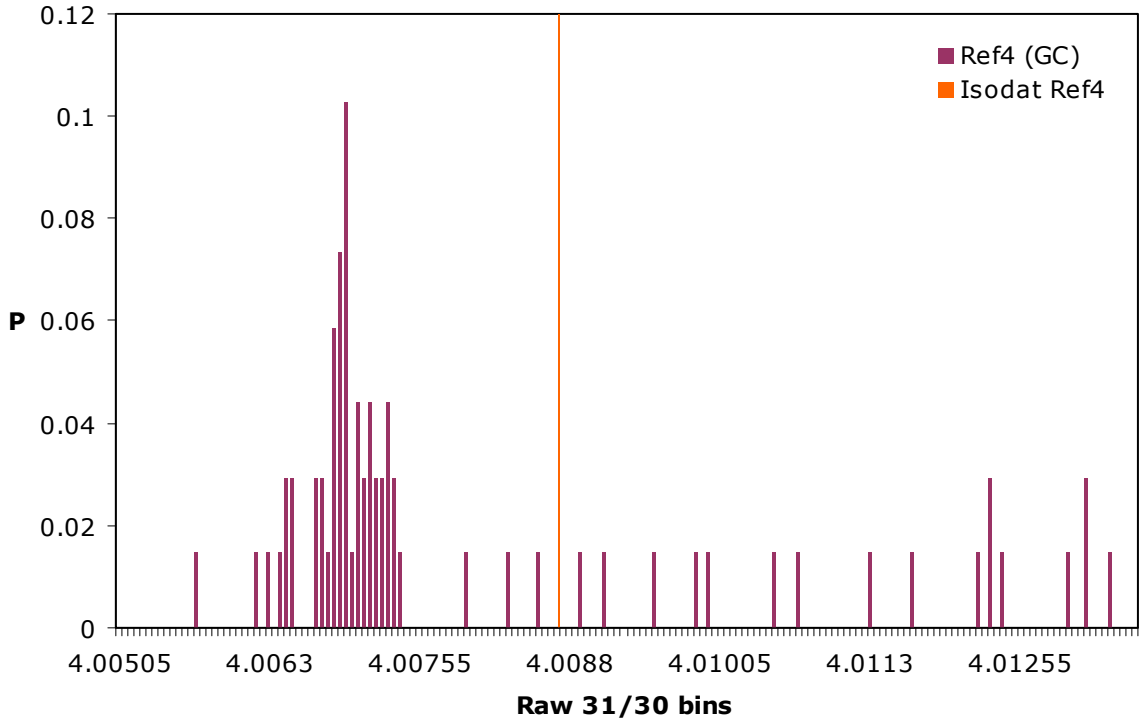

To verify this method several later samples were run so that the GC was under one reference peak and thus creating the same contamination while leaving another reference peak free from GC effluent. This is shown in Figure A4.3 where the reference without GC interference (Ref3) PDF maximum, Isodat integration of the uncontaminated peak (Isodat Ref3), and PDF maximum of the contaminated peak (Ref4) all align at the same 31/30 value within uncertainty. The erroneous Isodat integration 31/30 result of the contaminated peak is marked by the orange line. In total, 16 sample runs verified that the PDF maximum of a contaminated peak indeed corresponded to the Isodat uncontaminated reference integration.

Even though it was verified that this novel method matched the Isodat integrated 31/30 ratio in later samples that had no reference peak interference, to avoid any slight potential bias from the PDF referencing method this method was performed for the 31/30 ratio in the reference for all runs of all samples.

Figure A4.3 Example verification of PDF referencing method by bracketing a sample with one square reference peak with no underlying interference ("Ref3 (no GC)", blue PDF) and one reference peak with pre-concentration device effluent interference ("Ref4 (GC)", pink PDF). Isodat peak area integration results for 31/30 ratio are indicated for each reference peak. Both reference peaks are with the same reference gas and only separated on the IRMS by ~45 seconds and thus should be of equal 31/30 ratio. Apparent is the largely incorrect Isodat 31/30 ratio for the Ref4 peak with interference, and the concurrence of the two PDF maximums and the correctly determined Isodat area integration ratio for the peak without interference.

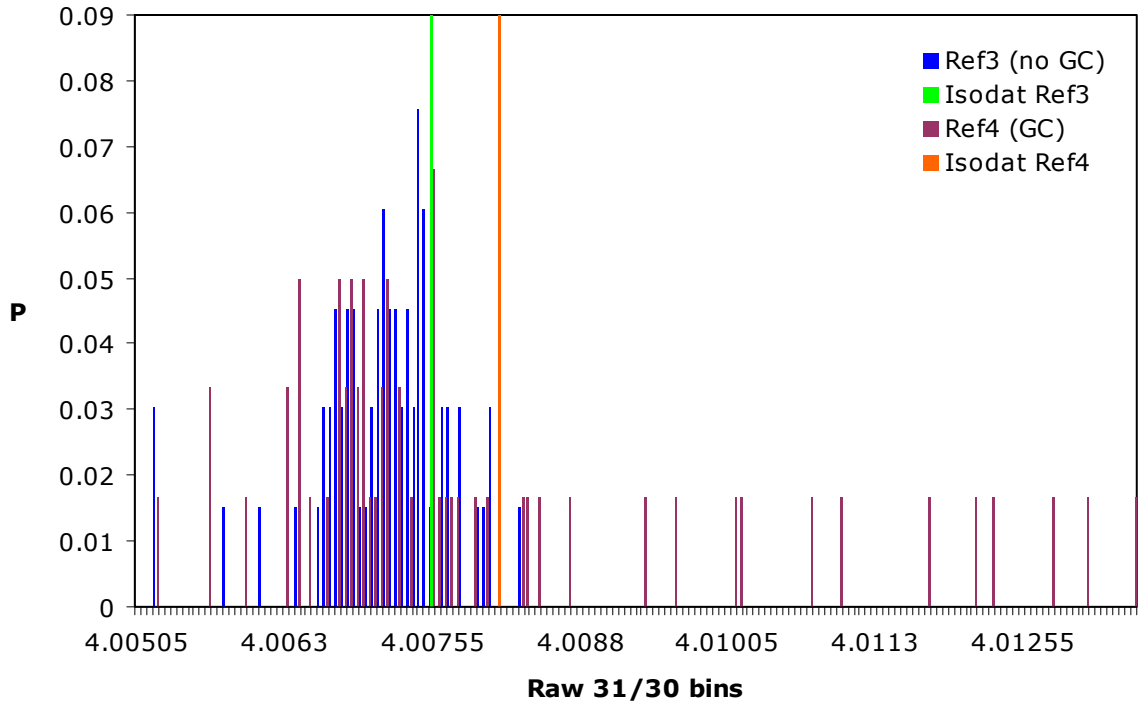

III. Air sampling at Mace Head

Air samples were collected regularly (anywhere from ~3 times per week to ~2 times per month) starting in January 2010 until January 2011 from the Mace Head Atmospheric Research Station on the Atlantic Ocean coast of Ireland (53.32°N, 9.90°W) (Figure A4.4). The Mace Head region is characterized as generally wet and boggy with about 20% of exposed rock and few trees. Immediately beneath the tower is a peat bog surface. Wind speed and direction measurements are made at ~25m on the tower. Reported wind measurement is a single point for the end of sampling.

Figure A4.4 Mace Head Atmospheric Research Station, Ireland

Two types of sample flasks are used: 2.9L spherical stainless steel flasks (Biospherics Research Corp) electropolished by Electromatic, Inc. with a single inlet with a bellows valve (Nupro SS-4H), or 3L cylindrical stainless steel flasks (Lab Commerce, Santa Clara, CA, X23L-2N) with two inlets each with bellows valves (Nupro SS-4H) (Figure A4.5).
For the double inlet flasks one of the valves is attached to a dip tube to the bottom of the canister and is the preferred inlet for inputting sample and withdrawing sample for analysis.

Figure A4.5. Air sampling setup with double inlet flask. Stainless steel inlet line is connected to a Viton-free diaphragm pump which is used to flush and then fill the flask to ~3-4 bar a through the dip-tube inlet.

Air from Mace Head enters through an inlet at 10 m on the Mace Head tower, 14 m above sea level and situated 90 m from the shoreline and 50 m from high water. Air is pulled through a 7 μm filter and 1/4" stainless steel line dedicated to flasks (Figures A4.6 and A4.7). Prior to sampling the line is flushed for ~30 minutes using a diaphragm pump (KNF UN86SNI, 316SS head, EPDM diaphragm,

Neoprene valves). This pump used for air sampling is specially designed to avoid typical Viton materials to avoid known Viton offgassing contamination (e.g. Rockmann et al 2003, Kaiser et al 2003a, Miller et al 2008). Double inlet flasks are simultaneously flushed for 30 minutes prior to closing the second valve and pressurizing with the KNF pump to ~3-4 bar a for about 10-15 minutes. Evacuated single inlet flasks are filled through the flushed sample line and pressurized to ~3-4 bar a for about 10-15 minutes.

Figure A4.6 Inlets on the Mace Head tower at ~10 m. Flask sampling line is the lower small inlet, AGAGE instrumentation is the upper small inlet.

Figure A4.7 Inlets for flask sampling line and AGAGE instrumentation at 10m on the Mace Head tower.

Collected flasks are returned to MIT for N_2O isotope analysis, and flasks are typically analyzed by the preconcentation+GC-IRMS system within 2-3 weeks after sampling. N_2O mole fractions in the flask are taken to be the simultaneously measured concentration on the AGAGE GC-MD. Although this arrangement does not measure N_2O mole fraction in exactly the same air as that analyzed for isotopic composition, the proximity of the two inlets on the Mace Head tower and the relatively uniform concentration of the long-lived N_2O especially over such short timescales strongly support the use of this approximation.

Flask integrity leak check

Prior to use for sampling, all flasks were checked for leaks (associated with the valves and valve connections). Because our pressure measuring capabilities are much more precise at vacuum pressures rather than higher pressures, flask and tank leaks were tested for by evacuating to <10mTorr and testing for any increases in pressure after 3 weeks. Though the tank and flasks might be kept in use for longer than these times, these lengths are adequate to detect any leaks that would be within the precision of measurements. It is assumed that the pressure difference between the low pressure evacuated tank and external atmospheric pressure adequately will detect leaks which would occur in the other direction (i.e. when the standard tank is at high pressure above the external atmospheric pressure). Initially a small pressure increase (~ a few mTorr) would be expected due to off-gassing from interior walls, mostly water. After repeated "cleaning" cycles of evacuations and pressurizing with nitrogen this off-gassing was eliminated to commence the leak test.

IV. Flask observations data

Table A4.1 Data table of flask observation collection date and sampling time, N_2O mole fraction (ppb) (from AGAGE in situ instrument), and isotopic composition (‰) with associated standard error (SD/√n; n = 3-5 repeated measurements). Observations in orange correspond to baseline categorized air samples. Mole fractions marked 'P' were pollution-flagged according to the AGAGE algorithm.

Date	Time (GMT)	N_2O (ppb)	$\delta^{15}N^{\alpha}$ (‰)		$\delta^{15}N^{\beta}$ (‰)		$\delta^{15}N^{bulk}$ (‰)		SP (‰)		$\delta^{18}O$ (‰)	
20-Jan-10	1503-1542	322.94	17.21	0.053	-3.88	0.064	6.67	0.028	21.09	0.092	43.98	0.029
27-Jan-10	1050-1110	323.17	16.91	0.064	-3.87	0.091	6.52	0.034	20.78	0.129	43.98	0.073
29-Jan-10	1120-1140	323.48	16.83	0.050	-3.92	0.065	6.46	0.058	20.75	0.090	43.89	0.064
1-Feb-10	1100-1115	323.23	16.57	0.067	-3.90	0.085	6.34	0.054	20.47	0.127	43.83	0.059
25-Feb-10	1325-1335	324.068 P	16.62	0.060	-3.72	0.084	6.45	0.041	20.34	0.119	44.17	0.068
1-Mar-10	1545-1555	323.19	16.77	0.068	-3.75	0.087	6.51	0.017	20.51	0.130	44.27	0.038
5-Mar-10	1635-1645	323.49	16.68	0.034	-3.79	0.042	6.45	0.039	20.47	0.051	44.24	0.040
11-Mar-10	1625-1635	323.29	16.83	0.028	-3.94	0.057	6.45	0.019	20.77	0.061	44.24	0.066
15-Mar-10	1330-1342	323.63	16.59	0.068	-3.80	0.088	6.39	0.023	20.39	0.131	44.03	0.046
18-Mar-10	1400-1415	323.85	16.75	0.056	-3.96	0.094	6.39	0.043	20.71	0.125	44.02	0.097
22-Mar-10	1105-1120	323.39	16.72	0.046	-3.84	0.057	6.44	0.022	20.56	0.078	44.15	0.025
23-Mar-10	1040-1055	323.77	16.59	0.055	-3.69	0.086	6.45	0.042	20.29	0.115	44.12	0.085
25-Mar-10	1150-1200	324.429 P	16.11	0.058	-3.23	0.081	6.44	0.045	19.35	0.114	44.45	0.070

30-Mar-10	1000-1015	323.30	16.51	0.092	-3.39	0.119	6.56	0.050	19.90	0.187	44.07	0.074
1-Apr-10	1045-1115	323.33	16.61	0.079	-3.62	0.116	6.49	0.021	20.23	0.169	44.12	0.091
30-Apr-10	1030-1040	323.51	16.70	0.057	-3.23	0.072	6.73	0.036	19.93	0.108	44.07	0.054
5-May-10	1417-1440	323.54	16.81	0.140	-3.55	0.204	6.63	0.044	20.36	0.320	44.26	0.051
6-May-10	1220-1240	323.51	16.52	0.061	-3.54	0.078	6.49	0.071	20.06	0.114	43.96	0.077
7-May-10	1155-1210	323.940 P	16.61	0.089	-3.70	0.106	6.45	0.075	20.30	0.170	44.00	0.068
11-May-10	1153-1205	no data	16.61	0.044	-3.66	0.070	6.48	0.038	20.27	0.089	44.15	0.073
25-May-10	1350-1405	323.55	16.47	0.038	-3.38	0.065	6.55	0.015	19.85	0.078	44.10	0.066
27-May-10	1050-1100	323.05	16.78	0.068	-3.32	0.102	6.73	0.045	20.09	0.145	44.14	0.092
23-Jun-10	1250-1300	323.11	16.41	0.068	-3.33	0.083	6.54	0.039	19.74	0.126	44.31	0.035
1-Jul-10	0910-0930	323.15	17.07	0.030	-2.84	0.104	7.11	0.025	19.91	0.109	44.61	0.137
23-Jul-10	1510-1525	322.89	16.66	0.054	-3.52	0.080	6.57	0.029	20.18	0.109	44.05	0.069
26-Jul-10	1145-1200	323.668 P	16.58	0.056	-3.55	0.089	6.52	0.007	20.14	0.120	44.11	0.078
3-Aug-10	1617-1631	322.73	16.82	0.033	-3.59	0.055	6.61	0.027	20.41	0.063	44.18	0.060
5-Aug-10	0947-1002	322.48	16.72	0.057	-3.66	0.068	6.53	0.047	20.38	0.101	44.13	0.042
7-Sep-10	1150-1200	323.15	16.68	0.061	-3.32	0.074	6.68	0.022	20.00	0.110	44.10	0.003
7-Sep-10	1618-1628	323.00	16.66	0.059	-3.46	0.075	6.60	0.015	20.12	0.108	44.24	0.032
9-Sep-10	1016-1031	323.16	16.33	0.049	-3.10	0.061	6.61	0.017	19.42	0.085	44.14	0.022
13-Sep-10	1018-1032	323.13	16.60	0.067	-3.42	0.076	6.59	0.042	20.01	0.117	44.37	0.012
27-Oct-10	1017-1103	323.64	16.41	0.057	-2.92	0.069	6.75	0.042	19.33	0.101	44.23	0.038
29-Oct-10	1000-1015	323.49	16.38	0.050	-2.99	0.079	6.70	0.039	19.37	0.104	44.19	0.078
1-Nov-10	1000-1015	323.90	16.19	0.058	-2.80	0.072	6.69	0.039	18.99	0.104	44.24	0.042
2-Nov-10	1030-1040	323.77	16.41	0.058	-3.23	0.073	6.59	0.024	19.64	0.106	44.34	0.032
8-Nov-10	1200-1240	324.22	16.40	0.028	-2.83	0.032	6.79	0.020	19.22	0.035	44.18	0.016
12-Nov-10	1100-1115	323.82	16.81	0.060	-3.94	0.099	6.44	0.071	20.75	0.134	43.78	0.116

15-Nov-10	1125-1135	323.37	16.56	0.072	-3.27	0.101	6.65	0.027	19.83	0.149	44.25	0.073
18-Nov-10	1120-1130	324.03	16.75	0.038	-3.32	0.045	6.72	0.027	20.07	0.058	44.22	0.019
3-Dec-10	1145-1200	323.82	16.43	0.037	-3.16	0.089	6.64	0.014	19.59	0.101	44.20	0.107
6-Dec-10	1145-1205	324.07	16.58	0.042	-3.47	0.066	6.55	0.024	20.06	0.082	44.10	0.061
12-Dec-10	1150-1202	325.097 P	16.39	0.047	-3.11	0.062	6.64	0.046	19.50	0.084	44.30	0.055
28-Dec-10	1200-1212	324.23	16.39	0.055	-2.78	0.074	6.80	0.062	19.17	0.104	44.19	0.073
4-Jan-11	1150-1200	324.05	16.72	0.018	-3.55	0.042	6.59	0.014	20.27	0.035	44.24	0.051
5-Jan-11	1136-1150	324.23	16.65	0.075	-3.17	0.080	6.74	0.062	19.82	0.129	44.22	0.012
10-Jan-11	1630-1645	324.20	16.70	0.049	-3.27	0.059	6.72	0.035	19.97	0.083	44.26	0.034
12-Jan-11	1050-1100	324.08	16.54	0.035	-3.33	0.050	6.60	0.032	19.87	0.060	44.08	0.047